Comprehensive Study of Semicontinuous Emulsion Polymerisation Processes for Producing Nanoparticles

Chen, Yan

Awarding institution:
King's College London

Title: Comprehensive Study of Semicontinuous Emulsion Polymerisation Processes for Producing Nanoparticles

Author: Yan Chen

Comprehensive Study of Semicontinuous Emulsion Polymerisation Processes for Producing Nanoparticles

Yan Chen

Thesis submitted for the degree of
Doctor of Philosophy
University of London

King's College London
Division of Engineering
May 2012

This thesis is dedicated to my parents and my wife.

For their endless love, support and encouragement

Abstract

Semicontinuous emulsion polymerisation offers flexibility and versatility for manufacturing colloids for a wide range of applications. The technique has been studied since 1950s, however, its importance has only recently realized as evidenced by increasing attentions it has received in recent years. Despite all attentions, the potentials of this process to produce novel materials have not been well recognized yet by polymer industry. The main aim of the thesis is to investigate the underlying mechanisms of semicontinuous emulsion polymerisation processes in order to improve and/or control the properties of resulting polymer latexes, and design new colloids.

Polymerisations have been carried out in a jacketed glass reaction vessel. The conversions of monomers were measured by gravimetric method. Particle sizes and size distributions, their zeta potentials and molecular weights were measured by dynamic and static light scattering techniques. Turbidity as well as phase transition behaviour of latexes was measured by UV-visible spectroscopy. Glass transition temperature of polymers was measured by differential scanning calorimetry. Morphologies of particles were investigated by transmission electron microscopy and scanning electron microscopy.

Semcontinuous microemulsion polymerisation of styrene has first been carried out in order to study the true features of nucleation stage. A major step has been taken forward to reconcile experimental data with theory. The average diameter of particles (D) decreased and the particle size distribution (PSD) narrowed with decreasing rate of monomer addition (R_a). Nanolatexes with extremely sharp particle size distribution with average particle size as small as 10 nm could be easily produced by the end of feeding. Consistent with recent theoretical developments, D at the end of nucleation was found to be independent of surfactant concentration ([S]). Furthermore, the weight-average molecular weight ($\bar{M}_w$) of polymer decreased with decreasing R_a due to chain termination by secondary entry of free radicals. Single-chain polymer particles could be produced at early stage of nucleation. It was also found that the average diameter of particles practically approached a limit with decreasing R_a, and increasing [S] and reaction temperature. Particles as small as 6 nm, which is close to the size of micelles, were detected in the early stage of feeding using an extremely low R_a. As an alternative way for reducing particle size, a water-soluble chain transfer agent (CTA) was used to terminate the growing radicals inside the particles. Comparing with conventional process, semicontinuous process was found to provide a better controllability over D and $\bar{M}_w$ of polymer in the presence of CTA. Furthermore, the average diameter of particles was successfully reduced by almost 25%.

Thermosensitive and water-soluble poly(n-isopropylacrylamide) (polyNIPAM) colloids have recently attracted increasing attentions for many applications. A set of kinetic data has been reported for the batch polymerisation of neat NIPAM using a wide range of monomer and surfactant concentrations for the first time. A novel method has been applied to produce fast

dissolving polyNIPAM latexes with high solids content, based on layered structures produced via semicontinuous process. The application of above method has been extended to fabrication of ultrafine thermal-sensitive nanocapsules. The core material produced via semicontinuous process could be easily and completely removed via self-removing process in water, in comparison with the conventionally made core material. Furthermore, the thickness of crosslinked polyNIPAM shells could also be precisely controlled via semicontinuous process.

In recent years, considerable effort has been expended on research in polymer/silica core-shell hybrid systems due to their promising applications in surface coatings and biotechnology. Comparing with conventional batch process, hybrid particles obtained by semicontinuous surfactant–free emulsion polymerisation can incorporate more silica nanoparticles into the shell. The incorporation of silica nanoparticles into the shell can be further improved by gradually feeding silica dispersion during polymerisation. A mechanistic scheme for particle formation of hybrid particles under different pH has been developed. Monomers with intermediate water solubility like methyl methacrylate (MMA) can only produce stable composite particles at acidic conditions, at which silica nanoparticles are less stable. By contrast, more water-soluble monomers like vinyl acetate (VA) can easily yield composite particles at both basic and acidic conditions. Polymerisation on the surface of silica nanoparticles is believed to occur in the course of polymerisation for water-soluble monomers, which can suppress the electrostatic repulsion between both negatively charged silica and polymer particles and thus promote the adhesion of silica to polymer particles. For highly water-soluble monomers such as NIPAM, uniform silica armoured polyNIPAM particles could only be obtained under basic conditions. Interestingly, under acidic conditions, agglomeration of growing polymer particles with silica particles was extensive, resulting insoluble gels (even in the absence of crosslinker). TEM images revealed that under basic conditions, polymer-core/silica-shell structures were produced by batch process, but homogenous hybrids of polyNIPAM/silica nanoparticles by semicontinuous process.

Table of Contents

Abstract ……... iii

Table of Contents ……..…….. v

Acknowledgment ……..……... xi

Nomenclature ……..…… xii

List of Figures ……..…… xiii

List of Tables ……..……. xxi

Chapter 1 Literature Review ……. 1

1.1 Introduction ……...…….…… 1

1.2 Free radical Polymerisation ……...…….…… 2

1.3 General Features of Emulsion Polymerisation ……...… 3

1.4 General Features of Microemulsion Polymerisation ……...…... 7

1.5 Semibatch Approaches ……..…….…….…….. 8

1.5.1 Introduction ……. 8

1.5.2 Features ……...……...…….. 8

1.5.2.1 Monomer-starved conditions ……..…… 8

1.5.2.2 Control of overall rate of polymerisation …….. 10

1.5.2.3 Control of particle size, particle size distribution and number of particles 11

1.5.2.4 Control of polymer composition and morphology ……. 15

1.5.2.5 Control of molecular weight ……...…… 17

1.5.2.6 Smart and hybrid particles (organic-inorganic) ……...…….. 19

1.6 Main Conclusions from the Literature Study ……..…….. 20

1.7 Objectives ……..……..…….. 22

1.8 Thesis Outline ……..…….. 23

1.9 Reference ……..……...….. 24

Chapter 2 Experimental Procedures …… 32

2.1 Chemicals ……..... 32

2.2 Apparatus ……..……. 33

2.3 Measurements ……..…….. 34

2.3.1 Conversions ……...…….. 34

2.3.2 Size of Particles ……...…… 35

2.3.3 Number of Particles ……..…….. 36

2.3.4 Surface Coverage Ratio …….....…… 36

2.3.5 Molecular Weight of Polymer ……...…….. 37

2.3.6 Zeta Potential ……..…… 37

2.3.7 Glass Transition Temperature …….……..……... 38

2.3.8 Turbidimetric Measurement …… 38

2.3.9 Conductivity ……...……. 38

2.3.10 pH ……..…... 38

2.3.11 Reproducibility ……..……... 38

Chapter 3 Microemulsion Polymerisation of Styrene ……. 39

3.1 New Insights into Semicontinuous Microemulsion Polymerisation as a Mean to Produce Nanolatexes: Analysis of Nucleation Stage ……... 40

3.1.1 Introduction ……...…….. 41

3.1.2 Experimental Work ……..……... 43

3.1.2.1 Procedure ……..……... 43

3.1.2.2 Measurements ……...……... 43

3.1.3 Results and Analysis ……..……. 45

3.1.3.1 Rate of Polymerisation ……...…….. 45

3.1.3.2 Nucleation Period ……...…….. 46

3.1.3.3 Particle Growth and Formation ……...……. 49

3.1.3.4 Particle Size Distribution ……...…….. 51

3.1.3.5 Polymer Molecular Weight ……...……... 54

3.1.4 Conclusions ……...…..…… 56

3.1.5 Reference ...……...……... 57

3.2 Exploring the Minimum Particle Size Achievable via Semicontinuous Microemulsion Polymerisation 60

3.2.1 Introduction 61

3.2.2 Experimental Work 62

3.2.2.1 Procedure 62

3.2.2.2 Measurements 62

3.2.3 Results and Discussions 63

3.2.3.1 Effect of Temperature 63

3.2.3.2 Effect of Surfactant Concentration 67

3.2.3.3 Effect of Rate of Monomer Addition 70

3.2.3.4 Further Discussion 72

3.2.4 Conclusions 74

3.2.5 Reference 75

3.3 Synthesis of Ultrafine Nanolatexes using Chain Transfer Agent via Semicontinuous Microemulsion Polymerisation 77

3.3.1 Introduction 78

3.3.2 Experimental Work 79

3.3.2.1 Procedure 79

3.3.2.2 Measurements 79

3.3.3 Results 80

3.3.3.1 Conversions 80

3.3.3.2 Size of Particles 81

3.3.3.3 Molecular Weight of Polymer 82

3.3.4 Discussions 83

3.3.4.1 Particle Formation and Growth 83

3.3.4.2 Control of Molecular Weight 88

3.3.5 Conclusions 90

3.3.6 Reference 91

Chapter 4 Smart Particles ……. 93

4.1 Synthesis of Thermo-responsive Water-Soluble Poly(*N*-isopropylacrylamide) Colloids …… 94

4.1.1 Introduction ……...……. 95

4.1.2 Experimental Work ……. 96

4.1.2.1 Procedure …….. 96

4.1.2.2 Measurements ……... 97

4.1.3 Results and Discussions...…… 99

4.1.3.1 Effects of Monomer Concentration in Emulsifier-free Emulsion Polymerisation (EFEP) (Set A) ……..……. 99

4.1.3.2 Effects of SDS Concentration in Emulsion Polymerisation (Set F) ……. 106

4.1.3.3 Effects of Monomer Concentration in Emulsion Polymerisation in the Presence of Low SDS Concentration (Set B) ……..……. 109

4.1.3.4 Effects of TEMED Concentration in Emulsion Polymerisation (Set D) ….. 111

4.1.4 Conclusions .……...……...……. 118

4.1.5 Reference ……...……. 119

4.2 A Novel Method for Synthesis of Fast Dissolving PolyNIPAM Colloids via Semicontinuous Process …….……. 121

4.2.1 Introduction …….…….……..…. 122

4.2.2 Experimental Work ……..……..……. 123

4.2.2.1 Procedure ……...……...……. 123

4.2.2.2 Measurements ……..……. 123

4.2.3 Results and Discussions ..……...……. 124

4.2.4 Conclusions...……...……...……. 130

4.2.5 Reference ……...……. 131

4.3 A Novel Method for Preparation of Thermosensitive Nanocapsules via Semicontinuous Approaches ……...……. 133

4.3.1 Introduction …….…….……..……. 134

4.3.2 Experimental Work ……. 135

4.3.2.1 Procedure ……..……...……..…. 135

4.3.2.2 Characterizations ……..……. 135

4.3.3 Results and Discussions …….……. 136

4.3.3.1 Preparation of Core-Shell Nanoparticles ……..……. 136

4.3.3.2 Fabrication of Hollow Particles ……...……. 137

4.3.4 Conclusion ……...……...……. 143

4.3.5 Reference ……...…….. 144

Chapter 5 Composite Particles ……... 146

5.1 Synthesis and Characterisation of Polymer/SiO_2 Core-Shell Nanocomposite Particles by Semicontinuous Polymerisation ……...…… 147

5.1.1 Introduction ……...…….. 148

5.1.2 Experimental Work ……..……... 149

5.1.2.1 Procedure ……...……... 149

5.1.2.2 Measurements ……...…… 149

5.1.3 Results and Discussions ……..... 151

5.1.3.1 Colloidal Stability of Silica Latex …… 151

5.1.3.2 Rate of Reaction, Particle Morphology, Size, and Size Distributions ……. 153

5.1.3.2.1 Synthesis of PMMA/SiO_2 hybrid nanoparticles ……..... 153

5.1.3.2.2 Synthesis of PVA/SiO_2 hybrid nanoparticles ……. 159

5.1.3.3 Effect of pH ……...……... 165

5.1.3.4 Semibatchwise addition of silica nanoparticles …… 167

5.1.3.5 Glass transition temperature ……. 171

5.1.3.6 Mechanism of formation of hybrid core-shell particles ……... 173

5.1.4 Conclusions ……..……... 176

5.1.5 Reference ……...…….……. 177

5.2 Synthesis and Characterisation of Thermal-Sensitive SiO_2/polymer Nanocomposite Particles via Semicontinuous Polymerisation ……..…… 179

5.2.1 Introduction ……..……... 180

5.2.2 Experimental Work ……. 180

5.2.3 Crosslinker-free polyNIPAM/SiO_2 hybrid Particles …… 181

5.2.3.1 Primary Experiments ……...……. 181

5.2.3.2 Thermal behaviour ……..……. 187

5.2.3.3 Adsorption test ……...…….. 189

5.2.3.4 Morphology of composite particles ……..……. 191

5.2.4 PolyNIPAM/SiO_2 hybrid microgels ……..……..…. 191

5.2.4.1 Synthesis of hybrid microgels ……...……... 191

5.2.4.2 Morphology of hybrid microgels ……..…... 193

5.2.5 Conclusions ……..……..…….. 196

5.2.6 Reference ……...…….. 197

Chapter 6 Conclusions and Recommendations for Future Work ……. 198

6.1 The present Study ……..……. 198

6.2 Main Findings ……..……... 199

6.2.1 Microemulsion Polymerisation of Styrene ……..…... 199

6.2.2 Smart Particles ……...…….. 200

6.2.3 Polymer-Silica Hybrid Particles ……...……... 202

6.3 Recommendations for Future Work ……..…. 204

Appendixes ……..…… 205

Publications ……..……... 233

Acknowledgments

Completing a PhD is truly a marathon event, and I would not have been able to complete this journey without the aid and support of countless people over the past five years. It is a pleasure to convey my gratitude to them all in my humble acknowledgement.

In the first place I would like to express my most grateful thanks to my first supervisor Dr Shahriar Sajjadi for his supervision, advice and guidance from the very early stage of this research as well as giving me extraordinary experiences throughout the work, which enable me to develop an understanding of the subject. I also appreciate his patience, encouragement and assistance in writing reports, which make it possible for me to finish this thesis.

I am also grateful to my second supervisor, Dr Stavroula Balabani for her constructive advice and help.

I would like to thank all my colleagues in the ECLAT, who have encouraged and supported me. I am especially grateful to Mr Julian Greenberg for his high efficiency and enthusiastic support. He supported me with arranging almost everything for the experimental works.

I have the deepest thanks to my family for their unconditional love and support that made me what I am and what I have achieved today.

Last but not least, a special thank to my wife, Yan Qian, for her selfless support and thoughtful kindness.

Nomenclature

Symbol	Description	Unit
C_f	Conversion factor from z-average mean size to volume average mean size	-
D_n	Number-average particle diameter	nm
D_v	Volume-average particle diameter	nm
D_z	Z-average particle diameter	nm
k_d	Decomposition rate constant for initiator	s^{-1}
k_p	The propagation rate constant for monomer	$l \cdot mol^{-1}s^{-1}$
k_{tr}	The rate constant for chain transfer reaction	$l \cdot mol^{-1}s^{-1}$
m_p	Mass of polymer	g
M_{mon}	Molecular weight of monomer	$g \cdot mol^{-1}$
[M·]	The radical concentration within the particle	$mol \cdot l^{-1}$
$[M]_p$	Monomer concentration in the polymer phase	$mol \cdot l^{-1}$
$[M]_w$	Monomer concentration in the water phase	$mol \cdot l^{-1}$
$\bar{M}_n$	Number-average molecular weight of polymer	Da
$\bar{M}_w$	Weight-average molecular weight of polymer	Da
$\bar{n}_c$	The average number of chains in each particle	-
N_A	Avogadro's constant	-
N_p	Number of particles	$1 \cdot l_{aq}^{-1}$
R_a	Rate of monomer addition	$mol \cdot l_{aq}^{-1} \cdot min^{-1}$
R_I	Rate of radical generation in water phase	$mol \cdot l_{aq}^{-1} \cdot min^{-1}$
R_p	Rate of polymerisation	$mol \cdot l_{aq}^{-1} \cdot min^{-1}$
[S]	The concentration of emulsifier per unit volume of water	$g \cdot l_{aq}^{-1}$
S_c	The equilibrium surfactant concentration in the water phase	$g \cdot l_{aq}^{-1}$
S_d	Amount of adsorbed surfactant at the interface	$g \cdot l_{aq}^{-1}$
S_t	Total amount of surfactant in the system	$g \cdot l_{aq}^{-1}$
$\bar{X}_n$	The number-average degree of polymerisation of a single polymer chain	-
α_s	The adsorption area occupied by a molecule of emulsifier on the surface on polymer particles	nm^2
ρ_m	Density of monomer	$g \cdot ml^{-1}$
ρ_p	Density of polymer	$g \cdot ml^{-1}$
ρ_s	Density of silica	$g \cdot ml^{-1}$
θ	Surface coverage ratio of particles by surfactant	-

List of Figures

Figure 1.1. Schematic representation of both micellar nucleation and homogeneous nucleation models …….. 5

Figure 1.2. Schematic presentation of typical rate of polymerisation as a function of monomer conversion. Three distinct intervals of the polymerisation process are also shown [10] ……. 7

Figure 2.1. Schematic of experimental rig ……....…… 33

Figure 2.2. A typical PSD obtained from TEM or SEM …..…….…….…….…….. 36

Figure 3.1.1. Conversion of styrene versus time for different t_{add} at [*S*]: (a) 5 $g \cdot l_{aq}^{-1}$; (b) 10 $g \cdot l_{aq}^{-1}$; (c) 15 $g \cdot l_{aq}^{-1}$; and (d) 20 $g \cdot l_{aq}^{-1}$. The closed and open symbols represent x_o and x_i, respectively. The small inset in Figure a shows the magnified conversion-time for the early 10 min…….….. 45

Figure 3.1.2. R_a versus R_p for different [*S*] during nucleation stage…….. 46

Figure 3.1.3. Time evolution of number of particles for different [*S*] at t_{add} of (a) 1h; (b) 2h; (c) 4h; and (d) 6h……. 47

Figure 3.1.4. Variations in nucleation periods in terms of t_{add} for different [*S*]: (a) 5 $g \cdot l_{aq}^{-1}$; (b) 10 $g \cdot l_{aq}^{-1}$; (c) 15 $g \cdot l_{aq}^{-1}$; and (d) 20 $g \cdot l_{aq}^{-1}$; The crystal and square symbol represent data from N_p and θ, respectively…… 48

Figure 3.1.5. Variation in D_v versus relative nucleation time with different [*S*] at t_{add} of (a)1h; (b)2h; (c)4h; and (d)6h;……...… 49

Figure 3.1.6. Variations in the size of particles at the end of nucleation versus (a) R_a and (b) [*S*], for different [*S*] and t_{add}, respectively…… 50

Figure 3.1.7. Number of particles at the end of nucleation versus (a) R_a and (b) [*S*], for different [*S*] and t_{add}, respectively……..…… 50

Figure 3.1.8. TEM images of the latexes 1 h into addition for t_{add} = 2h for different [*S*] of (a) 10 $g \cdot l_{aq}^{-1}$ and (b) 20 $g \cdot l_{aq}^{-1}$…….…… 51

Figure 3.1.9. PSD at the end of nucleation obtained by TEM for (a) semicontinuous process at different t_{add} and batch process with 10 $g \cdot l_{aq}^{-1}$ [*S*]; (b) semicontinuous process with different [*S*] at t_{add} = 2h…… 52

Figure 3.1.10. Evolution of PSD during nucleation obtained by TEM at different t_{add}: (a)2h; and (b)6h; [S]=10 $g \cdot l_{aq}^{-1}$……. 53

Figure 3.1.11. Variations in weight-average molecular weight of the polymer produced at the end of the nucleation stage versus relative nucleation time with different processes. (a) Conventional batch, (b) t_{add} = 2h and (c) t_{add} = 6h semicontinuous process. [*S*]:10$g \cdot l_{aq}^{-1}$, [M]: 75.75 $g \cdot l_{aq}^{-1}$. ……..…… 54

Figure 3.1.12. Average number of chains per particle during nucleation period for the batch and semicontinuous processes (same conditions as mentioned in Figure 3.1.11)…… 55

Figure 3.2.1. (a) Conversions of polymerisation, (b) size of particles and (c) number of particles versus reaction time at different T (t_{add}= 4h; [*S*]= 10 $g \cdot l_{aq}^{-1}$)……... 63

Figure 3.2.2. (a) Initiator concentration decay and (b) the rate of radical formation as a function of time for the polymerisation of styrene at different temperatures (ºC) using 4 mM KPS as initiator……. 64

Figure 3.2.3. Final size and number of particles produced with different temperatures. ([*S*]=20 g·l_{aq}^{-1}. t_{add} = 4h). ……..… 65

Figure 3.2.4. (a) Conversions of polymerisation, (b) size of particles and (c) number of particles versus reaction time at different T([*S*]= 20 g·l_{aq}^{-1}, t_{add}=2h)…… 66

Figure 3.2.5. Final size and number of particles produced with different temperatures. ([*S*]=20g·l_{aq}^{-1}. t_{add} = 2h). …… 67

Figure 3.2.6. (a) Conversions of polymerisation, (b) size of particles and (c) number of particles versus reaction time for different [*S*] (t_{add} = 4h, T: 70ºC)……...…… 68

Figure 3.2.7. Final Size and number of particles produced with different [*S*]. t_{add} = 4h…… 70

Figure 3.2.8. (a) Conversions of polymerisation, (b) size of particles and (c) number of particles versus relative addition time at different feed rate. [*S*]: 20 g·l_{aq}^{-1}. T: 70ºC…….… 71

Figure 3.2.9. Final size and number of particles produced with different t_{add}. [*S*]: 20 g·l_{aq}^{-1} 72

Figure 3.2.10. (a) Size of particles and (b) number of particles versus addition time at different R_a. [*S*]: 5 g·l_{aq}^{-1}. T: 70ºC. …… 73

Figure 3.3.1. Conversion versus time for polymerisations with various CTA concentrations for different processes (a) Batch and (b) Semicontinuous…… 81

Figure 3.3.2. D_v versus time for polymerisations with various CTA concentrations for different processes: (a) Batch and (b) Semicontinuous…… 81

Figure 3.3.3. Conversion evolution of weight-average molecular weight ($\bar{M}_w$) of produced polymer versus conversion in the course of batch and semicontinuous microemulsion polymerisation. CTA: 0.25wt%.…….…… 82

Figure 3.3.4. Weight average molecular weight ($\bar{M}_w$) versus CTA concentration for different processes. The dotted line represents model predictions for the semicontinuous process…… 82

Figure 3.3.5. N_p versus time for various CTA concentrations for different processes (a) batch and (b) semicontinuous. Arrows show end of nucleation…… 84

Figure 3.3.6. Particle surface coverage ratio in the course of polymerisation for various CTA concentrations via (a) batch process, (b) semicontinuous process…… 85

Figure 3.3.7. (a) Conversions, (b) volume-average size of particles, and (c) number of particles produced in the course of semicontinuous microemulsion polymerisation for runs with 4wt% CTA and different SDS addition policy. The arrows indicate the period of addition of SDS……..… 86

Figure 3.3.8. Particle surface coverage ratio in the course of repeated semicontinuous emulsion polymerisation with 4wt% CTA…… 86

Figure 3.3.9. (a) Final N_p and (b) final size of particle versus CTA concentration for different processes. Dashed lines indicate the final size of particles as well as the number of particles produced by semicontinuous process with excess addition of SDS during particle growth stage….……. 87

Figure 3.3.10. (a) Conversions, (b) size of particles and (c) number of particles versus reaction time. CTA: 4wt% of 1-C10. …… 88

Figure 3.3.11. Average number of chains per particle versus CTA concentration for batch and semicontinuous processes. …… 89

Figure 4.1.1. The time evolution of (a) polymer produced, (b) volume-average diameter of particles and (c) the number of particles for different NIPAM concentrations via surfactant-free emulsion polymerisation ([KPS] = 4 mmol·l_{aq}^{-1}, T = 60ºC)……..… 100

Figure 4.1.2. Weigh-average molecular weight of the sol for different monomer concentrations (Set A). …… 101

Figure 4.1.3. The evolution of transmittance and z-average size of particles with temperature for (a) 0.25wt%, (b) 1.0wt% and (c) 2.0wt% NIPAM monomer concentration (Set A). Inset: The variation of the logarithm of the transmittance of latex with temperature…….. 103

Figure 4.1.4. The intensity size distribution of final particles for (a) 0.25wt%, (b) 1.0wt% and (c) 2.0wt% NIPAM monomer at different temperatures obtained by DLS…… 104

Figure 4.1.5. The turbidimetric measurements of the final latex produced with 1.0wt% NIPAM monomer (set A). Inset: The variation of the logarithm of the transmittance of latex with temperature. …….. 105

Figure 4.1.6. The variations in transmittance with temperature of the final latex produced with 2.0wt% NIPAM monomer (set A) for 0h and 27h incubation periods. …… 106

Figure 4.1.7. The time evolution of (a) polymer produced, (b) volume-average size of particles and (c) the number of particles for different SDS concentrations, ([KPS] = 4 mmol·l_{aq}^{-1}, [NIPAM] = 8.0wt%, T = 60ºC) …… 107

Figure 4.1.8. Variation of (a) z-average diameter and (b) number of particles of the final latexes produced with different SDS concentrations (8.0wt% NIPAM, 4 mmol·l_{aq}^{-1} KPS). 109

Figure 4.1.9. The time evolution of (a) polymer produced, (b) volume-average size of particles and (c) the number of particles for different monomer concentrations ([KPS] = 4 mmol·l_{aq}^{-1}, [SDS] = 0.5 g·l_{aq}^{-1}, T = 60ºC). …… 110

Figure 4.1.10. Comparison of (a) initial rate of polymerisation and (b) initial (empty symbol) and final (filled symbol) numbers of particles versus monomer concentration for set A (emulsifier-free emulsion polymerisation) and set B (emulsion polymerisation in the presence of SDS). ……..…… 111

Figure 4.1.11. The time evolution of (a) polymer produced, (b) volume-average size of particles and (c) the number of particles for different TEMED concentrations. ([KPS] = 4 mmol·l_{aq}^{-1}, [NIPAM] = 1.0wt%, T = 60°C). ……..…… 113

Figure 4.1.12. The initial and final number of particles for different concentrations of TEMED (set D). …… 113

Figure 4.1.13. The time evolution of (a) polymer produced, (b) volume-average size of particles and (c) the number of particles for different monomer concentrations. ([TEMED] = 10 mmol·l_{aq}^{-1}, [SDS] = 0.5 g·l_{aq}^{-1}, [KPS] = 4 mmol·l_{aq}^{-1}, T = 60ºC)……..... 114

Figure 4.1.14. Weigh-average molecular weight of the final products versus monomer concentration for set E ([TEMED] = 10 mmol·l_{aq}^{-1}, [SDS] = 0.5 g·l_{aq}^{-1}) and set A (EFEP). [KPS] = 4 mmol·l_{aq}^{-1}, T = 60ºC. …… 115

Figure 4.1.15. The evolution of (a) z-average hydrodynamic size and transmittance and (b) intensity size distribution with temperature of the final latex produced using 1.0wt% NIPAM monomer, 10 mmol·l_{aq}^{-1} TEMED and 0.5 g·l_{aq}^{-1} SDS……. 115

Figure 4.1.16. Final N_p versus monomer concentration for Set A (EFEP), B ([SDS] = 0.5 g·l_{aq}^{-1}) and E ([TEMED] = 10 mmol·l_{aq}^{-1}, [SDS] = 0.5 g·l_{aq}^{-1})……..… 116

Figure 4.1.17. Variations in initial rate of polymerisation versus monomer concentration of Set A(EFEP), B([SDS]=0.5 g·l_{aq}^{-1}) and E([TEMED]=10 mmol·l_{aq}^{-1}, [SDS]=0.5 g·l_{aq}^{-1}).. 117

Figure 4.2.1. The reaction time evolution of (a) polymer produced, (b) volume-average size of particles and (c) the number of particles for different rates of monomer addition via semicontinuous process. [NIPAM] = 3.0wt%, T = 60ºC. Batch processes with 0.25wt% and 3.0wt% NIPAM were shown for comparison. …… 124

Figure 4.2.2. Z-average hydrodynamic size and transmittance versus temperature for the final samples obtained via semicontinuous process with 3.0wt% NIPAM monomer, feeding rate: (b) 0.27 g·min^{-1}·l_{aq}^{-1}; (c) 0.15 g·min^{-1}·l_{aq}^{-1}. The sample produced with 2.0wt% NIPAM monomer was studied for the sake of comparison. …… 125

Figure 4.2.3. The reaction time evolution of (a) polymer produced, (b) volume-average size of particles and (c) the number of particles for different rates of monomer addition via semicontinuous process. [NIPAM] = 1.0wt%, T = 60ºC. Batch processes with 0.25wt% and 1.0wt% NIPAM monomer concentrations were shown for comparison. ..… 126

Figure 4.2.4. Temperature evolution of z-average hydrodynamic size and transmittance of the final samples obtained via batch and semicontinuous process with 1.0wt% NIPAM monomer. Feeding rate for the semicontinuous process: (b) 0.38 g·min^{-1}·l_{aq}^{-1}; (c) 0.15 g·min^{-1}·l_{aq}^{-1}……. 127

Figure 4.2.5. Comparison of $\bar{M}_w$ of samples produced with different monomer concentration via batch and semicontinuous process.T=60ºC,feeding rate:0.15g·l_{aq}^{-1}·min^{-1} 128

Figure 4.2.6. Scheme of behaviour of polymer nanoparticles produced via (a) batch process; (b) semicontinuous process below LCST. The red dot represents the free radical. The blue colour represents NIPAM monomer. …… 129

Figure 4.3.1. Time evolution of (a) conversion, (b) particle size, (c) number of particles for different processes. The dashed lines indicate the starting point of the stage 2. Samples: HBS1 and HSS1 (1.0wt% NIPAM core and 1.0wt% NIPAM shell)…… 137

Figure 4.3.2. SEM images of (a) batch-semi and (b)semi-semi samples after three weeks storage at 25°C. Bar size: 500 nm……..…… 138

Figure 4.3.3. SEM images of washed particles produced via (a) batch-semi and (b) semi-semi routes. Bar size: 500 nm…….. 139

Figure 4.3.4. TEM images of washed particles produced via (a) batch-semi and (b) semi-semi routes. Bar size: 500 nm…… 139

Figure 4.3.5. Time evolution of (a) conversion, (b) particle size, (c) number of particles for different processes. The dashed lines indicate the starting point of the stage 2. Samples: HBS2 and HSS2 (1.0wt% NIPAM core and 2.0wt% NIPAM shell)…… 140

Figure 4.3.6. Percentage release as a function of release period for batch-semi and semi-semi routes. Samples: HBS2 and HSS2 (1.0wt% NIPAM core and 2.0wt% NIPAM shell) 141

Figure 4.3.7. TEM images of particles produced via (a) batch-semi and (b) semi-semi routes after 7 day release. Bar size: 500 nm. …… 141

Figure 4.3.8. Z-average particle size evolution with temperature for both core-shell particles and hollow particles produced via (a) batch-semi and (b) semi-semi routes…….. 142

Figure 4.3.9. Scheme of core removing process of core-shell particles produced via (a) batch-semi and (b) semi-semi routes. ……..……. 143

Figure 5.1.1. (a) The zeta potential, z-average size of particles and conductivity evolution of pH of the silica latex; (b) The intensity PSDs of silica nanoparticles for different pH of the dispersion. ……... 152

Figure 5.1.2. (a) Conversions, (b) volume-average diameter of particles, and (c) number of particles produced versus reaction time for batch process. [KPS] = 2 mmol·l_{aq}^{-1}; water: 450 ml; MMA: 50 ml; SiO2/MMA (g/g): 1:1. pH = 5.2±0.2…… 153

Fgure 5.1.3. Conversion evolution of PSD during batch polymerisation of MMA in the presence of silica nanoparticles, the same reaction as shown in Figure 5.1.2……..… 154

Figure 5.1.4. (a) Conversions, (b) volume average size of particles and (c) number of particles produced versus reaction time for semicontinuous process, [KPS] = 2 mmol·l_{aq}^{-1}; water: 450 ml; MMA: 50 ml; SiO2/MMA(g/g): 1:1, 2h feeding. pH = 5.2±0.2……..… 155

Figure 5.1.5. Overall conversion evolution of PSD during semicontinuous polymerisation of MMA in the presence of silica nanoparticles, the same reaction as shown in Figure 5.1.4…….. 156

Figure 5.1.6. SEM images of nanocomposite particles produced via (a-d) batch process, bar: (a, and b) 375 nm; (c, and d) 1000 nm and (e-f) semicontinuous process, bar: (e) 1000 nm; (f) 800 nm. Recipes can be found from Figure 5.1.2 and 5.1.4…… 157

Figure 5.1.7. TEM images of nanocomposite particles produced via (a-b) batch process, (c-d) semicontinuous process (100 min reaction), bar: 100 nm. Samples are stained with a negative stain agent, 1wt% phosphotungstic acid solution. Recipes can be found from Figures 5.1.2 and 5.1.4. …… 157

Figure 5.1.8. (a) Cross-section of particles at different positions inside the film. (b) The normal view of the particles morphologies under TEM…… 158

Figure 5.1.9. TEM images of the cross-section of final hybrid samples obtained from (a) batch process (c) semicontinuous process (at reaction time of 100 min). bar: 100nm. Samples are unstained. Recipes can be found from Figure 5.1.2 and 5.1.4…….…… 159

Figure 5.1.10. (a) Conversion, (b) volume average size of particles and (c) number of particles produced versus reaction time for batch reactions. [KPS] = 2 mmol·l_{aq}^{-1}; water: 450 ml; VA: 50 ml; SiO2/VA(g/g): 1:1. pH = 5.0±0.5……..…… 160

Figure 5.1.11. Conversion evolution of PSD during batch polymerisation of VA in the presence of silica nanoparticles, the same reaction as shown in Figure 5.1.10…… 161

Figure 5.1.12. (a) Conversions, (b) volume average size of particles, and (c) number of particles produced versus reaction time for semicontinuous reactions, same recipe as batch process, 2h feeding time. pH = 5.0±0.5. …… 161

Figure 5.1.13. Overall conversion evolution of PSD during semicontinuous polymerisation of VA in the presence of silica nanoparticles, the same reaction as shown in Figure 5.1.12…….. 162

Figure 5.1.14. SEM images of PVA/SiO_2 nanocomposite particles produced via (a) batch process and (b) semicontinuous process in the presence of silica nanoparticles, bar: 500 nm; pH = 5.0±0.5. ……. 162

Figure 5.1.15. TEM images of PVA/SiO_2 nanocomposite particles produced via (a-b) batch process, bar: 20 nm; Samples are stained with a negative stain agent, 1wt% phosphotungstic acid solution; (c-d) semicontinuous process. Bar: 100 nm. pH = 5.0±0.5.. 164

Figure 5.1.16. TEM images of the cross-section of nanocomposite particles obtained via semicontinuous process. (a) unstained; (b) stained by negative stain agent, 1wt% phosphotungstic acid solution. Bar: 100nm. Recipes can be found from Figure 5.1.12….. 164

Figure 5.1.17. Conversions versus reaction time for semicontinuous process. [KPS] = 2 mmol·l_{aq}^{-1}; water: 450 ml; MMA: 50 ml; SiO2/MMA(g/g): 1:1. pH = 9.8±0.2…… 165

Figure 5.1.18. SEM images of particles produced via semicontinuous polymerisation of MMA in the presence of basic silica particles. Bar: 600 nm. pH = 9.8±0.2…….. 165

Figure 5.1.19. (a) Conversions, (b) volume-average diameter of particles and (c) number of particles produced versus reaction time for batch process under basic conditions. pH = 9.8±0.2. [KPS] = 2 mmol·l_{aq}^{-1}; water: 450 ml; VA: 50 ml; SiO2/VA(g/g): 1:1. Batch polymerisation of VA/SiO_2 under acidic conditions is shown for comparison…….…… 166

Figure 5.1.20. Evolution of PSD during batch polymerisation of VA in the presence of silica nanoparticles under basic conditions. …….. 167

Figure 5.1.21. SEM images of PVA/SiO_2 nanocomposite particles produced batchwise in the presence of original silica nanoparticles. pH = 9.8±0.2, bar: 500nm…….. 167

Figure 5.1.22. (a) Conversions, (b) volume average size of particles and (c) number of particles produced versus reaction time for semicontinuous polymerisation of MMA in the presence of silica with different feeds. pH = 5.0±1.0…….. 168

Figure 5.1.23. SEM images of PMMA/SiO2 nanocomposite particles produced via semicontinuous process with silica dispersion feed. Bar: (a) 500nm; (b) 900nm; (c) 1000nm. pH = 5.0±1.0. ……. 169

Figure 5.1.24. (a) Conversions, (b) volume average size of particles and (c) number of particles produced versus reaction time for semicontinuous process. [KPS] = 2 mmol·l_{aq}^{-1}; water: 450 ml; VA: 50 ml; SiO2/VA(g/g): 1:1. pH = 5.25±0.75……... 170

Figure 5.1.25. SEM image of the PVA/SiO_2 nanocomposite particles produced via semicontinuous process with addition of silica nanoparticle, bar: 200nm. pH = 5.25±0.75 170

Figure 5.1.26. Morphology of polymer/silica nanocomposite particles produced via (a) batch and (b) semicontinuous process. …….. 174

Figure 5.1.27. Scheme of particle formation of nanocomposite particles under different pH……... 174

Figure 5.1.28. TEM images of stained samples from the early stage (x ≈ 30%) of batch polymerisation of VA in the presence of silica nanparticles under acidic conditions. Black layers represent stained polymer and spheres are silica nanparticles. Bar: 20 nm. pH = 5.0±0.5……..... 175

Figure 5.2.1. (a) Conversions, (b) volume average diameter of particles and (c) number of particles produced versus reaction time for semicontinuous process. Water: 450 ml; [NIPAM] = 0.5wt%; T = 60°C, [KPS] =2 mmol·l_{aq}^{-1}. pH = 5.0±0.5; R_a = 0.06 g·min^{-1}·l_{aq}^{-1} 182

Figure 5.2.2. (a) Conversions, (b) volume-average size of particles and (c) number of particles produced versus reaction time for batch reactions with different concentrations of silica latex. Water: 450 ml; [NIPAM] = 3wt%; T = 60°C, [KPS] = 4 mmol·l_{aq}^{-1}……. 183

Figure 5.2.3. (a) Conversions, (b) volume-average size of particles and (c) number of particles produced versus reaction time for batch process with different NIPAM/SiO_2 ratios. [KPS] = 4 mmol·l_{aq}^{-1}; water: 450 ml; [NIPAM] = 2wt%; T = 60°C…….. 184

Figure 5.2.4. Evolution of PSD during batch polymerisations with different concentration of NIPAM monomer and silica nanoparticles (a) 3wt% NIPAM, NIPAM/SiO_2 = 1:1; (b) 3wt% NIPAM, NIPAM/SiO_2 = 1:3; (c) 2wt% NIPAM, NIPAM/SiO_2 = 1:1; (d) 2wt% NIPAM, NIPAM/SiO_2 = 1:3. …… 185

Figure 5.2.5. (a) Conversions, (b) volume-average size of particles, and (c) number of particles produced versus reaction time for semicontinuous reactions in the presence of different concentrations of silica nanoparticles. [KPS] = 4 mmol·l_{aq}^{-1}; water: 450 ml; NIPAM: 3wt%; T = 60°C. R_a = 0.18±0.03 g·min^{-1}·l_{aq}^{-1}. ……... 186

Figure 5.2.6. Evolution of PSD with overall conversion during semicontinuous polymerisation of 3wt% NIPAM in the presence of different concentrations of silica nanoparticles (a) NIPAM/SiO_2 = 1:1; (b) NIPAM/SiO_2 = 1:3, the same reaction as shown in Figure 5.2.5…… 187

Figure 5.2.7. The evolution of (a) transmittance and (b) z-average size of particles with temperature of final products from batch process using 2wt% NIPAM with different concentration of silica latex. ……. 188

Figure 5.2.8. Particle size and transmittance versus temperature for final products via semicontinuous process with 3wt% NIPAM. [KPS] = 4 mmol·l_{aq}^{-1}; water: 450 ml; NIPAM/SiO2 = 1:1; T = 60°C. ……. 189

Figure 5.2.9. Incubation time evolution of PSD of 1wt% polyNIPAM particles in the presence of 1wt% silica nanoparticles under (a) basic conditions, pH = 9.8; (b) acidic conditions, pH = 5.0. ……. 190

Figure 5.2.10. SEM images of samples obtained after 30min of stirring under (a-b) basic conditions, pH = 9.8; and (c-d) acidic conditions, pH = 5.0. Bar: 1000nm……... 191

Figure 5.2.11. SEM images of samples produced with (a) 2wt% NIPAM via batch process and (b) 3wt% NIPAM via semicontinuous process. [KPS] = 4 mmol·l_{aq}^{-1}; water: 450 ml; T = 60°C…… 191

Figure 5.2.12. SEM images of samples produced with (a) 2wt% NIPAM via batch process, bar: 1000 nm and (b) 3wt% NIPAM via semicontinuous process, bar: 900 nm. [KPS] = 4 mmol·l_{aq}^{-1}; water: 450 ml; T = 60°C, NIPAM/silica(g/g) = 1:1; MBA/NIPAM(g/g) = 1:50; pH = 9.8±0.2…….. 192

Figure 5.2.13. (a) Conversion, (b) volume average size of particles and (c) number of particles produced versus reaction time for batch reactions with different concentrations of NIPAM monomer. [KPS] = 4 mmol·l_{aq}^{-1}; water: 450 ml; NIPAM/silica(g/g) = 1:1; MBA/NIPAM(g/g) = 1:10; T = 60°C. pH = 9.8±0.2. ……... 192

Figure 5.2.14. (a) Conversions, (b) volume-average size of particles and (c) number of particles produced versus reaction time for semicontinuous reactions with different concentrations of NIPAM monomer. [KPS] = 4 mmol·l_{aq}^{-1}; water: 450 ml; NIPAM/silica(g/g) = 1:1; MBA/NIPAM(g/g) = 1:10; T = 60°C; pH = 9.8±0.2; R_a=0.18±0.03 g·min^{-1}·l_{aq}^{-1}…….. 193

Figure 5.2.15. SEM images of microgels produced with (a) 1wt% NIPAM via batch process, bar: 250 nm; (b) 1wt% NIPAM semicontinuous process, bar: 250 nm; and (c) 3wt% NIPAM semicontinuous process, bar: 250 nm. [KPS] = 4 mmol·l_{aq}^{-1}; water: 450 ml; T = 60°C, NIPAM/silica(g/g) = 1:1; MBA/NIPAM(g/g) = 1:10; pH = 9.8±0.2……. 194

Figure 5.2.16. TEM images of polyNIPAM/SiO_2 nanocomposite particles produced via (a) 1wt% batch process and (b) 1wt% semicontinuous process. (c) 3wt% semicontinuous process, Bar: 100 nm. [KPS] = 4 mmol·l_{aq}^{-1}; water: 450 ml; T = 60°C, NIPAM/silica(g/g) = 1:1; MBA/NIPAM(g/g) = 1:10. …… 195

List of Tables

Table 3.1.1. Recipe for the semicontinuous microemulsion polymerisation of styrene…… 44

Table 3.2.1. Recipe of the experiments…….. 62

Table 3.2.2. Surface coverage ratio at the end of polymerisations with various T. t_{add} = 2h, [*S*] = 20 $g \cdot l_{aq}^{-1}$ …… 67

Table 3.2.3. Surface coverage ratio at the end of polymerisations with various [*S*]. t_{add} =4h 69

Table 3.2.4. Surface coverage ratio at the end of polymerisations with various t_{add}…….. 72

Table 3.3.1. Recipe used for the study of polymerisations in the presence of CTA. T=70°C. ……. 79

Table 3.3.2. Physical properties of some mercaptans……. 80

Table 4.1.1. Recipes for synthesis of polyNIPAM nanoparticles. Reaction temperature: 60°C; $C_{KPS} = C_{buffer}$ = 4 $mmol \cdot l_{aq}^{-1}$; 200 ml water…… 98

Table 4.1.2. Zeta potential of particles produced with different amount of TEMED, 1.0wt% NIPAM, T = 60ºC……. 114

Table 4.2.1. Recipes for synthesis of polyNIPAM nanoparticles in water by semicontinuous process. Reaction temperature: 60°C. $C_{KPS} = C_{buffer}$ = 4 $mmol \cdot l_{aq}^{-1}$. 200 ml water……... 123

Table 4.3.1. Recipes for synthesis of polyNIPAM core-shell nanoparticles in water. Reaction temperature: 60°C, $C_{KPS} = C_{buffer}$ = 4 $mmol \cdot l_{aq}^{-1}$. [NIPAM]/[MBA](g/g)=10:1….. 135

Table 5.1.1. Typical recipes for the polymer latexes prepared by surfactant-free emulsion polymerisation in the presence of Ludox TM-50 silica nanoparticles. [KPS] = 2$mmol \cdot l_{aq}^{-1}$. Water: 450 ml……. 151

Table 5.1.2. Solids content (wt%) of the top layer of the samples in the centrifuged tube for different experiments…… 163

Table 5.1.3. Summary of T_g (°C) of nanocomposite particles…… 172

Table 5.2.1. Typical recipes for the polyNIPAM latexes prepared by surfactant-free emulsion polymerisation in the presence of Ludox TM-50 silica nanoparticles. [KPS]=4$mmol \cdot l_{aq}^{-1}$. Water: 450 ml……..... 180

Chapter 1 Literature Review

1.1 Introduction

Emulsion polymerisation has been a very important industrial method to produce polymeric latexes since 1920s. A wide range of specialty polymers can be synthesised via emulsion polymerisation for applications including adhesives, paints and coatings, paper making, synthetic rubber, impact modifiers for plastic matrices, diagnostic tests, sensor and drug delivery systems [1-7]. The first successful theory to explain the distinct features of emulsion polymerisation was developed by Smith and Ewart [8] in 1948 on the basis of the achievements made by Harkins and co-workers [9]. Later on, further developments were introduced as reviewed by Gilbert [10], Chern [11], and Nomura [12] et al. Comparing with conventional batch process, semicontinuous process, which has been studied since 1950s, offers flexibility and versatility for manufacturing colloids for a wide range of applications.

In this chapter, a brief introduction of conventional (micro)emulsion polymerisation has first been presented, followed by a review of semicontinuous (semibatch) approaches in the present literature. The control of the properties of resulting latex, such as average size and size distribution as well as number of particles, composition and morphology of particles, have been discussed. The main conclusions and the gaps from the literature study have been defined. Finally, the objectives of the present study have been outlined.

1.2 Free radical polymerisation

Emulsion polymerisation is a free radical polymerisation process which involves three kinetic steps in sequence: initiation, propagation and termination. Additionally, chain transfer may be involved [10]. Initiation can be considered as the beginning of the propagation. The free radicals can be generated from radical initiators thermally or by irradiation. A free radical can react with a molecule of monomer to yield a new species that is still a radical. This process can be inhibited by the oxygen and other impurities. This step can be represented as:

$$\mathrm{I-I} \xrightarrow{k_d} 2\dot{\mathrm{I}} \tag{1.1}$$

$$\dot{\mathrm{I}} + \mathrm{M} \xrightarrow{k_{p,i}} \mathrm{I\dot{M}} \tag{1.2}$$

where I-I, $\dot{\mathrm{I}}$, M and $\mathrm{I\dot{M}}$ represent the initiator, initiator radical, monomer molecule and free radical with one monomer molecule, respectively. The kinetic parameters k_d and $k_{p,i}$ are the decomposition rate constant for initiator and the initial rate constant for the primary radical, respectively.

Propagation is a rapid reaction, in which the free radical unit at the end of the growing polymer chain continuously reacts with monomer molecules to increase until further length.

$$\mathrm{I\dot{M}} + \mathrm{M} \xrightarrow{k_{p,1}} \mathrm{I\dot{M}_2} \tag{1.3}$$

$$\mathrm{I\dot{M}_n} + \mathrm{M} \xrightarrow{k_{p,n}} \mathrm{I\dot{M}_{n+1}} \tag{1.4}$$

where $\mathrm{I\dot{M}_n}$ (n = 1,2,3…) represents the free radical with n monomer units. The kinetic parameter $k_{p,n}$ is the propagation rate constant for the reaction between one free radical with n monomer units and one monomer molecule. The dependence of propagation rate constant on radical length is practically important [13].

Termination, either combination or disproportionation, occurs when a radical reacts in a way that stops the further chain propagation. The two radical species can react with each other and form terminated chains. Therefore, termination can suppress the rate of polymerisation by decreasing the concentration of the living radicals.

$$\mathrm{I\dot{M}_m} + \mathrm{I\dot{M}_n} \xrightarrow{k_{t,c}} \mathrm{IM_{m+n}I} \tag{1.5}$$

$$\mathrm{I\dot{M}_m} + \mathrm{I\dot{M}_n} \xrightarrow{k_{t,d}} \mathrm{IM_m} + \mathrm{IM_n} \tag{1.6}$$

where $\mathrm{IM_n}$ represents the dead polymer chains with n monomer units. $k_{t,c}$ and $k_{t,d}$ are the rate constants for combination and disproportionation termination between two free radicals, respectively, which are also chain length dependent [14].

A chain transfer reaction is also a side-reaction during the polymerisation and serves to reduce the average chain length. Chain transfer of a propagating radical to monomer or chain transfer agent (CTA) can be represented as follow:

$$I\dot{M}_m + M \xrightarrow{k_{tr,m}} IM_m + \dot{M} \quad (1.7)$$

$$I\dot{M}_m + T \xrightarrow{k_{tr,T}} IM_m + \dot{T} \quad (1.8)$$

where T indicates the CTA. $k_{tr,m}$ and $k_{tr,T}$ are rate constants for chain transfer reaction of a propagating radical with monomer and CTA, respectively. Both $\dot{M}$ and $\dot{T}$ can react with monomer molecule and continue propagating.

1.3 General features of emulsion polymerisation

A typical emulsion polymerisation system starts with water, monomer, surfactant and a water-soluble initiator. The monomer is present in large droplets and micelles. The polymerisation results in the formation of a particle phase, comprising monomer molecules and polymer chains, stabilized by surfactant. The main locus of polymerisation is in the particle phase. Typical monomers used in emulsion polymerisation include styrene (St), methyl methacrylate (MMA), butyl acrylate (BA), butyl methacrylate (BMA), methyl acrylate (MA), methacrylic acid (MAA) and vinyl acetate (VA), etc. Surfactant (e.g. sodium dodecyl sulfate (SDS)) and water-soluble initiator (e.g. potassium persulfate (KPS) and ammonium persulfate (APS)) are usually used for reaction.

Since the early work of Smith and Ewart, a great effort has been placed on investigation of the kinetic events of emulsion polymerisation. According to the micellar nucleation model, proposed by Harkins [9,15] and Smith and Ewart [8,16] and modified by Gardon [17], free radicals first polymerise with monomer dissolved in the aqueous phase resulting in the increased hydrophobicity and decreased solubility of oligomeric radicals. When a critical chain length is achieved, these oligomeric radicals reach the limitation of their solubility and undergo phase transition in the aqueous phase. They become so hydrophobic that they tend to be captured by monomer-swollen micelles with extremely large oil-water interfacial area and continue to propagate by reacting with the monomer inside. In general, monomer droplets do not have a strong position for competing with micelles in capturing free radicals generated in the aqueous phase due to their relatively small surface area. As a consequence, particle nuclei are formed in the micelles. These particles continue to grow by acquiring monomer from monomer droplets and monomer-swollen micelles. A considerably large oil-water interfacial area is generated as the particle nuclei form and grow in size with the process of the polymerisation. In order to maintain the adequate colloidal stability of the growing particle nuclei, micelles that have not taken part in the particle nucleation disband to supply the increasing demand for surfactant by

growing particles. In addition, the surfactant molecules adsorbed on monomer droplets may also desorb out of the droplets surface, diffuse across the continuous aqueous phase and then adsorb on the expanding particle surface.

The particle nucleation stage (Interval I) ends immediately when the micelles are used up. Based on the Smith-Ewart theory, the number of latex particles nucleated per unit volume of water (N_p) can be predicted as follows:

$$N_p = k(k_d[\mathrm{I}]/\mu)^{2/5}(\alpha_s[S])^{3/5} \tag{1.9}$$

Where k is a numerical constant, [I] is the initiator concentration and μ represents the rate of volume growth per particle for a particle containing one free radical. α_s is the surface area occupied by a single surfactant molecule and [S] is the surfactant concentration. However, the simple Smith-Ewart model cannot provide a complete picture of particle formation and suffers from major limitations [8]. One such limitation is that this model predicts that particle number should be zero for zero surfactant concentration, which contradicts with the experimental results.

The observation of particle formation with no surfactant present suggests that there is another mechanism of particle formation in the aqueous phase. Priest [18], Roe [19] and Fitch and Tsai [20] proposed the homogeneous nucleation for the formation of particle nuclei in the continuous aqueous phase in the absence or presence of a low amount of surfactant. The waterborne initiator radicals generated by the thermal decomposition of initiator grow in size via the propagation reaction with the monomer dissolved in the aqueous phase. The oligomeric radicals continue to grow until they reach a critical chain length at which they become surface active - *i.e.* a surfactant. At this critical size, they may have a number of fates. If they terminate in the aqueous phase, they will act as an ***in-situ*** surfactant. They may also enter either an existing polymer particle or may continue to propagate. After further propagation the polymer chain reaches another critical size, J_{crit}, at which becomes fully hydrophobic and the resulting hydrophobic radical coils up, by increased surface tension from the interface, to form a precursor particle in the aqueous phase. Precursor particles are only marginally stable since small particles have a large amount of free energy across their surface. Therefore, the formation of stable primary particles occurs with limited flocculation and adsorption of surfactant molecules on the particles surfaces. The surfactant molecules used for stabilizing the primary particles come from those terminated surface active oligomers in the water phase. The above ideas were incorporated into the following kinetic model developed by Fitch and Tsai [20]

$$dN_p/dt = R_i - R_c \tag{1.10}$$

where t is the reaction time, R_i is the effective rate of radical generation in the aqueous phase, R_c is the rate of capture of free radicals by the pre-existing particles. As N_p decreasing, the rate of radical capture (R_c) will approach to the effective rate of radical generation (R_i) until a steady

state is finally reached where N_p levels off. The schematic representation of the comparison between micelle nucleation and homogeneous nucleation models are shown in Figure 1.1.

The period of particle nucleation or interval I is relatively short, but it is the most important stage which controls the particle population and particle size distribution of latex products. Generally, nucleation is a complex process. It is not straightforward to determine which particle nucleation mechanism (micellar nucleation or homogeneous nucleation) predominates in a particular emulsion polymerisation system.

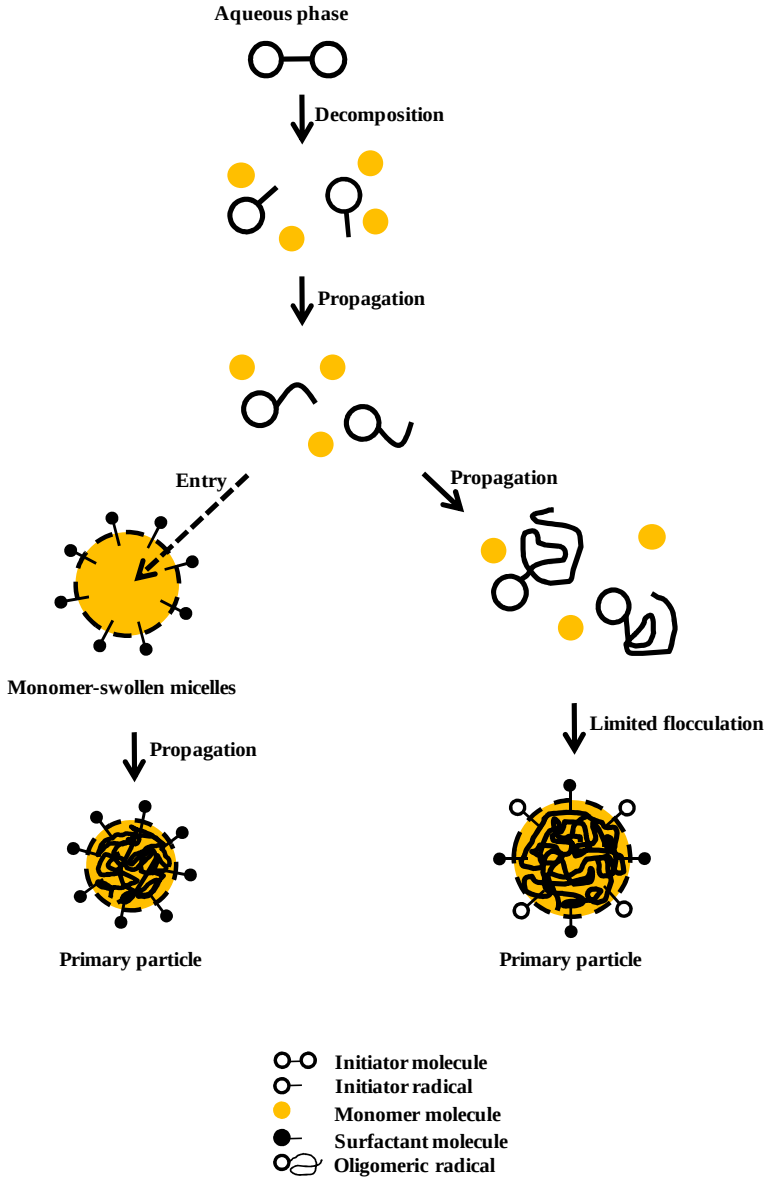

Figure 1.1. Schematic representation of both micellar nucleation and homogeneous nucleation models.

After the particle nucleation process is completed, the number of latex particles stays relatively constant towards the end of the reaction. The propagation reaction of free radicals with monomer takes place primarily in the monomer-swollen particles. Monomer droplets play a role

as a reservoir to supply the particles to grow by diffusing through the continuous aqueous phase. During particle growth stage (Interval Π), the monomer concentration in the particle does not change with the progress of polymerisation in the presence of monomer droplets.

Three limiting cases for interval Π were defined by Smith and Ewart:

Case 1: the radical desorption rate is much faster than the rate of radical entry and the average number of free radicals per particle is small; $\bar{n} \ll 0.5$.

Case 2: when the radical desorption rate is zero and instantaneous termination occurs when a radical enters a polymer particle already containing one radical; $\bar{n} = 0.5$.

Case 3: the rate of radical entry into particles is much higher than the rate of radical termination so that the concentration of radicals in the polymer particles approaches that of bulk polymerisation; $\bar{n} \gg 0.5$.

The rate of polymerisation (R_p) can be expressed by:

$$R_P = k_p[\mathrm{M}]_\mathrm{P}(\bar{n}N_p/N_A) \tag{1.11}$$

where k_p is the propagation rate constant, $[\mathrm{M}]_p$ is the concentration of monomer in the particles, $\bar{n}$ is the average number of free radicals per particle, and N_A is the Avogadro's number.

Equation 1.11 can adequately describe Case 2 kinetics that can usually be achieved when particles are sufficiently small. As a result, a constant polymerisation rate is attained. This model can successfully apply to emulsion polymerisation of relatively water-insoluble monomers such as St [21-22] and butadiene [23-24].

Interval Π ends when monomer droplets disappear in the polymerisation system. In Interval Ш, latex particles become monomer-starved and concentration of monomer in the reaction system continues to decrease until the end of the reaction [25]. Thus, the steady polymerisation rate observed in Interval Π cannot be maintained anymore and decreases during the Interval Ш. On the other hand, the rate may increase with increasing monomer conversion, due to the greatly reduced termination reaction between two polymeric radicals within the high viscous particle when the polymerisation is carried out at a temperature below the glass transition temperature of the monomer-starved polymer solution. This phenomenon is called ***the gel effect*** [26]. The schematic representation of rate of polymerisation as a function of monomer conversion is shown in Figure 1.2.

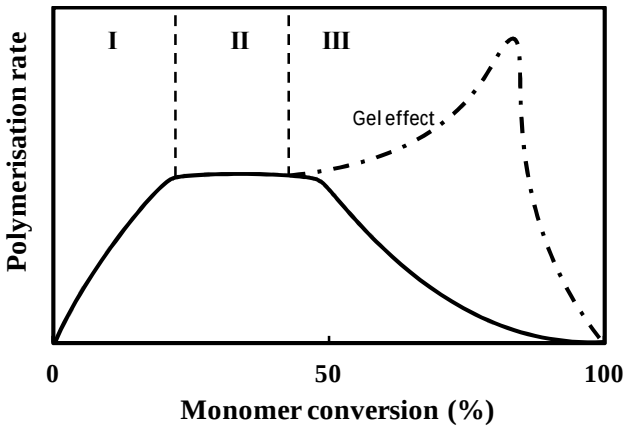

Figure 1.2. Schematic presentation of typical rate of polymerisation as a function of monomer conversion. Three distinct intervals of the polymerisation process are also shown in the figure [10].

1.4 General features of microemulsion polymerisation

Microemulsion polymerisation was first reported in the early 1980's [27-28]. This process can produce transparent or translucent polymer microlatexes with particle size of about 10 to 100 nm by using a surfactant and in some cases, a cosurfactant. Compared with emulsion polymerisation, a major difference comes from the amount of surfactant needed to stabilize the respective systems. Much more surfactant is needed for microemulsion polymerisations (≈10wt% of the total mass), due to necessity of stabilizing a large internal interfacial area. This is a drawback that can considerably limit the potential applications of microemulsion polymerisation [29]. Guo et al. [30-31], Morgan et al. [32] and Nomura and Suzuki [33] developed mechanistic models to predict the evolution of latex particles during St microemulsion polymerisation. Particle nuclei are found to be continuously generated throughout the polymerisation [34]. Kim and Napper [35] showed that micellar nucleation is dominant in polymerisation of St, whereas homogeneous nucleation plays an important role in polymerisation of MMA. Antonietti et al [36-37] and Wu [38] established a quantitative relation between particle size and the monomer to surfactant ratio for a range of compositions with ratios ranging from 1/3 to 3/1. It has been desired to obtain nanosized latexes containing higher polymer contents at lower surfactant concentrations. Two approaches to achieve this goal can be found in the literature. The first way is using more effective surfactant systems [39-43]. The second approach involves various semicontinuous microemulsion polymerisation techniques.

1.5 Semibatch approaches

1.5.1 Introduction

Semibatch or semicontinuous process is widely used in the chemical industry for the production of a wide variety of polymer latexes with special particle morphology and compositions, because of its several advantages over batch processes. In addition to its operational flexibility, the semibatch process can easily remove the enormous heat generated during the reaction. The most striking difference between the semibatch and conventional batch processes is that reaction ingredients such as monomer, surfactant, initiator or water can be added to the semibatch reaction system throughout the polymerisation, which makes the mechanisms and kinetics of the system more complicated in comparison with batch counterpart [11].

The research works on the kinetic features of semibatch emulsion polymerisation was pioneered by Naidus and Krackler [44-45], Gerrens [46] and Wesseling [47], who have compared conventional batch and semibatch with different types of feeding (neat monomer feed and monomer emulsion feed). Generally, semicontinuous emulsion polymerisation includes three stages: a batch period in which a small fraction of total monomer in the recipe is added and polymerised; an addition period in which the rest of monomer is fed into the reactor; a postaddition period to allow for polymerisation of residual monomer.

Two conditions of semibatch operations have been defined in the literature: monomer-flooded and monomer-starved [44-45,47]. Under monomer-flooded condition, the rate of monomer addition is higher than the polymerisation rate. The monomer accumulates in the reactor as droplets and the polymer particles are saturated with monomer, as interval II of a batch process. Under monomer-starved condition, the rate of monomer addition is lower than the rate of polymerisation and the reaction occurs in the interval III where particles are not fully swollen with monomer.

1.5.2 Features

1.5.2.1 Monomer-starved conditions

Chaterjee et al. [48] and Nomura and Harada [49] found that a larger number of latex particles is formed at very low monomer/water ratio (M/W) than that at high M/W ratio using a constant emulsifier concentration via batch process. Krackler and Naidus [45] first explained reduced growth in a semibatch emulsion polymerization reactor and introduced the concept of monomer-starved particle formation. They showed that a larger number of particles can be produced in a semibatch process under monomer-starved conditions, compared with that produced by batch process.

One good example of monomer-starved conditions was demonstrated by Gan et al. who pioneered the work in the area of semi-continuous microemulsion polymerization, focusing on producing higher solids content latex with lower surfactant concentration. A ***Winsor I-like system*** [50] was firstly designed for polymerising St [51] and MMA [52], in which the pure monomer phase was placed on the top of monomer in water (o/w) microemulsion. Polymerisation took place only in the microemulsion phase which contained a small amount of monomer and all of the surfactant and redox initiator pair. Particles formed initially in the microemulsion phase were considered as seeds for further growth. The upper monomer phase acted only as a reservoir and continuously supplied monomer to the lower microemulsion phase for polymerisation. Later, the system was further studied by Sajjadi [53] under highly diffusion-controlled conditions, with the underneath emulsion layer being gently stirred. The rate of polymerisation and particle growth were substantially reduced due to limitations in monomer transport and thus a large number of particles formed. Agitation speed was used as a manipulating variable to produce the desired number of particles by controlling the rate of particle growth. Ming's group [54-55] later modified the Winsor I-like method by directly adding monomer ***dropwise*** to a pre-polymerized ternary microemulsion and named it as 'modified microemulsion polymerisation'. Different monomers such as St, MMA, BA, BMA and MA were studied. Gan's group designed a ***hollow-fiber feeding*** setup and applied in modified Winsor I-like systems of St, BMA and MMA, using 1wt% cationic surfactant (CTAB) [56-57]. The monomer was continuously introduced to the polymerisation system via diffusion from the hollow fibers. The rate of monomer diffusion was regulated by external nitrogen pressure applied to the monomer reservoir at the top of the hollow fibres.

Puig et al. [58] produced a high solids-content (ca. 40wt%) polySt latex by ***shot addition*** of St every 20 min to a microemulsion initially consisting a 6wt% St, 14.1wt% surfactant (DTAB) and 79.9wt% water. Another approach to induce starved conditions was demonstrated by Sajjadi and Brooks [59] who used a low initial monomer charge and continuous addition of monomer at a low rate. They showed the initial monomer loading in a semibatch emulsion polymerisation have a major effect on particle formation and growth. By varying the monomer initial charge, the contribution of monomer-flooded and monomer-starved nucleation to the whole nucleation process will be varied. The presence of a sufficient amount of monomer in the initial charge causes particle formation to occur at monomer-flooded conditions where particle growth rate is a maximum. Under such conditions, no significant difference in the particle nucleation was observed between batch and semibatch processes [60]. A low amount of monomer in the initial charge will drive the system to monomer-starved conditions where the particle growth rate is controlled by the rate of monomer addition and more particles can be formed. Maximum number of particles can be produced if polymerization starts at highly monomer-starved conditions with no monomer in the initial charge [59]. However, the mixing was found to become difficult as polymerization proceeded due to significant increase in the

viscosity of the latex in the presence of a large number of small particles [59]. Consequently, the advantage of monomer-starved nucleation can be taken to produce small particles by using a semibatch process which starts with a small quantity of monomer, with the rest being fed to the reactor in the course of polymerisation [61-63].

Later, a term of differential microemulsion polymerisation was proposed by Rempel et al. [64,123], in which a reaction system similar to semibatch emulsion polymerisation is involved. This method uses a much smaller amount of surfactant, comparing with traditional microemulsion polymerisation.

1.5.2.2 Control of overall rate of polymerisation

For a semibatch process under monomer-starved conditions, the rate of polymerisation (R_p) can be controlled by the rate of monomer addition. It has been found that as time increases, the rate of polymerisation approaches a constant value; a steady state. According to Wessling model [47] for a non-swollen seeded semibatch emulsion polymerisation system with case II kinetics:

$$\lim_{t\to\infty} R_p = \frac{KR_a}{K+R_a} \tag{1.12}$$

or

$$1/R_p = 1/K + 1/R_a \tag{1.13}$$

Equation 1.13 is hereafter called 'first type' [72]. If K approaches infinity and radical concentration in the polymer particles is constant, a special case of the first type can be regarded as second-type correlation [72]:

$$R_p = R_a \tag{1.14}$$

The literature shows a wide range of dependence of R_p on R_a. Gerrens [65] investigated the semicontinuous emulsion polymerisation of a sparingly water-soluble monomer (ie. St) and MA as a monomer with moderate water solubility. It was reported that for both monomers at monomer-starved conditions, the rate of polymerisation was equal to the rate of addition (second type) for both neat monomer and monomer emulsion feeds. The same relationship was reported for the St/BA system [66]. Li and Brooks [67] modelled the semibatch emulsion polymerisation of St using literature values for St and found that first type can virtually predict the correlation between R_p and R_a. Bataille et al. [68] applied the monomer emulsion feed technique to the emulsion polymerisation of VA in the presence of non-ionic surfactant (polyethylene oxide propylene oxide). The first-type correlation was found to be dominant. However, Equation 1.14 was found to be valid for neat monomer feed semibatch process of VA using polyvinyl alcohol as surfactant [69]. Wessling and Gibbs [70] showed that, for both

vinylidene chloride (VDC) and VDC/BA semibatch polymerisation systems, the overall polymerisation rate is proportional to, but not equal to, the total feeding rate at starved conditions. A correlation equation $R_p = \emptyset_p R_a$ was used, where $\emptyset_p$ is the volume fraction of polymer in the monomer-swollen particles. A value of $\emptyset_p = 0.91$ was found for both systems, which is not confined to the form originally suggested by Wessling [47]. Aguilar et al. [71] applied the same correlation to their system and found that the value of $\emptyset_p$ approached 1.0 with increasing SDS concentration, which demonstrated a more monomer-starved condition.

Sajjadi and Brooks claimed that in the semibatch emulsion polymerisation of BA with monomer feed, the rate of polymerisation follows the Equation 1.13 [59,72]. The parameter K, which is an indicator of process capability to consume monomer, was found proportional to k_p, N_p and $\bar{n}$. Any increase in initiator concentration, surfactant concentration or temperature can increase the K value. As K increases, the rate of polymerisation approaches the rate of monomer. For BA semibatch emulsion polymerisation with case I kinetics, the steady-state rates of polymerisation shows little difference on the number of particles [59]. Thus, the increase in the rate of polymerisation with surfactant (SDS) concentration was explained by the acceleration in the rate of initiator decomposition in the presence of SDS and BA [59,73-74]. This is in contrast to monomer emulsion feed of BA semibatch emulsion polymerisation where a correlation of the type $R_p = R_a$ was applied [73,75] due to possible secondary nucleation because of continuous addition of surfactant and an increase in the average radical number because of addition of initiator. The discussion above implies that different rate expressions can be applicable to a system under different conditions [73].

1.5.2.3 Control of particle size, particle size distribution and number of particles

Particle formation and particle growth can compete in the course of emulsion polymerisation reaction. Any variation in the rate of particle growth may result in an opposite effect on the rate of particle formation. A depressed rate of growth can be achieved by starving polymer particles using a semibatch process. Under monomer-starved conditions, the rate of particle growth can be controlled by the rate of monomer addition. It has been reported in the literature that semibatch emulsion polymerisation processes produced a larger number of polymer particles compared with conventional batch process [45,59,61].

Sajjadi [61,76] extended the Smith and Ewart theory (Equation 1.9) to include particle formation under monomer-starved conditions. The model, together with a comparison with experimental data, was presented for the prediction of particle formation in the semibatch emulsion polymerisation of St. The model was derived as:

$$N_p = k(a_s[S])^{1.0} R_I^{2/3} R_a^{-2/3} \quad (1.15)$$

where N_p is the number of particles, k is a numerical constant, R_I the rate of radical generation in the water phase, a_s the adsorption area occupied by a molecule of emulsifier on the surface of polymer particles. R_a represents the rate of monomer addition. The above equation indicates that under monomer starved conditions, population of particles produced is proportional to [S], and inversely proportional to $R_a^{2/3}$. The effect of decrease in rate of particle growth, caused by radical desorption from polymer particles and /or termination in the particles, on the number of particles was indirectly taken into account by the assumption that the rate of growth of particles is controlled by the rate of monomer addition. The model was further developed by including the kinetic of the water phase. The critical degree of radical propagation for entry, z, of 2 was found to give the best fit to the experimental data. The simulation results suggest an increasing rate of particle formation with monomer concentration in the water phase ($[M]_w$). However, experimental data was not available to verify this. The article suggests that more experimental work is needed to focus on the evolution of N_p in the early minutes of polymerisations. It was also suggested that the models can be improved by incorporation of some significant omissions from the real events during polymerisation under monomer-starved conditions, such as limitation in monomer diffusion from fed-in monomer droplets to emulsifier micelles and growing polymer particles; the decreased rate of radical entry into micelles, caused by variation in the structure of monomer-starved micelles with monomer conversion; and the monomer concentration in very small polymer particles formed under monomer-starved condition that might be significantly different from what assumed based on current understanding [76].

Sajjadi and Brooks observed a bimodal particle size distribution (PSD) in semibatch emulsion polymerisation of BA with either a neat monomer feed [59] or a monomer emulsion feed [73] when nucleation started under flooded conditions and then continued into starved conditions, which was also confirmed by simulation [77]. This condition may occur when the rate of monomer addition is sufficiently high to allow polymerisation to start under flooded conditions, but not too high to prevent extension to starved conditions [87].

Lopez et al. published a work, which employed SDS/AOT surfactant mixture and potassium peroxodisulfate as initiator in the seeded semibatch microemulsion polymerization of BA [78]. It was found that nucleation of particles occurred regardless of swollen micelles being present or not. Questions concerning the mechanism of particle nucleation were beyond the scope of this contribution, but some ideas were discussed. The experimental results showed that formation of new particles stops at the same time as the monomer feeding is switched off leading to the conclusion that the monomer concentration in the water phase is crucial for particle formation. They also claimed that during the equilibration period the monomer is nonhomogeneously and favorably distributed in the continuous phase resulting in nonmicellar nucleation.

Nomura's group found that in batch emulsion polymerisation, the particle formation can be enhanced in the presence of highly water-soluble chain transfer agents (CTAs) (C_2, n-C_4, n-C_7

and n-C_{12}) [79]. They pointed out that [79-80] the chain transferred radicals can be desorbed from particle to water phase and form new particles via re-entry to the micelles during nucleation stage. Furthermore, the rate of particle growth as well as the consumption rate of micelles can be suppressed by decreasing the number of radicals within the growing particles. It was found that with an increase in the amount of CTA charged, the number of polymer particles produced increases initially, but then decreases due to significant water-phase termination among initiator and desorbed radicals [79]. The effects were expected to be more promising when mercaptans with higher water solubility are used.

Chern et al. [81-83] demonstrated that injecting SDS into the reaction medium induced a second nucleation of tiny particles in the semibatch seeded emulsion polymerisation of acrylic monomers (e.g. MAA). As a result, latex products with bimodal particle size distributions were obtained. Retarded secondary particle nucleation during the monomer addition period was achieved when the concentration of seed particles or the time when surfactant was added increased.

Sajjadi studied the effect of feeding policy on the secondary particle formation for a seeded semibatch emulsion polymerisation of St [84]. Different types of monomer emulsion feedings were applied to the reactor in the presence of seed particles with average diameter of 119 nm, using either a stream of the emulsified monomer or two streams of the neat monomer feed and an aqueous solution of an emulsifier. The results showed that secondary particle formation did not occur with either type of feedings. The incoming monomer-swollen micelles were disintegrated to supply emulsifier molecules for the stability of growing particles, before they can capture radicals and become polymer particles. Similar observation was made by Gan's group [56-57]. Chu and Tang [85] produced high solids content latexes of poly(St-BA-MMA) in the presence of *N*-hydroxymethacrylic amide (NMA) through semicontinuous emulsion polymerisation. Latexes with relatively low viscosity were obtained via a two-stage feeding process due to their bimodal particle size distributions (PSD). By contrast, one-stage feeding process results in latexes with a high viscosity and low mechanical and chemical stability, which is attributable to a narrow PSD.

It has been claimed that polymer particles with broad PSDs are produced via semibatch process due to its longer nucleation time [11,86]. Sajjadi claimed that the PSDs of particles, when presented in terms of volume, are characterized by a positive skewness due to the declining rate of the growth of particles during nucleation stage in the semibatch emulsion polymeisation of St. However; there was a lack of data of PSD evolution during the nucleation stage.

Later, the author demonstrated the evolution of PSD in the monomer–starved semibatch emulsion polymerization of St with a neat monomer feed, using a population balance model [87]. The effect of rate of monomer addition was studied under conditions ranging from

conventional batch emulsion to semicontinuous (micro)emulsion polymerization. It was shown that the broadness of PSD is not necessarily associated with the length of nucleation period, which is contrary to what was often believed. The PSDs at the end of nucleation were theoretically found to be independent of surfactant concentration. An interesting prediction is yet to be confirmed experimentally. Simulation results indicated that particle size was reduced and PSD narrowed with decreasing rate of monomer addition despite nucleation time increasing. The broad PSD usually obtained in semibatch emulsion polymerization was attributed to stochastic broadening during the growth stage [87].

Generally, the PSD of latexes produced via emulsion polymerization broadened with time as a result of stochastic broadening associated with a zero-one system [61,87]. This occurs due to the increase in difference of particle size between growing particles and nongrowing ones. The growing particles continuously grow for a long time, thus their sizes become quite large compared with that of nongrowing particles. Simple analytical equation was derived for the volume average size of particles at the end of nucleation as follows [87]:

$$d_{\mathrm{v}} = (6/\pi)^{1/3}(R_{\mathrm{a}}/R_{\mathrm{I}})^{1/3} \tag{1.16}$$

This equation predicts that the average size of particles at the end of nucleation is independent of surfactant concentration but proportional to ${R_{\mathrm{a}}}^{1/3}$. Surprisingly, no attempt has been made in literature to verify this prediction experimentally.

Rempel's group synthesized polyMMA nanoparticles by a differential microemulsion polymerisation process [64]. SDS and APS were used as surfactant and initiator, respectively. Particles smaller than 20 nm were achieved with surfactant/monomer and surfactant/water weight ratios of 1:18 and 1:120, respectively. With the increase in the amount of surfactant, the particle sizes became smaller. However, beyond a certain level, the amount of surfactant had little effect on particle size. This was also confirmed by their later mathematical kinetic model [88]. The same limitation for the effect of surfactant concentration on particle size was mentioned in the later works of Pan et al. [89,123]. Furthermore, the effect of temperature on particle size in the semibatch emulsion polymerisation of poly(ethyl acrylate) has also been studied. Particle size decreased with reaction temperature, which is consistent with results reported elsewhere [72-73,55]. However, the increase in particle size became insignificant above 82°C, which was explained by the effect of temperature on the initiator decomposition. They discussed that when temperature reaches a certain level, its contribution to increase in the radical concentration may be offset by the increase in the radical termination rate. In contrast, larger particles were produced at 80°C by Ming et al [55], which was explained by the aggregation of small particles.

1.5.2.4 Control of polymer composition and morphology

The semibatch approach, by which selected reagents are fed to the reactor, can be used to control composition and morphology of latexes during polymerisations under monomer-starved conditions, no matter how large the difference of monomer reactivity ratios [85,90-93]. If a given mixture of monomers is fed so that the rate of polymerisation is practically equal to the rate of monomer addition, a copolymer can be obtained with the same composition as that of the feed. However, in a batch process, copolymer composition drift is inevitable as long as there is a difference in monomer reactivity [94].

A early description was made of the synthesis and characterization of full acrylic latex (MMA/EA/MAA) using a variable feed rate via semicontinuous emulsion terpolymerisation by Arzamendi et al. [95-97] and Amalvy [98]. Terpolymers with almost constant compositions were achieved. Gualiotta et al. [99] developed a new approach to estimate the monomer conversion and copolymer composition in semibatch emulsion polymerisation based on reaction calorimetric measurements. The validity of this technique was confirmed by the semibatch emulsion copolymerisations of both the St-BA and VA-BA pairs.

It has been reported that homopolymerisation of n-BA yield a gel both in batch [100] and semibatch reactions [101-102], which is mainly due to intermolecular transfer to polymer plus termination by combination [102]. Plessis et al. [103] claimed that the amount of gel as well as the level of branches can be controlled by incorporating a small amount of St as comonomer in the seeded semibatch emulsion copolymerisation. A mathematical model was also developed by them for predicting the effect of St on the kinetics, the fraction of gel, the level of branches and molecular weight distribution of poly(*n*-BA). Alternatively, several works based on n-BA/MMA, which is another commonly used monomer systems, can be found in the literature [104-107]. The level of branches in n-BA polymerisations was reduced by the introduction of MMA as a comonomer. The kinetics, gel fraction and molecular weight distribution were determined both from experimental work and mathematical model. It was found that the larger the weight ratio of MMA to BA in the copolymer, the greater the amount of coagulum produced [108].

Mendizabal et al. [109] have studied the effect of monomer addition rate in the semicontinuous microemulsion copolymerisation of VA and BA under monomer-starved conditions. Homogeneous copolymer compositions were observed throughout the reaction, which cannot be obtained by the conventional batch process. Kabiri et al. [110] produced poly(BA-*co*-glycidyl methacrylate) latexes via semibatch emulsion copolymerisation. The effects of operating variables such as agitation speed, surfactant concentration, initator concentration, feeding rate and comonomers ratio were investigated based on monomer conversion and particle size distribution. Optimised copolymerisation conditions were obtained. Hsu et al. [111] studied the

MMA/St/BMA three-component system through surfactant-free semibatch emulsion copolymerisation. From the analysis of the results of GC and ^{1}H NMR, the instantaneous composition of polymers was found to have been effectively controlled.

Chern and Lin [112] studied the effects of functional monomers (acrylic acid (AA), MAA and hydroxyethyl methacrylate) on the emulsion polymerisation of BA. The final particle size decreased with increasing concentration of SDS, NP-40 or functional monomer. The colloidal stability of polyBA particles incorporated with a small amount of AA or MAA [113-114] in the semibatch emulsion polymerisation was further investigated both in the presence and absence of surfactant. It was found that the latex stability was greatly improved and particles sizes decreased with increasing concentration of comonomer, which was attributed to increase in the particle surface charge density and therefore, increasing the repulsive force among the particles [113]. Recently, Xu et al. reported synthesis of poly(BA/MMA/AA) latexes, as pressure-sensitive adhesives, at the solids content of 50wt% via semicontinuous emulsion polymerisation. The effects of addition of MMA on the gel fraction and molecular weights of copolymer were studied.

Alternatively, polymerisable surfactants, which are chemically incorporated onto the particle surface during polymerisation, can be used [115-116]. As a result, the water sensitivity of latex products arising from the immobilized surfactant molecules near the particle surface layer can be minimized. Xu and Chen [117] used polymerisable surfactants with different alkyl chain length, to stabilize the semibatch emulsion copolymerisation of butyl methacrylate. X-ray photoelectron spectroscopy data showed that polymerisable surfactant molecules were preferably located near the particle surface layer.

Sequential monomer addition in semicontinuous emulsion polymerisation can be employed to produce core-shell or onion type structured nanoparticles [118-121]. At a low rate of monomer addition, monomer molecules polymerise at the surface before they can penetrate deep into particles resulting in formation of layer-by-layer structure [121-122]. He and Pan [123] reported that PMMA/PS nanoparticles of diameter less than 20 nm could by prepared by a differential microemulsion polymerisation at a low surfactant concentration, involving the use of a small amount of PMMA as the seeds. Later Pan et al. [124-125] investigated the synthesis of glycidyl-functionalized PMMA latexes using a differential microemulsion polymerisation method via a two step process. A core-shell structure was formed which was composed of very high molecular weight PMMA as core and poly(MMA-*ran*-(glycidyl methacrylate)) as the shell. Kim and co-workers [126] prepared PMMA/PS nanocomposites under monomer-starved condition. PMMA nanoparticles were used as seed and St monomer was fed as gas phase. Aguiar et al. [127] prepared core-shell PS/PBA particles by a two-stage microemulsion polymerisation. The process was optimised by producing a larger number of PS nanoparticles with smaller size via a semicontinuous process, which were then used as seeds to form core-shell particles by adding

BA monomer. The resulting film exhibited harder and more rigid with larger Young moduli and ultimate strength compared with conventional core-shell polymer made by emulsion polymerisation. Puig's group have also synthesised core-shell particles of St and BA by seeded semicontinuous microemulsion polymerisation process [128]. The monomers for core and shell were altered to produce hard-core/soft-shell and soft-core/hard-shell particles. The results showed that by varying the core-shell composition and the initial location of the polymers, it is possible to obtain materials with a broad range of mechanical properties.

In recent years, polymer nanocapsules, have gained great interest in many fields, such as nanoreator, targeted drug delivery, control release, photocatalysis, macromolecule encapsulation, etc [129-132]. A number of methods, such as template method [133-135], dynamic swelling method [136-137], acid/alkali osmotic swelling [138], emulsion droplets [139], self-assembly [140], polymer micelles [141], have been developed for the synthesis of hollow polymer particles. Among all above, the synthesis of core-shell particles followed by removal of core materials is the most commonly used method for producing hollow structures [142-145].

1.5.2.5 Control of molecular weight

Molecular weight and molecular weight distribution (MWD) are important parameters that determine processability and final use properties of polymers (i.e., mechanical properties such as stress, impact behaviour, adhesion, glass transition temperature, rate of crack propagation, etc.) for different applications. In semibatch emulsion polymerisation, the molecular weight of polymer can be controlled by monomer feed rate [146]. It has been reported that the number-average molecular weight increases with increasing monomer feed rate [46,147]. However, Lee [148] and El-Aasser et al. [149-150] found that the latex copolymers prepared by semibatch polymerisation have lower number-average and weight-average molecular weights than those formed via the corresponding batch copolymersation. Sajjadi and Yianneskis [151] investigated semibatch emulsion polymerisation of MMA with a neat monomer feed in the presence of SDS and KPS, as emulsifier and initiator, respectively. They found that the molecular weight of resulting polymer decreased and MWD became narrower with decreasing R_a. This is opposite to what had been obtained earlier [68,149-150,152], in which broader MWDs with bimodal characteristics were observed for relatively highly water-soluble monomers (i.e., VA [68]) in seeded semicontinuous process, comparing with batch process.

Puig et al. [58] produced high solids content latexes (ca. 40wt%) containing small particles (< 40 nm) of high weight-average molecular weight ($\bar{M}_w > 10^6$ g·mol^{-1}) using semicontinuous microemulsion polymerisation. The molecular weight was found remaining fairly constant throughout the process, which was explained by chain transfer reactions to monomer as controlling chain termination event [153-156]. Such high molecular weight of polymer was also obtained by Rempel and co-workers [157], using differential microemulsion polymerisation of

MMA initiated by Azobisisobutyronitrile (AIBN). It was found that the M_w and MWD of the produced polymer are independent of SDS concentrations (5.78 and 17.34 $mmol \cdot l_{aq}^{-1}$). Furthermore, the MWD was found to be constant over the polymerisation time.

Puig et al. [71-158] reported a series of work on semicontinuous polymerisation of MMA under monomer-starved conditions, using KPS as initiator. They found molecular weight of polymer formed was practically independent of the SDS concentration and remained constant all throughout the reaction [71]. Furthermore, both particle size and molecular weight decreased with decreasing rate of monomer addition [158]. The authors tried to explain the low $\bar{M}_w$ ($\sim 10^5$ $g \cdot mol^{-1}$) produced as a consequence of chain stoppage by secondary entry of another radical before that of stoppage by transfer to monomer. Considering an almost instantaneuous mutual annihilation between two radicals in a small particle (< 30 nm), the ratio of overall number of polymer chains produced to the number of free radicals generated by initiator decomposition at the end of polymerisation was expected to be 0.5 [158]. However, their calculated values were above one, which suggests another contributing termination mechanism, such as chain transfer reaction to AOT [158]. Gugliotta's group applied semibatch process to control the molecular weight of polyAA through an adequate selection of both initiator concentration and the AA feeding rate [159].

Chain transfer agents (CTA) are commonly used in the polymer industry to control the MWD of the resultant polymers. Several publications have appeared on the molecular weight control of semibatch emulsion polymerizations. Uraneck and Burleigh [160] experimentally studied the addition of mercaptans along a St-Butadiene copolymerization, with the aim of reducing the final polydispersity of molecular weight. Baus [161] investigated the addition of CTAs along the reaction, as a means of broadening the MWD of polyAA press adhesives. Paine et al. [162] patented a starved technique for controlling the MWD of a St-BA copolymer by slow addition of preemulsified CTA-monomer mixture. Harelle et al. [163] carried out a slow seeded semibatch polymerization for controlling the MWD of PS. However, starved conditions for the monomer and modifier were not reached; and relatively broad MWDs were obtained [164]. Salazear et al. obtained a constant MWD along the polymerisation using a starved feed of a mixture of St and CTA (tert-dodecyl or tert-nonyl mercaptan) [164-165]. A mass transfer resistance to tert-docecyl mercaptan was found by a mathematical model. However, this extra mass transfer resistance could be neglected in the case of more water-soluble CTAs (tert-nonyl mercaptan) [164]. Such improvements in mass transfer resistance have also been observed by Asua' group in semicontinuous emulsion polymerisation of BA and VA/BA [166-167].

1.5.2.6 Smart and hybrid particles (organic-inorganic)

The application of semicontinuous process to advanced materials such as hybrid particles or smart particles have received very little attention in literature. One category of smart particles, thermal-sensitive one, is based on n-isopropylacrylamide (NIPAM). Thermal-responsive microgels based on poly(n-isopropylacrylamide) (polyNIPAM) have been widely studied for many applications, especially for the controlled release of pharmaceuticals. However, semicontinuous process was only used in a small number of researches. Candau et al. [168] synthesized stimuli-responsive polyelectrolytes and polyampholytes based on *N*-isopropylacrylamide (NIPAM) by a semicontinuous microemulsion polymerisation technique. The required surfactant concentration for the formation of microemulsion was little comparing to conventional microemulsion polymerisation. Zhang et al. [169] prepared pH- and temperature-sensitive nanogels, based on NIPAM, via semibatch process in the absence of surfactant. It was found that the particle size decreased with increasing amount of acrylic acid. Comparing to gel, water-soluble temperature-sensitive polyNIPAM colloids have received little attention in the literature despite their wide range of potential applications [170-171].

Hybrid particles have received a great deal of attentions in recent years due to their improved mechanical properties [172-173]. Due to commercial availability of silica nanoparticles at different radii, many academic works on hybrid particles used silica nanoparticles as the model inorganic component. There is little explored in the literature about potentials of semicontinuous process for fabrications of hybrid polymer-silica particles. Bourgeat-Lami et al. [174] prepared polySt/silica and poly(St-co-MMA)/silica composite latex particles by emulsion polymerisation in the presence poly(ethylene glycol) monomethylether methacrylate (PEGMA) macromonomer. Semicontinuous process was also applied to reduce the amount of monomer present in the reaction medium during the formation of particles in order to enhance their colloidal stability. As a result, a decrease in particles size as well as an increase in particle number was gained by using semicontinuous process [174]. Zhang et al. prepared polyNIPAM/PS core/shell particles both above and below the volume phase transition temperature (VPPT) using unseeded and seeded semibatch polymerisation process. 'Raspberry' structures were obtained in which PS formed small domains on the surface of the polyNIPAM particles.

1.6 Main conclusions from the literature study

The main findings from the literature review are listed below:

1) Several aspects of semicontinuous polymerisation such as rate of polymerisation and copolymer composition have been studied in depth in literature and processes for fabrication of particles with uniform compositions have been developed. There appears to be no lack of understanding in this area.

2) Although particle formation and growth in semicontinuous (mirco)emulsion has been extensively studied, there are still several controversial issues unresolved. One important reason for this is the lack of appropriate experimental data. Most data reported in the literature were either collected at intermediate conversions or final conversions, which cannot reveal the true features of particle nucleation in semicontinuous process. Experimental data and analysis based on the evolution of particle size and size distributions in the course of particle nucleation stage, and in particular at the completion of nucleation, are required.

3) Although it has been reported that the molecular weights of polymer can be controlled in semicontinuous process, there are still controversial issues regarding the mechanism of chain termination events occurring during the process and the way M_w varies with monomer addition rate. Several hypotheses have been proposed for termination reactions, such as chain transfer to monomer, chain transfer to surfactants, and termination by secondary entry of another radical.

4) There is a great need for small polymeric particles for applications such as ultrathin films, high performance coating materials, drug delivery nanocarriers, etc. While semicontinuous emulsion polymerisation can be used to produce such particles, its full potentials are still unexplored. Although particle size can be controlled by altering the reaction parameters, such as surfactant concentration and rate of monomer addition, it is not clear yet under what conditions minimum size can be achieved.

5) Ideally, chain transfer agents (CTA) should only control the molecular weight of the polymer product but should not affect the rate of polymerisation. However, it was found that CTAs with higher water solubility can also affect the rate of polymerisation due to desorption of chain transferred radicals from polymer particles to the water phase. The possibility of enhanced particle nucleation by desorbed radicals has been reported. However, this idea was only partly experimentally tested via batchwise emulsion polymerisation. The effects are expected to be more promising when CTAs with higher water solubility are used.

6) Most reports in the literature on nucleation in semicontinuous microemulsion polymerisation were experimental. Little attempt has been made to explain the features of the semicontinuous process using theoretical models available in the literature.

7) Application of semicontinuous process for synthesis of NIPAM based temperature-sensitive particles is scarce. Furthermore, most works reported in the literature on temperature-sensitive polyNIPAM particles focused on the applications of the final products. There is a lack of understanding above the kinetics of NIPAM polymerisation.

8) 'Smart' colloidal hollow hydrogels have attracted great attentions due to their wide applications in encapsulation, carriers, sensors and microreactors. Hollow structures are usually produced via precipitation polymerisation in the presence of core templates, followed by removing the core materials. The process always involves complicated and time-consuming steps that may limit its applications. Furthermore, the accurate control of the core-shell structure, which is usually used to produce hollow structure, is difficult to maintain in the conventional method. Therefore, a new method is needed to be thought.

9) Only few works have been reported on hybrid and smart hybrid (organic-inorganic) nanocomposites using semicontinuous processes. There appears to be significant potentials for semicontinuous process in this area. Actually, semicontinuous process can not only control the particle size but also the particle morphology and structure. Core-shell or structured particles made by semicontinuous emulsion polymerisation have found wide range of applications. However, the methodology to produce such particles, via semicontinuous process, has not been extended to hybrid systems yet.

1.7 Objectives

In view of the aforementioned considerations and conclusions made in the literature review, the objectives of the present study are summarised as:

- To decouple particle formation from growth and refine the true relation between number of particles (particle size) and process variables.
- To investigate PSD variations in the course of nucleation, and at the completion of nucleation with process variables.
- To verify and explain variations in molecular weight with process variables.
- To verify the theoretical models available in the literature by their comparison with the experimental data produced.
- To investigate the formulation and process conditions under which smallest nanoparticles can be produced using semicontinuous emulsion polymerisation.
- To further explore reducing the particle size threshold by using supplementary materials such as chain transfer agents.
- To explore application of semicontinuous emulsion polymerisation to fabrication of smart materials, such as thermal-sensitive colloids, and organic/inorganic hybrid particles.
- To take advantage of molecular orientations of polymer chains inside particles produced by semicontinuous emulsion polymerisation to design new processes for making advanced materials.
- To discover new potentials for semicontinuous polymerisation to produce advanced colloids.

1.8 Thesis outline

The remainder to this thesis is organised into six chapters. In the following chapter, the chemicals and apparatus used in this work have been described. Characterization methods, such as conversion of monomers, average size and size distributions and zeta potentials of particles, molecular weight and glass transition temperature of polymer produced, turbidity of latexes as well as the morphology of colloids, have been explained.

In Chapter 3, semicontinuous microemulsion polymerisations of a conventional monomer (styrene) under monomer-starved conditions have been carried out. Experimental data, such as conversion, average size of particles and average molecular weight of polymer chains have been closely monitored in the course of reaction. Particle formation has been decoupled from growth in order to be able to investigate the true relations between the properties of the resulting latexes and process parameters. The minimum sizes of particles achievable have then been explored by optimizing the reaction conditions as well as process parameters. As an alternative way of reducing the particle size via semicontinuous process, a water-soluble chain transfer agent has been used to decrease the average length of polymer chains and thus the size of particles.

Chapter 4 presents the study of thermo-responsive water-soluble poly(*n*-isopropylacrylamide) (polyNIPAM) colloids. The effects of monomer concentration on the kinetics of batch polymerisation under monomer-starved conditions and characterizations of resulting crosslinker-free particles have first been investigated. The conclusions have then been used for semicontinuous process for polyNIPAM. The potentials of semicontinuous processes, such as producing fast-dissolving colloids, have also been explored.

In Chapter 5, polymer/silica hybrid particles have been synthesized via different processes. Monomers with different water solubility, such as methyl methacrylate (MMA), vinyl acetate (VA) and NIPAM have been explored. The role of silica nanopaticles throughout the polymerisations, the mechanism of particle formation as well as the evolution of morphology of nanocomposite particles in semicontinuous processes, and its advantages over batch process have been explored and discussed.

Finally, conclusions and recommendation for future work have been provided in Chapter 6, where the main findings of the present work have been summarised and suggestions for future work have been made.

1.9 Reference

[1] Williams, M.M. Chemical Binders for Nonwovens Fabrics. *TAPPI Nonwovens Conference*, 1999, pp1-11.

[2] Michalak, J. Polymer Modified Factory-Made Dry Mortars as Modern Building Materials. *Polimery*, 2004, v49, pp346-349,

[3] Snowden, M.J., Hadgraft, J. The Use of Colloidal Microgels as a (trans)dermal Drug Delivery System. *International Journal of Pharmaceutics*, 2005, v292, pp137-147.

[4] Riedinger, A., Leal, M.P., Deka, S.R., George, C., Franchini, I.R., Falqui, A., Cingolani, R., Pellegrino, T. 'Nanohybrids' Based on pH-Responsive Hydrogels and Inorganic Nanoparticles for Drug Delivery and Sensor Applications. *Nano Letters*, 2011, v11, pp3136-3141.

[5] Koskinen, M., Wilen, C.E. Preparation of Core-Shell Latexes for Paper Coatings. *Journal of Applied Polymer Science*, 2009, v112, pp1265-1270.

[6] Szabo, T., Molnar-Nagy, L., Bognar, J., Nyikos, L., Telegdi, J. Self-healing Microcapsules and Slow Release Microspheres in Paints. Progress in Organic Coatings. 2011, v72, pp52-57.

[7] Juntuek, P., Ruksakulpiwat, C., Chumsamrong, P., Ruksakulpiwat, Y. Glycidyl Methacrylate Grafted Natural Rubber: Synthesis, Characterization and Mechanical Property. *Journal of Applied Polymer Science*, 2011, v122, pp3152-3159.

[8] Smith, W.V., Ewart, R.H. Kinetics of Emulsion Polymerisation. *Journal of Chemical Physics*, 1948, v16, pp592-599.

[9] Harkins, W.D. A General Theory of the Mechanism of Emulsion Polymerisation. *Journal of the American Chemistry Society*, 1947, v69, pp1428-&.

[10] Gilbert, R.G. Emulsion Polymerization: A Mechanistic Approach. *Academic Press*, 1995, London.

[11] Chern, C.S. Emulsion Polymerisation Mechanisms and Kinetics. *Progress in Polymer Science*, 2006, v31, pp443-486.

[12] Nomura, M. Kinetic and Mechanisms of Emulsion Polymerisation. *Journal of Industrial and Engineering Chemistry*, 2004, v10, pp1182-1215.

[13] Gridnev, A.A., Ittel, S.D. Dependence of Free-radical Propagation Rate Constants on the Degree of Polymerisation. *Macromolecules*, 1996, v29, pp5864-5874.

[14] Buback, M., Busch, M., Kowollik, C. Chain-length Dependence of Free-radical Termination Rate Deduced from Laser Single-Pulse Experiments. *Macromolecular Theory and Simulations*, 2000, v9, pp442-452.

[15] Harkins, W.D. A General Theory of the Reaction Loci in Emulsion Polymerisation. *Journal of Chemical Physics*, 1945, v13, pp381-382.

[16] Smith, W.V. The Kinetics of St Emulsion Polymerisation. *Journal of the American Chemical Society*, 1948, v70, pp3695-3702.

[17] Gardon, J.L. Emulsion Polymerisation .1. Recalculation and Extension of Smith-Ewart Theory. *Journal of Polymer Science Part A-1-Polymer Chemistry*, 1968, v6, pp623-&.

[18] Priest, W.J. Particle Growth in the Aqueous Polymerisation of Vinyl Acetate. *Journal of Physical Chemistry*, 1952, v56, pp1077-1082.

[19] Roe, C.P. Surface Chemistry Aspects of Emulsion Polymerisation. *Industrial and Engineering Chemistry*, 1968, v60, pp20-&.

[20] Fitch, R.M., Tsai, C.H. Homogeneous Nucleation of Polymer Colloids. *Proceeding of the National Academy of Sciences of the United States of America*, 1969, v64, pp1424-&.

[21] Lansdowne, S.W., Gilbert, R.G., Napper, D.H., Sangster, D.F. Relaxation Studies of the Seeded Emulsion Polymerisation of St Initiated by Gamma-Radiolysis. *Journal of the Chemical Society-Faraday Transactions*, 1980, v76, pp1344-1355.

[22] Hawkett, B.S., Napper, D.H., Gilbert, R.G. Seeded Emulsion Polymerisation of St. J*ournal of the Chemical Society-Faraday Transactions*, 1980, v76, pp1323-1343.

[23] Weerts, P.A., German, A.L., Gilbert, R.G. Kinetic Aspects of the Emulsion Polymerisation of Butadiene. *Macromolecules*, 1991, v24, pp1622-1628.

[24] Verdurmen, E.M., Dohmen, E.H., Verstegen, J.M., Maxwell, I.A., German, A.L., Gilbert, R.G. Seeded Emulsion Polymerisation of Butadiene.1.The Propagation Rate Coefficient. *Macromolecules*, 1993, v26, pp268-275.

[25] Chern, C.S. Emulsion Polymerisation Mechanisms and Kinetics. *Progress in Polymer Science*, 2006, v31, pp443-486.
[26] Friis, N., Hamielec, A.E. Gel-effect in Emulsion Polymerisation of Vinyl Monomers. *Acs Symposium Series*, 1976, v24, pp82-91.
[27] Stoffer, J.O., Bone, T. Polymerization in Water-in-oil Microemulsion Systems .1. *Journal of Polymer Science Part A. Polymer Chemistry*, 1980, v18, pp2641-2648.
[28] Atik, S.S., Thomas, J.K. Polymerized Microemulsions. *Journal of the American Chemical Society*, 1981, v103, pp4279-4280.
[29] Candau, F., Pabon, M., Anquetil, J.Y. Polymerizable microemulsions: some criteria to achieve an optimal formulation. *Collioids and Surfaces A-Physicochemical and Engineering Aspects*, 1999, v153, pp47–59.
[30] Guo, J.S., Sudol, E.D., Vanderhoff, J.W., El-Aasser, M.S. Particle Nucleation and Monomer Partitioning in Styrene O/W Microemulsion Polymerization. *Journal of Polymer Science Part A-Polymer Chemistry*, 1992, v30, pp691-702.
[31] Guo, J.S., Sudol, E.D., Vanderhoff, J.W., El-Aasser, M.S. Modeling of the Styrene Microemulsion Polymerization. *Journal of Polymer Science Part A-Polymer Chemistry*, 1992, v30, pp703-712.
[32] Morgan, J.D., Lusvardi, K.M., Kaler, E.W. Kinetics and Mechanism of Microemulsion Polymerization of Hexyl Methacrylate. *Macromolecules*, 1997, v30, pp1897 -1905
[33] Nomura, M., Suzuki, K. A New Kinetic Interpretation of the Styrene Microemulsion Polymerization. *Macromolecular Chemistry and Physics*, 1997, v198, pp3025-3039.
[34] Guo, J.S., Sudol, E.D., Vanderhoff, J.W., El-Aasser, M.S. Particle Nucleation and Monomer Partitioning in Styrene O/W Microemulsion Polymerization. *Journal of Polymer Science Part A-Polymer Chemistry*, 1992, v30, pp691-702.
[35] Kim, D.R., Napper, D.H. Experimental Discrimination Between Competing Nucleation Theories in Microemulsion Polymerizations. *Macromolecular Rapid Communications*, 1996, v17, pp845-851.
[36] Antonietti, M., Bremser, W., Muschenbom, D., Rosenauer, C. Schupp, B., Schmidt, M. Synthesis and Size Control of PolyStyrene Latices via Polymerisation in Microemulsion, *Macromolecules*, 1991, v24, pp6636-6643.
[37] Antonietti, M., Basten, R., Lohmann, S. Polymerization in Microemulsions - A New Approach to Ultrafine, Highly Functionalized Polymer Dispersions, *Macromolecular Chemistry Physics*, 1995, v196, pp441-466.
[38] Wu, C. Laser-light Scattering Determination of the Surfactant Interface Thickness of Spherical Polystyrene Microlattices. *Macromolecules*, 1994, v27, pp7099-7102.
[39] Texter, J., Oppenheimer, L., Minter, J.R. Microemulsion Polymerization in the Water, Aerosol-OT, Tetrahydrofurfuryl Methacrylate System. *Polymer Bulletin*, 1992, v27, pp487–494.
[40] Full A.P., Puig J.E., Gron L.U., Kaler E.W., Minter J.R., Mourey T.H., Texter, J. Polymerization of Tetrahydrofurfuryl Methacrylate in Three-component Anionic Microemulsions. *Macromolecules*, 1992, v25, pp5157–5164.
[41] Macias E.R., Rodriguez-Guadarrama L.A., Cisneros B.A., Castaneda A., Mendizabal E., Puig J.E. Microemulsion Polymerization of Methylmethacrylate with the Functional Monomer *N*-methylolacrylamide. *Colloids and Surfaces A: Physicochemical and Engineering Aspects*, 1995, v103, pp119–126.
[42] Sosa, N., Zaragoza, E.A., Lopez, R.G.,Peralta, R.D., Katime, I., Becerra, F., Mendizabal, E., Puig, J.E. Unusual Free Radical Polymerization of Vinyl Acetate in Anionic Micro-emulsion Media. *Langmuir*, 2000, v16, pp3612–3619.
[43] Xu, X., Zhang, Z., Wu, H., Ge, X., Zhang, M. Polymerization of Styrene in Anionic Microemulsion with High Monomer Content. *Polymer*, 1998, v39, pp5245-5248.
[44] Naidus, H. Emulsion Polymers for Paints. *Industrial and Engineering Chemistry*, 1953, v45, pp712-717.
[45] Krackler, J.J., Naidus, H. Particle Size and Molecular Weight Distributions of Various Polystyrene Emulsions, *Journal of Polymer Science Part C-Polymer Symposium*, 1969, v27, pp207-235.
[46] Gerrens, H. On Semicontinuous Emulsion Polymerisation, *Journal of Polymer Science Part C-Polymer Symposium*, 1969, v27, pp77-&.
[47] Wessling, R.A. Kinetic of Continuous Addition Emulsion Polymerisation, *Journal of Applied Polymer Science*, 1968, v12, pp309-319.

[48] Chatterjee, S.P., Barnerjee, M., Konar, R.S. Molecular-Weight of Polystyrene Polymer Obtained in the Emulsion Polymerisation at Low Monomer Concentration and the Harkins-Smith-Ewart-Gardon (HSEG) Theory, *Journal of Polymer Science Part A-Polymer Chemistry*, 1979, v17, pp2193-2207.
[49] Nomura, M., Harada, M. In Emulsion Polymers and Emulsion Polymerisation; Basset, D. R.; Hamielec, A. E., Eds. *American Chemical Society*: Washington, DC, 1981, pp121.
[50] Winsor, P. Solvent Properties of Amphiphilic Compounds, *Butterworth,* London 1954.
[51] Gan, L.M., Lian, N., Chew, C.H., Li, G.Z. Polymerization of Styrene in a Winsor-like System. *Langmuir*, 1994, v10, pp2197-2201.
[52] Loh, S.E., Gan, L.M., Chew, C.H., Ng, S.C. Polymerization of Methyl Methacrylate in Winsor I-like system. *Journal of Macromolecular Science-Pure and Applied Chemistry*, 1996, v33, pp371–384.
[53] Sajjadi, S. Diffusion-Controlled Particle Growth and Its Effects on Nucleation in Stirred Emulsion Polymerisation Reactors, *Macromolecular Rapid Communications*, 2004, v25, pp882-887.
[54] Ming, W., Jones, F.N., Fu, S.K. High Solid-Content Nanosize Polymer Latexes Made by Microemulsion Polymerisation, *Macromolecular Chemistry and Physics*, 1998, v199, pp1075-1079.
[55] Ming, W.H., Jones, F.N., Fu, S.K. Synthesis of Nanosize Poly(methyl methacrylate) Microlatexes with High Polymer Content by a Modified Microemulsion Polymerisation, *Polymer Bulletin*, 1998, v40, pp749-756.
[56] Xu, X.J., Chew, C.H., Siow, K.S., Wong, M.K., Gan, L.M. Microemulsion Polymerisation of Styrene for Obtaining High Ratios of Polystyrene/Surfactant, *Langmuir*, 1999, v15, pp8067-8071.
[57] Xu, X.J., Siow, K.S., Wong, M.K., Gan, L.M. Microemulsion Polymerisation via Hollow-Fiber Feeding of Monomer, *Langmuir*, 2001, v17, pp4519-4524.
[58] Rabelero M, Zacarias M, Mendizabal E, Puig JE, Dominguez JM, Katime I. High-content polystyrene latex by microemulsion polymerization. *Polymer Bulletin*, 1997, v38, pp695-700.
[59] Sajjadi S, Brooks BW. Semibatch Emulsion Polymerization of Butyl Acrylate. I. Effect of Monomer Distribution, *Journal of Applied Polymer Science*, 1999, v74, pp3094–3110.
[60] Gerrens, H. On Semicontinuous Emulsion Polymerization. *Journal of Polymer Science Part C-Polymer Symposium,* 1969, v27, pp77.
[61] Sajjadi, S. Particle Formation under Monomer-Starved Conditions in the Semibatch Emulsion Polymerisation of Styrene.1.Experimental, *Journal of Polymer Science: Part A: Polymer Chemistry*, 2001, v39, pp3940-3952.
[62] Sajjadi, S., Yianneskis, M. Analysis of Particle Formation under Monomer-Starved Conditions in Emulsion Polymerisation Reactors, *Macromolecular Symposia*. 2004, v206, pp201-213.
[63] Sajjadi, S. Nanoparticle Formation by Monomer-Starved Semibatch Emulsion Polymerisation, *Langmuir*, 2007, v23, pp1018-1024.
[64] He, G.W., Pan, Q.M., Rempel, G.L. Synthesis of Poly(methyl methacrylate) Nanosize Particles by Differential Microemulsion Polymerisation, *Macromolecular Rapid Communications*, 2003, v24, pp585-588.
[65] Gerrens, H. On Semicontinuous Emulsion Polymerization. *Journal of Polymer Science Part C-Polymer Symposium,* 1969, v27, pp77-&.
[66] Snuparek, J.J., Kreska, F. Semicontinuous Emulsion Copolymerization of Styrene and Butyl Acrylate. *Journal of Applied Polymer Science*, 1976, v20, pp1753-1764.
[67] Li, B., Brooks, B.W. Modeling and Simulation of Semibatch Emulsion Polymerization. *Journal of Applied Polymer Science*, 1993, v48, pp1811-1823.
[68] Bataille, P., Van, B. T., Pham, Q. B. On Semicontinuous Polymerization of Vinyl acetate. *Journal of Applied Polymer Science*, 1978, v22, pp3145-3161.
[69] Moritz, H.U. In: Reichert, K.H., Geisler, W.(Eds). Steric Stabilized Emulsion Polymerization of Vinyl Acetate. Influence of Process Conditions on Kinetics and Product Properties. *Polymer Reaction Engineering,* 1986, pp101-124.
[70] Wessling, R.A., Gibbs, D.S. A Study of Emulsion Polymerization Kinetics by the Method of Continuous Monomer Addition. *Journal of Macromolecular Science Chemistry*, 1973, v7, pp647-676.
[71] Aguilar, J., Rabelero, M., Nuno-Donlucas, S.M., Mendizabal, E., Martinez-Richa, A., Lopez, R.G., Arellano, M., Puig, J.E. Narrow Size-Distribution Poly(methyl methacrylate) Nanoparticles Made by Semicontinuous Heterophase Polymerisation, *Journal of Applied Polymer Science*, 2011, v119, pp1827-1834.

[72] Sajjadi S, Brooks BW. Semibatch Emulsion Polymerization Reactors: Polybutyl Acrylate Case Study. *Chemistry Engineering Science*, 2000, v55, pp4757

[73] Sajjadi S., Brooks BW. Unseeded Semibatch Emulsion Polymerization of Butyl Acrylate: Bimodal Particle Size Distribution. *Journal of Polymer Science Part A: Polymer Chemistry*, 2000, v38, pp528.

[74] Okubo, M., Fujimura, M., Mori, T. Studies on Suspension and Emulsion.120.The Acceleration of Decomposition of Potassium Persulfate in the Presence of Sodium Dodecyl-Sulfate and Polymer Particles as a Model of Emulsion Polymerisation System. *Colloid and Polymer Science,* 1991, v269, pp121-123.

[75] Sajjadi, S. Particle Formation and Coagulation in the Seeded Semibatch Emulsion Polymerisation of Butyl Acrylate. *Journal of Polymer Science: Part A: Polymer Chemistry*, 2000, v38, pp3612-3630.

[76] Sajjadi, S. Particle Formation under Monomer-Starved Conditions in the Semibatch Emulsion Polymerisation of St. Part II. Mathematical Modelling. *Polymer*, 2003, v44, pp223-237.

[77] Zeaiter, J., Romagnoli, J.A., Barton, G.W., Gomes, V.G., Hawkett, B.S., Gilbert, R.G. Operation of Semi-batch Emulsion Polymerisation Reactors: Modelling, Validation and Effect of Operating Conditions. *Chemical Engineering Science*, 2002, v57, pp2955–2969.

[78] Ramirez, A.G., Lopez, R.G., Tauer, K. Studied on Semibatch Microemulsion Polymerisation of Butyl Acrylate Influence of the Potassium Peroxodisulfate Concentration, *Macromolecules*, 2004, v37, pp2738-2747.

[79] Nomura, M., Minamino, Y., Fujita, K., Harada, M. The role of Chain Transfer Agents in the Emulsion Polymerisation of Styrene, *Journal of Polymer Science: Polymer Chemistry Edition*, 1982, v20, pp1261-1270.

[80] Suzuki, K., Nomura, M., Harada, M., Kinetics of Microemulsion Polymerisation of Styrene, *Colloids and Surfaces A-Physicochemical and Engineering Aspects*, 1999, v153, pp23-30.

[81] Chern, C., Chen, T.J., Wu, S.Y., Chu, H.B., Huang, C.F. Semibatch Seeded Emulsion Polymerization of Acrylic Monomers: Bimodal Particle Size Distribution. *Journal of Macromolecular Science: Pure and Applied Chemistry,* 1997, v34, pp1221-1236.

[82] Chern, C.S., Hsu, H., Lin, F.Y. Stability of Acrylic Latices in a Semibatch Reactor. *Journal of Applied Polymer Science,* 1996, v60, pp1301.

[83] Chern C.S., Lin F.Y. Stability of Carboxylated Poly(butyl acrylate) Latices During Semibatch Emulsion Polymerization. *Journal of Applied Polymer Science*, 1996, v61, pp989-1001.

[84] Sajjadi, S. Study of Different Types of Monomer Emulsion Feedings To Semibatch Emulsion Polymerisation Reactors, *Journal of Applied Polymer Science*, 2001, v82, pp2472-2477.

[85] Tang, C.B., Chu, F.X. Semicontinuous Emulsion Polymerisation of St-Butyl Acrylate-Methacrylic Acid with High Solid Content, *Journal of Applied Polymer Science*, 2001, v82, pp2352-2356.

[86] Krackeler, J.J., Naidus, H. Particle Size and Molecular Weight Distributions of Various Polystyrene Emulsions. *Journal of Polymer Science Part C: Polymer Symposia.* 1969, v27, pp207–235.

[87] Sajjaidi, S. Population Balance Modelling of Particle Size Distribution in Monomer-Starved SemibatchEmulsion Polymerisation, *AICHE Journal*, 2009, v55, pp3191-3205.

[88] He, G.W., Pan, Q.M., Rempel, G.L. Differential Microemulsion Polymerisation of St; A Mathematical Kinetic Model, *Journal of Applied Polymer Science*, 2007, v105, pp2129-2137.

[89] Liu, J.M., Pan, Q.M. Synthesis of Nanosized Poly(ethyl acrylate) Particles via Differential Emulsion Polymerisation, *Journal of Applied Polymer Science*, 2006, v102, pp1609-1614.

[90] Snuparek, J.J., Krska, F.J. Semicontinuous Emulsion Copolymerization of Styrene and Butyl Acrylate. *Journal of Applied Polymer Science,* 1976, v20, pp1753-1764.

[91] Misra, S.C., Pichot, C., El-Aasser, M.S., Vanderhoff, J.W. Effect of Emulsion Polymerization Process on the Morphology of Vinyl Acetate-Butyl Acrylate Copolymer Latex Films. *Journal of Polymer Science Part C-Polymer Letters*, 1979, v17, pp567-572.

[92] Chujo, K., Harada, Y., Tokuhara, S., Tanaka, K. Effects of Various Monomer Methods on Emulsion Copolymerization of Vinyl Acetate and Butyl Acrylate, *Journal of Polymer Science Part C-Polymer Symposium*, 1983, v21, pp321-&.

[93] Omi, S., Negishi, M., Kushibiki, K., Iso, M. Experimental and Modeling Study of Semi-continuous Emulsion Copolymerization of Styrene and Acrylonitrile. *Die Makromolekulare Chemie*, 1985, v10/11, pp149-158.

[94] Lovell, P.A. In Emulsion Polymerization and Emulsion Polymers; Lovell, P.A.; El-Aasser, M.S., Eds.; Wiley: Chichester, 1997; pp239

[95] Arzamendi, G., Leiza, J.R., Asua, J.M. Semicontinuous Emulsion Copolymerization of Methyl Methacrylate and Ethyl Acrylate. *Journal of Polymer Science Part A-Polymer Chemistry*, 1991, v29, pp1549-1559.
[96] Arzamendi, G., Asua, J.M. Copolymer Composition Control During the Seeded Emulsion Copolymerization of Vinyl Acetate and Methyl Acrylate. *Macromolecular Symposia*, 1990, v35-36, pp249-268.
[97] Arzamendi, G., Asua, J.M. Copolymer Composition Control of Emulsion Copolymers in Reactors with Limited Capacity for Heat Removal. *Industrial & Engineering Chemistry Research*, 1991, v30, pp1342-1350.
[98] Amalvy, J.I. Semicontinuous Emulsion Polymerization of Methyl Methacrylate, Ethyl Acrylate, and Methacrylic Acid, *Journal of Applied Polymer Science*, 1996, v59, pp339-344.
[99] Gugliotta, L.M., Arotcarena, M., Leiza, J.R., Asua, J.M. Estimation of Conversion and Copolymer Composition in Semicontinuous Emulsion Polymerization Using Calorimetric Data. *Polymer*, 1995, v36, pp2019–2023.
[100] Charmot, D. In *Polymeric Dispersions: Principles and Applications*; Asua, J.M., Ed.; NATO ASI Series; Kluwer, Academic Publishers, 1997; Vol. E-335, p79.
[101] Plessis, C., Arzamendi, G., Leiza, J.R., Schoonbrood, H.A.S., Charmot, D., Asua, J.M. A Decrease in Effective Acrylate Propagation Rate Constants Caused by Intramolecular Chain Transfer. *Macromolecules*, 2000, v33, pp4-7.
[102] Plessis, C., Arzamendi, G., Leiza, J.R., Alberdi, J. M., Schoonbrood, H.A.S., Charmot, D., Asua, J.M. Seeded Semibatch Emulsion Polymerisation of Butyl Acrylate: Effect of the Chain Transfer Agent on the Kinetic and Structural Properties, *Journal of Polymer Science Part A: Polymer Chemistry*, 2001, v39, pp1106-1119.
[103] Plessis, C., Arzamendi, G., Leiza, J.R., Schoonbrood, H.A.S., Charmot, D., Asua, J.M. Kinetics and Polymer Microstructure of the Seeded Semibatch Emulsion Copolymerisation of n-Butyl Acrylate and Styrene, *Macromolecules*, 2001, v34, pp5147-5157.
[104] Chern, C.S., Hsu, H. Semibatch Emulsion Copolymerization of Methyl Methacrylate and Butyl Acrylate. *Journal of Applied Polymer Science.* 1995, v55, pp571.
[105] Sayer, C., Lima, E.L., Pinto, J.C., Arzamendi, G., Asua, J.M. Kinetics of the Seeded Semicontinuous Emulsion Copolymerization of Methyl Methacrylate and Butyl Acrylate. *Journal of Polymer Science Part A: Polymer Chemistry*, 2000, v38, pp367.
[106] Elizalde, O., Arzamendi, G., Leiza, J.R., Asua, J.M. Seeded Semibatch Emulsion Copolymerisation of n-Butyl Acrylate and Methyl Methacrylate, *Industrial & Engineering Chemistry Research*, 2004, v43, pp7401-7409.
[107] Unzueta, E., Forcada, J. Semicontinuous Emulsion Copolymerization of Methyl Methacrylate and n-butyl acrylate: 2. Effect of Mixed Emulsifiers in Unseeded Polymerization. *Polymer*, 1995, v36, pp4301-4308.
[108] Chern C.S., Hsu H., Lin F.Y. Stability of acrylic latices in a semibatch reactor. *Journal of Applied Polymer Science*, 1996, v60, pp1301–1311.
[109] Ovando-Medina, V.M., Peralta, R.D., Mendizabal, E. Semicontinous Microemulsion Copolymerisation of Vinyl Acetate and Butyl Acrylate: High Solid Content and Effect of Monomer Addition Rate, *Colloid and Polymer Science*, 2009, v287, pp561-568.
[110] Bakhshi, H., Bouhendi, H., Zohyriaan-Mehr, M.J., Kabiri, K. Semibatch Emulsion Copolymerisation of Butyl Acrylate and Glycidyl Methacrylate: Effect of Operating Variables, *Journal of Applied Polymer Science*, 2010, v117, pp2771-2780.
[111] Hsu, S.C., Chiu, W.Y., Lee, C.F., Chang, H.S. Composition Control of Copolymer in Semibatch Emulsion Copolymerisation.II. MMA/St/BMA Three-Component System, *Journal of Polymer Science: Part A: Polymer Chemistry*, 2000, v38, pp3253-3269.
[112] Chern, C.S., Lin, F.Y. Semibatch Emulsion Polymerization of Butyl Acrylate: Effect of Functional Monomers. *Journal of Macromolecular Science: Pure and Applied Chemistry*, 1996, v33, pp1077-1096.
[113] Chern, C.S., Lin, F.Y. Stability of Carboxylated Poly(butyl acrylate) Latices During Semibatch Emulsion Polymerization. *Journal of Applied Polymer Science*, 1996, v61, pp989-1001.
[114] Chern, C.S., Lin, C.H. Semibatch Surfactant-free Emulsion Polymerization of Butyl Acrylate in the Presence of Carboxylic Monomers. *Polymer Journal*, 1996, v28, pp343–351.

[115] Chern, C.S., Chen, Y.C. Semibatch Emulsion Polymerization of Butyl Acrylate Stabilized by a Polymerizable Surfactant. ***Polymer Journal***, 1996, v28, pp627–632.

[116] Chern, C.S., Chen, Y.C. Kinetics of Semibatch Emulsion Polymerization of Butyl Acrylate Stabilized by a Reactive Surfactant. ***Journal of Macromolecular Science: Pure and Applied Chemistry***, 1998, v35, pp965–983.

[117] Xu, X.J., Chen, F. Semi-continuous Emulsion Copolymerization of Butyl Methacrylate with Polymerizable Anionic Surfactants. ***Polymer***, 2004, v45, pp4801–4810.

[118] Segall, I., Dimonie, V.L., Elaasser, M.S., Soskey, P.R., Mylonakis, S.G. Core-Shell Structured Latex-Particles.2.Synthesis and Characterization of Poly(n-Butyl Acrylate)/Poly(Benzyl Methacrylate-Styrene) Structured Latex-Particles, ***Journal of Applied Polymer Science***, 1995, v58, pp401-417.

[119] Sherman, R.L., Ford, W.T. Small Core/Thick Shell Polystyrene/poly(methyl methacrylate) Latexes, ***Industrial & Engineering Chemistry Research***, 2005, v44, pp8538-8541.

[120] Li, C., Wang, D., Liu, C.C. Preparation and Characterization of Polymer Core-shell Latex Particles, ***Journal of Dispersion Science and Technology***, 2008, v29, pp347-350.

[121] Facundo, I.A., Soria, M.J., Rosales, M.G., Elizalde, L.E., Diaz de Leon, R., Saade, H., Lopez, R.G. Synthesis and Characterization of Thermosensitive Core-shell Polymeric Nanoparticles, ***Polymer Bulletin***, 2011, v67, pp985-995.

[122] Mu, Y.C., Qiu, T., Li, X.C., Guan, Y.D., Zhang, S.W., Li, X.Y. Layer-by-Layer Synthesis of Multilayer Core-Shell Latex and the Film Formation Properties, ***Langmuir***, 2011, v27, pp4969-4978.

[123] He, G.W., Pan, Q.M. Synthesis of PolySt and PolySt/Poly(methyl methacrylate) Nanoparticles, ***Macromolecular Rapid Communications***, 2004, v25, pp1545-1548.

[124] Norakankorn, C., Pan, Q.M., Rempel, G.L., Kiatkamjonwong, S. Synthesis of Core/shell Structure of Glycidyl-Functionalized Poly(methyl methacrylate) Latex Nanoparticles via Differential Microemulsion Polymerisation, ***European Polymer Journal***, 2009, v45, pp2977-2986.

[125] Norakankorn, C., Pan, Q.M., Rempel, G.L., Kiatkamjonwong, S. Factorial Experimental Design on Synthesis of Functional Core/shell Polymeric Nanoparticles via Differential Microemulsion Polymerisation, ***Journal of Applied Polymer Science***, 2010, v116, pp1291-1298.

[126] Chen, W.B., Liu, X.Y., Liu, Y.S., Bang, Y., Kim, H. Synthesis of PMMA and PMMA/PS nanoparticles by Microemulsion Polymerisation with a New Vapor Monomer Feeding System, ***Colloids and Surfaces A: Physicochemical and Engineering Aspects***, 2010, v364, pp145-150.

[127] Aguiar, A., Gonzalez-Villegas, S., Rabelero, M., Medizabal, E., Puig, J.E. Core-shell Polymers with Improved Mechanical Properties Prepared by Microemulsion Polymerisation, ***Macromolecules***, 1999, v32, pp6767-6771.

[128] Rabelero, M., Lopez-Cuenca, S., Puca, M., Mendizabal, E., Esquena, J., Solans, C., Lopez, R.G., Puig, J.E. Composition Effects on the Mechanical Properties of Microemulsion-Made Core/Shell Polymers, ***Polymer***, 2005, v46, pp6182-6191.

[129] Shchukin, D.G., Sukhorukov, G.B. Selective YF3 Nanoparticle Formation in Polyelectrolyte Capsules as Microcontainers for Yttrium Recovery from Aqueous Solutions, ***Langmuir***, 2003, v19, pp4427-4431.

[130] Brand, T., Ratinac, K., Castro, J.V., Gilbert, R.G. Hollow Latex Particles as Submicrometer Reactors for Polymerization in Confined Geometries, ***Journal of Polymer Science Part A-Polymer Chemistry***, 2004, v42, pp5706-5713.

[131] Lajoinie, G., Gelderblom, E., Chlon, C., Bohmer, M., Manohar, S., Versluis, M. Characterization of an Innovative Drug Carrying Photoacoustic Contrast Agent: Fluorescent Polymer Microcapsules, ***The Journal of the Acoustical Society of America***, 2012, v131, pp3247.

[132] Costa, N., Sher, P., Mano, J.F. Liquefied Capsules Coated with Mutilayered Polyelectrolyte Films for Cell Immobilization, ***Advanced Engineering Materials***, 2011, v13, ppB218-B224.

[133] Donath, E., Sukhorukov, G.B., Caruso, F., Davis, H., Mohwald, H. Novel Hollow Polymer Shells by Colloid-templated Assembly of Polyelectrolytes, ***Angewandte Chemie International Edition***, 1998, v37, pp2005-2201.

[134] Park, M.K., Xia, C., Advincula, R.C., Schutz, P., Caruso, F. Cross-linked, Luminescent Spherical Colloidal and Hollow-shell Particles, ***Langmuir***, 2001, v17, pp7670-7674.

[135] Marinakos, S.M., Shultz, D.A., Feldheim, D.L. Gold Nanoparticles as Templates for the Synthesis of Hollow Nanometer-sized Conductive Polymer Capsules, ***Advanced Material***, 1999, v11, pp34-37.

[136] Okubo, M., Konishi, Y., Minami, H. Production of Hollow Polymer Particles by Suspension Polymerisation, *Colloid and Polymer Science*, 1998, v276, pp638-642.
[137] Okubo, M., Konishi, Y., Minami, H. Production of Hollow Polymer Particles by Suspension Polymerisations for Divinylbenzene/toluene Droplets Dissolving Various Polymers, *Colloidal and Polymer Science*, 2000, v278, pp659-664.
[138] McDonald, C.J., Devon, M.J. Hollow Latex Particles: Synthesis and Applications, *Advances in Colloid and Interface Science*, 2002, v99, pp181-213.
[139] Zoldesi, C.I., Imhof, A. Synthesis of Monodisperse Colloidal Spheres, Capsules, and Microballoons by Emulsion Templating, *Advanced Material*, 2005, v17, pp924-928.
[140] Discher, B.M., Won, Y.Y., Ege, D.S., Lee, J.C.M., Bates, F.S., Discher, D.E., Hammer, D.A. Polymersomes: Tough Vesicles Made From Diblock Copolymers, *Science*, 1999, v284, pp1143-1146.
[141] Chen, D.Y., Jiang, M. Strategies for Constructing Polymeric Micelles and Hollow Spheres in Solution via Specific Intermolecular Interaction, *Accounts of Chemical Research*, 2005, v38, pp494-502.
[142] Zhang, Y.W., Jiang, M., Zhao, J.X., Ren, X.W., Chen, D.Y., Zhang, G.Z. A Novel Route to Thermosensitive Polymeric Core-Shell Aggregates and Hollow Spheres in Aqueous Media, *Advanced Functional Materials*, 2005, v15, pp695-699.
[143] Dejugnat, C., Sukhorukov, G.B. pH-Responsive Properties of Hollow Polyelectrolyte Microcapsules Templated on Various Cores, *Langmuir*, 2004, v20, pp7265-7269.
[144] Lv, H., Lin, Q., Zhang, K., Yu, K., Yao, T.J., Zhang, X.H., Zhang, J.H., Yang, B. Facile Fabrication of Monodisperse Polymer Hollow Spheres, *Langmuir*, 2008, v24, pp13736-13741.
[145] Lapeyre, V., Renaudie, N., Dechezelles, J.F., Saadaoui, H., Ravaine, S., Ravaine, V. Multiresponsive Hybrid Microgels and Hollow Capsules with a Layered Structure, *Langmuir*, 2009, v25, pp4659-4667.
[146] Li, B., Brooks, B.W. Semi-batch Processes for Emulsion Polymerisation, *Polymer International*, 1992, v29, pp41-46.
[147] Rios, L., Cruz, M.A., Palacios, J., Ruiz, L.M., Garcia-Rejon, A. *Makromol. Chem. Suppl.*, 1985, v10/11, pp477-488.
[148] Lee, K.C. PhD thesis, Lehigh university(1987), *Dissertation Abstracts International [Section] B: The Sciences & Engineering*, 1988, v49, pp176.
[149] El-Aasser, M.S., Makgawinata, T., Misra, T., Vanderhoff, S.C., Pichot, J.W., Llauro, M.F. In Emulsion Polymerisation of Vinyl Acetate, ed. El-Aasser, M.S., Vanderhoff, J.W. *Applied Science*, London, 1981, pp215-252.
[150] El-Aasser, M.S., Makgawinata, T., Vanderhoff, J.W. Batch and Semicontinuous Emulsion Co-polymerization of Vinyl Acetate Butyl Acrylate.1.Bulk, Surface, and Colloidal Properties of Co-polymer Latexes. *Journal of Polymer Science Part A-Polymer Chemistry*, 1983, v21, pp2363-2382.
[151] Sajjadi, S., Yianneskis, M. Semibatch Emulsion Polymerisation of Methyl Methacrylate with a Neat Monomer Feed, *Polymer Reaction Engineering*, 2003, v11, pp715-736.
[152] Vanderhoff, J.W. Mechanism of Emulsion Polymerisation. *Journal of Polymer Science-Polymer Symposia*, 1985, v72, pp161-198.
[153] Puig, J. E. in Encyclopedia of Polymeric Materials, Salamone, J.P.(Ed.), CRC Press, Boca Raton, 1996, v6, pp4333-4341.
[154] Rodriguez-Guadarrama, L. A., Mendizabal, E., Puig, J.E., Kaler, E.W. Polymerization of Methyl Methacrylate in 3-component Cationic Microemulsion. *Journal of Applied Polymer Science*, 1993, v48, pp775-786 .
[155] Escalante, J.I., Rodriguez-Guadarrama, L.A., Mendizabal, E., Puig, J.E., Lopez, R.G., Katime, I. Synthesis of Poly(butyl methacrylate) in Three-component Cationic microemulsions, *Journal of Applied Polymer Science*. 1996, v62, pp1313-1323.
[156] Full, A.P., Kaler, E.W., Arellano, J., Puig, J.E. Microemulsion Polymerization of Styrene: The Effect of Salt and Structure , *Macromolecules*, 1996, v29, pp2764-2775.
[157] Norakankorn, C.W., Pan, Q.M., Rempel, G.L., Kiatkamjornwong, S. Synthesis of Poly(methyl methacrylate) Nanoparticles Initiated by Azobisisobutyronitrile Using a Differential Microemulsion Polymerisation Technique, *Journal of Applied Polymer Science*, 2009, v113, pp375-382.
[158] Ledzema, R., Trevine, M.E., Elizalde, L.E., Perez-Carrillo, L.A., Mendizabal, E., Puig, J.E., Lopez, R.G. Semicontinuous Heterophase Polymerization under Monomer Starved Conditions to Prepare

Nanoparticles with Narrow Size Distribution, *Journal of Polymer Science: Part A: Polymer Chemistry*, 2007, v45, pp1463–1473.

[159] Minari, R.J., Caceres, G., Mandelli, P., Yossen, M.M., Gonzalez-Sierra, M., Vega, J.R., Gugliotta, L.M. Semibatch Aqueous-solution Polymerisation of Acrylic Acid: Simultaneous Control of Molar Masses and Reaction Temperature, *Macromolecular Reaction Engineering*, 2011, v5, pp223-231.

[160] Uraneck, C.A., Burleigh, J.E. Modification of Emulsion Polymerisation by Multiple Addition of Modifier, *Journal of Applied Polymer Science*, 1971, v15, pp1757-1768.

[161] Baus, R.E., Swift, G. US Patent No. 4 501 845, 1985.

[162] Paine, A.J., Pontes, F.M., Moffat, K.A. U.S. Patent No. 5 444 140, 1995.

[163] Harelle, L., Pith, T., Hu, G., Lambla, M. Chain Transfer Behavior of Fractionated Commercial Mercaptans in Emulsion Polymerisation of Styrene, *Journal of Applied Polymer Science,* 1994, v52, pp1105-1113.

[164] Salazar, A., Gugliotta, L.M., Vega, J.R., Meira, G.R. Molecular Weight Control in a Starved Emulsion Polymerisation of Styrene, *Industrial & Engineering Chemistry Research*, 1998, v37, pp3582-3591.

[165] Gugliotta, L.M., Salazar, A., Vega, J.R., Meira, G.R. Emulsion polymerisation of Styrene. Use of n-nonyl mercaptan for molecular weight control, *Polymer*, 2001, v42, pp2719-2726.

[166] Zubitur, M., Asua, J.M. Improving Chain Transfer Agent Mass Transfer in the Semicontinuous Emulsion Copolymerization of Vinyl Acetate/butyl Acrylate, *Macromolecular Materials and Engineering*, 2001, v286, pp362-368.

[167] Plessis, C., Arzamendi, G., Leiza, J.R., Alberdi, J.M., Schoonbrood, H.A.S., Charmot, D. and Asua, J.M. Seeded Semibatch Emulsion Polymerization of Butyl Acrylate: Effect of the Chain-transfer Agent on the Kinetics and Structural Properties. *Journal of Polymer Science: Part A: Polymer Chemistry*, 2001, v39, pp1106-1119.

[168] Braun, O., Selb, J., Candau, F. Synthesis in Microemulsion and Characterization of Stimuli-responsive Polyelectrolytes and Polyampholytes Based on *N*-isopropylacrylamide, *Polymer*, 2001, v42, pp8499-8510.

[169] Zhang, Q.S., Zha, L.S., Ma, J.H., Liang, B. A Novel Route to Prepare pH- and Temperature-Sensitive Nanogels via a Semibatch Process, *Journal of Colloid and Interface Science*, 2009, v330, pp330-336.

[170] Li, H.H., O'Shea, J.P., Franks, G.V. Effect of Molecular Weight of Poly(n-isopropylacrylamide) Temperature-Sensitive Flocculants on Dewatering, *AIChE Journal*, 2009, v55, pp2070-2080.

[171] Shiraishi, Y., Adachi, K., Tanaka, S., Hirai, T. Effects of Poly-n-isopropylacrylamide on Fluorescence Properties of Cds/Cd(OH)2 Nanoparticles in Water, *Journal of Photochemistry and Photobiology A: Chemistry*, 2009, v205, pp51-56.

[172] Chai, S.G., Zhang, J.Z., Yang, T.T., Yuan, J.J., Cheng, S.Y. Thermoresponsive Microgel Decorated with Silica Nanoparticles in Shell: Biomimetic Synthesis and Drug Release Application, *Colloids and Surfaces A: Physicochemical and Engineering Aspects*, 2010, v356, pp32-39.

[173] Chuayjuljit, S., Boonmahitthisud, A. Natural Rubber Nanocomposites Using Polystyrene-Encapsulated Nanosilica Prepared by Differential Microemulsion Polymerization, *Applied Surface Science*, 2010, v256, pp7211-7216.

[174] Sheibat-Othman, N., Bourgeat-Lami, E. Use of Silica Particles for the Formation of Organic-Inorganic Particles by Surfactant-free Emulsion Polymerisation, *Langmuir*, 2009, v25, pp10121-10133.

Chapter 2 Experimental Procedures

This chapter focuses on the chemicals, apparatus and measurements involved in the present study for the synthesis and characterization of resulting polymeric latexes. Different methods has been explained for the characterization of monomer conversion, particle size and size distributions, zeta potential and morphology of particles, molecular weight and glass transition temperature of resulting polymers and turbidity, pH as well as conductivity of the latexes.

2.1 Chemicals

Analytical grade potassium persulfate (Aldrich), sodium lauryl sulfate (Aldrich) and sodium hydrogen carbonate (Aldrich), were used as initiator, emulsifier and buffer, respectively. 2-Butanethiol and 1-Decanethiol (Aldrich) were used as chain transfer agents (CTAs). The styrene (St), vinyl acetate (VA) and methyl methacrylate (MMA) monomers were supplied at 99.9% purity by Aldrich and inhibited against thermal polymerisation with trace quantities of an inhibitor. This inhibitor was removed prior to the use by an ion exchange column (Aldrich). Uninhibited monomer was stored at -20ºC and used within a week. *N*,*N*,*N*′,*N*′-Tetramethylethylenediamine (TEMED, 99%, Aldrich) was used as initiator accelerator. *N*-isopropylacrylamide (NIPAM) was supplied at 99% purity by ACROS, inhibited against thermal polymerisation with trace quantities of an inhibitor. The monomer was stored at -8ºC and used directly. *N*,*N*'-Methylene bisacrylamide (MBA, Aldrich) was used as crosslinker. LUDOX TM-50 colloidal silica latex was purchased from Aldrich-sigma. 0.1M hydrochloric acid (HCl) was supplied by Aldrich.

2.2 Apparatus

The apparatus for semibatch emulsion polymerisation experiments is shown in Figure 2.1. A round-bottomed jacketed glass reaction vessel was equipped with a four-bladed stainless steel flat turbine-type impeller with a width of half of vessel diameter, a standard four baffle plates with the width of 1/10 of vessel diameter located at 90° intervals, a thermocouple, a sampling device, a port for nitrogen purge and an inlet for feeding ingredients. Two different sizes of reaction vessel, which are 0.5 and 1 L, were used. The agitation rate was always set at a given value that was maintained in the course of reaction by the motor stirrer. The temperature of the reactor contents was controlled by pumping water with appropriate temperature from a water bath through the jacket and monitored by a digital thermometer. A syringe pump with a high precision was used for monomer feeding. Sampling was carried out through a port at the desired time intervals by removing an aliquot of 1-2 g latex by a hypodermic syringe.

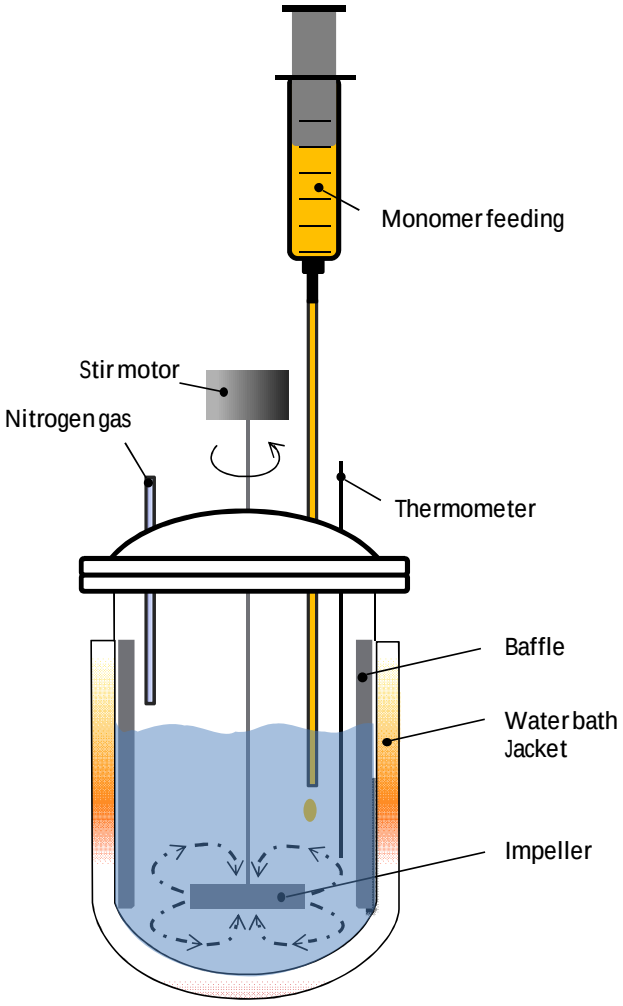

Figure 2.1. Schematic of experimental rig

2.3 Measurements

2.3.1 Conversions

Conversions were all measured by a gravimetric method. The latex mixtures taken from the reactor were placed in aluminium foil plates and quickly weighed by a four figure scale followed by addition of a few droplets of methanol at once to precipitate the polymer and stop the possible reaction. The samples were dried in an oven until constant weight, usually achieved within 18 h at 65°C.

For batch process, the conversion (x) can be calculated as:

$$x = \frac{weight\ of\ polymer\ formed}{weight\ of\ monomer\ in\ the\ recipe} = \frac{w_{dry} - w_{salt}}{w_{latex} - w_{water} - w_{salt}} \tag{2.1}$$

where w_{latex}, w_{water}, $w_{\text{salt,}}$ and w_{dry} are the weight of sample of latex, water, and salt in it (i.e. KPS and buffer) and dried sample.

For semibatch process, there are two types of conversions involved. One is the instantaneous conversion at a given time t, x_{i}, defined as the weight ratio of the polymer formed in the reactor to the total monomer fed into the reactor by the time t. The instantaneous conversion can be considered as a measure of polymer particle composition (monomer-polymer ratio). It can be obtained from Equation 2.1.

The other one is the overall conversion (x_{o}), which is defined as the weight ratio of the polymer produced in the reactor to the total monomer in the recipe. It can be calculated as:

$$x_o = \frac{weight\ of\ polymer\ formed}{weight\ of\ monomer\ in\ the\ receipe} = \frac{R_a t \rho_m x_i}{w_{mon}} \tag{2.2}$$

where w_{mon} is the total weight of monomer in the receipt, R_{a} is the rate of monomer addition, t is the addition time and ρ_{m} is the density of monomer.

The overall conversion is a measure of the overall rate of polymerisation (R_{p}), which its steady-state value can be calculated from the gradient of the linear part of the overall conversion-time curves for each experiment.

2.3.2 Size of particles

Z-average diameters of particles were measured using dynamic light scattering technique (DLS; see Appendix A) at desired temperature. DLS measures the Brownian motion and relates this to the size of particles using the Stokes-Einstein equation:

$$\mathrm{d(H)} = \frac{k\mathrm{T}}{3\pi\eta D} \tag{2.3}$$

where d(H) is the hydrodynamic diameter, k is the Boltzmann's constant, T is absolute temperature, D is translational diffusion coefficient and η is the viscosity of the continuous phase.

One should notice that the hydrodynamic diameter measured by DLS is a value that refers to how a particle diffuses with a fluid and is always affected by the surface structure of particles, conformation of polymer chains as well as the viscosity of the medium. Furthermore, if the shape of a particle changes in a way that affects the diffusion speed, the hydrodynamic size will change. The main advantage of the technique is that size information can be obtained in the order of minutes and it is almost completely automated so that routine measurements are easily reproduced.

Precautions need to be taken for the concentration of sample. If sample concentration is too low, there may not be enough light scattered to a make a measurement. If the sample is too concentrated, the light scattered by one particle will itself be scattered by another (known as multiple scattering). The upper limit of the concentration is also governed by the point at which the particles cannot freely diffuse, due to particle interactions. Generally, the sample concentration was selected such that the sample exhibits a slightly cloudy appearance. When the particle size of the sample was so small that even concentrated dispersions did not show any turbidity, various concentrations of the sample were measured in order to find the optimum conditions and avoid concentration dependent effects.

In order to obtain a reliable particle size distribution (PSD), selected samples were first diluted with de-ionized water and then dried onto glass slides and carbon-coated copper girds for the examination of scanning electron microscopy (SEM; Hitachi, S4000) and transmission electron microscopy (TEM; Nippon, 200kv), respectively. More than 2000 particles were counted for each example. For the PSD presentation, all particles in the range of a size increment were assigned to the higher bound of the size increment for the bin, as shown in Figure 2.2. The volume-average particle diameter (D_v) can be calculated with the following equation:

$$D_\mathrm{v} = \left[\frac{\sum_{\mathrm{i}=1}^{n} n_\mathrm{i} D_\mathrm{i}^3}{\sum_{\mathrm{i}=1}^{n} n_\mathrm{i}}\right]^{1/3} \tag{2.4}$$

where n_i is the number of particles with diameter D_i.

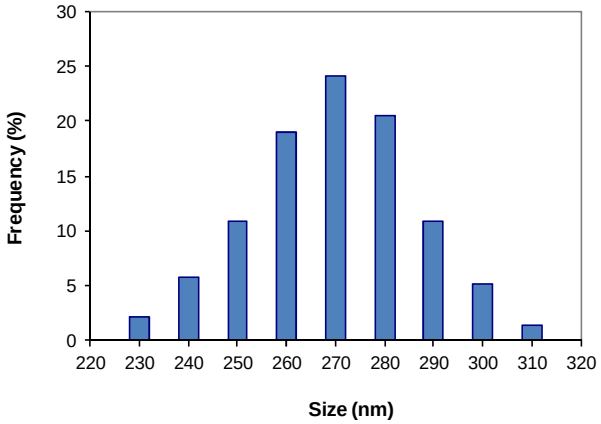

Figure 2.2. A typical PSD obtained from TEM or SEM

2.3.3 Number of particles (N_p)

Given the mass of polymer produced in the system and the average particle diameter, it is possible to calculate the number of particles according to the following equation:

$$N_{\mathrm{p}} = \frac{m_{\mathrm{p}}}{\pi/_{6} D_{\mathrm{v}}^{3} \rho_{\mathrm{p}}} \tag{2.5}$$

where m_p is the mass of polymer produced in the system at any given time and ρ_p is the polymer density. The volume-average diameter of unswollen polymer particles, D_v, can be obtained using a conversion factor, C_f, so that:

$$D_{\mathrm{v}} = C_f \cdot D_{\mathrm{z,dls}} \tag{2.6}$$

where $D_{z,dls}$ is the z-average diameter obtained by DLS. The conversion factor can be found from the comparison of volume-average obtained by TEM or SEM with $D_{z,dls}$.

2.3.4 Surface coverage ratio (θ)

Using D_v data and total amount of emulsifier in the reactor, it is possible to estimate the surface coverage ratio of particles (θ), which was calculated using Langmuir model:

$$\theta = \frac{K S_{\mathrm{c}}}{1 + K S_{\mathrm{c}}} \tag{2.7}$$

where S_c is the equilibrium surfactant concentration in the water phase, and K is the adsorption constant with a typical value of 6000 l·mol^{-1} for SDS [1]. The amount of adsorbed surfactant at the interface (S_d) is given by:

$$S_{\mathrm{d}} = \left(\frac{\pi D_{\mathrm{ps}}^{2} N_{\mathrm{p}} \theta (\mathrm{M_{SDS}}/N_{\mathrm{A}})}{\alpha_{\mathrm{s}}} \right) \tag{2.8}$$

[1] Kalinin, V.V., Radke, C.J. An ion-binding model for ionic surfactant adsorption at aqueous-fluid interfaces. *Colloids and surface a-Physicochemical and Engineering Aspects*, 1996, v114, pp337-350.

where α_s is the area occupied by an emulsifier molecule on the surface of polymer particles, which is 0.43 nm^2 for SDS [2]. N_A is Avogadro's constant and M_{SDS} is the molecular weight of SDS. D_{ps} is the average diameter of the monomer swollen particles, which can be calculated as:

$$D_{ps} = \left(\frac{6(m_p/\rho_p + m_m/\rho_m)}{\pi N_p}\right)^{1/3} \quad (2.9)$$

where m_m and ρ_m are the mass of unreacted monomer in the system and density of monomer. Equations 2.7 and 2.8 were simultaneously solved, using an overall mass balance equation for the surfactant as $S_t = S_c + S_d$, where S_t is the total amount of surfactant in the system, to give θ.

2.3.5 Molecular weight of polymer

The weight-average molecular weight ($\bar{M}_w$) of polymer was measured by static light scattering technique (SLS), where simplified Rayleigh equation is applied (see Appendix A):

$$\frac{KC}{R_\theta} = \left(\frac{1}{\bar{M}_w} + 2A_2C\right) \quad (2.10)$$

where K is a optical constant. R_θ, the Rayleigh ratio, is the ratio of scattered light to incident light of the sample. C and A_2 are the concentration of samples and the 2nd virial coefficient, respectively. The latter is a parameter describing the interaction strength between the macromolecules and the solvent (see Appendix A).

Selected samples were first precipitated in methanol and dried in the oven. The weighed and dried samples were then dissolved in a solvent (toluene or water, depending on the type of polymer). Polymer solutions with different concentrations, which are 0.25 g·l_{aq}^{-1}, 0.50 g·l_{aq}^{-1}, 0.75 g·l_{aq}^{-1} and 1.00 g·l_{aq}^{-1}, were produced. Each molecular weight measurement involves several individual measurements, from the solvent used only through polymer solutions at various concentrations. A Debye plot is then obtained by plotting the sample scattering intensity (KC/R_θ) against sample concentration. $\bar{M}_w$ is determined from the intercept at zero concentration and expressed in Daltons (or g·mol^{-1}).

2.3.6 Zeta potential

The Zetasizer calculates the zeta potential by determining the electrophoretic mobility which is obtained by performing an electrophoresis analysis on the sample and measuring the velocity of the particles using laser Doppler velocimetry (LDV; see Appendix A). A laser is used as the light source and split to provide an incident and reference beam. The incident laser beam passes through the centre of the sample cell, and the scattered light is detected at a forward angel (17º). In combination with the reference beam, a fluctuating intensity signal was obtained where the

[2] Sajjadi, S. Particle Formation under Monomer-starved Conditions in the Semibatch Emulsion Polymerisation of Styrene. Part II. Mathematical . *Polymer*, 2003, v44, pp223-237.

rate of fluctuation is proportional to the speed of the particles. In order to avoid any change in the existing state of the surface during the process of dilution, the original samples are directly used for the measurements. One should notice that a zeta potential value on its own without a quoted pH is a virtually meaningless number.

2.3.7 Glass transition temperature

The glass transition temperatures (T_g) of polymer is determined by dynamic scanning calorimeter (DSC; Mettler Toledo DSC822e). Aluminium pans are used for all measurements. The instrument is first calibrated with indium. Measurements are performed on samples of around 10 mg. The samples are first heated slightly above the melting point of the material at 20°C·min^{-1} heating rate and held at this temperature for 10 min to remove the thermal history, followed by quenching to room temperature. A heating rate of 10°C·min^{-1} is then used for the second heat run. The T_g is taken as the midpoint of the heat capacity change in the second heating run.

2.3.8 Turbidimetric measurement

Turbidity of the latex is determined using an ultraviolet-visible spectroscopy (UV-VIS; PerkinElmer, USA). The temperature of sample is monitored using a thermocouple. The transmittance is measured as a function of temperature (ºC) at a wavelength of 600 nm. In order to avoid the concentration effect (see Appendix B), the original samples were used without any dilution.

2.3.9 Conductivity

The conductivity of selected samples is measured by conductivity meter (MeterLab, CDM230). The device is first calibrated using standard solution with known conductivity. Measurements are preformed at desired temperature under mild stirring. The probe of the meter was fully immersed in the latex during measurements.

2.3.10 pH

The pH of the latexes is measured by pH meter (HANNA instruments, pH 213). The device is first calibrated with standard buffer solutions with different pH. Measurements are preformed at desired temperature under mild agitation.

2.3.11 Reproducibility

Some of experiments were repeated twice. The reproducibility of the results was quite good as there was no significant change in the rate of polymerisation and particle size. Only minor variations in the final conversions were recorded for some reproduced runs. Typical reproducibility tests are shown in Appendix C.

Chapter 3 Microemulsion Polymerisation of Styrene

In this chapter, semicontinuous microemulsion polymerisations of styrene under monomer-starved conditions have been carried out. Monomer conversions, particle sizes and molecular weight of polymer chains have been closely monitored in the course of reaction. In subsection 3.1, particle formation has been investigated during particle nucleation stage. Effects of process parameters on the kinetics of polymerisation as well as the properties of resulting polymer particles have been studied. In subsection 3.2, the minimum sizes of particles achievable via semicontinuous microemulsion polymerisations have been explored by optimizing the reaction conditions as well as process parameters. As an alternative way of reducing the particle size via semicontinuous process, a water-soluble chain transfer agent has been applied to control the average length of polymer chains as well as the particle growth. The work has been reported in subsection 3.3.

3.1 New Insights into Semicontinuous Microemulsion Polymerisation as a Means to Produce Nanolatexes: Analysis of Nucleation Stage

Abstract: In most researches on semicontinuous emulsion polymerisation, particle size average and size distributions have been reported for the end of polymerisation where monomer is depleted and micelles do exist. In many others, particles size distributions are reported when micelles are fully depleted and particles have grown during the growth stage. This implies that the history of particle size evolution, which is required for a mechanistic study, is either lost due to incomplete nucleation or is masked due to subsequent growth during post nucleation. In this research, particle formation is decoupled from particle growth by close monitoring of the end of nucleation. Effects of rate of monomer addition (R_a) and surfactant concentration ([*S*]) on the kinetics, particle size average and distribution, number of particles and molecular weight of product were studied. The results showed that the rate of polymerisation (R_p), the size of particles (*D*) as well as the particle size distribution (PSD) at the end of nucleation can be controlled by R_a. The variations in the number of particles with R_a and [*S*] were investigated and compared with a kinetic model. Nanolatexes with extremely sharp particle size distribution with particle size as small as 10 nm were obtained. Increasing [*S*] can increase the number of particles by providing more micelles for particle formation and prolonging the nucleation period. However, *D* at the end of nucleation was found to be independent of [*S*]. Furthermore, it is found that, chain termination by secondary entry of free radicals becomes progressively more important with decreasing R_a, which is different from what is often believed. As a result, the weight-average molecular weight ($\bar{M}_w$) of the polymer produced decreased with R_a. Single chain polymer particles could only be formed at early stage of nucleation.

3.1.1 Introduction

Semicontinuous microemulsion, or monomer-starved emulsion polymerisation is a novel and powerful technique that can produce concentrated nano-latexes (> 40wt%) using a low concentration of surfactant [1-7]. The resulting nanomatierials have a number of applications such as ultrathin films, high performance coating materials, modified materials, adhesives, semiconductor and drug delivery nanocarriers used for penetrating various biological barriers within the human body [8-14]. Nanolatexes of different monomers have been studied, such as butyl acrylate (BA), methyl methacrylate (MMA), styrene (St), butyl methacrylate (BMA), vinyl acetate (VA), ethyl acrylate (EA), methyl acrylate (MA) and n-isopropylacrylamide (NIPAM) [4,7,15-19]. Tiny particles with narrow size distribution have been produced [4,17,20-26]. Furthermore, particles with core-shell structures and functionalized groups have been synthesised as well [17,27-31] using this technique.

Nomura showed that if polymerisation is carried out in the presence of small quantity of monomer, particle formation is enhanced [32]. Sajjadi pointed out the presence of large quantity of monomer in the reactor initial charge or a high rate of monomer addition will cause flooded conditions to be dominant leading to rapid growth of particles and therefore smaller number of particles [33]. In a typical semicontinuous microemulsion polymerisation, the volume growth rate of particles is controlled at a very low value by the rate of monomer addition (R_a). This reduces the rate of depletion of emulsifier micelles. As a result, particle formation is prolonged and particles with narrow size distribution can be produced [2,34-35].

A few groups have studied particle nucleation in such systems and have indicated how particle size and number vary with reaction conditions. Puig's group [21,26] investigated the effect of surfactant concentration [S] and R_a on the particle size and particle number (N_p) for MMA. By decreasing R_a from 9.67 to 0.73 $g \cdot min^{-1} \cdot l_{aq}^{-1}$, the final weight-average size of particle (D_w) was decreased from 33.3 to 19.7 nm and the exponent of D_w in terms of R_a was 0.1971. N_p increased continuously during the whole course of monomer addition for all the addition rates used and the increase in N_p was more significant as R_a decreased. By increasing [S] from 10 to 50 $g \cdot l_{aq}^{-1}$, the final number-average size of particle (D_n) decreased from 32 to 23 nm. Furthermore, the molar masses remained practically unchanged throughout the reaction for all [S], ranged from 10 to 50 $g \cdot l_{aq}^{-1}$, but diminished as R_a decreased. Rempel's group studied the effect of [S] and R_a on particles size and N_p for MMA and St [22-23]. They called the process as differential microemulsion polymerisation probably because monomer was added in shots over the reaction time. Their results showed that the size of particles continuously decreased with increasing [S] for both monomers. In terms of number, N_p increased with increasing [S]; however, the rate of increase became slower at higher [S]. When R_a is high, larger particles were formed. Kim's group [16] worked on microemulsion polymerisation with a vapour monomer feeding system to

synthesis PMMA and PMMA/PS nanoparticles. Their results confirmed that the size of particles decreased slightly at higher [S] and lower R_a.

In the most previous works cited, the dependence of N_p on R_a and [S] was reported disregard of nucleation stage and there was no reference to the end of particle nucleation stage. In some of the works, particle nucleation was completed by the end of monomer feeding, whereas in many others particle nucleation continued well beyond monomer feeding time. Furthermore, the absence of monomer droplets in the systems under study was not verified in most cited articles. It comes as no surprise that there are such significant variations in N_p and D with process formulations. From above, it can be easily inferred that the exact relation between D and N_p versus R_a and [S] is not really known.

Sajjadi conducted semicontinuous microemulsion polymerisation of several monomers under the conditions that utilisation of surfactant micelles was assured (end of nucleation). He showed that N_p is proportional to [S] and R_a for the styrene microemulsion polymerisation. He developed a model based on the completion of nucleation which shows the effect of R_a and [S] on N_p for styrenic monomers [34]:

$$N_p = k(a_s[S])R_I^{2/3}R_a^{-2/3} \tag{3.1.1}$$

The details of this equation have been explained in page 13. This equation predicts that N_p is inversely proportional to $R_a^{2/3}$. Sajjadi also derived and equation for the volume size of particles at the end of nucleation [36].

$$d_v = (6/\pi)^{1/3}(R_a/R_I)^{1/3} \tag{3.1.2}$$

where d_v is the volume-average diameter of polymer particles at the end of nucleation. Equations 3.1.1 and 3.1.2 show that although N_p increases with [S], the size of latex particles is independent of [S]. On the other hand, the average size of latex particles at the completion of nucleation is proportional to R_a with an exponent of 1/3.

Despite all recent understanding of semicontinuous microemulsion polymerisation, there is no experimental data available in the literature on particle size at the end of nucleation. Most experimental data available in the literature are based on the size of particles at intermediate conversions or final conversions [2]. Such data cannot reflect true features of particle size and size distribution at the end of nucleation because of concurrent growth and possible coagulation in the course of addition. In this work, particle nucleation in the course of addition in semicontinuous microemulsion polymerisation of styrene has been closely monitored. The effects of [S] and R_a on kinetics, particle size and distribution, number of particles and average molecular weights are reported and compared with the theoretical developments reported in the literature.

3.1.2 Experimental Work

3.1.2.1 Procedure

The reactor was initially charged with most of the de-ionised water (570 ml), a weighed quantity of surfactant and buffer (0.2016 g) and allowed to heat up to the reaction temperature (70°C) while being purged with nitrogen under strong mixing (450 rpm). The purging was continued at the reaction temperature for another 15 min. Then the nitrogen line was lifted to sit well above the surface of the water to prevent evaporation. The nitrogen rate was turned down to provide only slight overpressure and the agitation speed was then reduced to 300 rpm. An amount of 0.6489 g of KPS dissolved in 30 ml of de-ionised water from the overall recipe was then added to the vessel. The system was allowed to return to reaction temperature. Prior to addition, the monomer was purged with nitrogen for 15 min to remove the oxygen dissolved. The monomer addition was started instantly with a dosing pump at a given rate. The onset of reaction was continuously monitored by sampling from the vessel and precipitating the sample in methanol. Generally, inhibition periods of 1-3 min were observed. The reaction time *zero* for the start of reaction was considered when the first droplet of monomer was added into the reactor. The micellar solution was initially clear and transparent but became translucent to opaque with the progress of polymerisation. The viscosity of the emulsion increased with the progress of reaction as the solids content increased.

3.1.2.2 Measurements

Conversions were measured gravimetrically. There are two types of conversion; one is the overall conversion, x_o, defined as the weight ratio of the polymer produced in the reactor to the total monomer in the recipe. The other is the instantaneous conversion at a given time t, x_i, defined as the weight ratio of the polymer formed in the reactor to the total monomer fed into the reactor by the time t. The details of calculation have been given in page 35.

The overall rate of polymerisation (R_p) was calculated from the gradient of the linear part (ignoring the first few min of addition) of the overall conversion-time curves for each experiment. In order to obtain a better understanding of particle growth, the z-average diameter of particles (D_z) was measured in the course of polymerisation using dynamic light scattering (Zetasizer, Malvern). Selected samples were examined by using transmission electron microscope (TEM; Nippon, 200kv). Particle size distribution as well as the volume-average particle diameter (D_v) was calculated with the following equation:

$$D_v = \left[\frac{\sum_{i=1}^{n} n_i D_i^3}{\sum_{i=1}^{n} n_i}\right]^{1/3} \qquad (3.1.3)$$

From the comparison of z-average and volume-average obtained by TEM with z-average obtained by dynamic light scattering ($D_{z,dls}$), the conversion factor of $C_f = 0.90$ was found so that $D_{v,} = C_f \cdot D_{z,dls}$.

The number of particles was calculated according to the following equation:

$$N_p = \frac{\rho_m R_a t x_i}{\pi/_6 D_v^3 \rho_p} \tag{3.1.4}$$

where x_i is the instantaneous conversion at time t, D_v is the volume-average diameter of unswollen polymer particles, R_a is the rate of monomer addition ($ml \cdot h^{-1}$), ρ_m and ρ_p are the density of styrene monomer and polystyrene, which is 0.909 $g \cdot ml^{-1}$ and 1.044 $g \cdot ml^{-1}$ [37], respectively.

Using the D_v data and total amount of emulsifier in the reaction mixture, it is possible to estimate the surface coverage ratio of particles (θ), which was calculated using Langmuir model:

$$\theta = \frac{KS_c}{1+KS_c} \tag{3.1.5}$$

This equation can be simultaneously solved with other equations, to give θ (see page 37).

The weight-average molecular weight ($\bar{M}_w$) of the polymer was measured using static light scattering technique (SLS) by Zetasizer, using simplified Rayleigh equation (see page 38):

$$\frac{KC}{R_\theta} = \left(\frac{1}{\bar{M}_w} + 2A_2C\right) \tag{3.1.6}$$

The evolution of $\bar{M}_w$ of polymer produced was monitored in the course of polymerisation.

Table 3.1.1. Recipe for the semicontinuous microemulsion polymerisation of styrene

Ingredients	Quantity
Styrene (ml)	50
Water (ml)	600
KPS ($mmol \cdot l_{aq}^{-1}$)	4
Buffer ($mmol \cdot l_{aq}^{-1}$)	4
Reaction temperature (°C)	70

3.1.3 Results and Analysis

The recipe for the polymerisations is shown in Table 3.1.1. The surfactant concentrations ([*S*]) of 5 $g \cdot l_{aq}^{-1}$, 10 $g \cdot l_{aq}^{-1}$, 15 $g \cdot l_{aq}^{-1}$, and 20 $g \cdot l_{aq}^{-1}$ were chosen for this study. The rate of monomer addition (R_a) of 100 $ml \cdot h^{-1}$, 50.7 $ml \cdot h^{-1}$, 24.6 $ml \cdot h^{-1}$, 13 $ml \cdot h^{-1}$ and 8.7 $ml \cdot h^{-1}$ were selected. Based on the amount of monomer used (Table 3.1.1), these correspond to monomer addition time (t_{add}) of 0.5h, 1h, 2h, 4h and 6h, respectively. A low feeding rate signifies a high t_{add}. We mainly used t_{add} in this article to indicate feeding rates.

3.1.3.1 Rate of polymerisation (R_p)

Figure 3.1.1 shows the variations in the overall (x_o) and instantaneous (x_i) conversions versus reaction time for different t_{add} and [*S*]. Before polymerisation can start, the added monomer has to dissolve in the water phase and diffuses in to micelles. This imposed some inhibition time, which decreased with decreasing t_{add}. The instantaneous conversion, which can be considered as a measure of monomer-polymer ratio in the system at any given time, started at high values (~40%) for all sets, except for the set with [*S*] = 5 $g \cdot l_{aq}^{-1}$ (see Figure 3.1.1a).

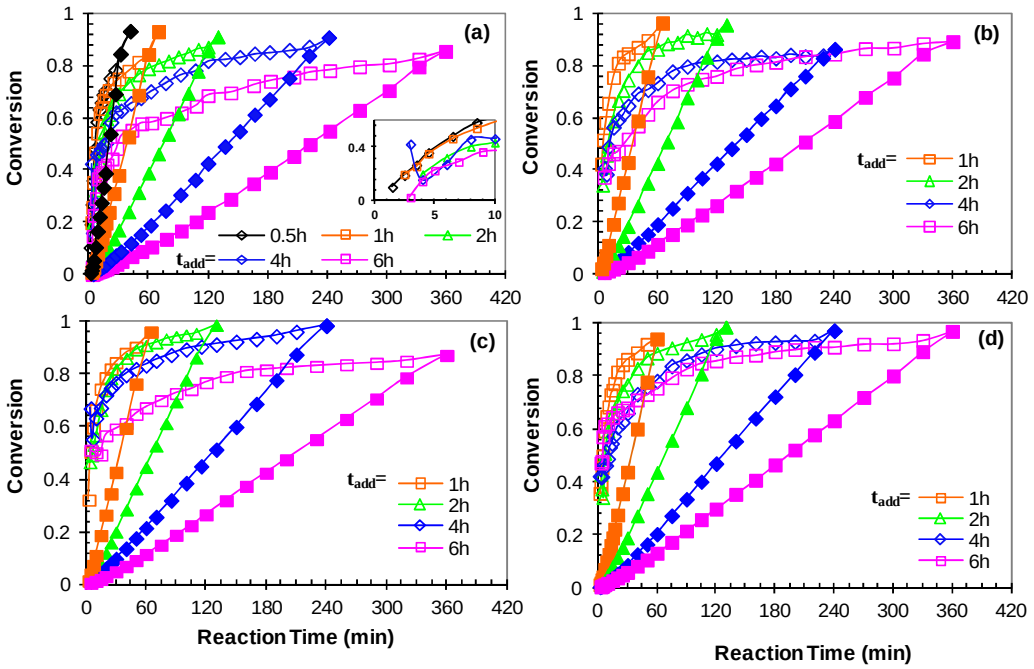

Figure 3.1.1. Conversions of styrene versus time for different t_{add} at [*S*]: (a) 5 $g \cdot l_{aq}^{-1}$; (b) 10 $g \cdot l_{aq}^{-1}$; (c) 15 $g \cdot l_{aq}^{-1}$; and (d) 20 $g \cdot l_{aq}^{-1}$. The closed and open symbols represent x_o and x_i, respectively. The small inset in Figure a shows the magnified conversion-time for the early 10 min.

Under monomer-starved conditions, monomer can reside in three locations; water phase, micelles, and polymer particles. Polystyrene particles can absorb one and half times their weight the styrene monomer (the critical ratio of polymer in the particle is x_{cr} = 0.40) [37]. Above this ratio, the particles are not fully swollen with monomer and are monomer starved. Therefore, a high polymer ratio at the beginning of reactions can signify fully monomer-starved condition. Micelles can enhance starved conditions by solubilising some monomers [40]. For the set with

[*S*] = 5 g·l_{aq}^{-1}, which uses a relatively low concentration of surfactant, there might not be sufficient micelles in the aqueous phase, compared to other sets, to absorb all the monomer fed to the system during inhibition period. As a result, monomer droplets could be formed leading to monomer-flood nucleation, at least partly. Generally, a higher monomer starvation in polymer particles could be obtained by increasing [*S*], as shown in Figure 3.1.1.

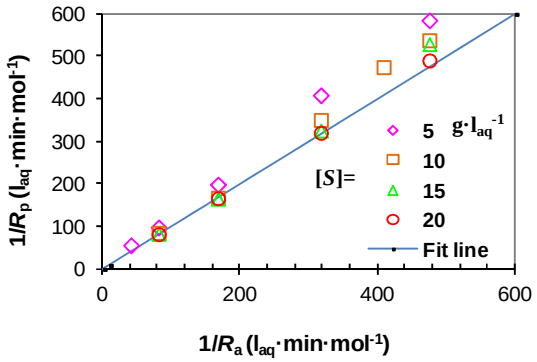

Figure 3.1.2. R_a versus R_p for different [*S*] during nucleation stage.

Figure 3.1.2 represents the relationship between the inverse of the R_a and R_p for different [*S*] during nucleation. An equality relationship, $R_p \approx R_a$, exists between the rate of feeding and the rate of polymerisation when either [*S*] or R_a is high. It appears that at a very low R_a, the rate of reaction becomes slower than the rate of addition; $R_p < R_a$, which indicates an accumulation of monomer in the system. This can be also found out from instantaneous conversions in Figure 3.1.1, which shows a decrease with decreasing R_a or increasing t_{add}.

One possibility could be the depletion of initiator with time, which may cause a decrease in R_p. Moreover, under a very low R_a, small particles (D_v < 15 nm) with low concentration of monomer are formed in the system, which are highly viscous and dense. In this case, it takes longer time for transportation of the monomer from the aqueous phase to the particles, which suggests the coexistence of monomer droplets and monomer-starved particles. Furthermore, as [*S*] is low, the number of 'active' micelles (containing monomer molecules) is limited. As a result, oligomer radicals would need longer time to enter either micelles or particles irreversibly; thus favouring the aqueous phase termination to occur. Consequently, R_p could be depressed.

Results in Figure 3.1.1 are grouped in terms of various t_{add} at a given [*S*]. By the cross comparisons of the rate of reactions for various [*S*] at a given t_{add}, it can be inferred that the R_p is independent of [*S*] (not shown). This supports the concept that the R_p is tightly controlled by the R_a or t_{add}.

3.1.3.2 Nucleation Period

Figure 3.1.3 shows the variations in N_p with time in the course of reactions. At any given R_a, or t_{add}, the number of particles was initially comparable for different values of [*S*], but the

difference gradually became wider with time. The number of particles increased with increasing either t_{add} or [*S*].

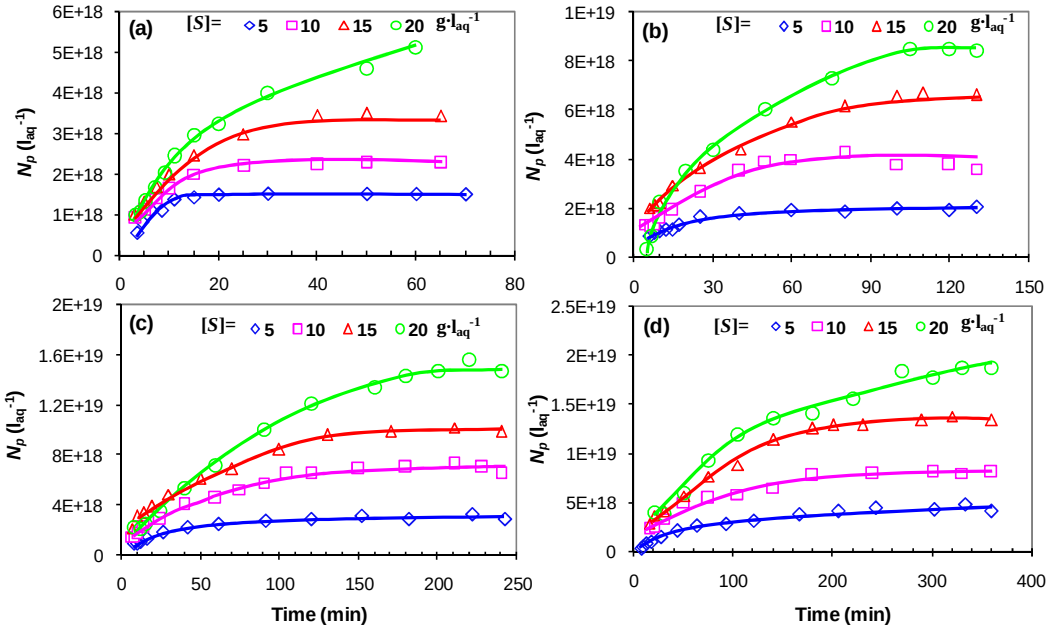

Figure 3.1.3. Time evolution of number of particles for different [*S*] at t_{add} of (a) 1h; (b) 2h; (c) 4h; and (d) 6h.

In a typical microemulsion polymerisation, particle formation and growth occur simultaneously. Particle growth leads to depletion of emulsifier micelles, thus inversely affects nucleation. In the case of high [*S*], particles are not saturated with monomer and grow at a rate controlled by the R_a. As t_{add} increases, the monomer starvation becomes more significant. Monomer-starved particles have smaller outer surface areas and thus absorb fewer surfactant molecules [41]. This can prolong the nucleation period by delaying the depletion of emulsifier micelles. Thus, the starvation of primary particles with monomer is in fact the prerequisite for prolonged nucleation period. Furthermore, small monomer-starved particles may have more chance to expel to the water-phase radicals formed by transfer to monomer, thus directly reducing the rate of particle growth and indirectly enhancing the rate of radical entry into micelles [37].

In order to investigate the nucleation stage, the nucleation period of each experiment is needed to be known. A rule of thumb is that nucleation period ends when the variations in N_p with time becomes negligible. However, one should note that according to micellar nucleation mechanism, micelles are consumed via particle formation and growth. In the absence of homogenous nucleation, the end of nucleation can be estimated by the time that all the micelles are depleted. Therefore, the surface coverage ratio (θ) of surfactant molecules on the polymer particles can give a reliable indication of presence of micelles in the reaction mixture. A complete surface coverage, $\theta = 1.0$, indicates that free micelles exist in the aqueous phase. Thus, the end of micellar nucleation can be theoretically predicted by the time when θ becomes smaller than 1.0.

Figure 3.1.4 shows the nucleation periods of experiments for different t_{add}. The micellar nucleation time is also shown on the graphs for the sake of comparison. The nucleation periods obtained by the two methods, overall and micellar, are comparable for high [*S*]. A difference emerges at the low [*S*] with a degree increasing with increasing t_{add}. Particle formation beyond the depletion of micelles has been previously reported for butyl acrylate microemulsion polymerisation [35] and styrene emulsion polymerisation [42].

The possible reason to explain such a difference could be homogeneous nucleation. Radicals formed in the water phase can propagate with monomer dissolved in the water phase to reach a critical size and then precipitate to form new particles. Precursor particles are extremely unstable and coagulate with each other until they acquire a sufficient number of stabilising ionic groups to become stable [2]. It is important to note that the rate of reaction was rather relatively slow at low [*S*] and R_a (high t_{add}) as seen in Figure 3.1.1 and 3.1.2. The instantaneous conversion was below 0.80 for all runs carried out using [*S*] = 5 $g \cdot l_{aq}^{-1}$. It should be noted that for sparingly water-soluble monomers such as styrene, homogenous nucleation has been found to be insignificant [43]. With decreasing monomer concentration in the water phase, a larger fraction of radicals are terminated in the water phase before they can enter micelles/particles. The continuous formation of such *in-situ* emulsifier molecules, formed by termination of initiator-derived oligomers in the water phase over long polymerisation time, is thought to be the main factor that contributes to stability of newly-formed particles. Formation of particles via homogenous nucleation is ceased when a large number of particles are present (high [*S*]. Ramirez and Tauer [44] also reported formation of particles by homogenous nucleation in semicontinuous microemulsion polymerisation of butyl acrylate.

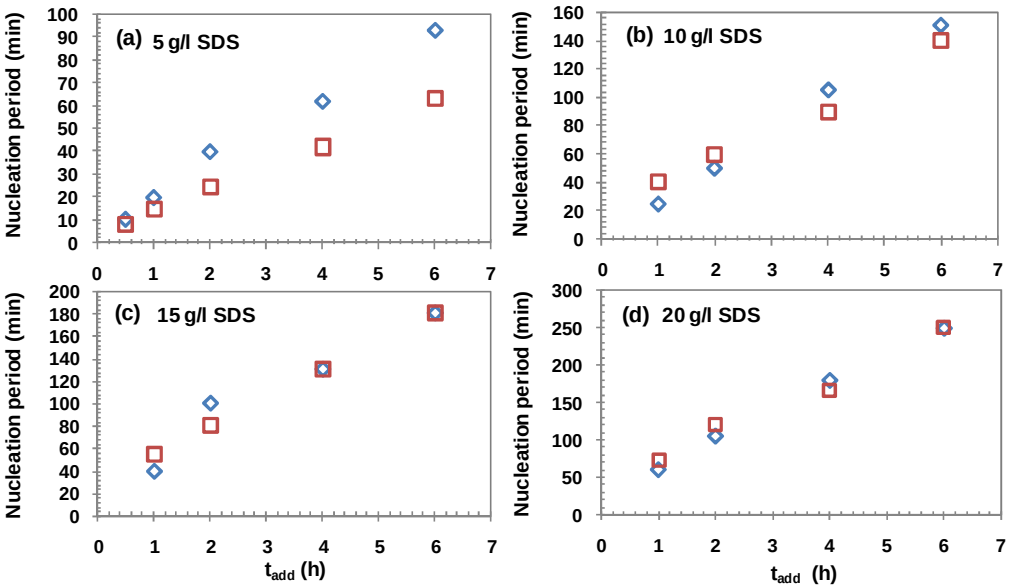

Figure 3.1.4. Variations in nucleation periods in terms of t_{add} for different [*S*]: (a) 5 $g \cdot l_{aq}^{-1}$; (b) 10 $g \cdot l_{aq}^{-1}$; (c) 15 $g \cdot l_{aq}^{-1}$; and (d) 20 $g \cdot l_{aq}^{-1}$; The crystal and square symbol represent data from N_p and θ, respectively.

3.1.3.3 Particle Growth and Formation

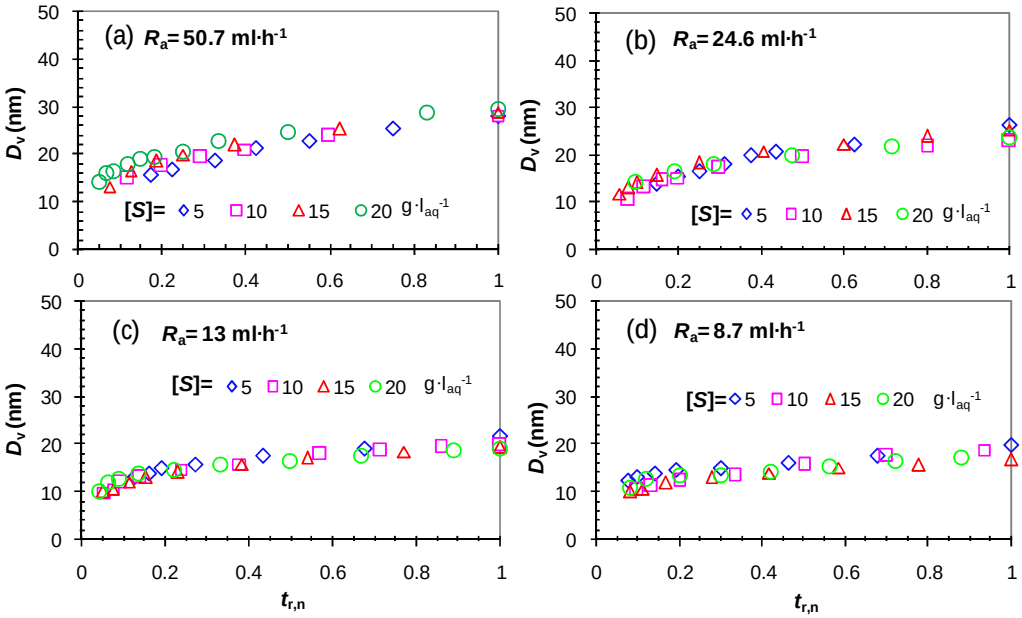

Figure 3.1.5. Variation in D_v versus relative nucleation time with different [*S*] at t_{add} of (a)1h; (b)2h; (c)4h; and (d)6h;

Figure 3.1.5 shows particle sizes versus relative nucleation time ($t_{r,n}$) for runs with different [*S*] and t_{add}. The relative nucleation time for any run is defined as the ratio of time over the nucleation time (the time at which overall particle nucleation is completed); $t_{r,n}$ = 1.0 indicates the end of nucleation. It is interesting to notice that during the nucleation stage, particles grew relatively at almost the same rate for various [*S*], with the exception of [*S*] = 5 g·l$_{aq}^{-1}$ at very high t_{add} (= 6h). Furthermore, the size of particles at the end of nucleation in polymerisations with different [*S*] was almost the same for a given rate of addition. The results imply that the relative rate of growth of particles is controlled by t_{add} but is independent of [*S*]. In order to compare the results with the theoretical predictions reported in the literature, the sizes of particles at the end of nucleation were drawn against t_{add} and [*S*] and the governing exponents calculated, as shown in Figure 3.1.6.

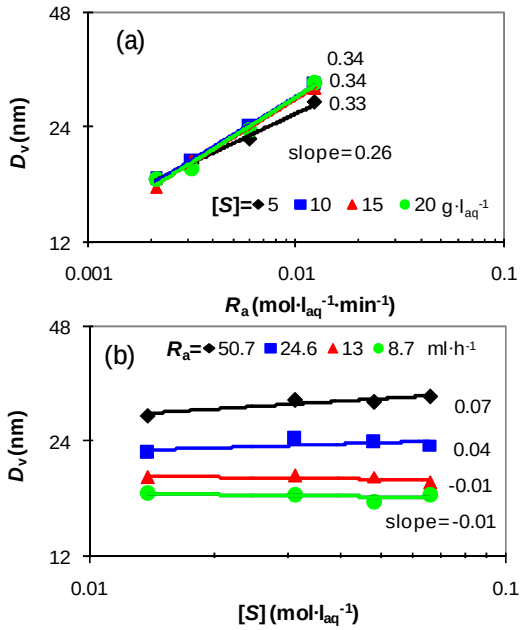

Figure 3.1.6. Variations in the size of particles at the end of nucleation versus (a) R_a and (b) [*S*], for different [*S*] and t_{add}, respectively.

Figure 3.1.6 shows the variations of the volume-average particle size at the end of nucleation with different R_a and [*S*]. The exponent value of D_v in terms of R_a approached 1/3 with increasing [*S*]. The exponent value of D_v in terms of [*S*] was within (-0.01)-0.07 for different R_a, and approached zero for intermediate range of R_a. These values are already in good agreement with the predictions from Equation 3.1.2. The highest deviations from theoretical predictions were found at high t_{add} and low [*S*].

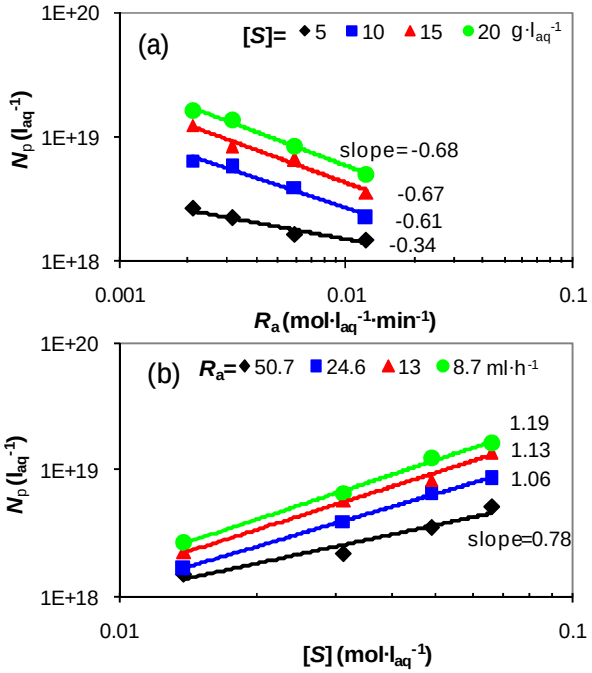

Figure 3.1.7. Number of particles at the end of nucleation versus (a) R_a and (b) [*S*], for different [*S*] and t_{add}, respectively.

Figure 3.1.7 shows the number of particles at the end of nucleation produced by various R_a and [*S*]. The exponent value of N_p in terms of R_a is around -0.34 for [*S*] = 5 $g \cdot l_{aq}^{-1}$ but approach -2/3 for higher [*S*]. This is again in good agreement with Equation 3.1.1.

The exponent value of N_p in terms of [*S*] was the lowest, 0.78, for the lowest t_{add} used, but gradually reached 1.12±0.07 with increasing [*S*]. This is in fair agreement with the value of 1.0 predicted by Equation 3.1.1. It should be noted that with decreasing either [*S*] or t_{add}, monomer droplets may form in the early stage of reactions (monomer-flooded condition) and causes the system to deviate from fully monomer-starved conditions, as is the case for the set with [*S*] = 5 $g \cdot l_{aq}^{-1}$. This can affect the exponent values.

3.1.3.4 Particle Size Distribution (PSD)

It was very interesting to see that polymer particles as small as 5-10 nm were formed (See Figure 3.1.8). This is around the size of fully swollen micelles measured by DLS. The particle size distributions (PSD) of latexes were obtained using images from TEM measurements.

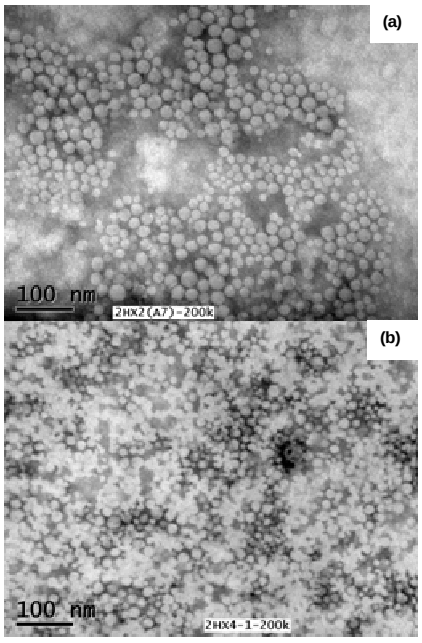

Figure 3.1.8. TEM images of the latexes 1 h into addition for t_{add} = 2h for different [*S*] of (a) 10 $g \cdot l_{aq}^{-1}$ and (b) 20 $g \cdot l_{aq}^{-1}$.

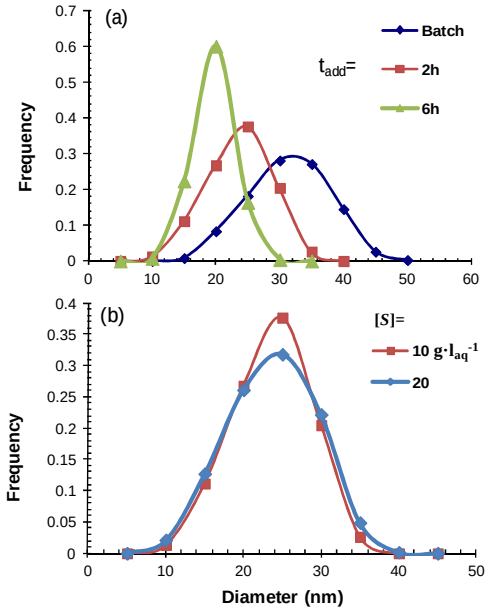

Figure 3.1.9. PSD at the end of nucleation obtained by TEM for (a) semicontinuous process at different t_{add} and batch process with [*S*] = 10 g·l$_{aq}^{-1}$; (b) semicontinuous process with different [*S*] at t_{add} = 2h.

Figure 3.1.9a shows the PSD of latexes at the end of nucleation for different t_{add}. Batch process produced the broadest distribution. PSD is much sharper for the semicontinuous process and moreover, the longer the t_{add} for the semicontinous process, the narrower was the particle size distribution. The PSD sharpening with increasing t_{add} can be explained by the reduced rate of particle growth under monomer-starved conditions. One should note that the nucleation time increased with increasing t_{add} suggesting a broader PSD should be expected as understood from conventional emulsion polymerisation [66]. However, particles formed under monomer-starved conditions grow slowly allowing more micelles, which otherwise had to disintegrate to provide stability to growing polymer particles, to be nucleated. This means that despite longer nucleation time, particles formed under semicontinuous mode became smaller with a sharper PSD with increasing t_{add}.

Figure 3.1.9b shows the PSD at the end of nucleation for two different [*S*] using the same rate of monomer addition (t_{add} = 2h). The average sizes of particles at the end of nucleation were almost the same for the two different [*S*]. This is because increase in nucleation time with [*S*] is counterbalanced with a reduction in the instantaneous rate of growth. This is in close agreement with recent developments in understanding of this process [36]. However, the PSD became slightly broader when [*S*] is increased, which may caused by stochastic broadening due to lower rate of radical entry at higher [*S*]. Stochastic broadening occurs in polymerisations with low average radical entry rate due to the difference in size of growing particles and nongrowing ones. The growing particles continuously grow for a long time, thus they become quite large, compared with that of nongrowing particles, and have more chance for secondary entry and further growth. This results in broadening of particle size distributions.

The average-number of radicals per particle ($\bar{n}$) can be calculated by Smith-Ewart equation (see page 7):

$$R_P = k_p[M]_P(\bar{n}N_p/N_A) \tag{3.1.7}$$

Assuming that the water-solubility of the styrene monomer and the amount of monomer solubilised in the micelles are negligible, the concentration of monomer in the particles ($[M]_p$) can be calculated as:

$$[M]_p = \frac{x_i/M_{mon}}{x_i/\rho_p+(1-x_i)/\rho_m} \tag{3.1.8}$$

where ρ_m is the density of monomer, M_{mon} is the molecular weight of monomer, and x_i is the instantaneous conversion.

The calculated $\bar{n}$ at the end of nucleation stage decreased from 0.015 to 0.012 as [*S*] increased from 10 to 20 g·l_{aq}^{-1}, which is consistent with the hypothesis put forward by Sajjadi [36] who pointed out that the stochastic broadening of PSD is expected to be greater for higher [*S*].

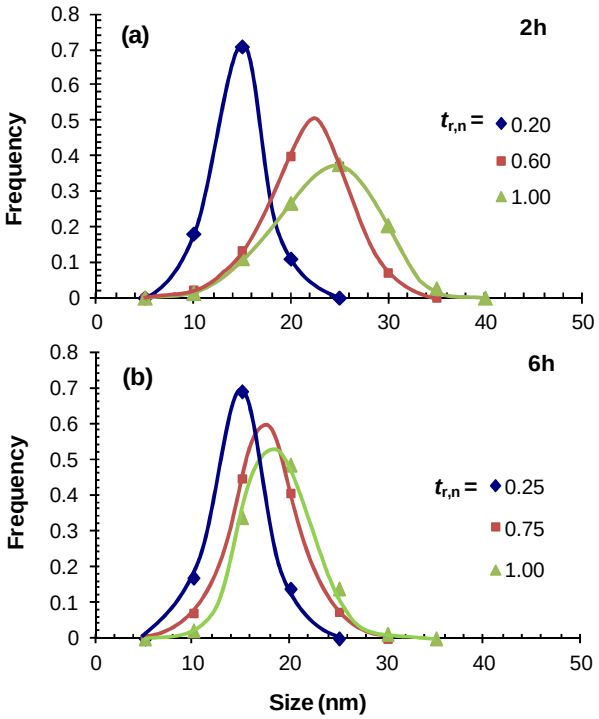

Figure 3.1.10. Evolution of PSD during nucleation obtained by TEM at different t_{add}: (a)2h; and (b)6h. [*S*] = 10 g·l_{aq}^{-1}.

Figure 3.1.10 shows the evolution of PSD during the nucleation stage for two different rates of monomer addition (t_{add} = 2h and 6h) at a constant [*S*] of 10 g·l_{aq}^{-1}. It can be observed that the average particle size increased and PSD became broader as the polymerisation reaction proceeds. This clearly suggests that particles continuously undergo growth during nucleation, which can also be found from Figure 3.1.5. This makes current system different from conventional

microemulsion polymerisation (in the presence of high concentration of surfactant) in which micelles (or particles) might only receive radicals once [85].

Under monomer-starved conditions, as has been discussed in a previous publication [2], the rate of particle growth, μ, is not constant even during the nucleation stage. Ignoring the density difference between the monomer and the polymer, the instantaneous rate of growth of particles can be simply described as:

$$\mu(t) = R_a / N_P(t) \tag{3.1.9}$$

This equation shows that at a fixed R_a, μ is decreasing as more particles are formed. The earlier particles can grow to a greater extent than the later ones. Moreover, Vanzo et al's result [45] shows that the monomer concentration in the particles, $[M]_p$, is highly size-dependant when particle size is smaller than 20 nm. The depressed rate of growth for tiny particles is more pronounced. As a result, the PSD becomes broader with time.

3.1.3.5 Polymer molecular weight

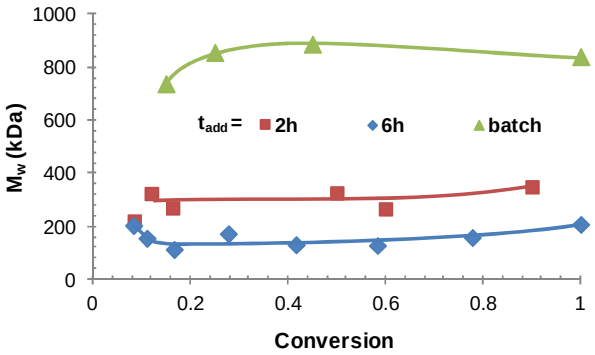

Figure 3.1.11. Variations in weight-average molecular weight of the polymer produced at the end of the nucleation stage versus relative nucleation time with different processes. (a) Conventional batch, (b) t_{add} = 2h and (c) t_{add} = 6h semicontinuous process. [*S*]: 10 g·l_{aq}^{-1}, [M]: 75.75 g·l_{aq}^{-1}.

Figure 3.1.11 shows the evolution of $\bar{M}_w$ with relative nucleation time for polymer latexes from batch and semicontinuous processes at constant [*S*] = 10 g·l_{aq}^{-1}. For all processes studied, the $\bar{M}_w$ values remained practically constant in the course of polymerisation reactions. However, it is clear that the batch process produced the highest $\bar{M}_w$. $\bar{M}_w$ decreased with decreasing rate of monomer addition for the semicontinuous process.

For a typical emulsion polymerisation, the number-average molecular weight ($\bar{M}_n$) can be simply calculated from the following equations:

$$\bar{M}_n = M_{mon}\bar{X}_n \tag{3.1.10}$$

$$\bar{X}_n = R_p / (R_t + R_{tr,m}) \tag{3.1.11}$$

where M_{mon} is the molecular weight of the monomer. $\bar{X}_n$ is the number-average degree of polymerisation of a single polymer chain. R_p, R_t and $R_{tr,m}$ represent the rates for propagation, termination and chain transfer to monomer in the particle, respectively. They are given by:

$$R_p = k_p[M]_p[M\cdot] \tag{3.1.12}$$

$$R_{tr,m} = k_{tr,m}[M]_p[M\cdot] \tag{3.1.13}$$

where k_p is the propagation rate constant in polymer phase, $k_{tr,m}$ is the rate constant for transfer to monomer. $[M]_p$ and $[M\cdot]$ represent the monomer and radical concentration within the particle, respectively.

If chain transfer to monomer is the dominant termination mechanism of the growing chain within the particles, R_t can be ignored. Therefore,

$$\bar{M}_n = M_{mon}R_p/R_{tr,m} = M_{mon}k_p/k_{tr,m} \tag{3.1.14}$$

Using Equation 3.1.14, for emulsion polymerisation of styrene at 70°C, with k_p = 480 l·mol^{-1}s^{-1} and $k_{tr,m}$ = 9.3×10^{-3} l·mol^{-1}s^{-1} [34], the value of $\bar{M}_n$ is obtained as 5375 kDa. As $\bar{M}_w$ is always larger than $\bar{M}_n$, it is ensured that $\bar{M}_w$ shown in Figure 3.1.11 is much smaller than 5375 kDa, which is the average size of polymer chains when chain transfer to monomer controls chain growth termination. Therefore, we come to a conclusion that in the system under study, termination by secondary entry of radicals to primary particles becomes progressively more dominant with decreasing rate of monomer addition (increasing addition time). This might seem to be odd as particles formed by semicontinuous process have less chance for secondary radical entry due to their small size. However, lower monomer concentration in polymer particles will allow for slower but longer propagation in the particles. This can enhance the chance of termination by secondary radical entry during the life time of a propagating radical [46].

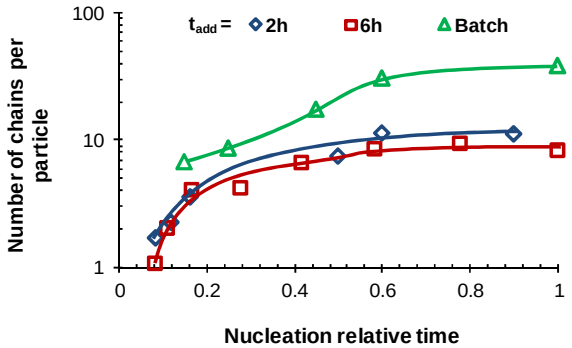

Figure 3.1.12. Average number of chains per particle during nucleation period for the batch and semicontinuous processes (same conditions as mentioned in Figure 3.1.11).

The average number of chains in each particle, $\bar{n}_c$, can be calculated by the average size of particles and $\bar{M}_w$ of the polymer chains according to the following equation:

$$\bar{n}_c = w_p N_A / \bar{M}_w = (\pi D_v^3 \rho) N_A / 6\bar{M}_w \quad (3.1.15)$$

where w_p is the average weight of single particle, D_v is the volume-average size.

The results are shown in Figure 3.1.12. The number of chains per particle is increasing during nucleation for both batch and semicontinuous processes. The number of chains per particle is much lower for the semicontinuous process than for the batch process. The number of chains per particle is in fact a reflection of growth mechanism of particles. The results clearly indicate that single-chain particles once formed in the early stage of reactions undergo subsequent growth by secondary radical entry.

By increasing the number of particles within the system via semicontinuous polymerisation, the chance of the secondary entry of radicals into particles is theoretically decreased, resulting in a smaller number of chains per particle. Single chain particles can only form in the early stage of nucleation where only micelles exist in the reaction medium.

3.1.4 Conclusions

Semicontinuous microemulsion polymerisation of styrene during particle nucleation stage was investigated in this work. The R_p-R_a relation showed that R_p can be controlled by R_a. It is found that particle nucleation period can be prolonged by either decreasing R_a or increasing [S]. As a result, particle formation is enhanced. When a low [S] and low R_a are combined, particle formation continues well beyond the depletion of micelles suggesting that homogeneous nucleation plays a part.

The exponent dependence of the number of particles in terms of R_a and [S] were found to approach those theoretically predicted, -2/3 and 1, respectively. The results indicate that the size of particles at the end of nucleation is almost independent of surfactant concentration for low R_a, but slightly decreased with increasing [S] at high R_a. The molecular weight of polymer decreased with decreasing rate of monomer addition. Secondary radical entry was found to be the dominant mechanism of chain termination in semicontinuous microemulsion polymerisation. The results suggest that the size of particles, the molecular weight of the polymer produced as well as the number of chains within particles can be controlled via semicontiunous process.

3.1.5 Reference

[1] Ming, W.H., Jones, F.N., Fu, S.K. Synthesis of Nanosize Poly(methyl methacrylate) Microlatexes with High Polymer Content by a Modified Microemulsion Polymerization. *Polymer Bulletin*, 1998, v40, pp749-756.

[2] Sajjadi, S. Particle Formation under Monomer-Starved Conditions in the Semibatch Emulsion Polymerisation of Styrene.1.Experimental. *Journal of Polymer Science Part A: Polymer Chemistry* 2001, v39, pp3940-3952.

[3]Rabelero, M., Zacarias, M., Mendizabal, E., Puig, J.E., Dominguez, J.M., Katime, I. High-content Polystyrene Latex by Microemulsion Polymerisation. *Polymer Bulletin*, 1997, v38, pp695-700.

[4] Roy, S., Devi, S. High Solids Content Semicontinuous Microemulsion Copolymerization of Methylmethacrylate and Butylacrylate. *Polymer*, 1997, v38, pp3325-3331.

[5] Xu, X.J., Chew, C.H., Siow, K.S., Wong, M.K., Gan, L.M. Microemulsion polymerization of styrene for obtaining high ratios of polystyrene/surfactant. *Langmuir*, 1999, v15, pp8067-8071.

[6] Moraes, R.P., Hutchinson, R.A., Mckenna, T.F.L. The Production of High Polymer to Surfactant Microlatexes. *Journal of Polymer Science: Part A: Polymer Chemistry* 2010, v48, pp48-54

[7] Ming, W., Jones, F.N., Fu, S. High Solids-content Nanosize Polymer Latexes Made by Microemulsion Polymerization. *Macromolecular Chemistry and Physics* 1998, v199, pp1075-1079.

[8] Chuayjuljit, S., Boonmahitthisud, A. Natural rubber nanocomposites using polystyrene-encapsulated nanosilica prepared by differential microemulsion polymerization. *Applied Surface Science*, 2010, v256, pp7211-7216.

[9] Pan, F.S., Jia, H.P., Cheng, Q.L., Jiang, Z.Y. Bio-inspired fabrication of composite membranes with ultrathin polymer-silica nanohybrid skin layer. *Journal of Membrane Science*, 2010, v362, pp119-126.

[10] Chen, B., Deng, J.P., Yang, W.T. Chiral Helical Polyacetylene-vinyl Polymer Core/shell Nanoparticles: Preparation and Application to Optically Active Composite Films. *Colloid and Polymer Science*, 2011, v289, pp133-139.

[11] Darwish, M.S.A., Peuker, U., Kunz, U., Turek, T. Bi-layered Polymer-magnetite Core/shell particles: Synthesis and Characterization. *Journal of Materials Science*, 2011, v46, pp2123-2134.

[12] Bait, N., Grassl, B., Derail, C., Benaboura, A. Hydrogel Nanocomposites as Pressure-sensitive Adhesives for Skin-contact Applications. *Soft Matter*, 2011, v7, pp2025-2032.

[13] Ho, C.T., Low, K.B., Klie, R.F., Maeda, K., Domen, K., Meyer, R.J., Snee, P.T. Synthesis and Characterization of Semiconductor Tantalum Nitride Nanoparticles. *Journal of Physical Chemistry C*, 2011, v115, pp647-652.

[14] Neubert, R.H.H. Potentials of New Nanocarriers for Dermal and Transdermal Drug Delivery. *European Journal of Pharmaceutics and Biopharmaceutics*, 2011, v77, pp1-2.

[15] Ming, W.H., Zhao, Y.Q., Cui, J., Fu, S.K., Jones, F.N. Formation of Irreversible Nearly Transparent Physical Polymeric Hydrogels During a Modified Microemulsion Polymerization. *Macromolecules* , 1999, v32, pp528-530.

[16] Chen, W., Liu, X., Liu, Y., Bang, Y., Kim, H. Synthesis of PMMA and PMMA/PS Nanoparticles by Microemulsion Polymerization with a New Vapor Monomer Feeding System. *Colloids and Surface A: Physicochemical and Engineering Aspects*, 2010, v364, pp145-150.

[17] Zhang, Q.S., Zha, L.S., Ma, J.H., Liang, B.R. A Novel Route to Prepare pH- and Temperature-sensitive Nanogels via a Semibatch Process. *Journal of Colloid and Interface Science*, 2009, v330, pp330-336.

[18] Sosa, N., Peralta, R.D., Lopez, R.G., Ramos, L.F., Katime, I., Cesteros, C., Mendizabal, E., Puig, J.E. A Comparison of the Characteristics of Poly(vinyl acetate) Latex with High Solid Content Made by Emulsion and Semi-continuous. *Polymer*, 2001, v42, pp6923-6928.

[19] Sarac, A., Berber, H., Yildirim, H. Semi-continuous Emulsion Copolymerization of Vinyl Acetate and Butyl Acrylate Using a New Protective Colloid. Part 2. Effects of Monomer Ratio and Initiator. *Polymers for Advanced Technologies*, 2006, v17, pp855-859.

[20] Kong, X.F., Wu, Q., Hu, W.C., Wang, Z.Q. Monodisperse Ultrafine Polystyrene Nanoparticles Prepared by a Semicontinuous Microemulsion Polymerization. *Journal of Polymer Science: Part A: Polymer Chemistry*, 2008, v46, pp4522-4528.

[21] Aguilar, J., Rabelero, M., Nuno-Donlucas, S.M., Mendizabal, E., Martinez-Richa, A., Lopez, R.G., Arellano, M., Puig, J.E. Narrow Size-Distribution Poly(methyl methacrylate) Nanoparticles Made by Semicontinuous Heterophase Polymerization. *Journal of Applied Polymer Science*, 2011, v119, pp1827-1834.

[22] He, G.W., Pan, Q.M., Rempel, G.L. Differential Microemulsion Polymerization of Styrene: A Mathematical Kinetic Model. *Journal of Applied Polymer Science*, 2007, v105, pp2129-2137.

[23] He, G.W., Pan, Q., Rempel, G.L. Synthesis of Poly(methyl methacrylate) Nanosize Particles by Differential Microemulsion Polymerization. *Macromolecule Rapid Communications*, 2003, v24, pp585-588.

[24] Liu, J.M., Pan, Q.M. Synthesis of Nanosized Poly(ethyl acrylate) Particles via Differential Emulsion Polymerization. *Journal of Applied Polymer Science*, 2006, v102, pp1609-1614.

[25] Smeets, N.M.B., Moraes, R.P., Wood, J.A., Mckenna, T.F.L. A New Method for the Preparation of Concentrated Translucent Polymer Nanolatexes from Emulsion Polymerization. *Langmuir*, 2011, v27, pp575-581.

[26] Ledezma, R., Trevino, M.E., Elizalde, L. E., Perez-Carrillo, L.A., Mendizabal, E., Puig, J.E., Lopez, R.G. Semicontinuous Heterophase Polymerization under Monomer Starved Conditions to Prepare Nanoparticles with Narrow Size Distribution. *Journal of Polymer Science: Part A: Polymer Chemistry*, 2007, v45, pp1463-1473.

[27] Aguiar, A., Gonzalez-Villegas, S., Rabelero, M., Mendizabal, E., Puig, J.E. Core-shell Polymers with Improved Mechanical Properties Prepared by Microemulsion Polymerization. *Macromolecules*, 1999, v32, pp6767-6771.

[28] Perez-Carrillo, L.A., Puca, M., Rabelero, M., Meza, K.E., Puig, J.E., Mendizabal, E., Lopez-Serrano, F., Lopez, R.G. Effect of Particle Size on the Mechanical Properties of Polystyrene and Poly(butyl acrylate) Core/shell Polymers. *Polymer*, 2007, v48, pp1212-1218.

[29] Norakankorn, C., Pan, Q.M., Rempel, G.L., Kiatkamjornwong, S. Factorial Experimental Design on Synthesis of Functional Core/Shell Polymeric Nanoparticles via Differential Microemulsion Polymerization. *Journal of Applied Polymer Science* 2010, v116, pp1291-1298.

[30] Norakankorn, C., Pan, Q.M., Rempel, G.L., Kiatkamjornwong, S. Synthesis of core/shell structure of glycidyl-functionalized poly(methyl methacrylate) latex nanoparticles via differential microemulsion polymerization. *European Polymer Journal* 2009, v45, pp2977-2986.

[31] He, G.W., Pan, Q.M. Synthesis of Polystyrene and Polystyrene/poly(methyl methacrylate) Nanoparticles. *Macromolecular Rapid Communications*, 2004, v25, pp1545-1548.

[32] Nomura, M., Harada, M. In: Basset, D.R., Hamielec, A.E. editors. *American Chemical Society*, 1981, 121.

[33] Sajjadi, S., Brooks, B.W. Semibatch Emulsion Polymerization of Butyl Acrylate. I. Effect of Monomer Distribution. *Journal of Applied Polymer Science*, 1999, v74, pp3094-3110.

[34] Sajjadi, S. Particle Formation under Monomer-starved Conditions in the Semibatch Emulsion Polymerisation of Styrene. Part II. Mathematical Modelling. *Polymer*, 2003, v44, pp223-237.

[35] Sajjadi, S., Brooks, B.W. Semibatch Emulsion Polymerisation Reactors: Polybutyl acrylate Case Study. *Chemical Engineering Science*, 2000, v55, pp4757-4781.

[36] Sajjadi, S. Population Balance Modeling of Particle Size Distribution in Monomer-Starved Semibatch Emulsion Polymerization. *Aiche Journal* 2009, v55, pp3191-3205.

[37] Sajjadi, S. Nanoparticle Formation by Monomer-starved Semibatch Emulsion Polymerization. *Langmuir*, 2007, v23, pp1018-1024.

[38] Kalinin, V.V., Radke, C.J. An Ion-binding Model for Ionic Surfactant Adsorption at Aqueous-fluid Interfaces. *Colloids and surface a-Physicochemical and Engineering Aspects*, 1996, v114, pp337-350.

[39] Sajjadi, S. Particle Formation under Monomer-starved Conditions in the Semibatch Emulsion Polymerisation of Styrene. Part II. Mathematical . *Polymer*, 2003, v44, pp223-237.

[40] Sajjadi, S., Brooks, B.W. Semibatch Emulsion Polymerization of Butyl Acrylate. II. Effects of Emulsifier Distribution. *Journal of Applied Polymer Science*, 2001, v79, pp582-597.

[41] Sajjadi, S. Particle Formation under Mnomer-Starved Conditions in the Semibatch Emulsion Polymerization of Styrene. I. Experimental. *Journal of Polymer Science Part A: Polymer Chemistry*, 2001, v39, pp3940-3952.

[42] Chern, C.S., Lin, S.Y., Hsu, T.J. Effects of Temperature on Styrene Emulsion Polymerisation Kinetics, *Polymer Journal*, v31, 1999, pp516-523.

[43] Sajjadi, S. Diffusion-controlled Particle Growth and Its Effects on Nucleation in Stirred Emulsion Polymerisation Reactors. ***Macromolecular Rapid Communications***, 2004, v25, pp882-887.

[44] Ramirez, A.G., Lopez, R.G., Tauer, K. Studies on Semibatch Microemulsion Polymerization of Butyl Acrylate: Influence of the Potassium Peroxodisulfate Concentration. ***Macroemolecules***, 2004, v37, pp2738-2747.

[45] Vanzo, E., Marchess, R.H., Stannett, V. Solubility and Swelling of Latex Particles, ***Journal of Colloid Science***, 1965, v20, pp62.

[46] Rodríguez-Guadarrama, L.A., Mendizábal, E., Puig, J.E., Kaler, E.W. Polymerization of Methyl Methacrylate in 3-Component Cationic Microemulsion. ***Journal of Applied Polymer Science***, 1993, v48, pp775.

3.2 Exploring the Minimum Particle Size Achievable via Semicontinuous Microemulsion Polymerisation

Abstract: The minimum size achievable by semicontinuous microemulsion polymerisation has been explored. Styrene was the monomer, and KPS and SLS were used as initiator and surfactant, respectively. Rate of monomer addition (R_a), surfactant concentration ([S]) and reaction temperature (T) were varied. For any given set, there is a critical rate of monomer addition, surfactant concentration or rate of radical generation at which particle formation and full monomer conversion coincide. The minimum particle size is usually achieved beyond the critical values, for which some rough measures were presented. Nanolatexes with particles as small as 17 nm were produced by using moderate concentration of surfactants. Using extremely low R_a, the size evolution of particles, starting from a size similar to that of micelles, could be monitored. Particle sizes as small as 6 nm, were detected in the early stage of reactions. It was found that particle size approached a constant value at extremely low monomer addition rate, high surfactant concentration, and high rate of radical generation.

3.2.1 Introduction

Semicontinuous microemulsion is a unique method for producing concentrated nanoparticles with relatively low amount of surfactant [1-3]. Nanolatexes have found increasing applications such as ultrathin films, high performance coating materials, modified materials, adhesives, semiconductor and drug delivery nanocarriers used for penetrating various biological barriers within the human body [4-10]. Most of these applications need nanoparticles which are extremely small.

The motives to produce small polymeric particles have found momentum in recent years due to their promise for new applications. Nomura [11] found that conventional emulsion polymerisation of styrene in the presence of small quantity of monomer (i.e., microemulsion) can produce a large number of particles. Sajjadi [2] showed that the pre-requisite for enhanced formation of particles is to maintain monomer-starved conditions during nucleation by continuous addition of monomer at low rate. He showed that the size of particles, as well as the number of particles, can be manipulated by varying the monomer distribution, the rate of monomer addition (R_a), surfactant concentration ([S]), initiator concentration or the rate of initiator decomposition [12-13,16]. However, monomer-flooded conditions should be avoided if a large number of small particles are sought [13].

Several groups have studied the effect of reaction conditions on the particle size. Rempel's group [14] have found that beyond a critical amount of surfactant, the effect of [S] had little effect on particle size for MMA. Kim's group [15] studied the effect of [S], monomer concentration and reaction temperature on particle size of PMMA nanoparticles via microemulsion polymerisation with a vapour monomer feeding system. Their results confirmed further increase of surfactant content (> 6.3 $g \cdot l_{aq}^{-1}$) did not give any noticeable change in size of nanoparticles. At very low monomer concentration in the water phase, the particle size did not vary much with monomer concentration. Moreover, the particle size stayed almost constant as the temperature increased from 50 to 70ºC, but further increase in temperature resulted in larger size of particles.

Sajjadi derived an analytical equation for formation and growth of nanoparticles in monomer-starved semicontinuous microemulsion polymerisation of styrene-like monomers, which shows that the number of particles (N_p) and the volume size of particles (d_v) at the end of nucleation vary according to [16-17]:

$$N_p = k(a_s[S])R_I^{2/3}R_a^{-2/3} \tag{3.2.1}$$

$$d_v = (6/\pi)^{1/3}(R_a/R_I)^{1/3} \tag{3.2.2}$$

However, one important point to notice is that this equation is only valid if all emulsifier micelles are depleted prior to full conversion of monomer. In other words, these equations provide guidelines as to the minimum size of particles that can be achieved under the optimised conditions, a sufficiently high solids content to allow for a full depletion of surfactant micelles, While these equations might imply that smallest particles can be obtained using very high [*S*] or low R_a, do not eliminate possibility of achieving a much smaller size under the conditions that micelles do persist by the end of monomer depletion. In this work, a wider range of reaction parameters, such as [*S*], R_a and reaction temperature (T), have been chosen to explore the minimum size of nanoparticles achievable via semicontinuous microemulsion polymerisation.

3.2.2 Experimental work

3.2.2.1 Procedure

Details of procedure have been given in the previous subchapter (see Chapter 3.1, page 44). The mixture of de-ionised water, surfactant and buffer was first placed in the reactor, followed by nitrogen purge to remove the dissolved oxygen. After adding initiator solution, the degassed styrene monomer was continuously fed into the reactor at a given rate. The onset of reaction was continuously monitored by sampling from the vessel and precipitating the sample in methanol. The reaction time *zero* for the start of reaction was considered when the first droplet of monomer was added into the reactor.

3.2.2.2 Measurements

Measurements of conversions, z-average diameter of particles (D_z), and weight-average molecular weight of the polymer have been explained in the previous subchapter (see Chapter 3.1, page 44). The volume-average particle diameters (D_v) were obtained using conversion fact of $C_f = 0.90$, so that: $D_{v,} = C_f \cdot D_z$. The number of particles (N_p) and the surface coverage ratio of particles (θ) have been calculated.

Table 3.2.1. Recipe of the experiments. Water: 600 ml; St: 50 ml; [KPS] = [buffer] = 4 mmol·l_{aq}^{-1}

No.	1*	2*	3*	4*	5*	6*	7*	8	9	10	11	12	13	14	15	16	17
	Effect of T							Effect of [*S*]					Effect of R_a				
t_{add} (h)	4	4	4	4	2	2	2	4	4	4	4	4	1	2	6	9	12
[*S*] (g·l_{aq}^{-1})	10	10	10	10	20	20	20	5	10	20	40	80	20	20	20	20	20
T (ºC)	60	70	80	85	60	70	80	70	70	70	70	70	70	70	70	70	70

*For the set with different temperature, an initial charge of monomer (1.3 g) was used.

3.2.3 Results and Discussions

The recipe for the polymerisations is shown in Table 3.2.1. The reaction temperature (T), the concentration of surfactant ([*S*]) and feeding period (t_{add}) were varied in a wide range in order to investigate the minimum size of particles as well as the maximum number of particles achievable.

3.2.3.1 Effect of Temperature (T)

High initiator concentration is known to adversely affect particle nucleation by degrading particle stability [19]. Therefore, in order to alter the rate of radical formation, we chose to vary the reaction temperature.

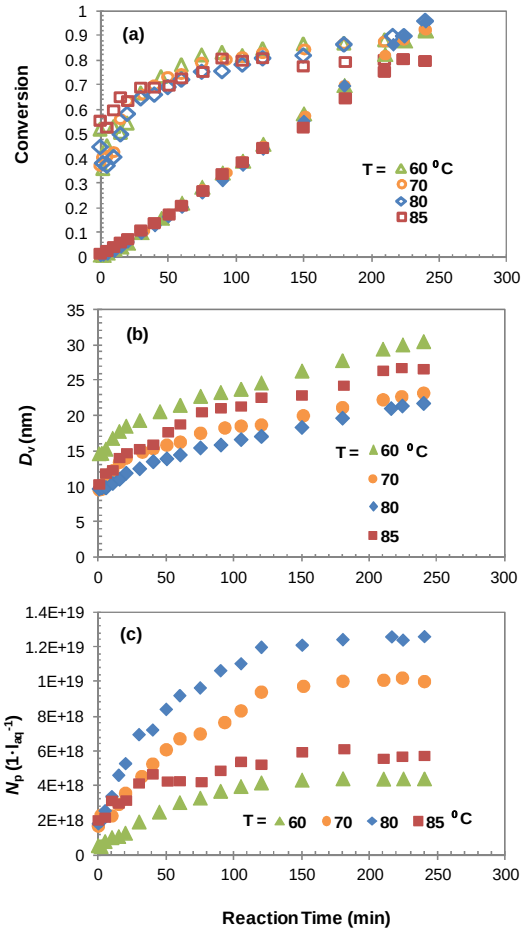

Figure 3.2.1. (a) Conversions of polymerisation, (b) size of particles and (c) number of particles versus reaction time at different T (t_{add}= 4h; [*S*]= 10 g·l_{aq}^{-1})

It is shown in Figure 3.2.1a that the rate of polymerisation is independent from the reaction temperature and tightly controlled by the rate of monomer addition. However, a slight decrease in the rate of reaction (after 2h) can be observed when reaction temperature was 85°C. Figure 3.2.1b shows that the early particles were as small as 10 nm at T > 70°C, and grew upto 30 nm depending on temperature. Overall, the size of particles decreases with increasing temperature

from 60 to 80°C. This is a rule of thump in emulsion polymerisation; the size of particles decreases with increasing rate of radical formation [19].

For all runs, particle formation was completed before the end of addition so that the numbers of particles have reached a plateau, as shown in Figure 3.2.1c. It is notable that the differences became smaller at higher temperatures for both size and number of particles (Figure 3.2.1b-c).

In order to explain the irregularities observed for T = 85°C, the kinetics of initiator decomposition is revisited. The rate of radical formation in the aqueous phase is of prime importance for the nucleation stage. For any given initiator, both concentration and temperature determine the rate of radical formation (R_i) as:

$$R_i = 2fk_d[I] \tag{3.2.3}$$

where k_d is the initiator dissociation rate coefficient and can be calculated with Arrhenius parameters for the persulfate decomposition [20]:

$$k_d(persulfate) = 8 \times 10^{15} s^{-1} e^{-135 kJ mol^{-1}/RT} \tag{3.2.4}$$

and [I] is the available initiator concentration which is given by [21]:

$$[I] = [I_0] e^{-k_d t} \tag{3.2.5}$$

Therefore, the initiator concentration decays as a function of time with a rate depending on temperature. Assuming the efficiency of the initiator, *f*, is 1.0 and the initial concentration of initiator is 4 mM, the values for $[I]/[I_0]$ and R_i were calculated and shown in Figure 3.2.2.

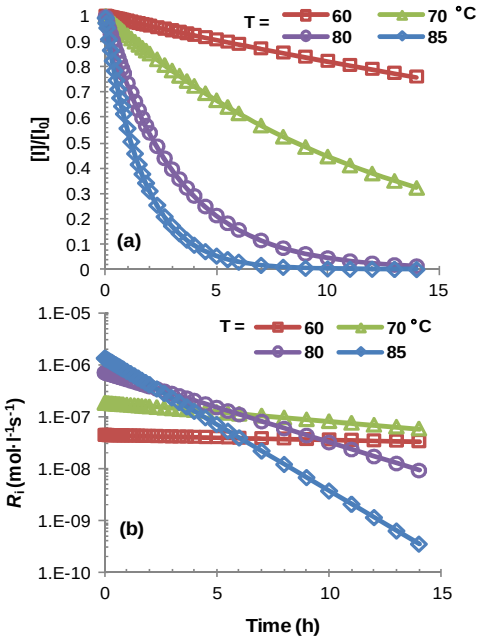

Figure 3.2.2. (a) Initiator concentration decay and (b) the rate of radical formation as a function of time for the polymerisation of styrene at different temperatures (°C) using 4 mM KPS as initiator.

Figure 3.2.2 clearly shows that the initial rate of initiator decomposition (Figure 3.2.2a) or radical formation increases with temperature (Figure 3.2.1b). As a result the half-life time ($t_{1/2}$) of the initiator became shorter and the rate of radical formation dropped faster as temperature increased. This suggests that the supply of radicals becomes increasingly more limited in the course of reaction with increasing temperature. The decaying radical generation is more pertinent to semicontinuous reactions with longer addition time.

Having clarified the effect of temperature on the rate of radical generation, the decrease in the rate of reactions and fall in the number of particles for the reaction carried out at 85ºC, in comparison to other runs, can now be attributed to the very fast decomposition of initiator or short life time of KPS ($t_{1/2}$=1.2h at 85°C). This can explain why the optimum temperature was found to be around at 80 ºC for the system under study at which the maximum number of particles is obtained, as shown in Figure 3.2.3.

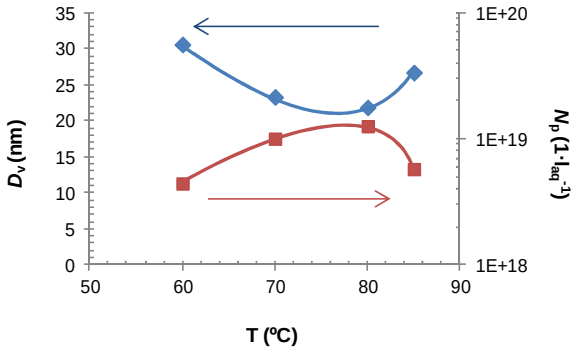

Figure 3.2.3. Final size and number of particles produced with different temperatures. ([*S*]=20 g·l$_{aq}^{-1}$. t_{add} = 4h).

While the simple treatment presented above, can predict the temperature at which the initiator becomes incapable of maintaining the rate of radical generation for formation of particles, it fails to reproduce the details. Comparing R_i for 85ºC with that at 80ºC, as shown in Figure 3.2.2b, one might expect to see a change in radical generation (i.e. number of particles) after 2h. However, experimental results point to much earlier time, as shown in Figure 3.2.1c. It should be noted that the concentration of radicals that take part in the polymerisation reaction, is balanced by the rates of decomposition of initiator and radical termination reaction. An explanation was given by Pan et al. [22] that when temperature reaches a critical level; the increase in the radical concentration via initiator thermal decomposition may be offset by the decrease in radical concentration via radical termination reactions. An approximate solution of the total aqueous phase radical concentration can be found as [20]:

$$\frac{d[\dot{R}]}{dt} = 2k_d[I] - 2k_{t,aq}\left[\dot{R}\right]^2 \qquad (3.2.6)$$

This is based on the assumptions that the radical entry into particles is ignored and $k_{p,aq}$ is independent of the degree of polymerisation. Therefore,

$$[\dot{R}] \approx \left(\frac{k_d[I]}{k_{t,aq}}\right)^{1/2} \tag{3.2.7}$$

where $k_{t,aq}$ is the water phase radical termination rate coefficient, which increases with temperature. As temperature rising, both the rate of radical formation and the rate of radical termination increase in the water phase. Unfortunately, the Arrhenius equation for $k_{t,aq}$ is not available in the literature in order to be able to estimate the time at which the radical concentration for 85°C falls below that of 80ºC.

As shown in Figure 3.2.1c, the conditions selected for this set were so that micelles were used up before the end of monomer addition for all runs. In order to further study the effect of reaction temperature on particle formation, another set of experiments was designed, in which the completion of particle nucleation is not guaranteed with variations in temperature. The results for this new set of conditions are shown in Figure 3.2.4c. At 60°C, number of particles continuously increased throughout the polymerisation. By contrast, a plateau of number of particles was reached at 80°C. The reaction temperature was not further increased due to the fast decomposition of KPS at higher temperature (≥ 85ºC).

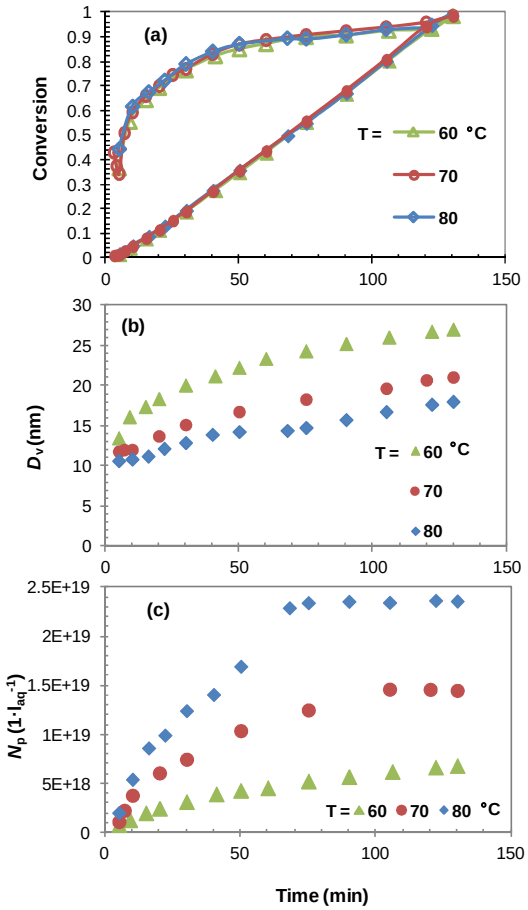

Figure 3.2.4. (a) Conversions of polymerisation, (b) size of particles and (c) number of particles versus reaction time at different T([*S*]= 20 g·l_{aq}^{-1}, t_{add}=2h).

In order to verify the presence of micelles in the reaction mixture, we calculated surface coverage ratio of particles (θ). θ can be estimated using the size and number of particles data given in Figure 3.2.4 and the value of the molecular surface coverage (a_s) for SDS [16]. The values of θ for the particles at the end of reaction for different T are listed in the Table 3.2.2. $\theta \leq$ 1.00 indicates that most of the available surfactant molecules are engaged in particle stabilization and there is no free micelle. θ = 1.00 indicates that particles are fully covered by the surfactant and there likely exists free surfactant micelles in the aqueous phase.

Table 3.2.2. Surface coverage ratio at the end of polymerisations with various T. t_{add} = 2h, [*S*] = 20 g·l_{aq}^{-1}

Temperature (°C)	θ
60	1.00
70	0.99
80	0.73

Figure 3.2.5 shows the same patterns as those given in Figure 3.2.3, for particle size and number. However, **c**omparing with Figure 3.2.3, steeper changes in the particle size as well as number of particles were observed, due to presence of uninitiated micelles by the end of polymerisation for the run with T = 60ºC.

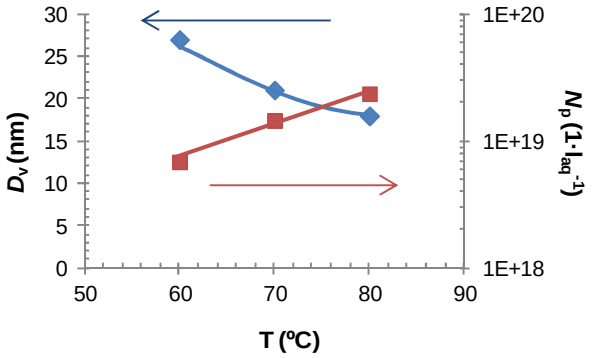

Figure 3.2.5. Final size and number of particles produced with different temperatures. ([*S*] = 20g·l_{aq}^{-1}. t_{add} = 2h).

3.2.3.2 Effect of Surfactant Concentration [*S*]

Surfactant concentration is one of the main factors contributing to the number and size of particles in microemulsion emulsion polymerisation. Various [*S*] were applied, which were 5, 10, 20, 40, and 80 g·l_{aq}^{-1}. The experimental data are shown in Figure 3.2.6.

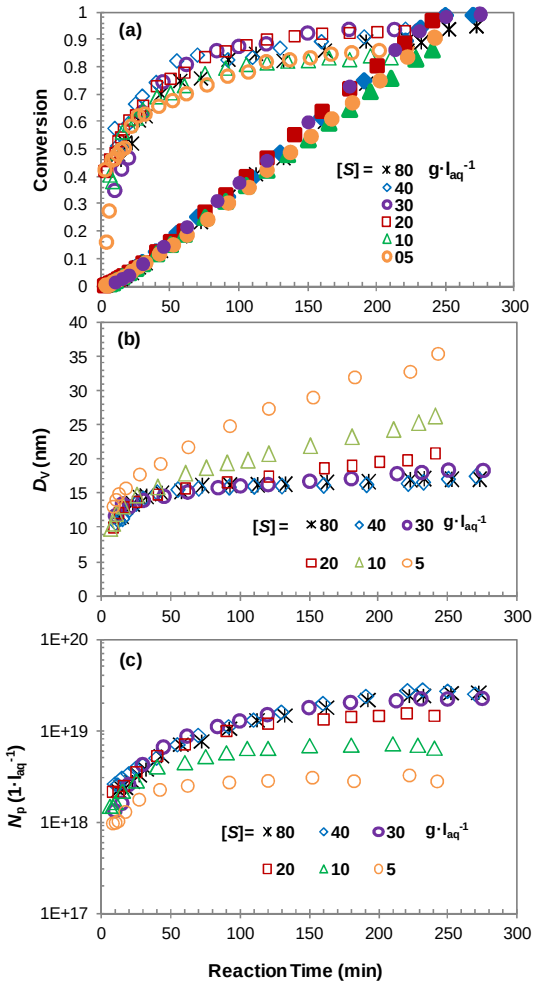

Figure 3.2.6. (a) Conversions of polymerisation, (b) size of particles and (c) number of particles versus reaction time for different [*S*] (t_{add} = 4h, T: 70°C).

Figure 3.2.6a shows that the rates of polymerisation only slightly fluctuated with variations in [*S*], which indicates that the rate of polymerisation was controlled by the rate of monomer addition.

The size of particles was initially almost independent of [*S*] and around 10 nm in diameter. However, the rate at which particles grew becomes slower with increasing [*S*] in particular at the later reaction times, as shown in Figure 3.2.6b, until it finally reduced to almost zero for higher [*S*], i.e, 40 and 80 $g \cdot l_{aq}^{-1}$. This means that the size of particles remains almost constant with time for [*S*] $\geq$ 40 $g \cdot l_{aq}^{-1}$ implying that particles did not grow further when they reached 15 nm at very high [*S*]. As a result, the rate of particle formation, as shown in Figure 3.2.6c, increased with [*S*] correspondingly and reached almost a constant value for higher [*S*].

It should be noticed that with increasing [*S*], the number of particles as well as viscosity of resulting latexes increased significantly. These can have opposing effects on the DLS measurements. Too concentrated latexes can cause multiple scattering effects during measurement, which leads to underestimation of particle size. On the other hand, highly viscose latexes are vulnerable to overestimation in particle size, because of the effect of viscosity. Both

effects can be overcome by severe dilution with deionised water prior to the measurements. However, too much dilution of samples may also cause coagulation of particles due to their insufficient colloidal stability. Therefore a considerable error (± 5%) may exist in the measurements of samples with very high [*S*].

One important point is that for [*S*] ≥ 40 $g \cdot l_{aq}^{-1}$, the number of particles does not appear to have reached a plateau, i.e. end of particle nucleation. For low [*S*], N_p has reached its final value in the early stage of reactions, while reactions with high [*S*] show continuous nucleation till the end of polymerisation. Table 3.2.3 shows that θ increases with [*S*] and finally reaches 1.00 for [*S*] ≥ 30 $g \cdot l_{aq}^{-1}$.

Table 3.2.3. Surface coverage ratio at the end of polymerisations with various [*S*]. t_{add} =4h.

[*S*] ($g \cdot l_{aq}^{-1}$)	θ
5	0.38
10	0.57
20	0.87
30	1.00
40	1.00
80	1.00

In a typical conventional semicontinuous microemulsion polymerisation, nucleation is usually completed before the end of monomer feeding so that primary particles always have sufficient time to grow. With a very high [*S*], particles are continuously formed until the end of the monomer feeding. As a result, the growth of particles is limited. Referring to the Equation 3.2.1, the number of particles should be proportional to [*S*] if nucleation is completed before monomer is fully depleted. However, as shown in Figure 3.2.7, it is clear that while the size of particles initially decreased with increasing [*S*], finally reached a plateau at higher [*S*]. The number of particles followed an opposite trend and reached a plateau too.

The run with [*S*] = 30 $g \cdot l_{aq}^{-1}$ is standing out among the rest of experiments as it represents a case in which the end of monomer addition and micellar nucleation almost coincide. This is probably the most efficient case as it assures all monomer is used up for generating particles and all surfactant micelles have contributed to nucleation. We can define it as $[S]_{cr}$, or as the minimum concentration of surfactant required to consume the whole monomer, which is 30 $g \cdot l_{aq}^{-1}$ under the experimental conditions. However, from Figure 3.2.6 it can be inferred that there still exists a rise in particle size during nucleation for $[S]_{cr}$ = 30 $g \cdot l_{aq}^{-1}$. This is in fact a general pattern for particle formation in which newly formed particles are likely to receive further radicals as the

number of micelles is decreased and the end of nucleation approached. Therefore, it appears that the minimum size may be achieved if excess surfactant concentration is used so that uninitiated micelles do remain in the reaction mixture before the end of monomer addition. In such cases, secondary entry into polymer particles becomes of less importance. Figure 3.2.7 clearly shows that the minimum final size was almost achieved when $[S] = 1.33\times[S]_{cr} = 40\ g\cdot l_{aq}^{-1}$ was used. Any further increase in $[S]$ did not noticeably affect the size of particles obtained.

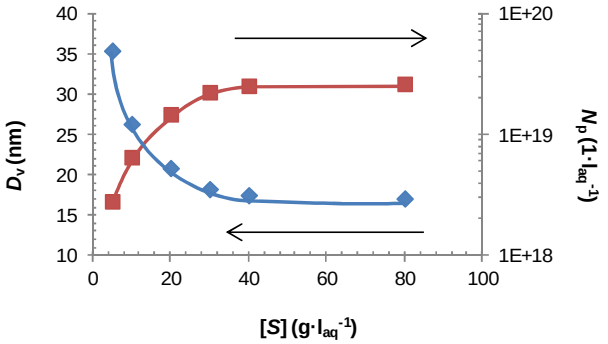

Figure 3.2.7. Final Size and number of particles produced with different [*S*]. t_{add} = 4h.

3.2.3.3 Effect of Rate of Monomer Addition - t_{add}

The rate of monomer addition, R_a, of 100 $ml\cdot h^{-1}$, 50.7 $ml\cdot h^{-1}$, 24.6 $ml\cdot h^{-1}$, 13 $ml\cdot h^{-1}$, 8.68 $ml\cdot h^{-1}$, 5.79 $ml\cdot h^{-1}$ and 4.34 $ml\cdot h^{-1}$, were selected, which were equivalently presented in terms of monomer addition time (t_{add}), 0.5h, 1h, 2h, 4h, 6h, 9h and 12h, respectively. One thing to be clarified is the data shown in this section are mainly based on t_{add}, for simplicity, which increases as decreasing R_a.

Rate of monomer addition (or addition time) is perhaps the most important parameter to control particle size in semicontinuous microemulsion polymerisation. Various t_{add} from 1h to 12h were used. In order to better compare the results for different t_{add}, the monomer addition time was normalised and shown in Figure 3.2.8. The rate of polymerisation is mainly controlled by the rate of monomer addition if $1h \leq t_{add} \leq 6h$. However, the relative rate of polymerisation decreased with increasing feeding time for $t_{add} \geq 9h$. This is because of the significant drop in the initiator concentration during monomer addition when t_{add} is much longer than the half life of KPS (ca. 8.5h at 70ºC). Figure 3.2.2a shows variations in $[I]/[I]_o$ versus time for KPS initiator at T = 70°C. With decreasing [I], the generation of primary radicals diminished and as a result, the instantaneous conversion as well as overall conversion decreased. The results suggest that while the rate of monomer addition is a useful variable to control the size of particles, it is not unbounded.

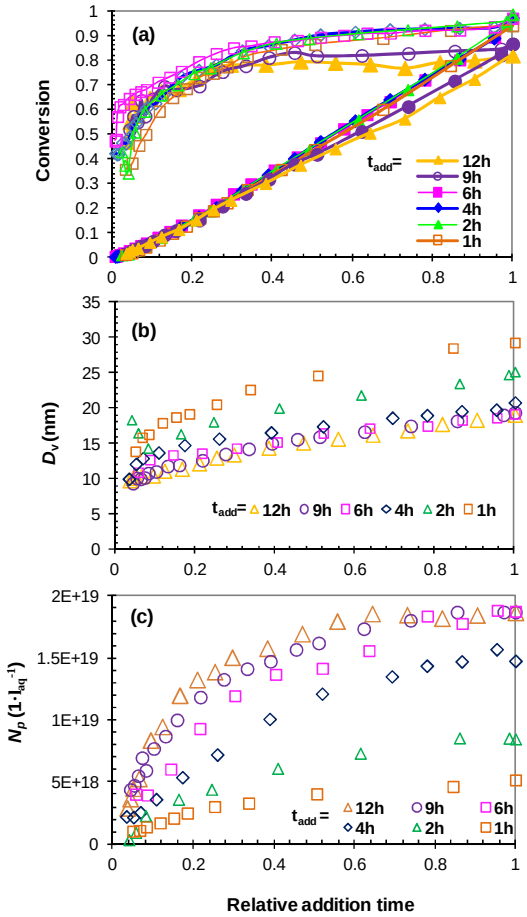

Figure 3.2.8. (a) Conversions of polymerisation, (b) size of particles and (c) number of particles versus relative addition time with different addition periods. [*S*]: 20 g·l_{aq}^{-1}. T: 70ºC

Figure 3.2.8b shows that the size of particles started from a value around 10 nm and increased with time for all t_{add}. Larger particles were obtained for lower t_{add}. The size of particles decreased with increasing t_{add}, but the difference gradually disappeared at the higher t_{add} (6h, 9h and 12h). From Figure 3.2.8c, it is seen that, N_p levelled off before the end of feeding for most feeding periods.

The values of θ at the end of polymerisation for different feeding rates are listed in Table 3.2.4. θ decreased with increasing t_{add} from a value of one to smaller than one passing through *the critical rate of monomer addition* for the run with t_{add} = 2h. This run represents the critical run in which particle formation and feeding ended at the same time so that θ = 1.0 with no micelles being present. For the runs with t_{add} > 2h, micelles were depleted during reaction and particle growth occurred during the remainder of the reactions. With increasing t_{add}, particle formation occurs along a longer time, more particles are formed, and larger surface area per unit weight is developed, leading to a decrease in θ.

Table 3.2.4. Surface coverage ratio at the end of polymerisations with various t_{add}.

t_{add} (h)	θ
1	1.00
2	1.00
4	0.87
6	0.80
9	0.73
12	0.73

Figure 3.2.9 depicts variations in the final N_p and D_v with t_{add}. The average size of particles initially decreases significantly with increasing t_{add}, however, reaches a plateau for $t_{add} \geq 6$h. These addition times are associated with the depletion of radicals (see Figure 3.2.8a), which is the main cause for constant number of particles and drop in the rate of reaction, as explained before. The minimum size is achieved when addition time is three times that of critical addition time; $t_{add} = 3.0 \times t_{add,cr} = 6$h.

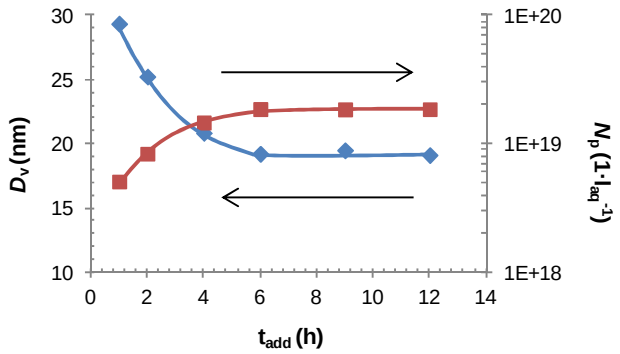

Figure 3.2.9. Final size and number of particles produced with different t_{add}. [*S*]: 20 $g \cdot l_{aq}^{-1}$.

3.2.3.4 Further Discussion

It can be concluded that one of the two the main reasons for emerging plateau in particle size variations with process variables is early depletion of initiator in the course of reaction. Continuous addition of initiator can be a way forward to make particle size patterns comply with Equations 3.2.1 and 3.2.2. While this can assure an optimum use of surfactant, cannot guarantee the minimum size, which can only be obtained if polymerisation reaction stops short of nucleation, in order to avoid re-entry and further growth of particles.

Having realised that the initiator and surfactant micelles depletions are the main restricting factors for achieving the smallest nanoparticles, we defined a set of new experiments in which

the addition time was fixed at 2h, in order to avoid fast depletion of KPS, and surfactant concentration at a high value (5 $g \cdot l_{aq}^{-1}$) in order to allow for nucleation to last for the substantial part of addition period, if not all. The rate of addition (R_a) was varied in a rather wide range. Note that in this set, the solids content was not constant and increased with R_a. Figure 3.2.10a clearly shows that the particle size decreased continuously with decreasing R_a, with no plateau reached even down to very low R_a (< 4.3 $ml \cdot h^{-1}$). The initial and final diameters of particles ranged from 6 to 18 nm, and 10 to 47 nm, respectively, depending on R_a (2.9 to 100 $ml \cdot h^{-1}$). The resulting particles were highly starved with monomer and grew at an extremely low rate, as shown in Figure 3.2.10a, for R_a < 4.3 $ml \cdot h^{-1}$. Under such conditions, as soon as the growing radicals reach the critical chain length for entry, they tend to be captured by micelles, which outnumber particles, avoiding secondary radical entry and enhancing generation of new particles (Figure 3.2.10b). The minimum detectable particle diameter, 6.0 nm, was obtained for the lowest monomer feed rate used; 2.9 $ml \cdot h^{-1}$. This is only slightly larger than the size of monomer swollen micelles. The results suggest that dilute nanolatexes can be easily produced using extremely low monomer addition rates.

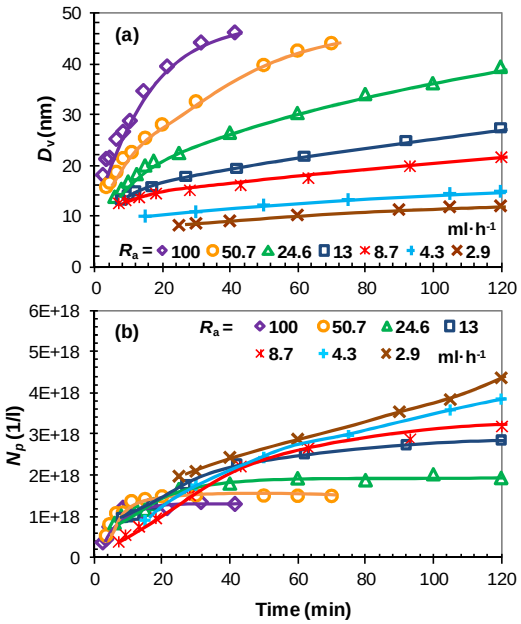

Figure 3.2.10. (a) Size of particles and (b) number of particles versus addition time at different R_a. [*S*]: 5 $g \cdot l_{aq}^{-1}$. T: 70°C.

3.2.4 Conclusions

In this part, particle formation in semicontinuous microemulsion polymerisation under extreme conditions, such as high [*S*], low rate of monomer addition and high reaction temperature, has been explored. The main aim was to find conditions under which the minimum particle size can be achieved. As general rules of thumb, high surfactant concentration and low rate of addition are pre-requisite to generation of small nanoparticles. However, results show a limit to which the size of particles can be reduced, as the size of particles approached constant values with increasing [*S*] and decreasing R_a. It was found that excess surfactant micelles at the end of addition are required in order to achieve smallest particles. Continuous addition of initiator should be considered if smaller particles at extremely low R_a are sought. Under the given experimental conditions, the lower limit of particle size was achieved with [*S*] > 40 $g \cdot l_{aq}^{-1}$, and t_{add}> 6h, and the reaction temperature of 80°C. These correspond to particle diameters of 14.9 nm, 19.1 nm and 21.9 nm, respectively. The results also show that by using extremely low R_a, the size evolution of particles starting from sizes similar to that of micelles can be monitored. Particles as small as 6 nm could be produced in the early stage of reactions.

3.2.5 Reference

[1] Ming, W.H. Jones, F.N., Fu, S.K. Synthesis of Nanosize Poly(methyl methacrylate) Microlatexes with High Polymer Content by a Modified Microemulsion Polymerization. *Polymer Bulletin*, 1998, v40, pp749-756.

[2] Sajjadi, S. Particle formation under monomer-starved conditions in the semibatch emulsion polymerization of styrene. I. Experimental. *Journal of Polymer Science Part A: Polymer Chemistry* 2001, v39, pp3940-3952.

[3] Xu, X.J., Chew, C.H., Siow, K.S., Wong, M.K., Gan, L.M. Microemulsion polymerization of styrene for obtaining high ratios of polystyrene/surfactant. *Langmuir*, 1999, v15, pp8067-8071.

[4] Chuayjuljit, S., Boonmahitthisud, A. Natural Rubber Nanocomposites using Polystyrene-encapsulated Nanosilica Prepared by Differential Microemulsion Polymerization. *Applied Surface Science*, 2010, v256, pp7211-7216.

[5] Pan, F.S., Jia, H.P., Cheng, Q.L., Jiang, Z.Y. Bio-inspired Fabrication of Composite Membranes with Ultrathin Polymer-silica Nanohybrid Skin Layer. *Journal of Membrane Science*, 2010, v362, pp119-126.

[6] Chen, B., Deng, J.P., Yang, W.T. Chiral Helical Polyacetylene-vinyl Polymer Core/shell Nanoparticles: Preparation and Application to Optically Active Composite films. *Colloid and Polymer Science*, 2011, v289, pp133-139.

[7] Darwish, M.S.A., Peuker, U., Kunz, U., Turek, T. Bi-layered Polymer-magnetite Core/shell particles: Synthesis and Characterization. *Journal of Materials Science*, 2011, v46, pp2123-2134.

[8] Bait, N., Grassl, B., Derail, C., Benaboura, A. Hydrogel Nanocomposites as Pressure-sensitive Adhesives for Skin-contact Applications. *Soft Matter*, 2011, v7, pp2025-2032.

[9] Ho, C.T., Low, K.B., Klie, R.F., Maeda, K., Domen, K., Meyer, R.J., Snee, P.T. Synthesis and Characterization of Semiconductor Tantalum Nitride Nanoparticles. *Journal of Physical Chemistry C*, 2011, v115, pp647-652.

[10] Neubert, R.H.H. Potentials of New Nanocarriers for Dermal and Transdermal Drug Delivery. *European Journal of Pharmaceutics and Biopharmaceutics*, 2011, v77, pp1-2.

[11] Nomura, M., Harada, M. In: Basset, D.R., Hamielec, A.E. editors. *American Chemical Society*, 1981, pp121.

[12] Sajjadi, S. Nanoparticle formation by monomer-starved semibatch emulsion polymerization. *Langmuir*, 2007, v23, pp1018-1024.

[13] Sajjadi, S., Brooks, B.W. Semibatch emulsion polymerization of butyl acrylate. I. Effect of monomer distribution. *Journal of Applied Polymer Science*, 1999, v74, pp3094-3110.

[14] He, G.W., Pan, Q.M., Rempel, G.L. Synthesis of Poly(methyl methacrylate) Nanosize Particles by Differential Microemulsion Polymerization. *Macromolecular Rapid Communications*, 2003, v24, pp585-588.

[15] Chen, W.B., Liu, X.Y., Liu, Y.S., Bang, Y., Kim, H. Synthesis of PMMA and PMMA/PS Nanoparticles by Microemulsion Polymerization with a New Vapor Monomer Feeding System. *Colloids and Surfaces A: Physicochem. Eng. Aspects*, 2010, v364, pp145-150.

[16] Sajjadi, S. Particle Formation under Monomer-starved Conditions in the Semibatch Emulsion Polymerisation of Styrene. Part II. Mathematical Modelling. *Polymer*, 2003, v44, pp223-237.

[17] Sajjadi, S. Population Balance Modeling of Particle Size Distribution in Monomer-Starved Semibatch Emulsion Polymerization. *Aiche Journal*, 2009, v55, pp3191-3205.

[18] Kalinin, V.V., Radke, C.J. An ion-binding model for ionic surfactant adsorption at aqueous-fluid interfaces. *Colloids and surface a-Physicochemical and Engineering Aspects*, 1996, v114, pp337-350.

[19] Smith, W.V., Ewart, R.H. Kinetics of Emulsion Polymerisation. *Journal of Chemical Physics*, 1948, v16, pp592-599.
[20] Gilbert, R.G. London: Academic press, 1995.
[21] Odian, G. Wiley: New York, 1995, Chapter 2, pp198-394.
[22] Liu, J.M., Pan, Q.M. Synthesis of Nanosized Poly(ethyl acrylate) Particles via Differential Emulsion Polymerization. *Journal of Applied Polymer Science*, 2006, v102, pp1609-1614.

3.3 Synthesis of Ultrafine Nanolatexes using Chain Transfer Agent via Semicontinuous Microemulsion Polymerisation

Abstract: As an alternative way to reduce the particle size, a water-soluble chain transfer agent (CTA), 2-Butanethiol, was used in semicontinuous microemulsion polymerisation for the synthesis of ultrafine nanolatexes. Batch emulsion polymerisations were carried out for comparison. It was found that for batch process, the termination of chain transferred radicals in the water phase become more important with increasing CTA concentration, resulting in formation of large particles. By contrast, for semicontinuous process, the application of the CTA reduced the average particle size by 25%, and provided a good controllability over molecular weight distribution as well as the rate of polymerisation.

3.3.1 Introduction

Many applications of nanolatexes with small size of particles (below 20 nm) also require sharp or at least narrow molecular weight distributions (MWDs) [1-4]. Semicontinuous microemulsion polymerisation is a powerful technique to produce concentrated nano-latexes using a low concentration of surfactant [5-9]. Lower molecular weights are usually obtained for latexes produced by semicontinuous process, comparing with those from batch process. Furthermore, it has also been found that the molecular weight of polymer can be controlled by the rate of monomer addition [10-12].

Mercaptans (C_4-C_{12}) are commonly used as chain transfer agent (CTA) to control the MWD by terminating the growing polymer chains and transferring the radical activity to the CTA molecules [13-15].

Ideally CTA affects only the molecular weight of the polymer product but not the kinetics of the polymerisation. However, Nomura found that in emulsion polymerisation, both the molecular weights and the rate of polymerisation are affected in the presence of highly water-soluble CTAs [14]. The effect is due to desorption of chain transferred radicals from polymer particles to water phase [16]. Harada and Nomura [14,17] pointed out that the desorbed radicals can re-enter the micelles and form new particles during nucleation stage. Moreover, as transferred radicals leave the particles, the rate of particle growth, as well as the consumption rate of micelles can be depressed. As a result, the particle formation can be enhanced (i.e. prolonged).

These ideas were partly experimentally tested by Nomura using four primary mercaptans (C_2, n-C_4, n-C_7 and n-C_{12}) via batchwise emulsion polymerisation [14]. It was found that with an increase in the amount of CTA charged, the number of polymer particles produced increases initially, but then decreases due to significant water-phase termination among initiator and desorbed radicals. The effects were expected to be more promising when mercaptans with higher water solubility are used.

In previous section, we explored the conditions under which smallest polymeric nanoparticles can be produced for conventional polymerisations. In the current section, we seek to further exploit this idea by reducing the polymer chain length within particles, as described above, in semicontinuous microemulsion polymerisation. The corresponding batch polymerisation was also conducted for the sake of comparison. By using a water-soluble chain transfer agent, we aim to terminate growing radicals inside particles in order to hinder the particle growth and therefore reduce the size of resulting nanoparticles. The main aim is to be able to control the polymer particle size via controlling the length of polymer chains formed during the reaction using a CTA.

3.3.2 Experimental Work

3.3.2.1 Procedure

For batch process: 50 ml styrene and a weighed quantity of CTA were firstly added into the reactor. After being purged for 5 min with nitrogen gas, KPS solution was then added to the vessel to initiate the reaction. An inhibition period of 1-2 min was observed for polymerisation reaction to start. The time zero for the start of reaction was considered when polymer was detected in the reaction mixture.

For semicontinuous process: The initiator solution was firstly added to the vessel. The system was allowed to return to reaction temperature. Styrene and a weighed quantity of the CTA were mixed and purged with nitrogen for 15 min before use to remove the oxygen dissolved in the monomer. The addition of monomer was started instantly with a dosing pump with a fixed feeding speed (13 $ml \cdot h^{-1}$). The onset of reaction was continuously monitored by sampling from the vessel and precipitating in methanol. The reaction time *zero* for the start of reaction was considered when the first droplet of monomer was added into the reactor.

3.3.2.2 Measurements

Conversions, z-average diameter of particles (D_z) and weight-average molecular weight ($\bar{M}_w$) have been measured. Details can found in the previous subchapter (see Chapter 3.1, page 44). A conversion factor of $C_f = 0.9$ was found so that $D_{v,} = C_f \cdot D_z$. The number of particles and the surface coverage ratio of particles (θ) have been calculated.

Table 3.3.1. Recipe used for the study of polymerisations in the presence of CTA. T = 70°C. St: 50 ml; Water: 600 ml; [KPS]=[Buffer]= 4 $mmol \cdot l_{aq}^{-1}$

Ingredients	Quantity
SDS ($g \cdot l_{aq}^{-1}$)	10
Feed rate ($ml \cdot h^{-1}$)	13
CTA (wt%)	0.5~4

3.3.3 Results

Considering that the reaction temperature is 70°C, the boiling point of the selected mercaptan should not be too low. For this reason we chose 2-Butanethiol, *sec*-butyl mercaptan, as CTA because of its relatively high boiling point and solubility in water (1.32 $g \cdot l_{aq}^{-1}$, at 20ºC, as shown in Table 3.3.2).

Two sets of experiments were carried out via batch and semicontinuous processes to investigate the effect of CTA on the kinetics of polymerisation. The concentrations of CTA used in this work have been varied from 0 to 4wt% based on the weight of monomer.

Table 3.3.2. Physical properties of some mercaptans

CTA	Boiling point (°C)	Solubility in water ($g \cdot l_{aq}^{-1}$) (20°C)
Ethanethiol	35	6.80
1-propanethiol	67-68	1.90
1-butanethiol	97-99	0.60
2-butanethiol	82-88	1.32
tert-butanethiol	63.7-64.2	2.00
1-pentanethiol	125-126	0.16
1-Decanethiol	114	None
1-Dodecanethiol	266-283	None

3.3.3.1 Conversions

Figure 3.3.1 shows the variations of conversions versus time for different CTA concentrations for both batch and semicontinuous processes. The overall rate of polymerisation was suppressed in the presence of CTA and decreased further with increasing CTA concentration for the batch process, as shown in Figure 3.3.1a. Similar experimental results have also been obtained by Fevotte et al. [16]. However, for semicontinuous process, the rate of polymerisation was not much sensitive to the amount of CTA (Figure 3.3.1b). This is simply because in the monomer-starved semicontinuous process, the rate of reaction was controlled by the rate of monomer addition.

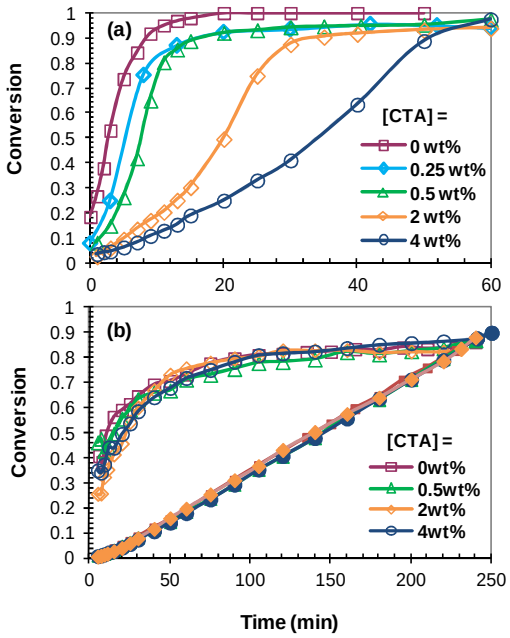

Figure 3.3.1. Conversion versus time for polymerisations with various CTA concentrations for different processes (a) Batch and (b) Semicontinuous

3.3.3.2 Size of Particles

The results for particle size in the course of reaction time are shown in Figure 3.3.2. For the batch process, the rate of particle growth was depressed when lower concentration of CTA was used (< 0.5wt%). However, in the presence of higher concentration of CTA (> 2wt%), the particles grew much faster, as shown in Figure 3.3.2a. For semicontinuous process, the size of particles decreased with increasing CTA concentration.

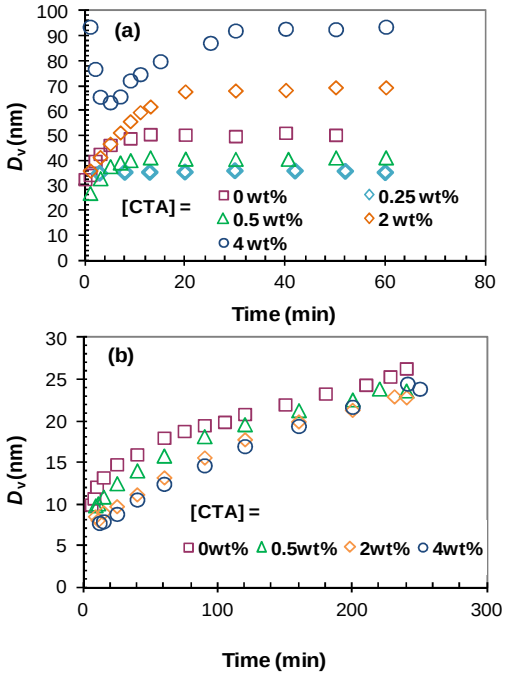

Figure 3.3.2. D_v versus time for polymerisations with various CTA concentrations for different processes: (a) Batch and (b) Semicontinuous

3.3.3.3 Molecular weight of polymer ($\bar{M}_w$)

The weight-average molecular weight of polymer produced ($\bar{M}_w$) in the course of polymerisation was monitored, as shown in Figure 3.3.3, for typical batch and semicontinuous runs. $\bar{M}_w$ is found to be continuously increasing during batch polymerisation, which indicates that $\bar{M}_w$ is not well controlled in the presence of CTA. By contrast, $\bar{M}_w$ is fairly constant throughout the semicontinuous process, which indicates a narrow MWD was obtained

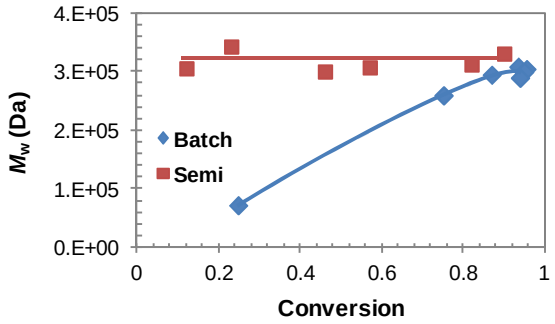

Figure 3.3.3. Conversion evolution of weight-average molecular weight ($\bar{M}_w$) of produced polymer versus conversion in the course of batch and semicontinuous microemulsion polymerisation. CTA: 0.25wt%.

The $\bar{M}_w$ of the final samples were drawn against CTA concentrations and shown in Figure 3.3.4. It shows that $\bar{M}_w$ decreased with increasing CTA concentration for both batch and semicontinuous processes. Note that despite similar $\bar{M}_w$ produced by both processes, the polydispersity, measured by variations in $\bar{M}_w$ in the course of reaction, is quite significant for polymers produced by batch process.

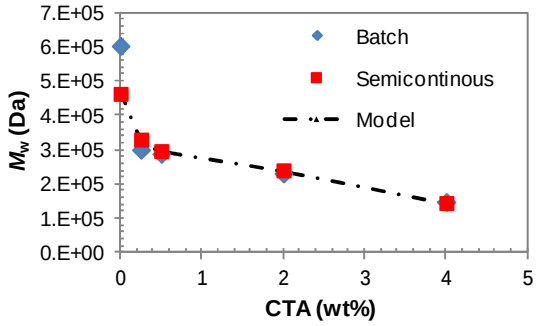

Figure 3.3.4. Weight average molecular weight ($\bar{M}_w$) versus CTA concentration for different processes. The dotted line represents model predictions for the semicontinuous process.

3.3.4 Discussions

3.3.4.1 Particle Formation and Growth

The results for the number of particles can demonstrate most clearly the effect of CTA on particle formation and growth. Using the size data shown in Figure 3.3.2, the number of particles for different runs was calculated and shown in Figure 3.3.5.

Since the CTA (2-C_4) is more water soluble than styrene (0.31 $g \cdot l_{aq}^{-1}$), the CTA is able to diffuse faster than monomer from monomer droplets to the growing polymer particles through the aqueous phase. The high diffusion rate, coupled with a high reactivity inside the polymer particles, could result in faster consumption of CTA in the course of polymerisation.

Furthermore, radicals arising from chain transfer reaction to CTA can be easily desorbed from particles and generally undergo four fates [14,16,20]:

(1) It can be terminated by another radical in the aqueous phase.

(2) It can re-enter an existing 'active' polymer particle and terminate with another radical inside the particle.

(3) It can re-enter an existing 'inactive' polymer particle and propagate inside the particle.

(4) It can re-enter a free micelle and form a new particle.

In cases of (1) and (2) there will a significant reduction in concentration of radicals within the system affecting adversely both rate of reaction and particle nucleation. For the batch process, a large number of chain transferred radicals could be generated in the early stage of polymerisation since all of CTA was initially charged in the reactor. Conversion data (Figure 3.3.1a) suggest that radical termination is dominant either in the water phase or in the particle phase. Particle number data, as shown in Figure 3.3.5a, supports this hypothesis at least for the runs with CTA > 2.0wt% which were associated with a significant drop in the number of particles. A depressed rate of particle formation can result in larger size of particles (Figure 3.3.2a).

Nevertheless, on the other hand, it can be found that new particles continuously formed in the course of batch polymerisation and particle nucleation period was prolonged with increasing CTA concentration (Figure 3.3.5a). It indicates that re-entry to free micelles to nucleate particles is also taking place in the system. When CTA concentration is low (< 0.5wt%), the contribution of desorbed radicals into nucleation (event 4) is more significant than theirs to radical termination. Consequently, the final number of particles produced using batch process with CTA is higher than that produced with neat monomer (Figure 3.3.5a), but the rate of polymerisation was retarded.

For the semicontinuous process, the monomer/CTA mixture was continuously fed into the reactor. The polymerisation occurred under starved conditions, as shown in Figure 3.3.1b. The rate of particle growth was controlled by the rate of monomer addition, and the nucleation period was prolonged due to a low rate of particle growth. This caused more micelles to remain in the system and contribute to nucleation, before they had to deplete in order to stabilise the growing particles. Therefore, a considerable chance of radical re-entry into micelles, rather than termination of the desorbed CTA radicals, arises. As shown in Figure 3.3.5b, particle formation was enhanced with the help of CTA. Larger population of particles were formed in the beginning of polymerisation when a higher concentration of CTA is used. As polymerisations proceeded, however, the particles underwent coagulation in the course of the reaction so that the number of final particles produced varied slightly with CTA concentration.

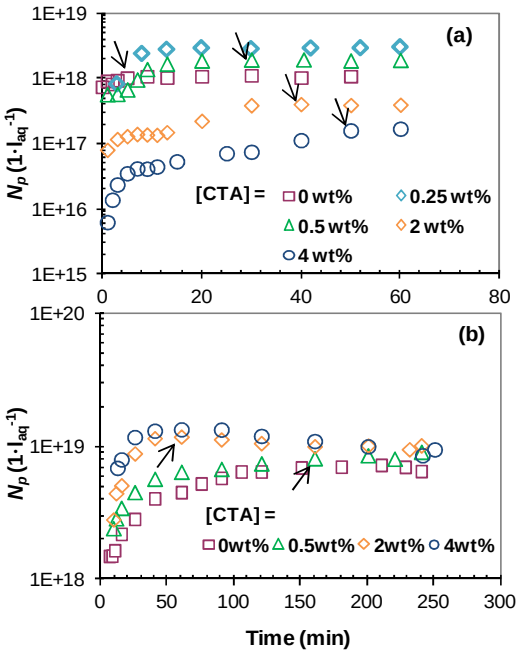

Figure 3.3.5. **N_p versus time for various CTA concentrations for different processes (a) batch and (b) semicontinuous. Arrows show end of nucleation.**

One possible reason to explain particle coagulation is that the amount of surfactant available in the system was not enough to stabilize such a large number of particles produced and limited particle coagulation occurred. In order to investigate this, the average particle surface coverage ratio (θ) during polymerisations was calculated and shown in Figure 3.3.6. One important point about the batch process, is that particles were completely covered by SDS and uninitiated micelles did exist by the end of polymerisation for all runs except those two that produced larger numbers of particles; [CTA] = 0.25wt% and 0.5wt%. This implies that the large variations in the final number of particles produced for runs with different CTA concentration might be partly due to early consumption of monomer and presence of uninitiated micelles in the latexes. However, the formation of large particles for high CTA concentration, as shown in Figure 3.3.21, indicates that such an effect is minor.

For the semicontinuous process, particle formation completed and θ dropped below 100% in the course of feeding. By comparing Figure 3.3.5b and 3.3.6b, it can be found that particles start to coagulate as soon as θ drops below 100%. This was not expected as surface coverage of as low as 50% has been found to produce sufficient stability to polymeric nanoparticles [21]. Particles formed by entry of desorbed radicals into micelles do not have the sulfate end group, and are comparatively less stable. This could be the reason why such particles are prone to coagulation even at intermediate range of surfactant coverage. Note that particles produced by batch process with [CTA] = 0.25 and 0.50wt% had θ of around 75-85% at end of polymerisation, but did not undergo coagulation. This was probably because particles had become glassy at high conversions by the time that θ dropped below 100% [22].

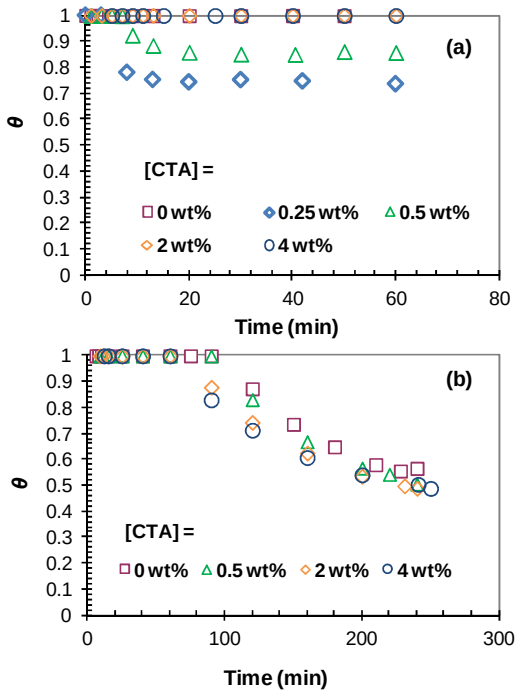

Figure 3.3.6. Particle surface coverage ratio in the course of polymerisation for various CTA concentrations via (a) batch process, (b) semicontinuous process

In order to improve colloidal stability of particles during the growth stage, we repeated the experiment with 4wt% CTA, but gradually added SDS (4.8 g) just after nucleation stage from 60 min onwards to 180 min. The results are shown in Figure 3.3.7. As we expected, particle coagulation was suppressed and more particles were maintained during the growth stage. One thing should be noticed is that the rate of SDS addition was controlled at a low level in order to avoid accumulation of SDS in the reaction mixture and induce secondary particle nucleation. The evolution of θ during reaction was compared with polymerisations with 0wt% and 4wt% CTA concentrations, as shown in Figure 3.3.8. It is found that a small increase in θ by feeding SDS was sufficient to hinder particle coagulation.

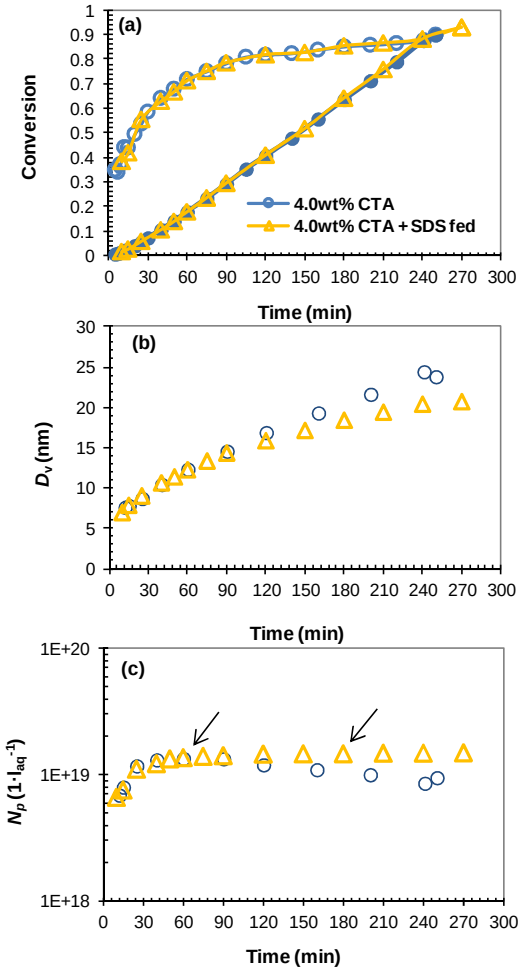

Figure 3.3.7. (a) Conversions, (b) volume-average size of particles, and (c) number of particles produced in the course of semicontinuous microemulsion polymerisation for runs with 4wt% CTA and different SDS addition policy. The arrows indicate the period of addition of SDS.

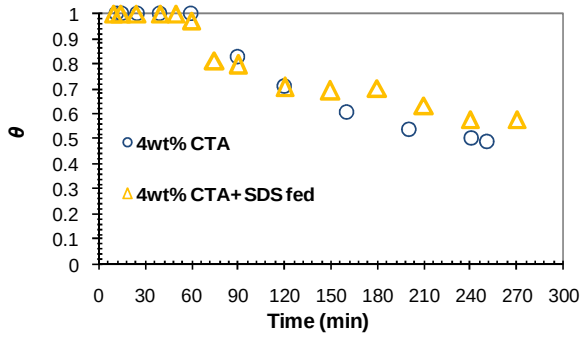

Figure 3.3.8. Particle surface coverage ratio in the course of repeated semicontinuous emulsion polymerisation with 4wt% CTA.

Figure 3.3.9 shows the final N_p and final particle size for different runs. For the batch process, the final size of particles initially decreased with CTA concentrations but later increased giving a minimum at 0.25wt% of CTA concentration (see Figure 3.3.9a). For semicontinuous process, the final size of particles decreased only slightly with increasing CTA concentration, as shown in Figure 3.3.9b. The maximum numbers of particles that could be produced by semicontinuous process, assisted by gradual addition of SDS during growth stage, are also shown. Moreover,

Figure 3.3.9 directly shows that the number of particles that can be produced via semicontinuous process is more than 10 times of that via batch process.

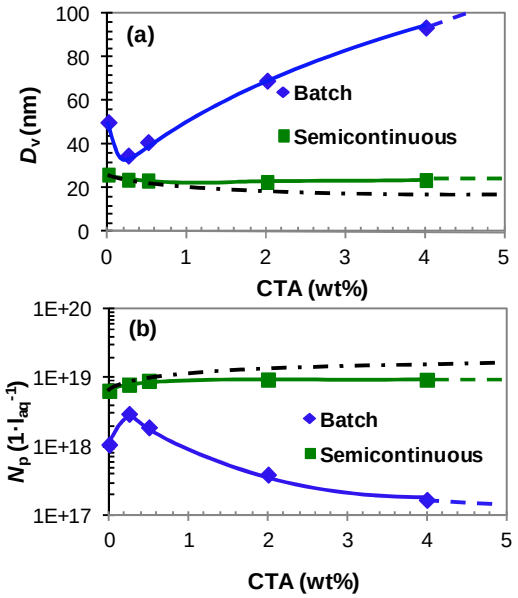

Figure 3.3.9. (a) Final N_p and (b) final size of particle versus CTA concentration for different processes. Dashed lines indicate the final size of particles as well as the number of particles produced by semicontinuous process with excess addition of SDS during particle growth stage.

In order to show the importance of water solubility of CTA in producing small particles, semicontinuous process in the presence of 1-Decanethiol (1-C10) was carried out. 1-Decanethiol is a chain transfer agent with almost no solubility in water (see Table 3.3.2). The results are shown in Figure 3.3.10. It is clear that there is no significant effect of 1-C10 on the particle growth and formation. This is simply because transferred radicals remain inside polymer particles and propagate there without leaving any significant effects on the kinetics of polymerisation.

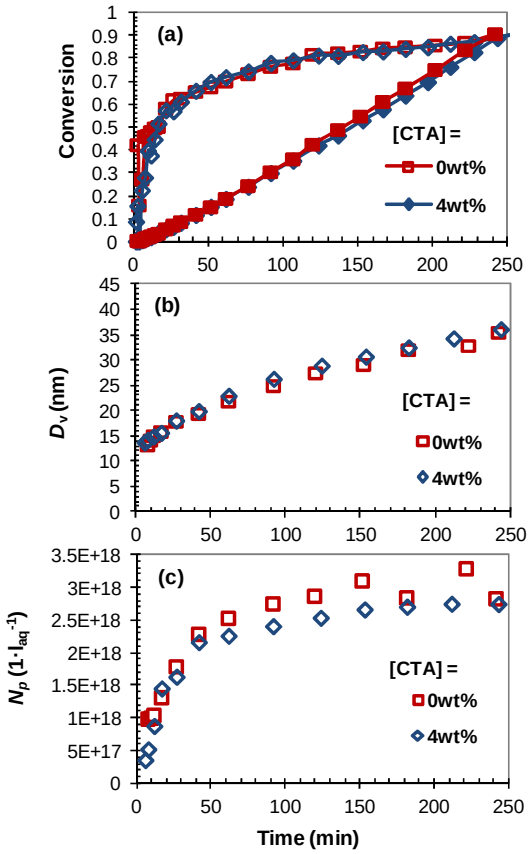

Figure 3.3.10. (a) Conversions, (b) size of particles and (c) number of particles versus reaction time. CTA: 4wt% of 1-C10.

3.3.4.2 Control of Molecular Weight

The polymer produced instantaneously has a number-average chain length ($DP_n = \bar{M}_n / M_{mon}$) given by [23]:

$$1/DP_n = 1/DP_0 + C_T[A]/[M] \quad (3.3.1)$$

where M_{mon} is the monomer molecular weight, [M] and [A] are the molar concentration of monomer and CTA in the polymer particle. DP_0 is the polymer number-average chain length in the absence of CTA. The transfer constant of CTA (C_T) is given as:

$$C_T = k_{tr}^A / k_p \quad (3.3.2)$$

where k_{tr}^A is the chain transfer rate constant of CTA and k_p is the propagation reaction rate constant of monomer.

Ideally, in a batch polymerisation, $\bar{M}_n$ can be determined by C_T, as shown in Equation 3.3.1. If chain transfer to CTA controls the molecular weight and $C_T = 1.0$, then $\bar{M}_n$ remains constant in the course of polymerisation. For reactive CTAs exhibiting $C_T > 1.0$, $\bar{M}_n$ increases along the reaction; otherwise it decreases for CTAs with $C_T < 1.0$. However, this is not always valid when

the water solubility of CTA is much different from that of monomer, or termination reactions are operative.

From Figure 3.3.3, it is seen that $\bar{M}_w$ of polymer increased in the course of batch polymerisation in the presence of 0.25wt% CTA. This may point to a relation of type $C_T > 1.0$ for the CTA. However, this is not conclusive as solubility of 2-butanethiol in water is several times greater than that of styrene. Before a CTA molecule can involve in a batch reaction, it has to transfer from monomer droplets to growing polymer particles via aqueous phase. Being relatively water-soluble substance, the CTA can easily transfer into polymer particles and react, while the styrene monomer diffuses much slower. As the CTA is consumed in polymer particles, then $\bar{M}_w$ would increase. This could be the reason why $\bar{M}_w$ in the batch process increased with conversion, and was even lower than that of semicontinuous process. Regarding the latter, the reverse was true when the CTA was absent from formulation (see Figure 3.3.4).

This picture can be changed in semicontinuous process in which the transport effects are minimised, as the rate of reaction as well as the concentration of CTA in the system is tightly controlled by the rate of monomer addition. Considering that $\bar{M}_w$ of polymer produced in semicontinuous process is controlled by chain termination reactions as well as transfer reaction to CTA, the value of C_T can be obtained by fitting Equation 3.3.1 with experimental data (assuming $\bar{M}_w = 2\bar{M}_n$ [24]), as shown in Figure 3.3.4. A value of 0.021 was found for C_T which is much smaller than the values of conventional CTAs reported in the literature. It also suggests a relation of type $C_T < 1.0$ for the CTA used.

Using molecular-weight and particle-size data, the average number of chains per particle were calculated and shown in Figure 3.3.11. For batch process, the number of polymer chains per particle increased significantly with CTA concentration. The results suggest that the re-entry of desorbed radicals to the growing particles is significant in the course of polymerisation. This fits with the size data, as shown in Figure 3.3.2a where the particles grew to a significant extent at higher concentration of CTA. Comparing with batch process, particles formed via semicontinuous process contain fewer chains whose number remained relatively constant with increasing CTA concentration even though the chains become shorter (see Figure 3.3.4).

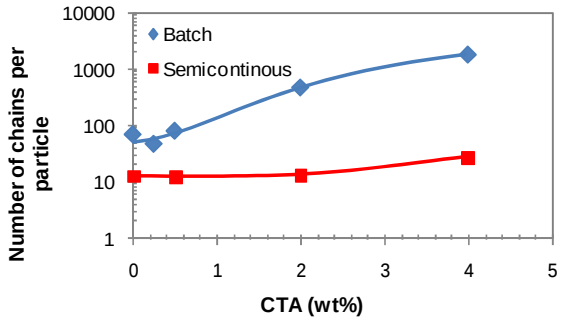

Figure 3.3.11. Average number of chains per particle versus CTA concentration for batch and

3.3.5 Conclusions

The effect of CTA on the formation of ultrafine particles via semicontinuous emulsion polymerisation was studied. The results show that using a CTA with relatively high solubility in water, 2-Butanethiol, makes desorption of chain transferred radicals to the water phase kinetically more important. Under batch condition, the rate of polymerisation as well as the molecular weight of final products decreased with increasing CTA concentration. Furthermore, except for the low concentration of CTA fewer particles with larger size were produced with increasing CTA concentration due to termination of active radicals in the water phase.

Comparing with batch process, semicontinuous process can produce much smaller particles at a constant rate of polymerisation and provide a better controllability over particles size and molecular weight in the presence of CTA. Using CTA, it was possible to reduce the particle size by almost 25%.

3.3.6 Reference

[1] Xia, H.M., Gao, X.L., Gu, G.Z., Liu, Z.Y., Zeng, N., Hu, Q.Y., Song, Q.X., Yao, L., Pang, Z.Q., Jiang, X.G., Chen, J., Chen, H.Z. Low Molecular Weight Protamine-Functionalized Nanoparticles for Drug Delivery to The Brain After Intranasal Administration, *Biomaterials*, v32, 2011, pp9888-9898.

[2] Hirsjarvi, S., Peltonen, L., Hirvonen, J. Layer-By-Layer Polyelectrolyte Coating of Low Molecular Weight Poly(lactic acid) Nanoparticles, *Colloids and Surfaces B-Biointerfaces*, v49, 2006, pp93-99.

[3] Mendoza, J., De La Cal, J.C., Asua, J.M. Kinetics of the Styrene Emulsion Polymerisation Using n-Dodecyl Mercaptan as Chain-Transfer Agent, *Journal of Polymer Science: Part A: Polymer Chemistry*, v38, 2000, pp4490-4505.

[4] Gugliotta, L.M., Salazar, A., Vega, J.R., Meira, G.R., Emulsion Polymerisation of Styrene. Use of n-nonyl Mercaptan for Molecular Weight Control, *Polymer*, v42, 2001, pp2719-2726.

[5] Ming, W.H. Jones, F.N., Fu, S.K. Synthesis of Nanosize Poly(methyl methacrylate) Microlatexes with High Polymer Content by a Modified Microemulsion Polymerization. *Polymer Bulletin*, 1998, v40, pp749-756.

[6] Sajjadi, S. Particle formation under monomer-starved conditions in the semibatch emulsion polymerization of styrene. I. Experimental. *Journal of Polymer Science Part A: Polymer Chemistry*, 2001, v39, pp3940-3952.

[7] Rabelero, M., Zacarias, M., Mendizabal, E., Puig, J.E., Dominguez, J.M., Katime, I. High-content Polystyrene Latex by Microemulsion Polymerization. *Polymer Bulletin*, 1997, v38, pp695-700.

[8] Roy, S., Devi, S. High Solids Content Semicontinuous Microemulsion Copolymerization of Methylmethacrylate and Butylacrylate. *Polymer*, 1997, v38, pp3325-3331.

[9] Chapter 3.2. Exploring the Minimum Particle Size Achievable by Semicontinuous Microemulsion Polymerisation

[10] Sajjadi, S., Yianneskis, M. Semibatch Emulsion Polymerisation of Methyl Methacrylate with a Neat Monomer Feed, *Polymer Reaction Engineering*, 2003, v11, pp715-736.

[11]Rios, L., Cruz, M.A., Palacios, J., Ruiz, L.M., Garcia-Rejon, A. *Macromolecular Chemistry*: *Supplement*, 1985, v10/11, pp477-488.

[12] Chapter 3.1. New Insights into Semicontinuous Emulsion Polymerisation as a Means to Produce Nanolatexes: Analysis of Nucleation Stage, Figure 3.1.11.

[13] Nomura, M., Suzuki, H., Tokunaga, H., Fujita, K., Mass Transfer Effects in Emulsion Polymerisation Systems.1.Diffusional Behaviour of Chain Transfer Agents in the Emulsion Polymerisation of Styrene, *Journal of Applied Polymer Science*, v51, 1994, pp21-31.

[14] Nomura, M., Minamino, Y., Fujita, K., Harada, M. The role of Chain Transfer Agents in the Emulsion Polymerisation of Styrene, *Journal of Polymer Science: Polymer Chemistry Edition*, v20, 1982, pp1261-1270.

[15] Harelle, L., Pith, T., Hu, G.H., Lambla, M., Chain Transfer Behaviour of Fractionated Commercial Mercaptans in Emulsion Polymerisation of Styrene, *Journal of Applied Polymer Science*, v52, 1994, pp1105-1113.

[16] Barudio, I., Guillot, J., Fevotte, G., Efficiency of Mercaptan Chain Transfer Agents in Emulsion Copolymerisations.1. Influence on Kinetics and Microstructure. Modeling of Radical Desorption, *Journal of Polymer Science: Part A: Polymer Chemistry*, 1998, v36, pp157-168

[17] Suzuki, K., Nomura, M., Harada, M., Kinetics of Microemulsion Polymerisation of Styrene, *Colloids and Surfaces A-Physicochemical and Engineering Aspects*, v153, 1999, pp23-30.

[18] Kalinin, V.V., Radke, C.J. An ion-binding model for ionic surfactant adsorption at aqueous-fluid interfaces. *Colloids and surface a-Physicochemical and Engineering Aspects*, 1996, v114, pp337.

[19] Sajjadi, S. Particle Formation under Monomer-starved Conditions in the Semibatch Emulsion Polymerisation of Styrene. Part II. Mathematical Modelling. *Polymer*, 2003, v44, pp223-237.
[20] Whang, B.C.Y., Lichti, G., Gilbert, R.G. The Effects of a Chain Transfer Agent on the Kinetics of the Emulsion Polymerisation of Styrene, *Journal of Polymer Science Part C: Polymer Letters*, 1980, v18, pp711-716.
[21] Sajjadi, S. Diffusion-Controlled Particle Growth and Its Effects on Nucleation in Stirred Emulsion Polymerisation Reactors. *Macromolecular Rapid Communications*, 2004, v25, pp882-887.
[22] Gilbert, R.G. London: Academic press, 1995.
[23] Hutchinson, R.A., Paquet, D.A., McMinn, J.H. Determination of Free-Radical Chain-Transfer Rate Coefficients by Pulsed-Laser Polymerisation. *Macromolecules*, 1995, v28, pp5655-5663.
[24] Sticker, M., Meyerhoff, G. *Macromolecular Chemie*, 1978, v179, pp2729.

Chapter 4 Smart Particles

In this chapter, the thermo-responsive and water-soluble poly(*n*-isopropylacrylamide) (polyNIPAM) colloids have been synthesized and studied. The work starts from batch polymerisation under monomer-starved conditions, as reported in subsection 4.1. The effects of monomer concentration on the kinetic of reaction as well as the properties of resulting particles have been investigated. The conclusions have then been applied to design a novel method via semicontinuous process. The advantages as well as the potentials of the novel method have also been explored.

4.1 Synthesis of Thermo-responsive Water-Soluble Poly(*N*-isopropylacrylamide) Colloids

Abstract: In comparison to gel, the water-soluble polyNIPAM colloids have received little attention in literature despite their wide range of potential applications. In this section, preparation of crosslinker-free poly(*n*-isopropylacrylamide) (polyNIPAM) nanoparticles is reported. A set of kinetic data is reported for NIPAM polymerisation using a wide range of monomer concentration and surfactant (SDS) concentration for first time. The rate of polymerisation, average size of particles and molecular weight of the final products increased with monomer concentration. In the presence of SDS, the number of particles showed a maximum at a critical SDS concentration. This unfamiliar observation was explained by enhanced swelling of polyNIPAM particles with water due to incorporation of SDS. From the study of dissolution behaviour of polymer particle in water via DLS and UV-vis, it was found that polyNIPAM chains were partly insoluble below LCST even in the absence of a crosslinker. The hydrodynamic size distributions measured by dynamic light scatting (DLS) were used to track dissolution of water-soluble chains and swelling of insoluble chains simultaneously. In order to improve the dissolution behaviour of the particles, *N,N,N′,N′*-Tetramethylethylenediamine (TEMED) was used as initiator accelerator. With the help of TEMED, completely water-soluble particles could be produced. However, on the other hand, the stability of the system was weakened due to too many uncharged radicals generated by TEMED. Addition of a small amount of sodium dodecyl sulfate (SDS) (0.5 $g \cdot l_{aq}^{-1}$), however, could provide sufficient electrostatic stability to the particles.

4.1.1 Introduction

Smart polymeric materials that can respond to changes in their environment have been in great demand in many emerging applications such as pharmaceuticals. poly(*N*-isopropylacrylamide) (polyNIPAM), first synthesised in the 1950s [1], is perhaps the best well known smart polymeric material due to its interesting phase transition temperature; its chain becomes hydrophilic below a temperature around 32°C, which is called lower critical solution temperature (LCST).

By copolymerising NIPAM with a cross-linker in aqueous media, such as *N,N'*-methylene-bis-acrylamide (MBA), polyNIPAM microgels can be produced. The temperature-sensitive uptake or release of drug and protein has been one of the most intensively investigated potential applications for polyNIPAM-based microgels [2-4]. Pelton's group was the first to synthesize surfactant-free polyNIPAM microgels [5]. The size of the particles was around 1 μm. Later, Mcphee et al. [6] found that the presence of low concentration of sodium dodecyl sulphate (SDS) well below its critical micelle concentration (CMC) in water had a significant positive effect on colloid size and stability. The resultant microgel latex contained smaller particles in higher concentrations.

In comparison to gel, the water-soluble polyNIPAM has received less attention. However, water-soluble polyNIPAM can be used for many purposes. Pelton was the first to suggest a novel method to produce particles by heating a solution of polyNIPAM through the LCST [7-8]. However, this method could only yield very low solids content (< 0.045wt%). Wu's group was interested in studying the coil-to-globule transition and internal motions of polyNIPAM chains in water in biological systems [9-11]. Hamielec et al. [12] studied the interactions between sodium dodecyl sulphate and polyNIPAM. Li et al. used polyNIPAM as temperature-sensitive flocculants [13]. They investigated the influence of molecular weight and dose of the polymer on sedimentation rate, sediment density and supernatant clarity of silica suspensions. Kizhakkedathu et al. used linear polyNIPAM chains produced by aqueous atom transfer radical polymerisation (ATRP) to synthesise well-defined environmentally responsive polymer brushes [14]. Ishifune et al. used aqueous solution of linear polyNIPAM as a matrix to produce high molecular weight polyacrylamide [15].

Despite increasing potential applications of water-soluble polyNIPAM, they have been studied to a very limited extent. Gao and Frisken [16-18], for example, carried out a series of work on the free radical polymerisation of NIPAM in water initiated by potassium persulfate in the absence of cross-linker at temperature well above the LCST of polyNIPAM. When the temperature of the resulting latexes was decreased to room temperature, the particles were not dissolved in the aqueous phase but formed stable microgels. This was attributed to the formation of network by self-cross-linking through chain transfer reaction both during and after

polymerisation.[13]C NMR spectra was done for both linear PNIPAM chains and self-cross-linked chains. Unfortunately, the difference could not be specified. Pelton's group also prepared polyNIPAM latexes in the absence of crosslinker but in the presence of SDS. They explained the presence of stable particles below LCST by the formation of branched chains and/or chain entanglement [6]. In a subsequent publication, Pelton et al. further investigated entanglements in the particles by allowing them to undergo variations in temperature and concluded that crosslinker-free particles would be fully dissolved in water when they are cooled down below LCST [19]. From the literature, it appears that the colloidal stability of crosslinker-free polyNIPAM partciels below LCST is not still clear.

Monomer concentration is usually considered as one of the most influential parameters in the kinetics of emulsion polymerisation [20], as it can affect the rate of polymerisation as well as the length of polymer chains, the average particle size and number of particles. Therefore monomer concentration was altered to investigate its effects on the kinetics of polymerisation and characteristics of the polymer particles. Variations in monomer concentration is usually utilised in semicontinuous process in order to be able to improve the control over the characteristics of the final products including their size, structure and morphology. In this research, monomer concentration is altered to investigate its effects on the kinetics of polymerisation and characteristics of the polymer particles produced. So the current work, which is carried out under monomer-starved conditions, can be considered as an introduction to semicontinuous process for polyNIPAM and the results from this chapter will be used in the subsequent sections. Another objective of this research is to clarify stability of cross-linker free polyNIPAM nanoparticles either above or below LCST. The effect of *N,N,N′,N′*-Tetramethylethylenediamine (TEMED), which can boost the rate of initiation and thus can reduce the polymer chain length, on the stability of particles was also studied.

4.1.2 Experimental Work

4.1.2.1 Procedure

Five sets of batch experiments were conducted as tabulated in Table 4.1.1. Most of the de-ionised water (130 ml), a weighed quantity of surfactant (if used) and buffer (4×10^{-3} mol·l_{aq}^{-1}) were initially charged in the reactor and heated up to the desired reaction temperature (60°C) while being purged with nitrogen under strong mixing (650 rpm). The purging continued at the reaction temperature for another 15 min. Then a weighed quantity of NIPAM monomer, defined as the weight percentage of the overall aqueous phase, was firstly dissolved in 40 ml of de-ionised water and then added into the reactor. After another 5 min purging, the agitation speed was reduced to 450 rpm and the initiator solution, 0.2163 g KPS dissolved in 30 ml of de-ionised water, including TEMED if used, was then added to the vessel. Generally, inhibition periods around 10 min were observed. Samples taken during the reaction for kinetic

measurements were quenched with water containing methyl hydroquinone. The reaction time zero for the start of reaction was considered when polymer was detected in the reaction mixture.

4.1.2.2 Measurements

Conversions were measured gravimetrically. Details of characterisations have been given in page 35. Test experiments clarified that the remaining NIPAM in a reaction sample evaporates at high temperature (60°C). The z-average diameters (D_z) and zeta potentials of particles during reaction were measured using Zetasizer (Malvern, UK). The samples for the size measurements were diluted with de-ionised water and kept in a water bath at the reaction temperature. The measurements were always carried out at the reaction temperature (60ºC). A conversion factor of C_f = 0.90 was used for volume-average diameter of particles (D_v) so that $D_v = C_f \cdot D_z$. The swelling ratio $(D_{v,s}/D_{v,c})^3$ of particles was calculated as the cube of the ratio of the volume-average diameter of particles at maximum swollen state to that of particles at collapsed state (60°C).

The number of particles was calculated according to the following equation:

$$N_p = 6m_p/\pi D_v^3 \rho_p \qquad (4.1.1)$$

where m_p gives the mass of polymer in the system at any given time and ρ_p is the density of polyNIPAM which is 1.269 g·ml^{-1} [21]. Considering two bound water molecules per isopropyl group above LCST [22], the bound water content of polyNIPAM phase was calculated to be 25wt% (based on 100% dried polymer) at the reaction temperature (60°C). On the basis of this assumption, a correction has been made in the calculation of N_p, so that $N_{p,\,corrected} = 1.25N_p$.

The weight-average molecular weight ($\bar{M}_w$) of the final products was measured by Zetasizer. In order to measure the molecular weights of the sol polymer, the samples were placed in the de-ionised water at room temperature for one week. The gel precipitated and the serum was used for the measurements.

Selected samples were extracted (Soxhlet) with tetrahydrofuran (THF) for one week to remove the linear chains. The resulting polymer was then dried in the oven to constant weight in order to calculate the weight ratio of the crosslinked chains.

The temperature dependence of the phase transition of the polyNIPAM was determined using an ultraviolet-visible spectroscopy (PerkinElmer, USA) (see page 39). The samples were first heated to 50ºC and then gradually cooled by heat transfer to the surroundings. The initial rate of cooling was around 3°C·min^{-1} until 33°C, but then decreased to around 1°C·min^{-1}.

Table 4.1.1. Recipes for synthesis of polyNIPAM nanoparticles. Reaction temperature: 60°C; $C_{KPS} = C_{buffer} = 4$ mmol·l_{aq}^{-1}; 200 ml water.

Description	Initial Monomer charge (wt%)	TEMED (mmol·l_{aq}^{-1})	SLS (g·l_{aq}^{-1})
Set A	0.25	0	0
	0.5	0	0
Effect of [M]	1.0	0	0
	2.0	0	0
	3.0	0	0
Set B	0.25	0	0.5
Effect of [M]	1.0	0	0.5
in the presence of	4.0	0	0.5
SDS	8.0	0	0.5
	16.0	0	0.5
Set D	1.0	5	0
Effect of	1.0	10	0
[TEMED]	1.0	15	0
	1.0	20	0
Set E	0.25	10	0.5
Effect of [M]	0.5	10	0.5
in the presence of	1.0	10	0.5
TEMED and SDS	2.0	10	0.5
	4.0	10	0.5
	8.0	10	0.5
Set F	8.0	0	0.125
Effect of [S]	8.0	0	0.25
	8.0	0	1.0
	8.0	0	2.0
	8.0	0	4.0
	8.0	0	8.0

[M]: monomer concentration;
[S]: surfactant concentration;
[TEMED]: TEMED concentration.

4.1.3 Results and Discussions

4.1.3.1 Effects of Monomer Concentration in Emulsifier-free Emulsion Polymerisation (EFEP) (Set A)

Experiments were conducted with various monomer concentrations (0.25-3.0wt% of water phase) in the absence of surfactant at 60°C via batch process. The amount of monomer used in this set was below the saturation concentration of NIPAM in water, which is around 20wt% [23]. Therefore, the polymerisations proceeded under monomer-starved conditions as no monomer droplet was present in the system. The solution was initially clear and transparent but became translucent to opaque with the progress of polymerisation.

The mass of polymer produced, the average particle size and the number of particles were shown as functions of reaction time in Figure 4.1.1. It is obvious (Figure 4.1.1a) that the initial rate of polymerisation (R_p; $mol \cdot l_{aq}^{-1} s^{-1}$) increases with the monomer concentration. A severe coagulation occurred at 3.0wt% NIPAM monomer. The average size of particles increased with monomer concentration for all runs (Figure 4.1.1b). In the literature, a limited range of monomer concentration, from 0.5wt% to 1.5wt%, was studied for a similar process at 70°C using 1.5 $mmol \cdot l_{aq}^{-1}$ KPS [17]. The final size of particles slightly increased with monomer concentration within the range studied, which is consistent with our results.

One should note that the procedure for measuring size of particles in this work is different from that used in the literature [16-18] in which the dispersions were cooled down to room temperature for characterisation. In this research, particles were kept at the reaction temperature during size measurements so the resulting size can reflect the real size of particles under polymerisation conditions. This point will be further discussed later.

Figure 4.1.1c shows the variation of the number of particles during the reaction. When monomer concentration is low (i.e. below 1.0wt%), the number of particles was almost constant. However, the colloidal stability of particles became weaker when monomer concentration was high because of a rapid growth of particles. Obviously, it is hard to simultaneously monitor particle formation and coagulation in the course of nucleation stage due to their fast dynamics. However, the N_p figure can still indicate that the number of particles formed at the early stage of polymerisation increased with monomer concentration. For monomer concentrations greater than 1.0wt%, a large number of particles initially formed so that they could not be maintained in the course of reaction due to continuous coagulation. As a result, the maximum number of particles that could be produced was 9.25×10^{14} l_{aq}^{-1}, which was achieved when monomer concentration was 1.0wt%. Therefore, the monomer concentration in the water phase plays an important role in determining the maximum number of particles that can be stabilised, a

conclusion which is consistent with the results from conventional emulsifier-free emulsion polymerisation of common vinylic monomers [24].

In the absence of surfactant, homogeneous nucleation mechanism is believed to be dominant in the system. NIPAM has a relatively high solubility in water (20wt% at 25ºC [23]). As radicals propagate with monomer to a certain extent, phase separation occurs. The growing chains are so unstable that they coagulate with each other to form colloidally unstable precursor particles. The precursor particles follow one of two competing processes. They can either deposit onto an existing colloidally stable particle or aggregate with other precursor particles to reach a sufficiently large size to become colloidally stable. The results indicate that it is difficult to prepare particles with small size in the absence of surfactant due to insufficient particle surface charge. It has been found that the surface charge density of polyNIPAM microgel latexes is about two orders of magnitude lower than corresponding surfactant-free polystyrene latexes [6].

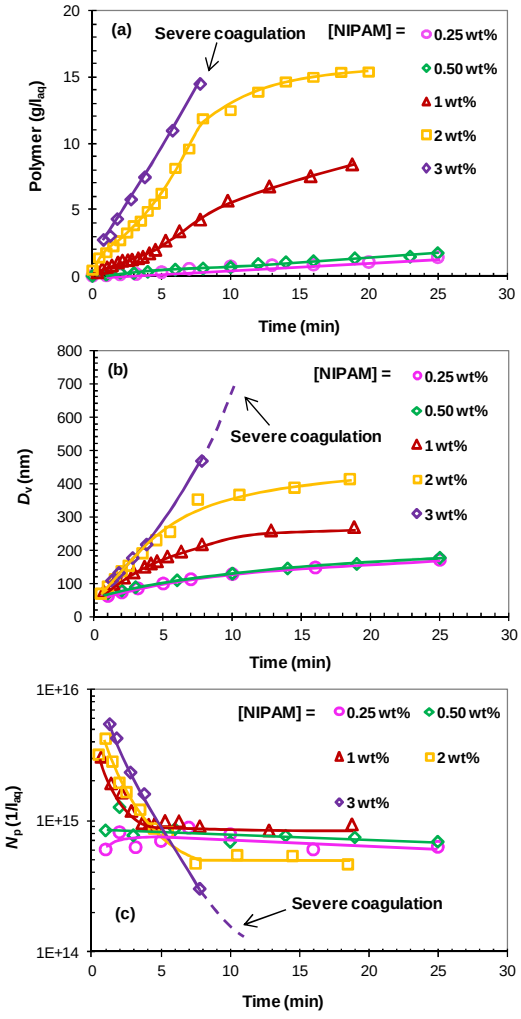

Figure 4.1.1. The time evolution of (a) polymer produced, (b) volume-average diameter of particles and (c) the number of particles for different NIPAM concentrations via surfactant-free emulsion polymerisation ([KPS] = 4 mmol·l_{aq}^{-1}, T = 60ºC).

The weight-average molecular weights of the final products ($\bar{M}_w$), as shown in Figure 4.1.2, increase with monomer concentration. In a conventional emulsion polymerisation, a polymer chain continues to grow until is terminated by reaction with either another radical or by abstraction of hydrogen atom from monomer molecules (i.e. chain transfer to monomer). A higher monomer concentration in water phase will result in a faster rate of monomer diffusion into the particles (i.e. higher monomer concentration in the particles) and allow the growing chains inside particles to propagate to a greater extent before termination reactions can occur. For a system with a constant number of particles, this can lead to a higher molecular weight.

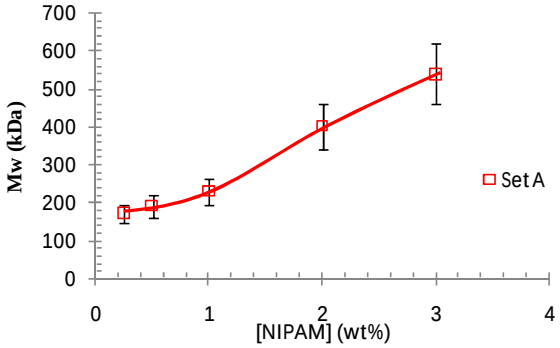

Figure 4.1.2. Weigh-average molecular weight of the sol for different monomer concentrations (Set A).

Typical emulsion/precipitation polymerisation of NIPAM at high temperature (> LCST) always results in formation of insoluble chains even in the absence of crosslinker [6,12,16,19,25-26]. Chain-transfer reaction to polymer chain was considered as the likely source of chain branching and cross-linking [6,16]. Transfer to polymer results in the formation of a radical site on a polymer chain, which can propagate with monomer to form a branched or cross-linked polymer chain either by termination with a small-molecule radical or by coupling termination with another macromolecular free radical, respectively.

To investigate this phenomenon, samples produced with 0.25wt%, 1.0wt% and 2.0wt% NIPAM concentrations via surfactant-free emulsion polymerisation (set A) were chosen for further characterization. The samples were not allowed to cool down prior to measurements. The DLS readings and transmittance data from the resulting latexes produced with 1.0wt% and 2.0wt% NIPAM monomer concentrations, as they were cooled down from the reaction temperature (60ºC), are shown in Figure 4.1.3.

For size measurements, the sample was cooled down at a constant rate of 1.0ºC·min^{-1}. The size of particles did not change with temperature until temperature within 30-35ºC was reached for all monomer concentrations. Within this critical temperature range, the size data show an abrupt jump in the size of particles, due to swelling, starting from temperatures around 35ºC. The maximum particle swelling ratio of 1.9, 15.8 and 15.3 were obtained for 0.25wt%, 1.0wt% and 2.0wt% NIPAM concentration, respectively. However, after being swollen to their maximum

sizes, the particles decreased in size with temperature very steeply. The hydrodynamic size of polymer particles for 0.25wt% and 1.0wt% NIPAM concentration finally reduced to 44 nm and 135 nm, respectively, when temperature dropped to room temperature (20ºC). For 2.0wt% NIPAM concentration, the size appeared to level off around 400 nm at room temperature.

The transmittance curve shows that the absorbance of the samples decreased on cooling as temperature dropped below 32-33ºC. These indicate that the difference in refractive index (RI) between the particles and the water phase became smaller as the particles started to swell with water and dissolve, which is consistent with the DLS data. It can be concluded, from both size and transmittance measurements, that the LCST of all samples is 32-33ºC. One important conclusion is that the transmittance of the samples with 1.0wt% and 2.0wt% NIPAM monomer could not reach 100% when temperature was below LCST implying that particles are not completely soluble in water. Furthermore, the logarithm of transmittance (inset) clearly shows the phase transition of the particles became a two-step process for the sample produced with 2.0wt% NIPAM monomer.

Interestingly, for 0.25wt% NIPAM monomer, the phase transition occurred at much higher temperature (45ºC), accompanied with a slight decrease in particle size, as shown in Figure 4.1.3a. Furthermore, the swelling was limited, followed by a steep rate of shrinking. A rather clear solution was obtained, as evidenced by the high value of transmittance. These indicate that a low monomer concentration results in formation of smaller particles with lower molecular weight (see Figure 4.1.2) and improved solubility in water. It has also been reported by Wu et al. that the LCST of polymer chain increases with decreasing molecular weight [11,27].

Dynamic light scattering (DLS) technique has been used to study the phase transition of polyNIPAM chains in the water phase [9-11,28]. It can measure the hydrodynamic size distribution of polymer chains in the solvent (i.e. water), which depends not only on the chain length distribution, but also on the relaxation of the chain conformation [29]. In this work, the dissolution process of particles has been closely monitored by measuring the hydrodynamic size distribution of latex as a function of temperature, as shown in Figure 4.1.4 for particles obtained using different monomer concentrations. For 1.0wt% and 2.0wt% NIPAM monomer, the particles slightly swelled as temperature dropped from 60ºC to 32ºC. It is interesting to note that below 32.1ºC the size distribution of particles transforms to binary distributions consisting of populations of large particles with average diameter range of 600-1000 nm and very small entities within the size range of 10-50 nm. The latter peak can be attributed to formation of linear polyNIPAM chains in water phase [30]. With lowering temperature, the water-soluble polymer chains started to be disentangled and then diffused out of particles into the water phase. It is noticeable that the peak representing the soluble chains moved to the larger size as temperature further decreased. This is thought to be due to dissolution pattern of mixed polymer chains in a solvent with time rather than necessarily an effect of temperature; the short chains

diffuse out more quickly and dissolve faster, while long chains need more time to disentangle and dissolve.

Another important point worthy of attention is that the average size data below LCST include information about the length (size) of polymer chains released to water. Comparing Figure 4.1.2 with Figure 4.1.3, it can be found that the hydrodynamic size at 20ºC increased with the molecular weight of polymer chains produced with different monomer concentrations. In fact, polymer particles do swell with lowering temperature despite the fact that they lose polymer chains to water, as clearly seen in Figure 4.1.4. Size measurements indicated very small change in drop diameter at room temperature within 10h (not shown) as the particles did not show any sign of shrinking during monitoring. The presence of such large particles below LCST proves that they contain insoluble polymer chains, which hinder further deformation and degradation of the particles. By contrast to 1.0wt% and 2.0wt% NIPAM concentrations, the whole PSD continuously shifts to smaller size range for 0.25wt% NIPAM monomer as temperature is reduced to below 30°C, which indicates that particles undergo shrinking with time as more polymer chains are dissolved in the water phase.

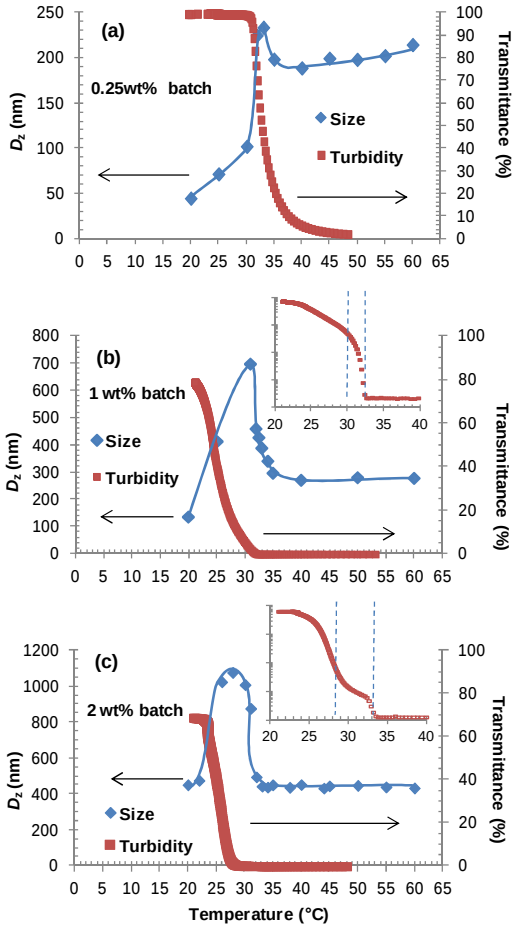

Figure 4.1.3. The evolution of transmittance and z-average size of particles with temperature for (a) 0.25wt%, (b) 1.0wt% and (c) 2.0wt% NIPAM monomer concentration (Set A). Inset: The variation of the logarithm of the transmittance of latex with temperature.

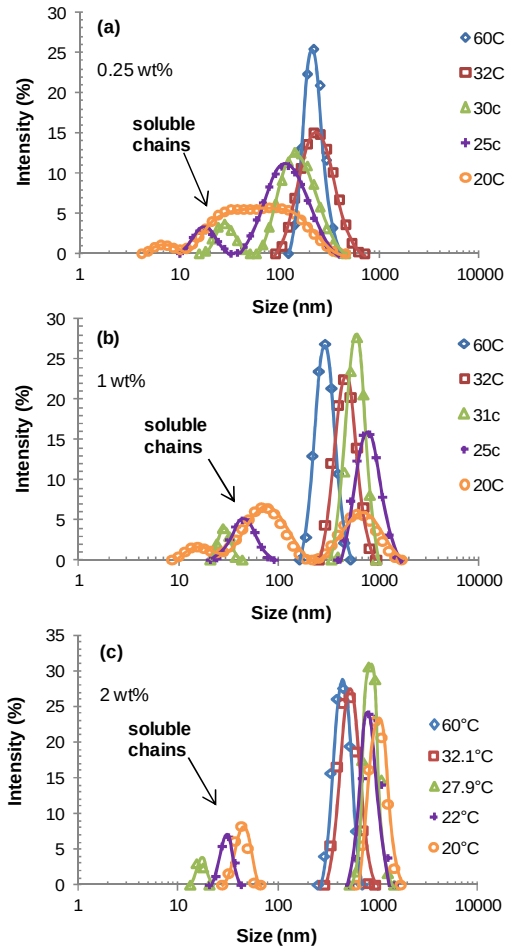

Figure 4.1.4. The intensity size distribution of final particles for (a) 0.25wt%, (b) 1.0wt% and (c) 2.0wt% NIPAM monomer at different temperatures obtained by DLS.

On the nature of crosslinking, a question to answer is whether the insolubility of particles in water is due to chemical crosslinking or physical entanglement of polymer chains. First we assume that severe physical entanglement is the reason for polymer insolubility in water. Before a chain contained in a particle can be dissolved in the water phase, it has to disentangle from other chains within the particle. It is quite likely that disentanglement, followed by transport of the chains out of the particles, is controlled by time. In order to study the kinetics of chain disentanglement, following cooling, the latex (with 1.0wt% monomer) was kept at room temperature up to 20 days. In order to measure any possible property change during storage, the samples were then heated rapidly above the LCST; 50±4°C. The transmittance was measured in terms of temperature as samples were gradually cooled down to room temperature; 20°C.

Figure 4.1.5 shows the transmittance data for the sample with 1.0wt% NIPAM monomer for different storage periods at room temperature (22ºC).

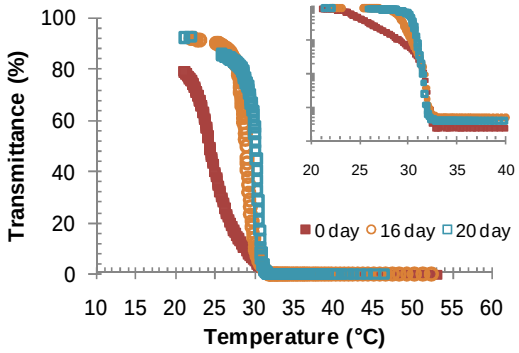

Figure 4.1.5. The turbidimetric measurements of the final latex produced with 1.0wt% NIPAM monomer (set A). Inset: The variation of the logarithm of the transmittance of latex with temperature.

Three features were noticed. One is that the LCST remains constant (= 32°C) and independent of the storage period at room temperature. Second, the transmittance at room temperature improved with increasing storage time, which indicates that more of polymer chains are disintegrated from the particles and dissolved in the water phase. Third is the phase transition of the sample that became sharper with increasing storage time. It is known that the phase transition temperature increases with decreasing the molecular weight of polymer chains [11,30]. The more monodisperse are the molecular weight of polymer chains, the sharper phase transition will be [9,11]. Therefore, as more chains were disentangled and dispersed in the water phase during storage period, the average molecular weight distribution of polymer chains within the sample became sharper as well as the range of phase transition temperature.

It appears that storage time longer than 16 days could only lead to a small improvement in transmittance. The transmittance of 100% was not achieved even after 20 days, which points to the presence of water-insoluble moieties in the latexes. This implies that particles were partially cross-linked. This conclusion is supported by the results from one week soxhlet extraction that shows around 20wt% of the polymer latexes obtained using 2.0wt% NIPAM monomer is composed of water-insoluble or chemically crosslinked chains.

Gao et al. claimed that the formation of insoluble particles is a result of self-crosslinking of polyNIPAM chains by chain transfer reaction rather than hyperbranching [16]. They incubated a transparent solution of polyNIPAM and KPS in the absence of monomer at 70°C for 4h in a nitrogen atmosphere. After cooling the sample to room temperature, a viscoelastic dispersion of colloidal particles with hydrodynamic size of 200 nm was formed, which indicates that permanent crosslinking between the chains had occurred. The molecular weight was found to be ~500 times larger than that of the linear chains before incubation [16].

In order to investigate the effect of incubation, a sample of the latex produced with 2.0wt% NIPAM monomer and 4 $mmol \cdot l_{aq}^{-1}$ KPS was taken directly from the reactor (x = 98%) and stored at reaction temperature (60°C) for 27h. Turbidmetric measurements were conducted as a function of temperature. Figure 4.1.6 shows transmittance data for the sample with 2.0wt%

NIPAM monomer before and after incubation. It is found that the temperature range of phase transition of the latex became wider and more gradual with longer incubation, which implies larger chains of polyNIPAM are formed during incubation. However, the extent of change in phase transition behaviour does not seem to be high enough to support any significant alteration in molecular weight and LCST of the resulting polymer. Noting that the reaction time, 1h, was much shorter than the incubation time, 17h, one can easily eliminate effect of reaction time (incubation time) on molecular weight within the context of this study.

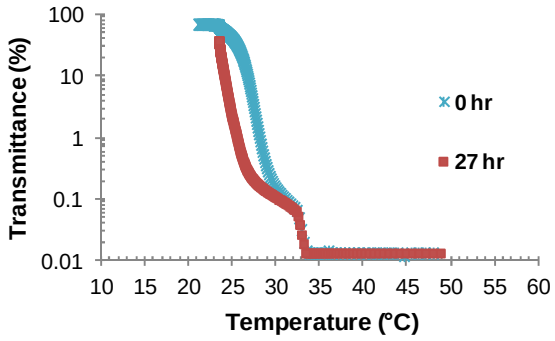

Figure 4.1.6. The variations in transmittance with temperature of the final latex produced with 2.0wt% NIPAM monomer (set A) for 0h and 27h incubation periods.

4.1.3.2 Effects of SDS Concentration in Emulsion Polymerisation (Set F)

Based on the results presented in previous section, it has been found that the surfactant-free emulsion polymerisation of NIPAM was not robust due to the low surface charge density of particles, and as a result produced latexes with large particle size and low solids content. The same issue has been reported for the synthesis of polyNIPAM microgels and the technique was refined by using sodium dodecyl sulfate (SDS) [6,19,31-32]. In the recipes reported by Wu et al., within SDS concentration range of 0.2-4 mmol·l_{aq}^{-1}, a dependence of hydrodynamic diameter of microgel (volume average size measured by DLS at 50°C, 1.4wt% NIPAM) versus SDS concentration has been found as: $D_v \propto [S]^{-0.71}$ [19]. Similar microgels (2.8wt% NIPAM) prepared using the same range of SDS concentration was also studied by McPhee et al. They found the intensity-average hydrodynamic diameter (measured by DLS at 25°C) becoming constant when SDS concentration was above 2 mmol·l_{aq}^{-1} [6]. Later, the use of higher concentrations of SDS up to 6.7 mmol·l_{aq}^{-1}, for making smaller microgel particles was reported [31-32]. However, no reports have been found in literature based on the effect of SDS on the synthesis of crosslinker-free polyNIPAM particles.

In this section, the effect of SDS concentration on particle formation and growth has been studied. Monomer concentration was kept constant at 8.0wt%. This is much higher than the ranges of NIPAM concentration that have ever been reported in the literature for the synthesis of polyNIPAM particles. Variations of SDS concentration from 0.125 g·l_{aq}^{-1} (0.43 mmol·l_{aq}^{-1}) to

8 g·l_{aq}^{-1} (27.74 mmol·l_{aq}^{-1}) have been applied in the polymerisation. As shown in Figure 4.1.7a, the rate of polymerisation is independent of SDS concentration. Similar observation has been reported by Pelton et al [19] for the synthesis of polyNIPAM microgels. A severe coagulation occurred in the later stage of polymerisation ($x \approx 92\%$) in the presence of the lowest SDS concentration used (0.125 g·l_{aq}^{-1}). By increasing the SDS concentration, as shown in Figure 4.1.7b-c, particle size decreased and particle formation was enhanced, except for the highest SDS concentration (i.e. 8 g·l_{aq}^{-1}).

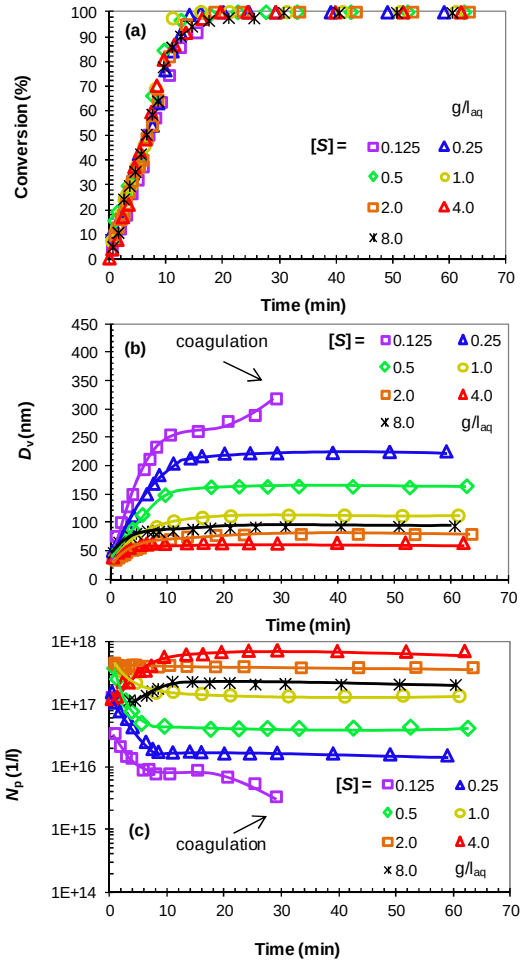

Figure 4.1.7. The time evolution of (a) polymer produced, (b) volume-average size of particles and (c) the number of particles for different SDS concentrations, ([KPS] = 4 mmol·l_{aq}^{-1}, [NIPAM] = 8.0wt%, T = 60ºC)

Considering the mechanism of particle nucleation, the initial particle sizes were above 30 nm for all surfactant concentrations used, as shown in Figure 4.1.7b. The evolution of particle population shown in Figure 4.1.7c indicates that the system undergoes coagulation right from the beginning of the reaction. At [*S*] = 2.0 g·l_{aq}^{-1}, particle coagulation was apparently absent and the particles initially formed were maintained in the course of reaction. At [*S*] = 4.0 g·l_{aq}^{-1}, particle formation lasted longer. However, particle formation was inversely affected, as shown in Figure 4.1.7c, when surfactant concentration increased to 8.0 g·l_{aq}^{-1}.

Figure 4.1.8 shows the dependence of z-average hydrodynamic size of particles as well as the number of particles on the SDS concentration within the range of 0.125-8.0 $g \cdot l_{aq}^{-1}$. The fitted lines on the double logarithmic plot predict $D_z \propto [S]^{-0.50}$ and $N_p \propto [S]^{1.68}$, upto $[S]$ = 2.0 $g \cdot l_{aq}^{-1}$, which are similar to what have been suggested for polyNIPAM microgels [19]. However, these relations break down as $[S]$ increased beyond $[S]$ = 4.0 $g \cdot l_{aq}^{-1}$.

A few investigations published on interactions of SDS with polyNIPAM have considered both microgels and polymer chains [12,33-35]. Pelton et al. studied SDS binding to polyNIPAM microgel latex by isothermal titration calorimetry at different temperatures. The results showed that SDS has a high binding affinity for polyNIPAM above LCST [33]. The LCST of polyNIPAM was found to increase with the amount of bound SDS, which was attributed to electrostatic contribution of the bound sulfate groups to the increased hydrophilicity of polyNIPAM chains [12]. The factors that influence the amount of bound SDS, such as SDS and polymer concentrations, also influence the LCST. With a certain amount of SDS, the LCST of polyNIPAM could be even higher than 60°C [34,36]. This suggests that polyNIPAM nanoparticles can swell with water during the reaction at the reaction temperature (60°C) when they have incorporated and adsorbed a certain amount of SDS. Since the range of SDS concentration used in this work was much higher than that applied in the literature, it was possible to observe such phenomenon for the first time. Therefore the presence of SDS imposes two contrary effects in the course of polymerisation. On the one hand, it provides electrostatic stability and decreases the size of particles; on the other hand, it binds to the polyNIPAM chain and causes further swelling of the particles at reaction temperature. There appears to be a critical SDS concentration, or SDS/polyNIPAM ratio, above which the decrease in size due to enhanced stability of particles is offset by increase in their size due to swelling leading to increasing particle size (or decreasing particle number) with SDS concentration. The critical SDS concentration for the current system with 8.0wt% NIPAM, is found to be $[S]$ = 4.0 $g \cdot l_{aq}^{-1}$. This is the reason for larger particles being obtained at 8.0 $g \cdot l_{aq}^{-1}$ SDS concentration, as shown in Figure 4.1.7b.

The incorporation of SDS, accompanied with water, into polyNIPAM particles casts some doubt on the accuracy of the number of particles calculated. The incorporation of SDS and water into hydrophilic polymers such as PVA has been reported in the literature before [37]. However, the diffusion process for such a system is quite slow and was only observed long after polymerisation was completed. The results suggest that for polyNIPAM, the diffusion of SDS into particles is rather fast so that the effect of SDS concentration on the kinetics of polymerisation is beyond what is usually foreseen for a conventional surfactant system.

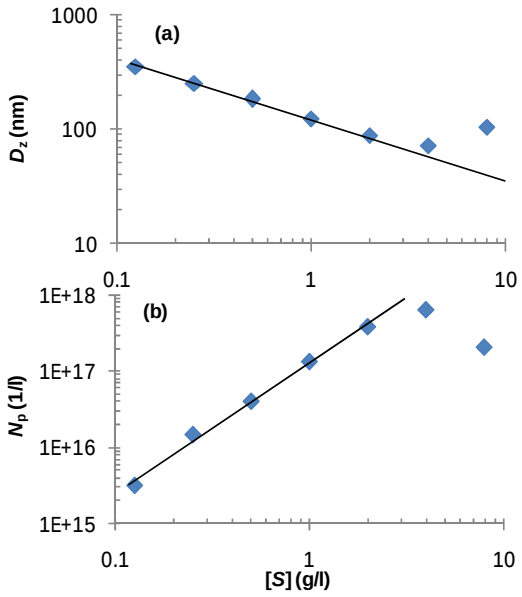

Figure 4.1.8. Variation of (a) z-average diameter and (b) number of particles of the final latexes produced with different SDS concentrations (8.0wt% NIPAM, 4 mmol·l_{aq}^{-1} KPS).

4.1.3.3 Effects of Monomer Concentration in Emulsion Polymerisation in the Presence of Low SDS Concentration (Set B)

In order to avoid a significant effect of binding of SDS with polyNIPAM, which changes the thermal sensitive property of polymer and thus affects potential applications, the use of SDS should be controlled at a low level. A set of polymerisation reactions was conducted with various monomer concentrations in the presence of 0.5 g·l_{aq}^{-1} of SDS (Set B), which is below the critical micelle concentration (CMC) of SDS in water under the reaction condition (around 1.0 g·l_{aq}^{-1}).

Figure 4.1.9 shows the polymer produced, the volume-average size of particles and number of particles versus time for various monomer concentrations. The rate of polymerisation and the rate of particle growth increased with monomer concentration (Figure 4.1.9a-b), similar to the trend observed for EFEPs (set A). Stable polyNIPAM latex could be produced with monomer concentration as high as 8.0wt%. A massive coagulation was observed for monomer concentration of 16.0wt% at high conversions. As shown in Figure 4.1.9c, particle formation was slow, and the number of particles reached a constant value after 15 min with 0.25wt% monomer. With 1.0wt% monomer, the number of particles remained constant in the course of reaction. For any monomer concentration greater than 1.0wt%, limited particle coagulation occurred during reaction.

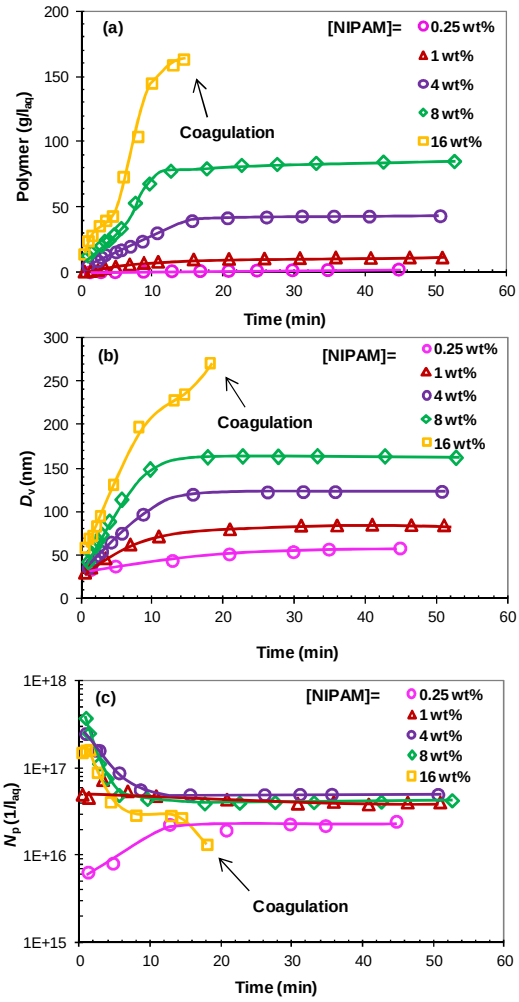

Figure 4.1.9. The time evolution of (a) polymer produced, (b) volume-average size of particles and (c) the number of particles for different monomer concentrations ([KPS] = 4 mmol·l_{aq}^{-1}, [SDS] = 0.5 g·l_{aq}^{-1}, T = 60°C).

Figure 4.1.10 shows the comparison of set A and set B in terms of initial rate of polymerisation and final number of particles. The exponent for the initial rate of polymerisation in terms of monomer concentration in the water phase, $R_p \propto [M]_w^{\partial}$, was found to be around 1.45±0.02 for both sets, which once again indicates that the presence of SDS did not affect the kinetic of the polymerisation. Figure 4.1.10b shows the comparison between maximum and final number of particles for different monomer concentrations, which can represent the extent of particle coagulation in the course of polymerisation. It is clearly shown that particle coagulation during the growth stage is negligible at very low monomer concentration (0.25-0.50wt%), but becomes progressively more important with increasing monomer concentration for both sets. The figure also shows that both maximum and final number of particles substantially increased in the presence of SDS, compared to that produced by the EFEP, as shown in Figure 4.1.10b. The maximum number of final particles was obtained with 4.0wt% NIPAM monomer in the presence of SDS, which is around 4.93×10^{16} l_{aq}^{-1}. The results clearly indicate that the role of SDS during particle nucleation is to increase the colloidal stability of precursor particles and thus hinder particle coagulation.

One important observation was that the presence of surfactant increased the number of particles and consequently the final conversion achieved. The final conversions of most experiments using SDS, however, exceeded 100%. This may point to the gel structure of the particles and their capability to incorporate some SDS, as explained before, that could lead to entrapment of some water inside particles (up to 10wt% of the particles) and erroneous conversion calculation.

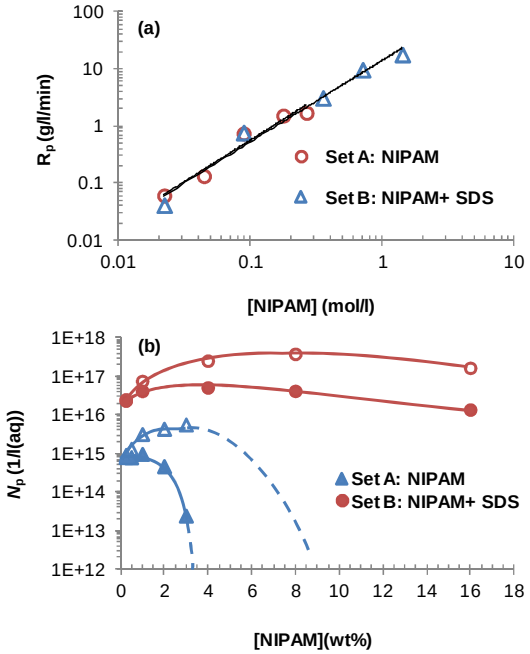

Figure 4.1.10. Comparison of (a) initial rate of polymerisation and (b) initial (empty symbol) and final (filled symbol) numbers of particles versus monomer concentration for set A (emulsifier-free emulsion polymerisation) and set B (emulsion polymerisation in the presence of SDS).

4.1.3.4 Effects of TEMED Concentration in Emulsion Polymerisation (Set D)

We have already shown that conventional crosslinker-free emulsion polymerisation of NIPAM at high temperature (> LCST), in the presence or absence of surfactant, produce entangled polymer matrix that cannot be easily dissolved in water, unless particles are small and have low molecular weight. These conditions can only partially met for low monomer concentrations (i.e., 0.25wt%).

To produce linear polyNIPAM chains, redox initiation system in the aqueous phase had been widely used. In one example, potassium persulfate (KPS) as the initiator and *N,N,N',N'*-Tetramethylethylenediamine(TEMED) as the accelerator were used at room temperature [1]. Gao's group claimed that precipitation polymerisation of NIPAM at 70°C results in a solution of polyNIPAM linear chains with the help of TEMED [16].

To investigate the effect of TEMED in emulsion polymerisation of NIPAM, polymerisations with 1.0wt% NIPAM monomer were carried out in the presence of various amounts of TEMED, from 5 mmol·l_{aq}^{-1} to 20 mmol·l_{aq}^{-1} (set D). The minimum concentration of TEMED used was 5 mmol·l_{aq}^{-1}, which is larger than 4 mmol·l_{aq}^{-1} used for the initiator. According to the redox

chemical reaction scheme for TEMED with persulfate, as represented by Equation 4.1.2, the stoichiometric ratio between KPS and TEMED is 1:1 [38].

$$S_2O_8^{2-} + (CH_3)_2NCH_2CH_2N(CH_3)_2 \rightarrow (CH_3)_2NCH_2CH_2NCH_3C\dot{H}_2 + S\dot{O}_4^- + SO_4^{2-} \quad (4.1.2)$$

This means the increase in TEMED concentrations above 4 mmol·l_{aq}^{-1}, which was used for the persulfate initiator, should have little effect on radical generation. However, a concentration larger than 4 mmol·l_{aq}^{-1} ensures that the rate of radical generation does not change with TEMED concentration.

The results are shown in Figure 4.1.11. With the help of TEMED, the rate of polymerisation increased significantly. This implies an enhanced rate of radical generation in the presence of TEMED. However, the rate of reaction did not change with the amount of TEMED used, as expected. Furthermore, the final conversion of around 100% was achieved for 5 mmol·l_{aq}^{-1} TEMED, but decreased with further increase in TEMED concentration due to coagulation, as shown in Figure 4.1.11b-c.

Particles were found to be quite unstable and underwent significant coagulation in the course of reaction. This is clearly inferred from Figure 4.1.12 which shows the difference between the initial and final number of particles produced with different amount of TEMED. The difference became wider with increasing TEMED concentration suggesting that TEMED serves to destabilise the particles.

Table 4.1.2 shows the zeta potential of particles produced with different amounts of TEMED. As coagulation proceeds during polymerisation, the zeta potential of particles might change due to the subsequent particle growth. Therefore, to have a better estimation of the effect of TEMED on the stability of newly nucleated particles, samples were taken for analysis during the early stage of polymerisation. The particles produced with KPS had negative zeta potentials, due to the presence of persulfate groups on their surfaces. A potential of around -30 mV is within the range of zeta potential that is required to produce a relatively stable colloidal system. Comparatively, the particles produced with TEMED (and KPS) had a quite low absolute value of zeta potential, around -1.40 mV, indicating that these particles are extremely unstable and prone to coagulation, as seen in Figure 4.1.11c. Such behaviour probably suggests that the radicals generated from TEMED ($(CH_3)_2NCH_2CH_2NCH_3C\dot{H}_2$) are hydrophilic and, cannot contribute to the colloidal stabilization. As a result, the addition of TEMED would depress the stability of particles. However, the reason for increasing size of particles with increasing TEMED concentration remains to be explained. This is particularly important as the rate of radical generation by redox initiation system does not appear to increase with TEMED for concentration above 5 mmol·l_{aq}^{-1}, as explained before. One important point that should be noticed is the generation of radicals by thermal decomposition of KPS. At reaction temperature

(60°C), the redox reaction for TEMED with KPS occurs in parallel with thermal decomposition of KPS. Therefore, with further addition of TEMED to the reaction medium, the initiation via the redox system becomes more favourable, at a constant overall rate, and more hydrophilic radicals will be produced causing further depression of colloidal stabilization, as shown in Figure 4.1.11b-c.

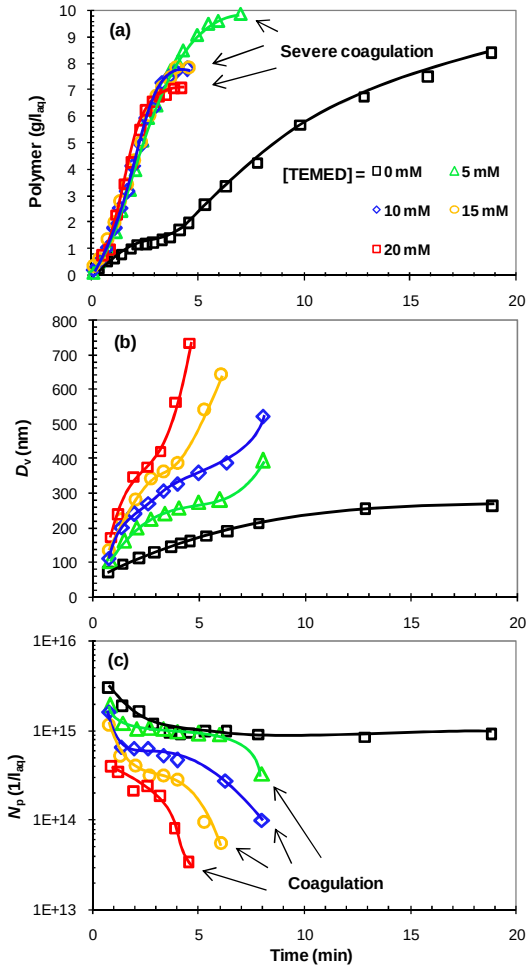

Figure 4.1.11. The time evolution of (a) polymer produced, (b) volume-average size of particles and (c) the number of particles for different TEMED concentrations. ([KPS] = 4 mmol·l$_{aq}^{-1}$, [NIPAM] = 1.0wt%, T = 60°C).

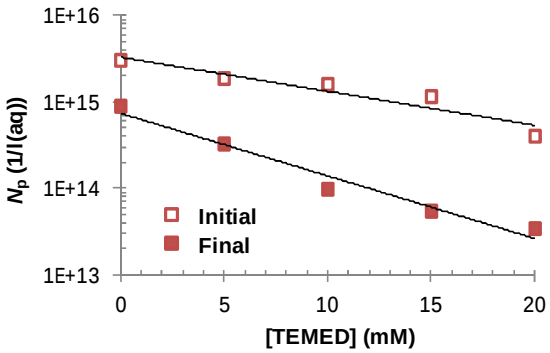

Figure 4.1.12. The initial and final number of particles for different concentrations of TEMED (set D).

Table 4.1.2. Zeta potential of particles produced with different amount of TEMED, 1.0wt% NIPAM, T = 60°C

TEMED (mmol·l_{aq}^{-1})	Zeta potential (mV)	pH
0	-28.1	7.0
10	-1.48	7.0
20	-1.40	7.0

The reaction results clearly show that stable particles cannot be produced via EFEP in the presence of TEMED. To improve the colloidal stability of particles, a small amount of SDS is needed. Several experiments were carried out with various monomer concentrations in the presence of 10 mmol·l_{aq}^{-1} of TEMED and 0.5 g·l_{aq}^{-1} of SDS (set E). Results of Set E are shown in Figure 4.1.13. The reactions occurred quickly and almost completed within a few min for most runs. The results clearly show that the rate of growth of particles, due to coagulation, was damped by using surfactant leading to formation of stable latexes. Because of the low concentration of surfactant used, however, there is still significant coagulation during the course of reaction. Particle coagulation continued till the full completion of reactions with monomer concentrations greater than 2.0wt%. The maximum number of particles that could be produced is around 4.59×10^{16} l_{aq}^{-1} when monomer concentration is around 2.0wt%.

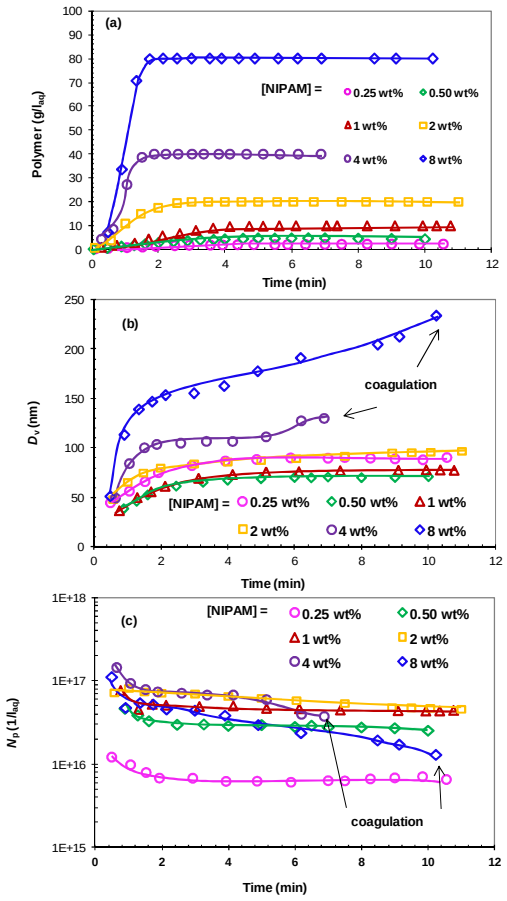

Figure 4.1.13. The time evolution of (a) polymer produced, (b) volume-average size of particles and (c) the number of particles for different monomer concentrations. ([TEMED] = 10 mmol·l_{aq}^{-1}, [SDS] = 0.5 g·l_{aq}^{-1}, [KPS] = 4 mmol·l_{aq}^{-1}, T = 60°C)

Figure 4.1.14 shows that $\bar{M}_w$ increased with monomer concentration, which is similar to the trend reported for EFEP. However, it appears that the presence of TEMED has led to a significant drop in molecular weight of polymer in particular at low monomer concentrations. However, the decrease became unobvious when higher monomer concentration is used (≥ 3.0wt%). This may be attributed to the higher consumption rate of TEMED than that for NIPAM monomer in the course of polymerisation.

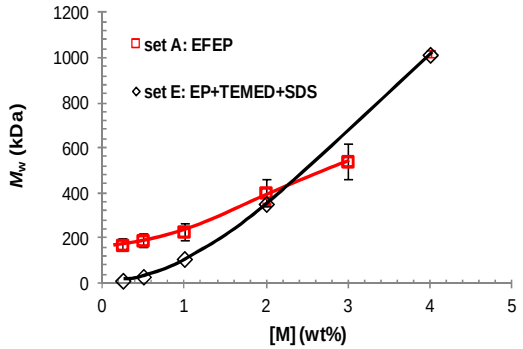

Figure 4.1.14. Weigh-average molecular weight of the final products versus monomer concentration for set E ([TEMED] = 10 mmol·l_{aq}^{-1}, [SDS] = 0.5 g·l_{aq}^{-1}) and set A (EFEP). [KPS] = 4 mmol·l_{aq}^{-1}, T = 60°C.

To verify the role of TEMED, the resulting polymer latexes produced with 1.0wt% NIPAM monomer were cooled from the reaction temperature (60°C) to room temperature and their size and turbidity were measured using DLS and UV, respectively.

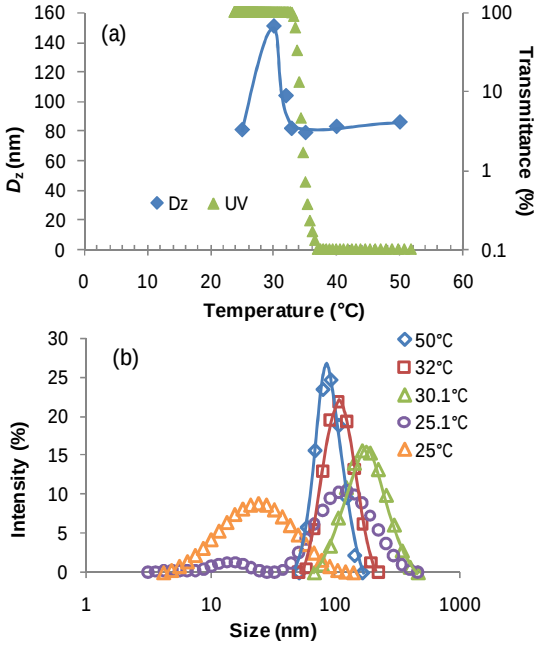

Figure 4.1.15. The evolution of (a) z-average hydrodynamic size and transmittance and (b) intensity size distribution with temperature of the final latex produced using 1.0wt% NIPAM monomer, 10 mmol·l_{aq}^{-1} TEMED and 0.5 g·l_{aq}^{-1} SDS.

The turbidimetric measurements by UV indicate that particles are fully dissolved in the water phase when temperature was below 32°C. Comparing with the sample produced by EFEP

(Figure 4.1.5), it can be found that the onset temperature of phase transition, as indicated by a sudden increase in transmittance, rises from 32 to 36°C implying that polyNIPAM chains become more hydrophilic with the help of TEMED. The maximum particle swelling ratio was found to be around 6.5, which is much lower than that produced in the absence of TEMED indicating that particles start to degrade before they swell to a great extent.

The dissolution of a polymer into solvent involves two steps, which are solvent diffusion (swelling) and chain disentanglement [39]. The results also suggest that when TEMED was involved, polymer chains were shorter and thus underwent lower degree of swelling before the disentanglement. This point is supported by the weight-average molecular weight ($\bar{M}_w$) of the polymer, which is 105 kDa and only half of that produced with 1.0wt% NIPAM (229 kDa) via EFEP (set A), as shown in Figure 4.1.14. Recently, Hu et al. further discussed self-crosslinking network structure of polyNIPAM chains and pointed out that TEMED can act as a transfer agent with NIPAM. According to them, the propagating polyNIPAM chains would likely undergo transfer with TEMED rather than undergo a chain termination reaction with other propagating chains. As a result, the residual TEMED in the system could hinder the chain branching and thus act to control the molecular weight of the resulting polymer chains [40].

Both increased hydrophilicity and reduecd length of polymer chains can improve the dissolution of polyNIPAM particles, as shown in Figure 4.1.15a. Below 30.1ºC, a smaller peak appears at the lower range of size representing water-soluble chains, as shown in Figure 4.1.15. In this region, the variations in the size of particles are thought to be a matter of time rather than subsequence of decrease in temperature, and are more likely a diffusion-controlled process. The curve shown by triangle symbols in Figure 4.1.15 indicates the PSD of the latex after being stored at 25°C for a day. The PSD consists of one single peak at lower end (< 100 nm) which represents the water-soluble chains. The result of soxhlet extraction also showed that there was no insoluble chains existed in the sample.

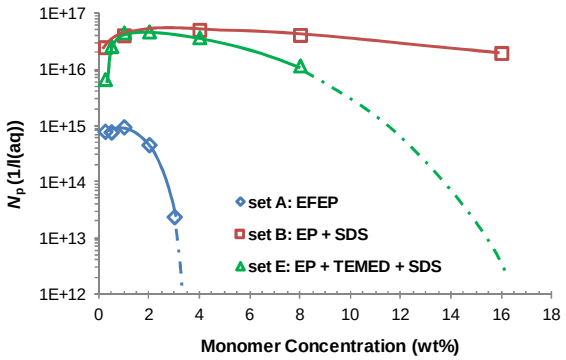

Figure 4.1.16. Final N_p versus monomer concentration for Set A (EFEP), B ([SDS] = 0.5 g·l_{aq}^{-1}) and E ([TEMED] = 10 mmol·l_{aq}^{-1}, [SDS] = 0.5 g·l_{aq}^{-1}).

Figure 4.1.16 summarises the number of particles produced in the final products for different sets of batch process. The poor colloidal stability of soft polyNIPAM particles makes it difficult

to synthesis high solids content latexes. Application of a low amount of SDS could improve the stability of the system. TEMED can prevent self-crosslinking but depresses the colloidal stability of the system; therefore, its concentration should be optimised.

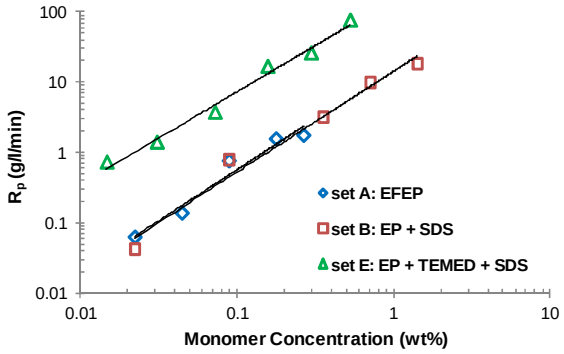

Figure 4.1.17. Variations in initial rate of polymerisation versus monomer concentration of Set A (EFEP), B ([SDS] = 0.5 g·l_{aq}^{-1}) and E ([TEMED] = 10 mmol·l_{aq}^{-1}, [SDS] = 0.5 g·l_{aq}^{-1}).

Figure 4.1.17 shows the variations of the rate of polymerisation during steady state versus initial monomer concentration for different sets. It is obvious that the rates of polymerisation in the absence of TEMED with and without SDS followed the same line, which indicates that the presence of SDS did not affect the mechanism of the polymerisation. On the other hand, the significant difference in the intercept of Set E, with that of other sets, indicates that TEMED did enhance the rate of polymerisation.

4.1.4 Conclusions

Thermal-sensitive water-soluble polyNIPAM nanoparticles have been synthesised in this work. A set of kinetic data is reported for NIPAM polymerisation using a wide range of monomer and SDS concentrations for the first time. Conversions, mostly ignored in previous reports, were closely monitored using a facile gravimetric method. Unlike other contributions, all particle sizes were measured at the reaction temperature.

The rate of polymerisation, z-average diameter of particles and molecular weight of the final products increased with NIPAM concentration. Unlike conventional emulsion polymerisation of monomers with high water-solubility, the rate of reaction was independent of SDS concentration. SDS was found to interact with polyNIPAM chains in the course of polymerisation in unusual way; by incorporating into polymer particles and causing them to swell with water at reaction temperature. As a result, the number of particles showed a maximum with increasing SDS concentration.

It was found that crosslinker-free polyNIPAM was partly insoluble in water below LCST. With decreasing temperature, the PSD of polymer latexes evolved as binary distribution representing two competing effects; particle swelling and particle shrinking by chain disintegration and dissolution in water. Only small particles formed using a low monomer concentration depicted a single shrinking PSD.

In order to improve the solubility of the polymer, TEMED was applied. This was proved to be a suitable approach in order to improve the dissolution of polymer, but depressed the colloidal stability of the particles at the same time. With the help of both TEMED and SDS, stable water-soluble nanoparticles were obtained.

4.1.5 Reference

[1] Schild, H.G. Poly(N-isopropylacrylamide): Experiment, Theory and Application. ***Progress in Polymer Science***, 1992, v17, pp163-249.
[2] Nerapusri, V., Keddie, J.L., Vincent, B., Bushnak, L.A. Absorption of Cetylpyridinium Chloride into Poly(N-isopropylacrylamide)-Based Microgel Particles, in Dispersion and as Surface-deposited Monolayers. ***Langmuir,*** 2007, v23, pp9572-9577.
[3] Liu, P.X., Luo, Q.F., Guan, Y., Zhang, Y.J. Drug Release Kinetics from Monolayer Films of Glucose-sensitive Microgel. ***Polymer***, 2010, v51, pp2668-2675.
[4] Zhang, J.T., Liu, X.L., Fahr, A., Jandt, K.D. A New Strategy to Prepare Temperature-sensitive Poly(N-isopropylacrylamide) Microgels. ***Colloid and Polymer*** Science, 2008, v286, pp1209-1213.
[5] Pelton, R.H., Chibante, P. Preparation of Aqueous Lattices with N-isopropylacrylamide. ***Colloids and Surfaces*** 1986, v20, pp247-256.
[6] Mcphee, W., Tam, K.C., Pelton, R. Poly(N-isopropylacrylamide) Latices Prepared with Sodium Dodecyl Sulfate. ***Journal of Colloid and Interface Science,*** 1993, v156, pp24-30.
[7] Pelton, R. Temperature-Sensitive Aqueous Microgels. ***Advances in Colloid and Interface Science,*** 2000, v85, pp1-33.
[8] Chan, K., Peltion, R., Zhang, J. On the formation of Colloidally Dispersed Phase-Separated Poly(N-isopropylacrylamide). ***Langmuir***, 1999, v15, pp4018-4020.
[9] Wu, C., Zhou, S.Q. Internal Motions of Both Poly(N-isopropylacrylamide) Linear Chains and Spherical Microgel Particles in Water. ***Macromolecules,*** 1996, v29, pp1574-1578.
[10] Gao, J., Wu, C. The 'Coil-to-globule' Transition of Poly(N-isopropylacrylamide) on the Surface of a Surfactant-free Polystyrene Nanoparticle. ***Macromolecules,*** 1997, v30, pp6873-6876.
[11] Wu, C. A Comparison Between the 'coil-to-globule' Transition of Linear Chains and the 'volume phase transition' of Spherical Microgels. ***Polymer,*** 1998, v39, pp4609-4619.
[12] Wu, X.Y., Pelton, R.H., Tam, K.C., Woods, D.R., Hamielec, A.E. Poly(***N***-isopropylacrylamide).1.Interactions with Sodium Dodecyl Sulfate Measured by Conductivity. ***Journal of Polymer Science: Part A: Polymer Chemistry***, 1993, v31, pp957-962.
[13] Li, H., O'Shea, J., Franks, G.V. Effect of Molecular Weight of Poly(N-isopropylacrylamide) Temperature-Sensitive Flocculants on Dewatering. ***AIChE Journal,*** 2009, v55, pp2070-2080.
[14] Kizhakkedathu, J.N. Synthesis of Well-Defined Environmentally Responsive Polymer Brushes by Aqueous ATRP. ***Macromolecules,*** 2004, v37, pp734-743.
[15] Ishifune, M., Suzuki, R., Yamane, M., Tanabe, H., Nakagawa, Y., Uchida, K. Polymerisation of Acrylamide in Aqueous Solution of Poly(N-isopropylacrylamide) at Lower Critical Solution Temperature. ***Journal of Macromolecular science,*** 2008, v45, pp523-528.
[16] Gao, J., Frisken, B.J. Cross-Linker-Free ***N***-isopropylacrylamide Gel Nanospheres. ***Langmuir,*** 2003, v19, pp5212-5216.
[17] Gao, J., Frisken, B.J. Influence of Reaction Conditions on the Synthesis of Self-Cross-Linked N-isopropylacrylamide Microgels. ***Langmuir,*** 2003, v19, pp5217-5222.
[18] Gao, J., Frisken, B.J. Influence of secondary components on the synthesis of self-cross-linked N-isopropylacrylamide microgels. ***Langmuir***, 2005, v21, pp545-551.
[19] Wu, X., Pelton, R.H., Hamielec, A.E., Woods, D.R., Mcphee, W. The Kinetic of Poly(N-isopropylacrylamide) Microgel Latex Formation. ***Colloid Polymer Science,*** 1994, v272, pp467-477.
[20] Chen, Y., Sajjadi, S., Particle Formation and Growth in ab initio Emulsifier-free Emulsion Polymerisation Under Monomer-Starved Conditions. ***Polymer,*** 2009, v50, pp357-365.

[21] Lele, A.K., Hirve, M.M., Badiger, M.V., Mashelkar, R.A. Predictions of Bound Water Content in Poly(*N*-isopropylacrylamide) Gel. *Macromolecules*, 1997, v30, pp157-159.
[22] Osada, Y., Rossmurphy, S.B. Intelligent Gels. *Scientific American*, 1993, v268, pp82-87.
[23] Gotoh, T., Okamoto, H., Sakohara, S. Dewatering of Organic Slurries Using Reinforced Thermosensitive Porous Gels. *Polymer Bulletin*, v58, 2007, pp213-223.
[24] Chen, Y., Sajjadi, S. Particle Formation and Growth in ab initio Emulsifier-free Emulsion Polymerisation Under Monomer-Starved Conditions. *Polymer*, v50, 2009, pp357-365.
[25] Smith, M.H., Herman, E.S., Lyon, L.A. Network Deconstruction Reveals Network Structure in Responsive Microgels. *Journal of Physical Chemistry B*, 2011, v115, pp3761-3764.
[26] Hu, X.B., Tong, Z., Lyon, L.A. Control of Poly(N-isopropylacrylamide) Microgel Network Structure by Precipitation Polymerisation near the Lower Critical Solution Temperature. *Langmuir*, 2011, v27, pp4142-4148.
[27] Wu, C., Zhou, S.Q., Au-yeung, S.C.F., Jiang, S.H. Volume Phase Transition of Spherical Microgel Particles. *Die Angewandte Makromolekulare Chemie*, 1996, v240, pp123-136.
[28] Meewes, M., Ricka, J. Coil-globule Transition of Poly(N-isopropylacrylamide), A Study of Surfactant Effects by Light Scattering. *Macromolecules*, 1991, v24, pp5811.
[29] Wu, C., Niu, A. Another Way to View the Chain Conformation Broadening of the Line-width Distribution Measured in Dynamic Light Scattering. *Science in China B*, 1999, v42, pp76-80.
[30]Wu, C., Zhou, S.Q. Volume Phase Transition of Swollen Gels: Discontinuous or Continuous? *Macromolecules*, 1997, v30, pp574-576.
[31] Andersson, M., Maunu, S.L. Structural Studies of Poly(*N*-isopropylacrylamide) Microgels: Effect of SDS Surfactant Concentration in the Microgel Synthesis. *Journal of Polymer Science: Part B: Polymer Physics*, 2006, v44, pp3305-3314.
[32] Deen, G.R., Alsted, T., Richtering, W., Pedersen, J.S. Synthesis and Characterization of Nanogels of Poly(*N*-isopropylacrylamide) by a Combination of Light and Small-angle X-ray Scattering. *Physical Chemistry Chemical Physics*, 2011, v13, pp3108-3114.
[33] Wang, G., Pelton, R., Zhang, J. Sodium Dodecyl Sulphate Binding to Poly(*N*-isopropylacrylamide) Microgel Latex Studied by Isothermal Titration Calorimetry. *Colloids and Surfaces A: Physiochemical and Engineering Aspects*, 1999, v153, pp335-340.
[34] Wu, C., Zhou, S.Q. Effects of Surfactants on the Phase Transition of Poly(*N*-isopropylacrylamide) in Water, *Journal of Polymer Science Part B Polymer Physics*, 1996, v34, pp1597-1604.
[35] Ricka, J., Meewes, M., Nyffenegger, R., Binkert, T.h. Intermolecular and Intramolecular Solubilization: Collapse and Expansion of a Polymer Chain in Surfactant Solutions. *Physical Review Letters*, 1990, v65, pp657-660.
[36] Tam, K.C., Ragaram, S., Pelton, R.H. Interaction of Surfactant with Poly(*N*-isopropylacrylamide) Microgel Latexes, *Langmuir*, 1994, v10, pp418-422.
[37] Lewis, K.E., Robinson, C.P. The Interaction of Sodium Dodecyl Sulfate with Methyl Celulose and Polyvinyl Alcohol, *Journal of Colloid and Interface Science*, 1970, v32, pp539-546.
[38] Feng, X.D., Guo, X.Q., Qiu, K.Y. *Makromolekulare Chemie-Macromolecular Chemistry and Physics*, 1988, v189, pp77-83.
[39] Narasimhan, B., Peppas, N.A. On the Importance of Chain Reputation in Models of Dissolution of Glassy Polymers. *Macromolecules*, 1996, v29, pp3283-3291.
[40] Hu, X.B., Tong, Z., Lyon, L.A. Control of Poly(*N*-isopropylacrylamide) Microgel Network Structure by Precipitation Polymerisation near the Lower Critical Solution Temperature, *Langmuir*, 2011, v27, pp4142-4148.

4.2 A Novel Method for Synthesis of Fast Dissolving PolyNIPAM Colloids via Semicontinuous process

Abstract: The dissolution behaviour of thermal-sensitive polymers plays a key role in many applications. Cross-linker free polyNIPAM nanoparticles produced by conventional emulsifier-free batch process do not easily dissolve in water phase, if at all. A semicountious approach was designed in which the growth of particles occurred at their surface. Nanoparticles produced via semicontinuous process underwent fast dissolution behaviour due to their layer by layer structure. For the batch process, particle swelling occurred at LCST followed by gradual release of disentangled chains into water. The extent of swelling decreased with decreasing monomer feed rate for semicontinuous process. At the lowest feed rate used, particles start shrinking as soon as LCST was reached without undergoing swelling. This suggests simultaneous chain disintegration and release from the surface of particles. Furthermore, relatively high solids content (6.0wt%) polymer latexes can be obtained via semicontinouous process.

4.2.1 Introduction

Nanomaterials based on polyNIPAM have gained great attention due to its thermal sensitive property and controllable phase transition temperature - LCST. In the absence of crosslinker monomer, polyNIPAM becomes water soluble below LCST, which is around 32°C. In the literature, water soluble polyNIPAM has been studied for different aims, such as thermal sensitive micelles for drug delivery, controllable flocculants, well-defined environmentally responsive polymer brushes and matrix for producing high molecular weight polymer [1-4].

The dissolution behaviour of the polymer can play a key role in such applications. For example, there is a growing interest in orally fast disintegrating tablets, which allow a fast dissolving drug to be absorbed directly into the systemic circulation. The improvement of drug dissolution can be obtained by incorporating the drug into a water soluble carrier [5]. The conventional method to produce polyNIPAM nanoparticles is emulsion polymerization at temperatures above LCST. This method, however, produces polymers that are not fully dissolved in water even in the absence of corsslinker (see Chapter 4.1). Similar phenomenon has also been reported in the literature [6-9]. The formation of non-soluble polyNIPAM has been attributed to physical entanglements of chains [7] or network formation due to chain transfer to polymer [6,9]. We showed that around 20wt% of the polymer chains formed by EFEP (emulsifier-free emulsion polymerisation) could not be dissolved in water at room temperature even after a week of soxhelet extraction [10]. One way around this, is to use redox initiation system such as KPS/TEMED to produce particles with more hydrophilic chains, low molecular weight and limited chain branching. However, such methods introduce significant instability to the particles so that the use of surfactants such as SDS becomes inevitable [10]. For many applications, the presence of additional components such as SDS is usually not desired because they may adversely affect the characteristics of the final products [11-12].

In this research we aim to produce nanoparticles with improved dissolution behaviour by using semicontinuous emulsion polymerization process via layer structures. Semicontinuous emulsion polymerisation is a traditional method to produce nanoparticles with core-shell structures [13-15]. Continuous addition of monomer into the reaction vessel in the course of reaction can cause new polymer chains to form at the surface of growing particles and therefore have a limited physical entanglement.

4.2.2 Experimental Work

4.2.2.1 Procedure

Most of the de-ionised water (170 ml) and buffer (4 mmol·l_{aq}^{-1}) were heated up to the desired reaction temperature while being purged with nitrogen under strong mixing (650 rpm). Then 0.25wt% of NIPAM, defined as the weight percentage of the overall aqueous phase, was added to the reactor. The rest of monomer was placed in a jacketed dosing funnel and heated to 70°C. With the help of a few drops of water, NIPAM crystals could be easily transformed to homogeneous solution and ready to be added. The agitation speed was then reduced to 450 rpm. The initiator solution, 0.2163 g KPS dissolved in 30 ml of de-ionised water, was then added to the vessel. Generally, inhibition periods around 10 min were observed. As soon as polymer was detected in the reaction mixture, the addition of monomer solution was started dropwise during a certain period. After addition was completed, the reaction was allowed to continue for another 10 min.

4.2.2.2 Measurements

Conversions, z-average diameters of particles (D_z) and zeta potentials have been measured, as described in the previous subchapter (see Chapter 4.1, page 100). The volume-average diameter of particles (D_v), swelling ratio $(D_{v,s}/D_{v,c})^3$ of particles and number of particles have been calculated.

Table 4.2.1. Recipes for synthesis of polyNIPAM nanoparticles in water by semicontinuous process. Reaction temperature: 60°C. $C_{KPS} = C_{buffer} = 4$ mmol·l_{aq}^{-1}. 200 ml water.

Exp.	Initial Monomer charge (wt%)	Total monomer charge (wt%)	Feed rate (g·min^{-1}·l_{aq}^{-1})
S1	0.25	3.0	0.27
S2	0.25	3.0	0.15
S3	0.25	1.0	0.38
S4	0.25	1.0	0.15

4.2.3 Results and Discussions

We found that (see Chapter 4.1) a larger number of particles were formed batchwise using low monomer concentration, comparing with that produced with higher monomer concentration (> 1.0wt%). Moreover, an enhanced solubility in water below LCST can be obtained with 0.25wt% NIPAM monomer. Therefore, an initial monomer concentration of 0.25wt% of NIPAM was used for all reactions, as shown in Table 4.2.1. The overall monomer concentration of 3.0wt% was used. Two rates of monomer addition were utilised.

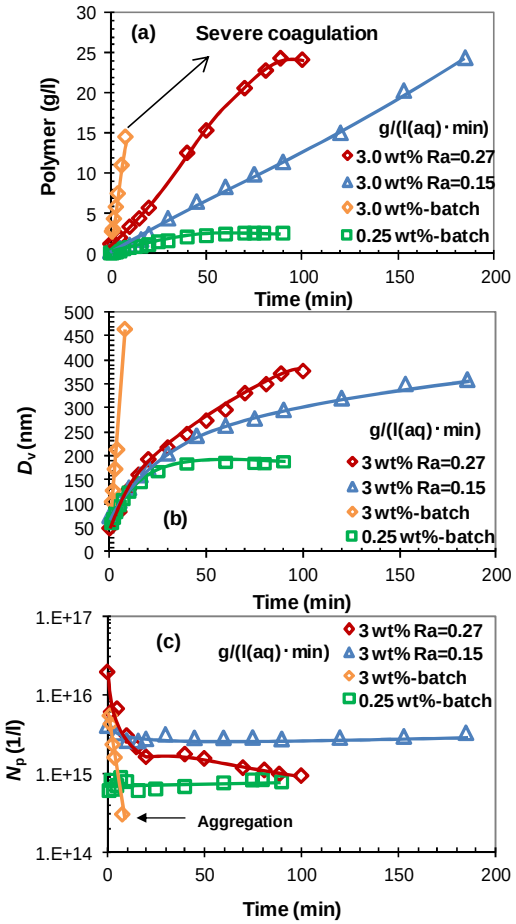

Figure 4.2.1. The reaction time evolution of (a) polymer produced, (b) volume-average size of particles and (c) the number of particles for different rates of monomer addition via semicontinuous process. [NIPAM] = 3.0wt%, T = 60°C. Batch processes with 0.25wt% and 3.0wt% NIPAM were shown for comparison.

Figure 4.2.1 shows the kinetic results of semicontinuous polymerisation with different rates of monomer addition (R_a). The data from batch processes with 0.25wt% and 3.0wt% NIPAM monomer concentrations were used for the sake of comparison. Comparing with batch process, it is easy to obtain stable latex with 3.0wt% NIPAM monomer via semicontinuous processes. The rate of reactions increased with increasing rate of monomer addition, as shown in Figure 4.2.1a. Particle growth in the semicontinuous process followed the same trend as batch process with 0.25wt% in the beginning of the polymerisation. A difference, however, became observable in the later stage of feeding. The batch polymerisation with [NIPAM] = 0.25wt%

produces stable particles at the end of reaction. However, the batch process with [NIPAM] = 3.0wt% showed severe coagulation in the intermediate stage of reaction (x = 48%). When polymerisation started semibatchwise with $[NIPAM]_0$ = 0.25wt%, followed by addition of the remainder of monomer (total [NIPAM] = 3.0wt%), the growth of particles was rather limited. The control over particle size improved with decreasing feed rate. At the higher feed rate, limited particle coagulation occurred. It is clear that semicontinuous process can control particle growth and maintain the population of particles initially formed.

In order to study the dissolution behaviour of polyNIPAM particles produced via semicontinuous processes, temperature evolution of particle size and turbidmetric of the final products were observed.

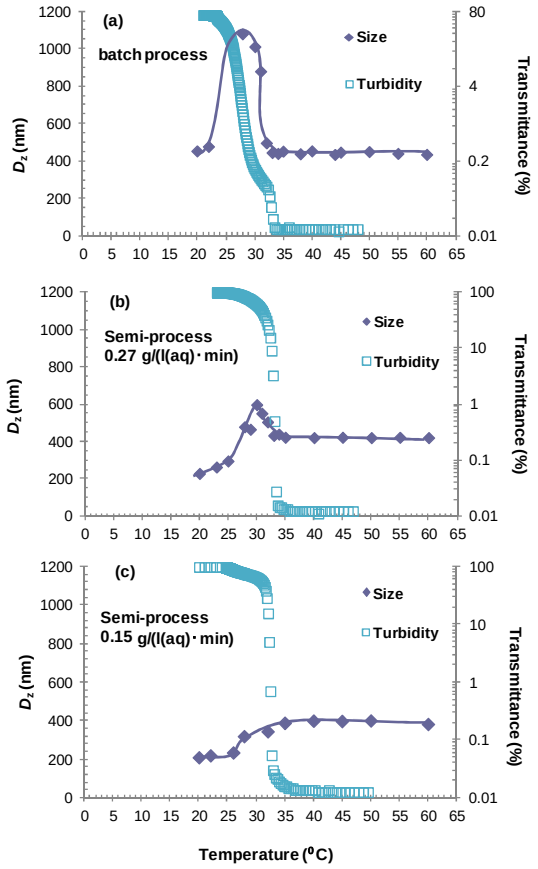

Figure 4.2.2. Z-average hydrodynamic size and transmittance versus temperature for the final samples obtained via semicontinuous process with 3.0wt% NIPAM monomer, feeding rate: (b) 0.27 g·min^{-1}·l$_{aq}^{-1}$; (c) 0.15 g·min^{-1}·l$_{aq}^{-1}$. The sample produced with 2.0wt% NIPAM monomer was studied for the sake of comparison.

Figure 4.2.2 shows the results for semicontinuous process with 3.0wt% NIPAM concentration at two different feed rates. Due to severe coagulation, the sample from batch process with 3.0wt% NIPAM was not suitable for investigation. Therefore, the sample produced via batch process with 2.0wt% was used for comparison. For the batch process, as shown in Figure 4.2.2a, the transmittance of the latex continuously increased when temperature went below 33°C, which indicates a decrease of solids content or dissolution of soluble chains. The final value

approached 69% as a part of polymer chains did not dissolve in water at 20°C. At the same time, the z-average hydrodynamic size reached 453 nm at 20°C. A maximum swelling ratio of 15.3 was obtained in the course dissolution. For the semicontinuous process, as shown in Figure 4.2.2b-c, the onset temperature of increase in transmittance was the same as that for the batch process. However, the final transmittance value reached 100% for both feeding rates indicating polymer colloids were fully dissolved in water. More interestingly, the degree of swelling diminished as feeding rate decreased within the phase transition range.

The semicontinuous process with 1.0wt% NIPAM monomer was carried out in order to study the effect of monomer concentration on the dissolution behaviour.

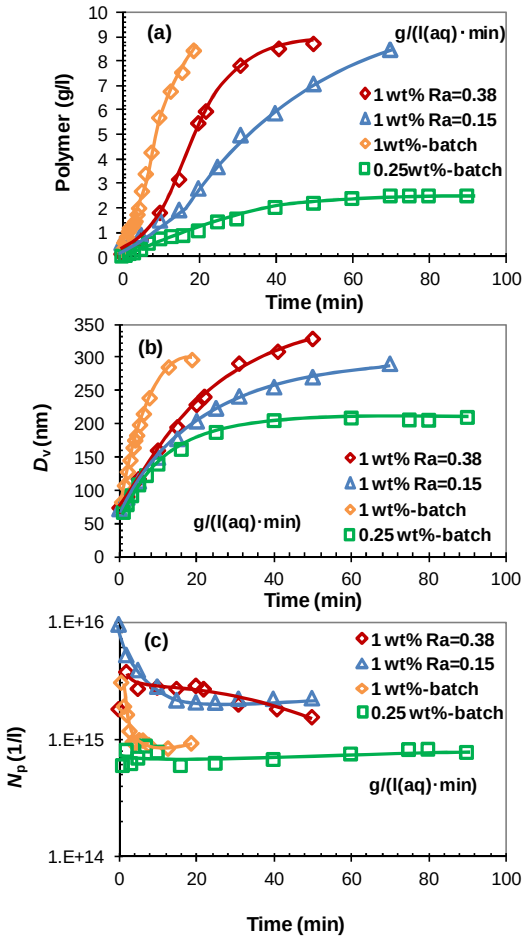

Figure 4.2.3. The reaction time evolution of (a) polymer produced, (b) volume-average size of particles and (c) the number of particles for different rates of monomer addition via semicontinuous process. [NIPAM] = 1.0wt%, T = 60°C. Batch processes with 0.25wt% and 1.0wt% NIPAM monomer concentrations were shown for comparison.

The polymerisation results show similar features as the set with 3.0wt% NIPAM, as shown in Figure 4.2.1. In addition, the final number of particles produced by the semicontinuous process was quite high, compared to batch processes.

Figure 4.2.4 shows the dissolution process of particles produced with 1.0wt% NIPAM. The maximum swelling ratio dropped from 15.8 to 1.2 by shift from batch to semicontinuous

process with R_a = 0.38 g·l_{aq}^{-1}·min^{-1}). For the lower feed rate (0.15 g·l_{aq}^{-1}·min^{-1}), particles did not swell at all but started shrinking right from beginning of the phase transition until they disappeared and a clear solution was obtained.

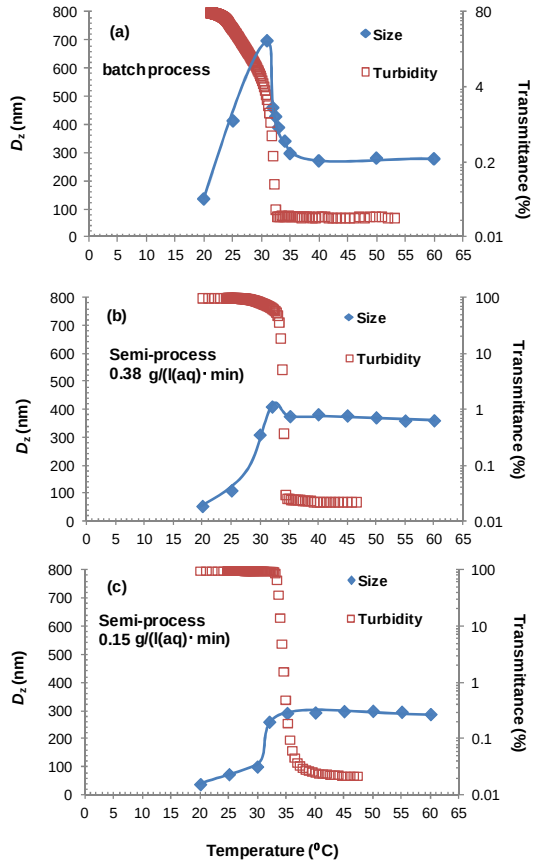

Figure 4.2.4. Temperature evolution of z-average hydrodynamic size and transmittance of the final samples obtained via batch and semicontinuous process with 1.0wt% NIPAM monomer. Feeding rate for the semicontinuous process: (b) 0.38 g·min^{-1}·l_{aq}^{-1}; (c) 0.15 g·min^{-1}·l_{aq}^{-1}

The results clearly show that the particles prepared by semicontinuous processes dissolve more easily and completely than those produced by batch process. Furthermore, a decrease in feeding rate can enhance the dissolution of particles and sharpen the LCST range during which dissolution occurs. One thing should be noticed; that is the average sizes of initial particles are similar for both batch and semicontinuous processes, which are around 300 nm and 400 nm for 1.0wt% and 3.0wt% (2.0wt% for batch) NIPAM monomer, respectively. Consequently, the effect of particle size on the dissolution behaviour in the two processes is negligible.

When an uncrosslinked, amorphous, glassy polymer is brought into contact with a thermodynamically compatible solvent, the latter dissociates into the polymer. When the solvent concentration in the swollen polymer reaches a critical value, chain displacement begins to dominate and the polymer is eventually dissolved [16]. Therefore, the dissolution of a polymer into solvent is associated with two transport processes, which are solvent diffusion (swelling) and chain disentanglement. When chains are extended at the surface of particles, rather than

toward the centre of particles, they are disintegrated from the particles and dissolved in the water phase almost simultaneously without any need to undergo swelling first (i.e. to disintegrate) and then dissolve.

One may argue that the improved dissolution behaviour could be attributed to the shorter chains produced via semicontinuous process rather than the morphology of the particles produced. To verify the effect of molecular weight, a semicontinuous reaction was carried out using 6.0wt% NIPAM and feeding rate of 0.15 $g \cdot l_{aq}^{-1} \cdot min^{-1}$. Samples for molecular weight measurements were taken at desired time to indicate the overall monomer concentration. The results are shown in Figure 4.2.5. It shows that $\bar{M}_w$ of polyNIPAM chains produced by semicontinuous process remained almost constant with increasing monomer content at a value around 400 kDa, which is similar to the $\bar{M}_w$ of particles produced batchwise with 2.0wt% NIPAM monomer. It is seen that below monomer concentration of 2.0wt%, molecular weight of polymer chains produced via batch process was always shorter than those from semicontinuous process. The reverse was true above NIPAM concentration of 2.0wt%.

For monomer concentration of 2.0wt%, in which the batch and semibatch processes have similar $\bar{M}_w$, Figure 4.2.2 clearly shows that particles produced by semicontinuous process dissolve in water very quickly. Furthermore, despite having a higher $\bar{M}_w$, a faster dissolution is still observed for the polymer produced with 1.0wt% NIPAM monomer using semicontinuous process, in comparison with the corresponding batch process, as shown in Figure 4.2.4c. This proves that the length of polymer chain is not the only factor affecting the dissolution behaviour. The morphology of polymer particles is the main parameter governing the dissolution behaviour.

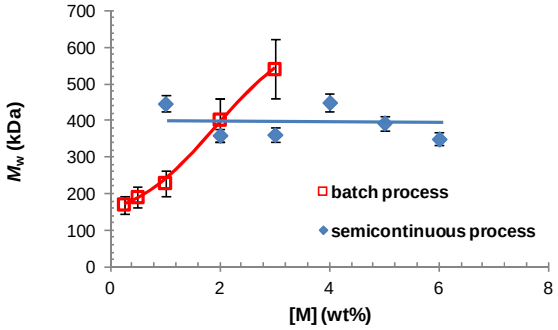

Figure 4.2.5. Comparison of $\bar{M}_w$ of samples produced with different monomer concentration via batch and semicontinuous process. T = 60°C, feeding rate: 0.15 $g \cdot l_{aq}^{-1} \cdot min^{-1}$.

There are two points to be concerned about. One is the main locus of polymerisation. The solubility of NIPAM in polyNIPAM has not been reported in the literature. In such cases that monomer is insoluble or sparingly soluble in the polymer, polymerisation always occurs at the surface of growing particles, independent of the type of process used. This means that application of semicontinuous process for such monomers expected to have little effect on the morphology of particles produced. However, we observed otherwise for the system under study. We think that water, which is also soluble in polyNIPAM to some extent, can plasticize the

polymer and enhance diffusion of monomer into particles. Since polyNIPAM can swell with 25wt% water above LCST [17] and the water solubility of NIPAM in water is around 20wt% [18], therefore the monomer percentage in the particle phase can be somehow estimated, as 5wt% × 20wt% = 5 wt%. Another point of concern is that chain transfer to polymer is often enhanced in semicontinuous process where particles are starved with monomer; rich in polymer. Had the chain transfer to polymer been the main cause for polymer insolubity in water, the semicontinuous approach would have led to formation of highly branched chains with adverse solubility in water. The results clearly eliminate such a possibility.

Figure 4.2.1 shows the schematic of orientation of polymer chains within particles produced via batch and semicontinuous processes. In batch process, where monomer concentration is relatively high within the particles, radicals propagate in any direction according to random walk theory [19]. This may lead to formation of chains extended to the centre of particles, resulting in highly entangled chains, as shown in Figure 4.2.1a. In semicontinuous process, the rate of polymerisation is controlled by the rate of monomer addition. Particles in semicontuous process are highly starved with monomer. As monomer diffuses from the aqueous phase into the particles, polymerisation is more likely to occur at the interface (Figure 4.2.1b). This is the reason why semicontinuous process is widely used to produce core-shell particles [14,20]. This feeding policy causes propagating chains to be oriented at the interface, leading to their fast disentanglement upon diffusion of water (solvent) below LCST.

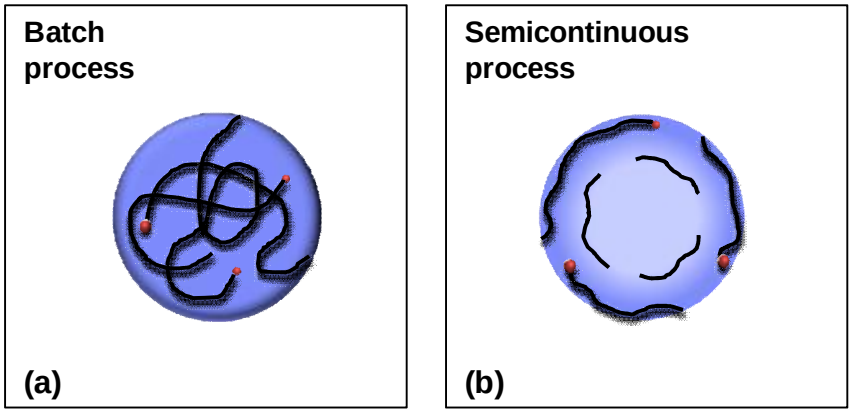

Figure 4.2.6. Scheme of behaviour of polymer nanoparticles produced via (a) batch process; (b) semicontinuous process below LCST. The red dot represents the free radical. The blue colour represents NIPAM monomer.

4.2.4 Conclusions

The results clearly show a novel way of making fast-dissolving temperature-sensitive colloids. The method was designed based on the understanding that chains formed via layer-by-layer polymerisation through semicontinous process, disintegrate and dissolve in water phase before they can swell to a measurable extent, making the dissolution time very short. For the particles formed via the batch process, particles had to swell first before chains could disintegrate and dissolve in the particles.

It can also be suggested that the semicontinuous technique can possibly be applied to produce water-soluble polyNIPAM particles at high solids content.

4.2.5 Reference

[1] Li, H., O'Shea, J., Franks, G.V. Effect of Molecular Weight of Poly(N-isopropylacrylamide) Temperature-Sensitive Flocculants on Dewatering. ***AIChE Journal,*** 2009, v55, pp2070-2080.

[2] Kizhakkedathu, J.N. Synthesis of Well-Defined Environmentally Responsive Polymer Brushes by Aqueous ATRP. ***Macromolecules,*** 2004, v37, pp734-743.

[3] Ishifune, M., Suzuki, R., Yamane, M., Tanabe, H., Nakagawa, Y., Uchida, K. Polymerisation of Acrylamide in Aqueous Solution of Poly(N-isopropylacrylamide) at Lower Critical Solution Temperature. ***Journal of Macromolecular science,*** 2008, v45, pp523-528.

[4] Talelli, M., Hennink, W.E. Thermosensitive Polymeric Micelles for Targeted Drug Delivery. ***Nanomedicine***, 2011, v6, pp1245-1255.

[5] Laitinen, R., Suihko, E., Toukola, K., Bjorkqvist, M., Riikonen, J., Lehto, V.P., Jarvinen, K., Ketolainen, J. Intraorally Fast-dissolving Particles of a Poorly Soluble Drug: Preparation and in vitro Characterization. ***European Journal of Pharmaceutics and Biopharmaceutics***, 2009, v71, pp271-281.

[6] Gao, J., Frisken, B.J. Cross-Linker-Free ***N***-isopropylcarylamide Gel Nanospheres. ***Langmuir,*** 2003, v19, pp5212-5216.

[7] Mcphee, W., Tam, K.C., Pelton, R. Poly(N-isopropylacrylamide) Latices Prepared with Sodium Dodecyl Sulfate. ***Journal of Colloid and Interface Science***, 1993, v156, pp24-30.

[8] Smith, M.H., Herman, E.S., Lyon, L.A. Network Deconstruction Reveals Network Structure in Responsive Microgels. ***Journal of Physical Chemistry B,*** 2011, v115, pp3761-3764.

[9] Hu, X.B., Tong, Z., Lyon, L.A. Control of Poly(***N***-isopropylacrylamide) Microgel Network Structure by Precipitation Polymerisation near the Lower Critical Solution Temperature. ***Langmuir***, 2011, v27, pp4142-4148.

[10] Charpter 4.1: Synthesis of Thermo-responsive and Water Soluble Poly(n-isopropylacrylamide) Colloids.

[11] Mcphee, W., Tam, K.C., Pelton, R. Poly(N-isopropylacrylamide) Latices Prepared with Sodium Dodecyl Sulfate. ***Journal of Colloid and Interface Science,*** 1993, v156, pp24-30.

[12] Wu, C., Zhou, S.Q., Effects of Surfactants on the Phase Transition of Poly(***N***-isopropylacrylamide) in Water. ***Journal of Polymer Science Part B Polymer Physics***, 1996, v34, pp1597-1604.

[13] Sajjadi, S. Nanoparticle Formation by Monomer-Starved Semibatch Emulsion Polymerisation, ***Langmuir***, 2007, v23, pp1018-1024.

[14] Sajjadi, S. Particle Formation and Coagulation in the Seeded Semibatch Emulsion Polymerisation of Butyl Acrylate, ***Journal of Polymer Science: Part A: Polymer Chemistry***, 2000, v38, pp3612-3630.

[15] Mu, Y.C., Qiu, T., Li, X.C., Guan, Y.D., Zhang, S.W., Li, X.Y. Layer-by-Layer Synthesis of Multilayer Core-Shell Latex and the Film Formation Properties, ***Langmuir***, 2011, v27, pp4968-4978.

[16] Narasimhan, B., Peppas, N.A. On the Importance of Chain Reputation in Models of Dissolution of Glassy Polymers. ***Macromolecules***, 1996, v29, pp3283-3291.

[17] Osada, Y., Rossmurphy, S.B. Intelligent Gels, ***Scientific American***, 1993, v268, pp82-87.

[18] Gotoh, T., Okamoto, H., Sakohara, S., Dewatering of Organic Slurries Using Reinforced Thermosensitive Porous Gels, ***Polymer Bulletin,*** v58, 2007, pp213-223.

[19] Croxton, C.A., Mills, M.F., Gilbert, R.G., Napper, D.H. Spatial Inhomogeneities in Emulsion Polymerisations: Repulsive Wall Calculations, ***Macromolecules***, 1993, v26, pp3563-3571.

[20] Facundo, I.A., Soria, M.J., Rosales, M.G., Elizalde, L.E., Diaz de Leon, R., Saade, H., Lopez, R.G. Synthesis and Characterization of Thermosensitive Core-shell Polymeric Nanoparticles. ***Polymer Bulletin***, 2011, v67, pp985-995.

4.3 A Novel Method for Preparation of Thermosensitive Nanocapsules via Semicontinuous Approaches

Abstract: Nanocapsules are usually difficult to produce due to difficulties involved in removing the core materials. PNIPAM nanocapsules were synthesized using a novel route. Crosslinker-free polyNIPAM nanoparticles were fabricated as core template via a semicontinuous process. The shell was made by continuous addition of NIPAM and a crosslinker. The core material was then removed via extraction with water below LCST. Traditionally batchwise made core materials could not be fully removed from the particles. However, the core produced by semicontinuous process undergoes fast dissolution and could be easily removed via self-removing process at room temperature.

4.3.1 Introduction

Functional nanomaterials with cavity-containing or hollow structures have found great interest in recent years due to their potential applications, such as drug carrier and delivery system, microreactors, protective shield for bioactive materials and bio-sensors [1-6]. Polymeric nanocapsules can be produced using a variety of approaches, including layer by layer assembly [7-11], polymer precipitation [12-13], and direct polymerisations [14-18].

Poly(*N*-isopropylacrylamide) (PNIPAM) has been extensively investigated as an ideal material due to its thermosensitive phase transition at the lower critical solution temperature (LCST) around 32°C in the water phase [19-21]. Wu et al. [22] proposed a novel one-pot route to prepare hollow PNIPAM nanocapsules. The formation of the shells and dissolution of the cores were fulfilled in the same medium. The whole synthetic procedure is composed of three stages. Crosslinker-free PNIPAM particles were firstly produced via precipitation polymerization. In the following stage, cross-linked shells were formed on the nuclei by adding a cross linker, *N,N'*-Methylene bisacrylamide (MBA) to give a core-shell structure. The final stage involves a 'self-removing' process in which the core was dissolved and diffused through the cross-linked shell to form hollow particles at temperatures below the LCST, without using organic solvents or etching agents.

However, in Chapter 4.2, we have shown that polyNIPAM particles produced via batchwise polymerization at temperatures above LCST are not fully soluble in water when they are cooled below LCST. This was mainly attributed to entanglements and self-crosslinking of polymer chains within the particles. The presence of insoluble polymer chains within the polyNIPAM particles suggests that it would be difficult to remove the core material completely. By comparison, particles produced via semicontinuous process were dissolved in water quickly and completely below the LCST temperature suggesting this process as an ideal process for making the core materials. In this work, in order to verify such hypothesis, semicontinuous process has been applied to produce PNIPAM nanocapsules. Crosslinker-free PNIPAM particles were synthesized semibatchwise and used as template to produce polyNIPAM nanocapsules. The conventional batch process was also carried out to produce the core material for the sake of comparison. The shells were produced using a semicontinuous approach for both types of the templates. This is a well-established technique to produce core-shell particles.

4.3.2 Experimental Work

4.3.2.1 Procedure

The details have been described in the previous chapter. Briefly, polymerisations were carried out at 60±1.0°C. Seed particles were first produced. For the batch process, the reactor was initially charged with 1.0wt% NIPAM. After degassing with nitrogen, initiator solution was added to initiate the polymerization. For the semicontinuous process, the polymerization was started with 0.25wt% NIPAM. The rest of the monomer was then added dropwise to the reaction vessel after 20 min. In the second stage, the crosslinked PNIPAM shell layers were fabricated on the crosslinker-free PNIPAM cores by feeding NIPAM and MBA (monomer:crosslinker = 10:1) via semicontinuous process. After polymerization was completed, the final product was diluted 10 times with pure water and was kept stirred at room temperature. Some of the dispersion was then washed by centrifugation twice and kept for further study. The same treatment is repeated for the rest of the dispersion after 3 week storage period.

4.3.2.2 Characterizations

Conversions, z-average hydrodynamic size of particles have been measured. Particle morphology and hollow structures were visualized by SEM (Hitachi, S4000) and TEM (Nippon, 200kv).

Table 4.3.1. Recipes for synthesis of polyNIPAM core-shell nanoparticles in water. Reaction temperature: 60°C, $C_{KPS} = C_{buffer} = 4$ mmol·l_{aq}^{-1}. [NIPAM]/[MBA](g/g)=10:1

Exp.	Stage 1: Seed			Stage 2: Shell	
	$[M]_o$[1] (wt%)	$[M]_f$[2] (wt%)	R_a[3]	$[M]_f$ (wt%)	R_a
HBS1	1.0	0		1.0	0.21
HSS1	0.25	0.75	0.20	1.0	0.21
HBS2	1.0	0		2.0	0.22
HSS2	0.25	0.75	0.18	2.0	0.24

1. Initially charged monomer concentration
2. Feeding monomer concentration
3. Rate of monomer addition, g·min^{-1}·l_{aq}^{-1}

4.3.3 Results and Discussions

4.3.3.1 Preparation of Core-Shell Nanoparticles

Typical PNIPAM core-shell nanoparticles were produced via two major stages: seed formation stage and shell formation stage. In the seed formation stage, two types of crosslinker-free PNIPAM cores were synthesized via batch and semicontinuous processes. After seed formation stage was completed, crosslinked shells were manipulated on the surface of seed particles by adding a mixture of NIPAM and MBA via semicontinuous process. The details of both stages are given in Table 4.3.1.

A monomer concentration of 1.0wt% was selected for the seed (core) stage. We found that (see Chapter 4.2) particles formed using 1.0wt% NIPAM monomer via semicontinuous process had enhanced solubility in water, comparing with that produced via batch process. Since the same composition of monomers is used for the shells (see Table 4.3.1), the comparison between the dissolution behaviour of different structures will display the properties of core particles produced by different processes.

Figure 4.3.1a-c show the results of the polymerizations for the two types of routes, which are labelled as batch-semi and semi-semi. During seed formation stage, conversions reached high values (x > 90%) for both routes, which indicate that most of the monomer was used up and particles were starved with monomer before monomer addition started. Figure 4.3.1b shows that the size of seed particles is around 235 and 260 nm for batch-semi and semi-semi routes, respectively. During shell formation stage, particles continuously grew indicating the formation of polyNIPAM shell layer on the seed particles. The shell thickness is around 51 and 67 nm for batch-semi and semi-semi routes, respectively. The number of particles was almost constant for both routes, which implies that secondary particle nucleation is not significant during shell formation stage.

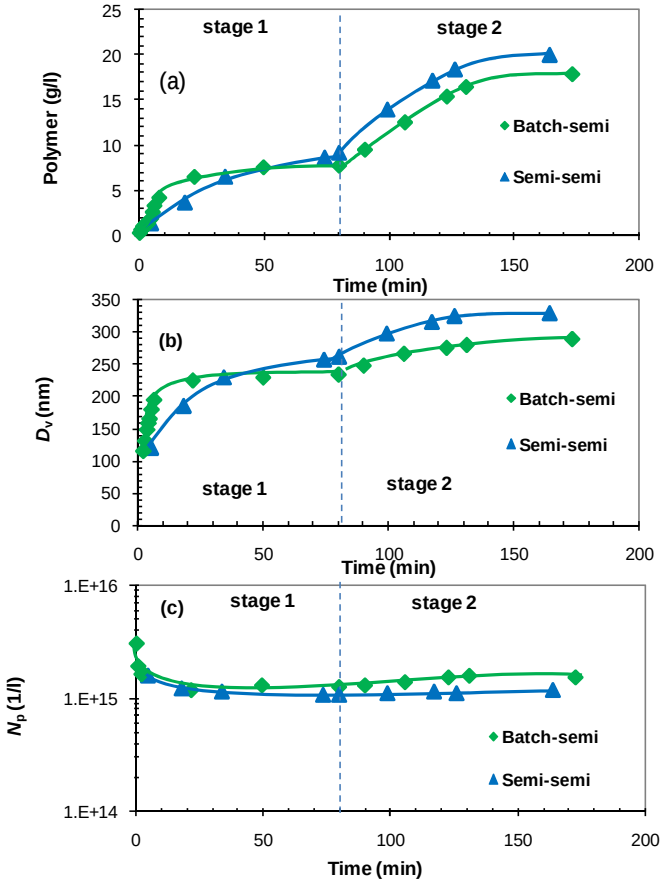

Figure 4.3.1. Time evolution of (a) conversions, (b) particle size, (c) number of particles for different processes. The dashed lines indicate the starting point of the stage 2. Samples: HBS1 and HSS1 (1.0wt% NIPAM core and 1.0wt% NIPAM shell)

4.3.3.2 Fabrication of Hollow Particles

In order to obtain hollow particles, the core needs to be removed. Crosslinker-free polyNIPAM core particles are expected to dissolve in water and diffuse out through the crosslinked shell when temperature drops below LCST.

Figure 4.3.2 shows the morphology of samples stored at room temperature for three weeks. Individual particles can be hardly indentified due to significant aggregations, especially for semi-semi particles. This is possibly caused by the presence of plenty of soluble chains in the water phase that promotes particle agglomeration. It also implies that dissolution and diffusion processes have taken place. On the other hand, a slight aggregation observed from the batch-semi particles indicates incomplete or partial polymer dissolution.

After being washed for twice using centrifuge to remove the polymer chains dissolved in water phase, the samples were once again observed using SEM. This time individual particles could be easily identified, as shown in Figure 4.3.3. Particles obtained via the batch-semi process appear to be more spherical than their counterpart from the semi-semi process. The latter

particles appear to be more collapsed. However, internal structure of the particles could not be easily observed via the SEM images.

Therefore, samples were stained with a staining agent (PTA, phosphotungstic acid) and observed under TEM. The images are shown in Figure 4.3.4. It is clearly shown that the core of the batch-semi particles was only partly removed even after three weeks of self-removing process. The micrographs also indicate that the entangled chains cannot easily diffuse out through the crosslinked shell before they are disentangled, which is consistent with the hypothesis described before. As a result, complete hollow structures were not obtained, as shown in Figure 4.3.4a. In fact, Wu et al [22] admitted that the particles they produced by batch process contained networks and were not fully soluble in the water phase below LCST. By contrast, the cores of the semi-semi particles were fully removed within the storage time and as a result hollow structures formed. Interestingly, most of the hollow particles were collapsed and form 'donut'-like particles under TEM, as shown in Figure 4.3.4b. This appears to be, however, an artifact as particles collapse under TEM when water evaporates from the internal core. Such collapse did not occur for batch-semi particles were polyNIPAM chains were still present in the core of particles.

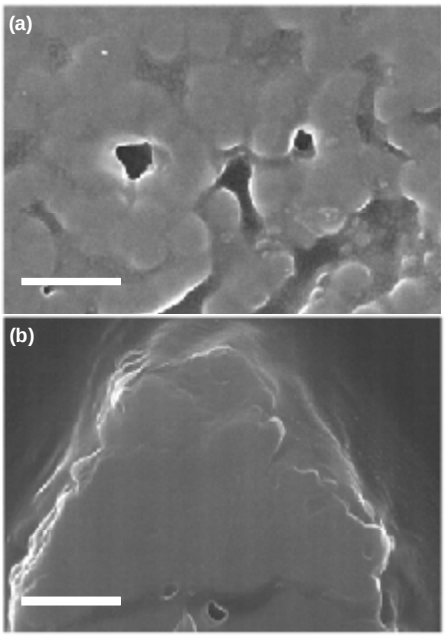

Figure 4.3.2. SEM images of (a) batch-semi and (b)semi-semi samples after three weeks storage at 25°C. Bar size: 500 nm.

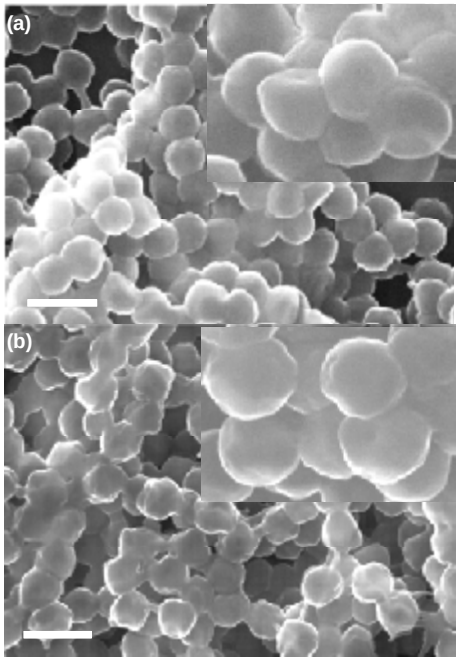

Figure 4.3.3. SEM images of washed particles produced via (a) batch-semi and (b) semi-semi routes. Bar size: 500 nm.

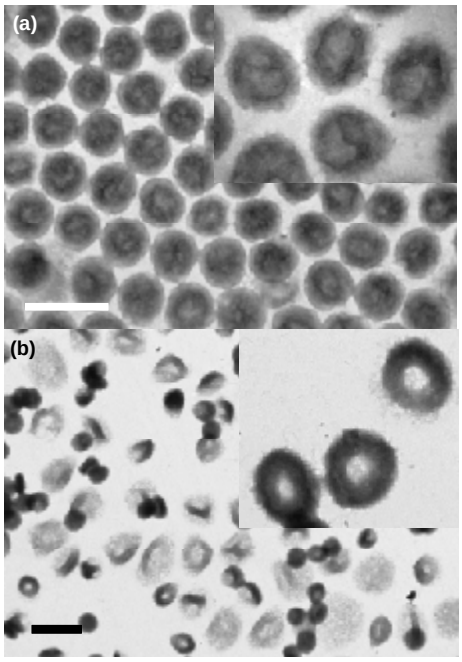

Figure 4.3.4. TEM images of washed particles produced via (a) batch-semi and (b) semi-semi routes. Bar size: 500 nm.

In order appreciate the importance of core size and look at the dynamic of core dissolution, another set of experiments was carried out with 1.0wt% NIPAM core and 2.0wt% NIPAM crosslinked shell (samples: HSB2 and HSS2). The polymerisation results are shown in Figure 4.3.5. Similar conclusions can be obtained as the samples of HBS1 and HSS1 (shown in Figure 4.3.1), except for the thicker shells (130 nm and 150 nm for batch-semi and semi-semi routes, respectively.)

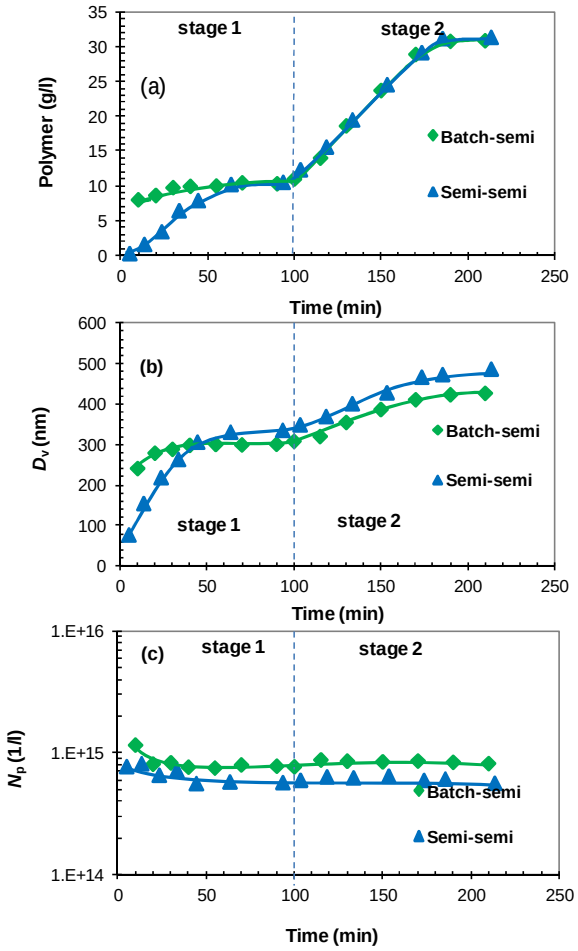

Figure 4.3.5. Time evolution of (a) conversion, (b) particle size, (c) number of particles for different processes. The dashed lines indicate the starting point of the stage 2. Samples: HBS2 and HSS2 (1.0wt% NIPAM core and 2.0wt% NIPAM shell).

During core removing process, samples were taken from the dispersion at desired times and centrifuged for 30 min. The solid content of the top layer in the centrifuge tube was measured gravimetrically and used for the estimation of the amount of the polymer chains released from the core-shell particles. The results of percentage release are shown in Figure 4.3.6 as a function of release period for different routes. It is clearly shown a progressive release of polymer chains for the core-shell particles produced via semi-semi route. By contrast, core-shell particles produced by the batch-semi route released at much slower rate. After 7 days of release, the samples were observed under TEM, as shown in Figure 4.3.7. The core of particles produced by the batch-semi route still exists while a hollow structure is obtained for the particles produced by the semi-semi route. It is clear from the TEM images that the release from core particles made with 1.0wt% shell was much more effective than the ones made with 2.0wt% monomer for shell (see Figure 4.3.4). This reduction in release can be explained by the thicker shell around the core particles. The results suggest that advantage of the semi-semi technique can particularly be taken in occasions when nanocapsules with a thick shell are required.

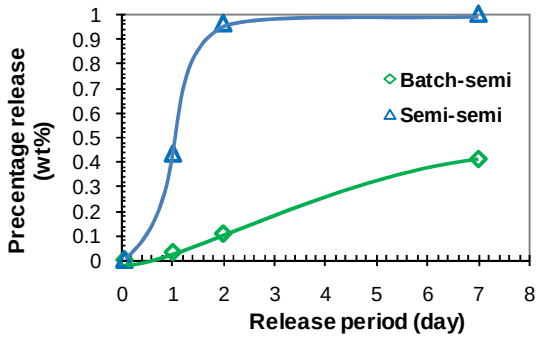

Figure 4.3.6. Percentage release as a function of release period for batch-semi and semi-semi routes. Samples: HBS2 and HSS2 (1.0wt% NIPAM core and 2.0wt% NIPAM shell).

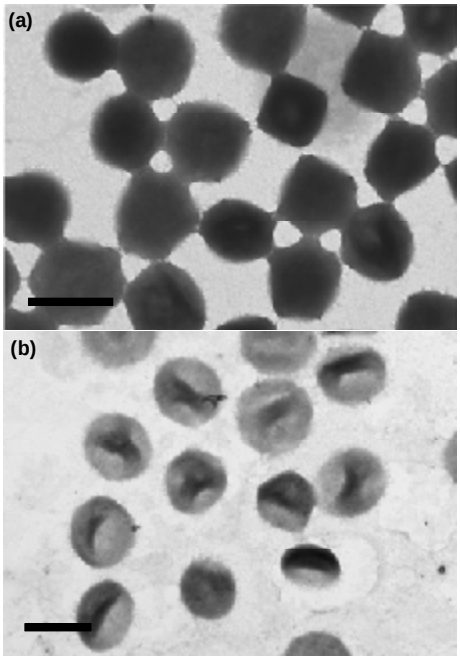

Figure 4.3.7. TEM images of particles produced via (a) batch-semi and (b) semi-semi routes after 7 day release. Bar size: 500 nm.

Thermal behaviour of particles produced via both batch-semi and semi-semi routes with 1.0 and 2.0wt% NIPAM as core and shell were further studied by DLS and shown in Figure 4.3.8. Samples, either at the end of polymerisation or after 7 day storage at room temperature, were heated up and size measurements were made. The former represents the synthesised core-shell particles, while the latter can represent hollow particles formed by removal of the core material.

It is found from Figure 4.3.6 that a complete hollow structure was obtained after 7 days of release for the semi-semi route, while for the batch process only half of the core had been removed during the same period. Figure 4.3.8 clearly shows that as temperature increases from 25°C to 60°C, the diameter of the particles decreased sharply from micron size to a unified value (around 500 nm) for the batch-semi process, but approached different values for the semi-semi process. A significant change in particle diameter occurred between 30 and 40°C; LCST. After the core being partly or fully removed, particles display a larger swelling ratio, in

comparison to corresponding core-shell ones, increasing from 8.8 to 14.6 and 10.9 to 26.7 for batch-semi and semi-semi route, respectively, as shown in Figure 4.3.8.

It is interesting to notice that hollow polyNIPAM particles or nanocapsules formed via semi-semi route vary in size to a greater extent than corresponding filled (core-shell) particles below LCST. This phenomenon can be explained by the release from the constraint of the core by the shell due to chain entanglement, as explained elsewhere [16,23]. Furthermore, the progressive shrinkage of hollow particles, produced by semi-semi route, above LCST also points to the presence of such constraint for core-shell particles, which could not shrink as such.

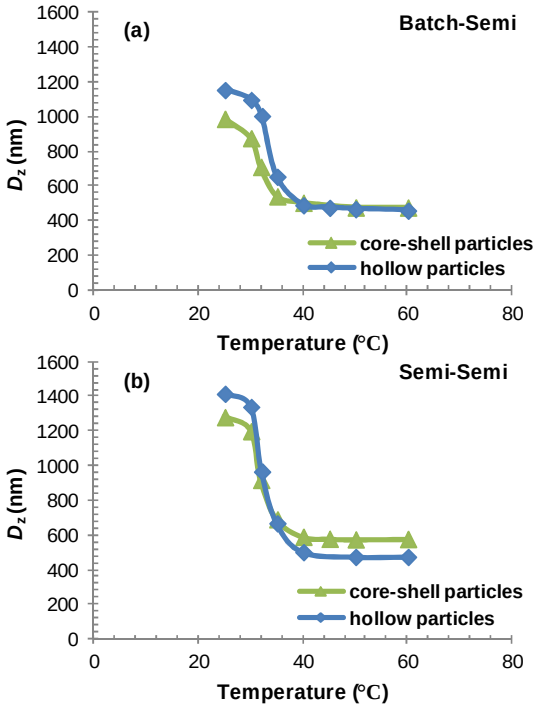

Figure 4.3.8. Z-average particle size evolution with temperature for both core-shell particles and hollow particles produced via (a) batch-semi and (b) semi-semi routes.

The results point to an enhanced dissolution of core materials produced via semi-semi process. Semicontinuous process produces particles with layer by layer structures that can allow a fast core removal for producing nanocapsules. The schematic of dissolution mechanism is shown in Figure 4.3.9.

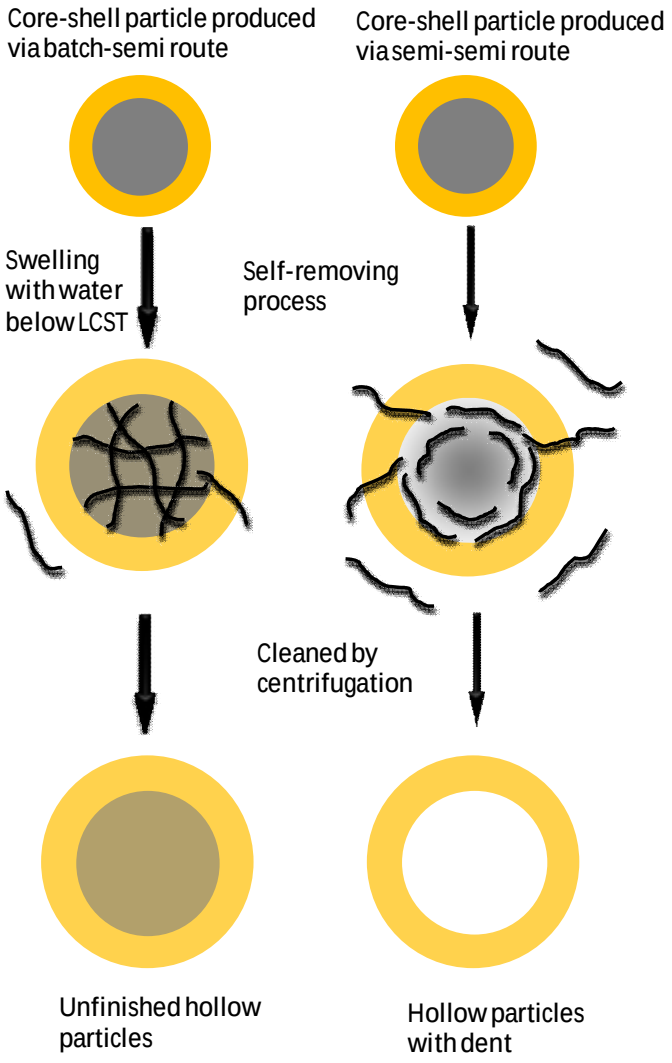

Figure 4.3.9. Scheme of core removing process of core-shell particles produced via (a) batch-semi and (b) semi-semi routes.

4.3.4 Conclusions

Thermally responsive nanocapsules were successfully fabricated via a novel method. Comparing with conventional routes reported in the literature, the core template can be easily and completely removed in the water phase below LCST, via self-removing process. The semicontinuous process was used and found to be an ideal method for the preparation of both core templates and crosslinked shells. The size of both core and shell can be easily controlled and manipulated via semicontinuous process.

4.3.5 Reference

[1] Khorram, M., Vasheghani-Farahani, E., Dinarvand, R. Preparation of Poly(*N*-isopropylacrylamide) Hollow Beads as Reservoir Drug Delivery Systems. *Journal of Controlled Release*, 2006, v116, ppe13-e33.

[2] Meier, W. Polymer Nanocapsules. *Chemical Society Reviews*, 2000, v29, pp295-303.

[3] Brand, T., Ratinac, K., Castro, J.V., Gilbert, R.G. Hollow Latex Particles as Submicrometer Reactors for Polymerization in Confined Geometries. *Journal of Polymer Science: Part A: Polymer Chemistry*, 2004, v42, pp5706-5713.

[4] Mora-Huertas, C.E., Fessi, H., Elaissari, A. Polymer-based Nanocapsules for Drug Delivery. *International Journal of Pharmaceutics*, 2010, v385, pp113-142.

[5] Antipov, A., Shchukin, D., Fedutik, Y., Zanaveskina, I., Klechkovskaya, V., Sukhorukov, G., Moehwald, H. *Macromolecular Rapid Communications*, 2003, v24, pp274-277.

[6] Glinel, K., Sukhorukov, G.B., Moehwald, H., Khrenov, V., Tauer, K. Thermosensitive Hollow Capsules Based on Thermoresponsive Polyelectrolytes. *Macromolecular Chemistry and Physics*, 2003, v204, pp1784-1790.

[7] Caruso, F. Colloids and Colloid Assemblies: Synthesis, Modification, Organization and Utilization of Colloid Particles; Wiley-VCH Verlag GmbH & Co. KGaA: Weinheim, 2004.

[8] Addison, T., Cayre, O.J., Biggs, S., Armes, S.P., York, D. Polymeric Microcapsules Assembled from a Cationic/Zwitterionic Pair of Responsive Block Copolymer Micelles. *Langmuir*, 2010, v26, pp6281-6286.

[9] Decher, G. Fuzzy Nanoassemblies: Toward Layered Polymeric Multicomposites, *Science*, 1997, v277, pp1232-1237.

[10] Dejugnat, C., Sukhorukov, G.B. pH-responsive Properties of Hollow Polyelectrolyte Microcapsules Templated on Various Cores. *Langmuir*, 2004, v20, pp7265-7269.

[11] Kinnane, C.R., Such, G.K., Antequera-Garcia, G., Yan, Y. Dodds, S.J., Liz-Marzan, L.M., Caruso, F. Low-Fouling Poly(N-vinyl Pyrrolidone) Capsules with Engineered Degradable Properties. *Biomacromolecules*, 2009, v10, pp2839-2846.

[12] Loxley, A., Vincent, B. Preparation of Poly(methylmethacrylate) Microcapsules with Liquid Cores. *Journal of Colloid and Interface Science*, 1998, v208, pp49–62.

[13] Lavergne, F.M., Cot, D., Ganachaud, F. Polymer Microcapsules with 'Foamed' Membranes. *Langmuir*, 2007, v23, pp6744–6753.

[14] Gao, Q.X., Wang, C.Y., Liu, H.X., Wang, C.H., Liu, X.X., Tong, Z. Suspension Polymerization Based on Inverse Pickering Emulsion Droplets for Thermosensitive Hybrid Microcapsules with Tunable Supracolloidal Structures. *Polymer*, 2009, v50, pp2587-2594.

[15] Ni, K., Bourgeat-Lami, E., Sheibat-Othman, N., Shan, G., Fevotte, G. Preparation of Hybrid Nanocapsules. *Macromolecular Symposia*, 2008, v271, pp120-128.

[16] Zhang, Y.W., Jiang, M., Zhao, J.X., Ren, X.W., Chen, D.Y., Zhang, G.Z. A Novel Route to Thermosensitive Polymeric Core-shell Aggregates and Hollow Spheres in Aqueous Media. *Advanced Functional Materials*, 2005, v15, pp695-699.

[17] Lv, H., Lin, Q., Zhang, K., Yu, K., Yao, T.J., Zhang, X.H., Zhang, J.H., Yang B. Facile Fabrication of Monodisperse Polymer Hollow Spheres. *Langmuir*, 2008, v24, pp13736-13741.

[18] Wu ,T., Ge, Z.S, Liu, S.Y. Fabrication of Thermoresponsive Crosslinked Poly(N-isopropylacrylamide) Nanocapsules and Silver Nanoparticle-Embedded Hybrid Capsules with Controlled Shell Thickness. *Chemistry of Materials*, 2011, v23, pp2370-2380.

[19] Schild, H.G. Poly(N-isopropylacrylamide): Experiment, Theory and Application. *Progress in Polymer Science*, v17, 1992, pp163-249.

[20] Pelton, R. Temperature-Sensitive Aqueous Microgels. *Advances in Colloid and Interface Science*, v85, 2000, pp1-33.

[21] Du, B.Y., Cao, Z., Li Z.B., Mei, A.X., Zhang X.H., Nie J.J., Xu J.T., Fan, Z.Q. One-Pot Preparation of Hollow Silica Spheres by Using Thermosensitive Poly(N-isopropylacrylamide) as a Reversible Template. ***Langmuir***, 2009, v25, pp12367-12373.

[22] Qian, J., Wu, F.P. Synthesis of Thermosensitive Hollow Spheres via a One-pot Process. ***Chemistry of Materials***, 2007, v19, pp5839-5841.

[23] Zhang, F., Wang, C.C. Preparation of Thermoresponsive Core-shell Polymeric Microspheres and Hollow PNIPAM Microgels. ***Colloid and Polymer Science***, 2008, v286, pp889-895.

Chapter 5 Composite Particles

In this chapter, organic/inorganic hybrid particles have been synthesized via different processes. Silica nanoparticles were first used for the sake of academic interests. Monomers with different water solubility, such as methyl methacrylate (MMA), vinyl acetate (VA) and NIPAM, have been explored. The stability of silica nanoparticles, the role of sililca nanoparticles throughtout the polymerisation, the affinity between silica and polymer particles and the mechanism of particle formation as well as the advantages of semicontinuous processes over batch processes have been investigated and discussed. As another example, composite thermo-responsive polyNIPAM- CdTe quantum dots (QDs) was also attempted. Water-soluble QDs were produced and charaterised (see Appendix D). However, due to difficulties involved in making stable polymer latexes and limited time available, the second stage of this work was discontinued and the focus was placed on the application of silica particles (see Appendix E).

5.1. Synthesis and Characterisation of Polymer/SiO2 Core-Shell Nanocomposite Particles by Semicontinuous Polymerisation

Abstract: Poly(methyl methacrylate, MMA)/silica and poly(vinyl acetate, VA)/silica core-shell nanocomposite particles were produced by semicontinuous surfactant-free emulsion polymerisation. Batchwise reactions were also carried out for the sake of comparison. Comparing with conventional batch process, semicontinuous process can produce much thicker silica shells at the cost of larger particles being obtained due to continuous growth of particles during monomer addition. Water solubility of monomers was found to be the key point not only for the adhesion between polymer and silica particles, but also for the associated surface polymerisation of monomers on the silica nanoparticles which facilitated hetero-coagulation. Sufficient information has been obtained to indicate that silica particles become partially covered by polymer before they are attached to the growing polymer particles. Furthermore, the effects of pH on the morphology of composite particles were reported. MMA can only produce composite particles under acidic conditions where silica nanoparticles are unstable enough to coagulate with growing polymer particles. By contrast, the highly water-soluble monomer, VA, can easily produce composite particles over a wide range of pH due to formation of layers of polymer on silica particles and resulting polymer-polymer affinity. Raspberry-like structures with smoother surfaces were obtained under basic conditions in comparison with those produced under acidic conditions. Based on this finding, a mechanism for evolution of morphology of hybrid particles in the course of polymerisation is presented.

5.1.1 Introduction

Colloidal nanocomposite materials have gained a great deal of interest for applications in many fields, particularly in catalysis, surface coatings, chromatography and biotechnologies [1-3]. The combination of properties of both organic and inorganic components exhibits improved properties (mechanical, electrical, optical, chemical, rheological, etc.) over those of either constitutes.

According to the literature, silica-polymer nanocomposite systems can be prepared by various synthesis routes using ***in-situ*** heterophase polymerisation methods mainly including emulsion, emulsifier-free emulsion, and miniemulsion polymerisation. The presence of silica nanoparticles not only has significant effect on the mechanical and physical properties of the final products but also plays a key role in the kinetic events occurring in the course of polymerisation. Early attempts on hybrid particles mainly focused on the core-shell morphology with an inorganic core protected by polymer shell in the presence of surfactants [4-6,15-16]. Later on new approaches have been developed in which inorganic phase acts as stabilizer and contributes to the stabilization of the resulting composite latex particles [7-10,22].

However, the hydrophilic nature of the silica particles and the hydrophobic nature of most polymers hinder the adhesion between two phases and reduce the possibility of forming nanocomposite particles. Therefore, improving the affinity between silica particles surface and polymers plays a key role to successful production of nanocomposite particles.

Auxiliary monomers or cationic initiators have been used to promote adhesion between anionic silica particles and the growing polymer chains. Armes and Wu [11-13] used 4-vinylpyride (4-VP) and 1-vinylimidazole (1-VID) as auxiliary monomers to prepare raspberry-like PMMA/SiO_2 hybrid particles. In these methods, the formation of nanocomposite particles was attributed to the acid-base interaction between hydroxyl groups (acidic) on silica particle surface and amino groups (basic) of 4-VP or 1-VID of the polymer. Wu's group [14] also used a cationic monomer, 2-(methacryloyl) ethyltrimethylammonium chloride (MTC), as an auxiliary monomer to prepare PMMA/SiO_2 hybrid particles. Nanosilica particles with negative charge were adsorbed on the surface of polymer particles via electrostatic interaction. Bourgeat-Lami's group [5] successfully obtained varied morphologies of silica-polymer composite latexes with different diameters in the presence of poly(ethylene glycol) monomethyl ether methacrylate (PEGMA) macromonomer. The absorption of PEGMA on the silica surface through hydrogen bonding was found to be the driving force of the assembly process. Bourgeat-Lami's group also used 2,2'-azobis(isobutyramidine) dihydrochloride (AIBA) as a cationic initiator to produce positively charged polymers in order to promote interaction of the polymers with the negatively charged surface of colloidal silica particles in aqueous solution [15-16].

Alternatively, the modifications of silica nanoparticles in order to enhance their affinity toward polymers have been widely reported. Ravaine et al. [17] produced core-shell composite particles using silica seeds grafted with a high density of γ-methacryloxypropyltrimethoxysilane (MPS). Bon's group [18,22] reported emulsifier-free emulsion polymerisation of styrene and acrylic monomers using Ludox silica particles. The pH of the suspension was fixed at 5.5 and the silica-to-monomer volumetric ratio found to be higher than 0.5 in order to get colloidally stable latex particles. Wu's group [19] prepared raspberry-like PVAc/SiO_2 composite particles using acidic nanosilica particles (pH = 3.0) with a small amount of 3-allyloxy-2-hydroxy-1-propanesulfonic acid sodium salt (HAPS) as stabilizer.

Except for a couple of short reports [15,22], no serious work has been aimed at using process type as a means to alter formation of hybrid polymer particles. In this work, we aim to investigate the effect of process type, semicontinuous versus batch, on surfactant-free emulsion polymerization of MMA and VA in the presence of Ludox silica nanoparticles.

5.1.2 Experimental Work

5.1.2.1 Procedure

The reactor vessel was initially charged with colloidal silica latex and most of the deionised water (420 ml). The dispersion was heated up to the reaction temperature and kept for 15 min under nitrogen purging and strong mixing (> 450 rpm). Then the pH of the dispersion was adjusted (mostly to 5.0±0.5) by addition of 0.1 $mol \cdot l_{aq}^{-1}$ HCl solution. After another 5 min of purging, the flow rate of nitrogen was turned down to provide only slight overpressure and the line was lifted to sit well above the surface of the dispersion to prevent evaporation of the mixture. The agitation speed was then reduced to 300 rpm. Two processes were used as follows:

Batch process: A measured amount of monomer (purged with nitrogen) was added. The polymerisation was started upon addition of KPS dissolved in 30.0 ml of water.

Semicontinuous process: The initiator solution was firstly added to the reactor. The system was allowed to return to reaction temperature. Degassed monomer was then continuously fed into the reactor at a given rate using a dosing pump.

5.1.2.2 Measurements

Conversions (x) were measured gravimetrically. Details have been given before. Z-average diameters (D_z) and zeta potential of particles were measured by DLS (Zetasizer, Malvern). We were not able to separate free silica nanoparticles from nanocomposite particles, by centrifugation for example, before size measurements due to relatively small sized silica particles used. Therefore, the size data presents the average size of all particles present in the latex.

The morphology of the nanocomposite particles was observed via scanning electron microscopy (SEM, Hitachi, S4000) and transmission electron microscopy (TEM, Nippon, 200 kv). The particle dispersions were first diluted with de-ionized water and then dried onto glass slide and carbon-coated copper grids before examination, for SEM and TEM, respectively.

From the comparison of z-average and volume average obtained by TEM with z-average obtained by DLS ($D_{z,dls}$), the conversion factor of C_f=1.0 was found, so that $D_v = C_f \cdot D_{z,dls}$.

The number of particles can be calculated as :

$$N_p = 6(m_p/\rho_p + v_{silica})/\pi D_v^3 \quad (5.1.1)$$

where m_p and v_{silica} give the mass of polymer produced and volume of silica nanoparticles incorporated at any given time. D_v is the volume-average diameter of nanocomposite particles. ρ_p is the density of polymer. The density of PMMA, PVA, polyNIPAM and silica was taken as 1.178 g·ml^{-1}, 1.160 g·ml^{-1}, 1.269 g·ml^{-1}, and 2.648 g·ml^{-1}, respectively.

The glass transition temperature (T_g) of the final products was determined by differential scanning calorimeter (DSC, Mettler Toledo DSC822e). Aluminum pans were used for all materials. The samples were first heated to 200ºC (for PMMA) or 120ºC (for PVA) at the heating rate of 20°C·min^{-1} and held at this temperature for 10 min to remove the thermal history, followed by quenching to room temperature. A heating rate of 10°C·min^{-1} was used for the second heat run. The T_g was taken as the midpoint of the heat capacity change in the second heating run.

The titration of silica was carried out at 20°C under equilibrium conditions. Silica latex was diluted with deionised water to 1.0wt% and the pH of the dispersion was adjusted by gradually adding 0.1 mol·l$_{aq}^{-1}$ HCl solution.

For observing the interior of the silica-polymer hybrid particles via TEM, selected samples were dried and grinded into powders. A small amount of the powder was mixed with a low viscosity epoxy resin, (< 10wt%), in order to make a composite. The composites were cured at 60°C for 24h. The samples were then microtomed to form slices of approximately 250 nm thickness. The resulting slices were then supported by standard Cu grids and used directly for TEM study.

Table 5.1.1. Typical recipes for the polymer latexes prepared by surfactant-free emulsion polymerisation in the presence of Ludox TM-50 silica nanoparticles. [KPS] = 2 mmol·l_{aq}^{-1}. Water: 450 ml.

Monomer	R_a ($g \cdot min^{-1} l_{aq}^{-1}$)	[NIPAM] (wt%)	NIPAM/silica (g/g)	T (°C)	[KPS] ($mmol \cdot l_{aq}^{-1}$)
MMA		10	1:1	70	2
	24.6	10	1:1	70	2
VA		10	1:1	65	2
	24.6	10	1:1	65	2

5.1.3 Results and Discussions

Surfactant-free emulsion polymerisations were carried out using methyl methacrylate (MMA) and vinyl acetate (VA) as monomers in the presence of Ludox TM-50 silica particles. Recipes are shown in Table 5.1.1.

5.1.3.1 Colloidal Stability of Silica Latex

Since KPS is used as initiator, the resulting polymer chains (particles) are anionic as they carry anionic sulfate group. The commercial silica particles, provided as dispersion in the water phase, had an average diameter of 25 nm and a zeta potential of -52.9 mV. As a result, there exists electrostatic repulsion between to-be-formed polymer chains and the silica particles, which works against agglomeration of polymer and silica phases. This suggests the colloidal stability of silica nanoparticles should be studied first before they can be used for polymerisation.

One important factor that can affect stability of nanoparticles is pH [20,22]. In order to address this, the colloidal stability of the silica latex was studied as a function of pH of the dispersion. The zeta potential and z-average diameter of silica particles and conductivity of the dispersion as a function of pH of the dispersion were measured and shown in the Figure 5.1.1a. The pH of the initial Ludox dispersion was around 10 and reduced by dropwise addition of HCl (0.1 $mol \cdot l_{aq}^{-1}$) solution. It is noticeable that the conductivity of the dispersion did not vary significantly by gradually decreasing pH from 10.0 to 2.8, but increased dramatically when pH was further reduced below 2.8.

Since the $SiOH/SiO^-$ acid/base dissociation reaction always occurs under equilibrium conditions in the silica nanoparticle dispersion [20], so:

$$Si - OH + OH^- \rightleftharpoons SiO^- + H_2O \qquad (5.1.2)$$

Silica nanoparticles carry negative charges, which derive from SiO^- species, under alkali conditions, as can be inferred from Figure 5.1.1. By adding HCl to the dispersion, the hydroxide

ions present in the dispersion are neutralized and replaced by chloride ions leading to decrease in pH. This was associated with a decrease in number of SiO^- species, as the equilibrium shifted to the left side (Equation 5.1.3), and thus in the absolute value of zeta potential. As a result, particles started to flocculate with each other, which caused an increase in z-average size of particles. Once all hydroxide ions are neutralized, further addition of acid contributes free electrolyte to the solution and the conductance increases significantly, as shown in Figure 5.1.1a (pH < 2.8). The isoelectric point was found to be close to pH=1.8, which is in agreement with the literature data (pH = 2.0) [15]. The particle size distributions (PSDs) obtained from DLS are shown in Figure 5.1.1b for different pH values. As the value of pH decreased, the PSD became narrower while shifted to the larger size range. Small silica particles showed stronger tendency for flocculation with decreasing pH than the large ones, which resulted in PSD narrowing. Unimodal PSDs were always observed.

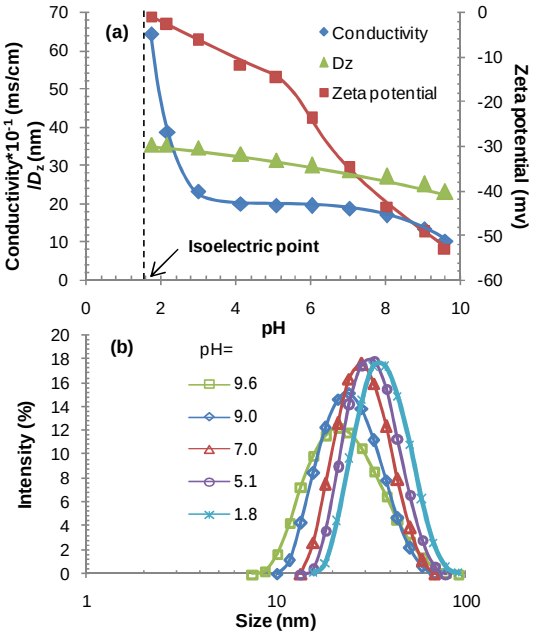

Figure 5.1.1. (a) The zeta potential, z-average size of particles and conductivity evolution of pH of the silica latex; (b) The intensity PSDs of silica nanoparticles for different pH of the dispersion.

If pH = 10 and pH = 2 represent most and least stable silica nanoparticles, respectively, then the mid points may represent particles with combined properties as filler and stabiliser. The stabilising property of silica nanoparticles is essential for emulsifier-free emulsion polymerisations because of their poor colloidal stability due to lack of surfactant in the system. Therefore, an effective pH of 4.5-5.50 for silica dispersions, prior to polymerisation, was adopted for this research. Within this range of pH values, the silica particles are expected to be stable enough to provide stability to polymer particles but not too stable to hinder interaction with polymeric particles. In order to elaborate this point, effects of pH on the reaction have been studied and discussed in a subsequent section.

5.1.3.2 Rate of Reaction, Particle Morphology, Size, and Size Distributions

5.1.3.2.1 Synthesis of PMMA/SiO_2 hybrid nanoparticles

Polymerisations were conducted using MMA in the presence of silica nanoparticles via batch and semicontinuous processes at 70°C. Polymerisations of MMA in the absence of silica nanopartcles were also carried out for the sake of comparison.

Batch Process

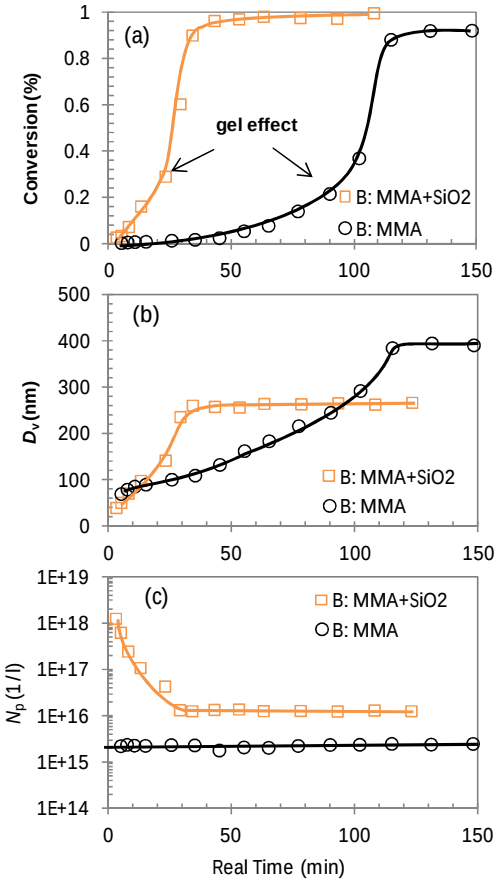

Figure 5.1.2. (a) Conversions, (b) volume-average diameter of particles, and (c) number of particles produced versus reaction time for batch process. [KPS] = 2 mmol·l_{aq}^{-1}; water: 450 ml; MMA: 50 ml; SiO2/MMA (g/g): 1:1. pH = 5.2±0.2.

Figure 5.1.2 shows the conversions, D_v and N_p with reaction time for batch process. Time zero of the reaction time is considered when polymer was detected in the system. Therefore, the inhibition periods have not been shown in the Figures. The rate of polymerisation was enhanced when silica particles were present, as shown in Figure 5.1.2a. As a result, the gel effect took place at the earlier reaction time in the presence of silica nanoparticles than that for the neat batch MMA polymerisation. Finally, smaller sized particles with larger population were obtained with the help of silica nanoparticles (Figure 5.1.2b-c).

One should note that the conversion at which the gel effect occurred ($x_{cr} \approx 33\%$ [21]) did not vary, and the rate of polymerisation inside particles during interval III (the gel effect) with most

free monomer contained inside particles, was not altered in the presence of silica nanoparticles. Furthermore, the rapid rate of reaction during early conversions implies that the transport of monomer and radicals into polymer particles were not controlled by diffusion. The effect of pH of the dispersion on radical generation should also be ruled out since a similar pH value was kept initially for both reactions (pH = 5.2±0.2). Therefore, the increase in rate of polymerisation may be simply because more particles are formed during the initial stage of the polymerisation, as shown in Figure 5.1.2c, which implies that silica nanoparticles could act as stabilizer and enhance particle formation in the course of reaction.

The presence of free silica nanoparticles in the water phase can affect the estimated size for nanocomposite particles. The maximum error in calculation occurs for the initial stage of reaction when the free silica nanoparticles outnumber composite particles. However, the effect of silica nanoparticles on size data becomes progressively less significant with reaction time. Furthermore, the intensity size distribution obtained from DLS is proportional to the square of volume of particles, and thus biased toward the larger particle sizes. In order to verify this, the conversion evolution of PSD in the batch polymerisation of MMA in the presence of silica nanoparticles was analysed and shown in Figure 5.1.3. The PSD at zero conversion represents that of silica nanoparticles. In the beginning of the reaction ($x \leq 16\%$), a broad PSD was observed in which the small size range (10-100 nm) may be attributed to the presence of free silica nanoparticles. It is quite likely that the average size of nanocomposite particles is underestimated in the presence of free silica nanoparticles during this period. As nanocomposite particles continuously grew by coagulation (see Figure 5.1.2c) in the course of polymerisation, the PSD evolved to a negatively skewed PSD and then became narrower while shifted to the large size range. The size range of silica particles was absent from the PSD of the subsequent samples indicating either silica nanoparticles were attached to the polymer particles or underwent homo coagulation. The latter can be assisted by the presence of soluble polymer chains formed in the solution, via termination of propagating radicals in water, which can glue together flocculated silica nanoparticles. The TEM images of latexes did not also show too many free silica nanoparticles in the background.

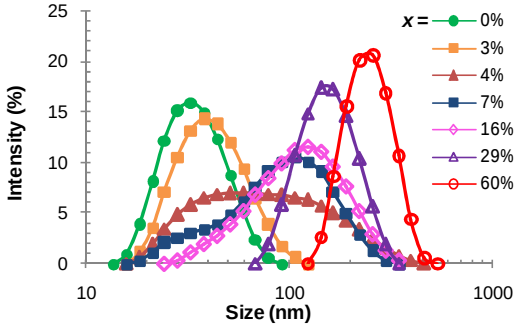

Fgure 5.1.3. Conversion evolution of PSD during batch polymerisation of MMA in the presence of silica nanoparticles, the same reaction as shown in Figure 5.1.2.

Semicontinuous Process

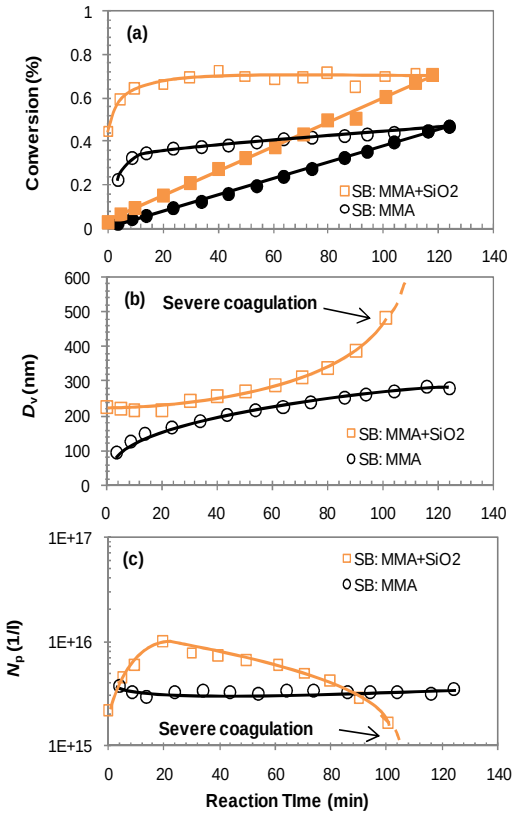

Figure 5.1.4. (a) Conversions, (b) volume average size of particles and (c) number of particles produced versus reaction time for semicontinuous process, [KPS] = 2 mmol·l_{aq}^{-1}; water: 450 ml; MMA: 50 ml; SiO2/MMA(g/g): 1:1, 2h feeding. pH = 5.2±0.2.

Figure 5.1.4 shows the conversions, D_v and N_p evolution with reaction time for semicontinuous process. For MMA monomer, the critical weight ratio of polymer in the particle is $x_{cr} = 0.33$ [21]. Above this ratio, the particles are not fully swollen with monomer and are monomer starved. As shown in Figure 5.1.4a, the instantaneous conversion of polymerisation in the presence of silica nanoparticles started at a high value ($x_i > 45\%$), which indicates a monomer-starved condition. By contrast, the initial instantaneous conversion for polymerisation of neat MMA was below 33%, which implies that polymerisation started under at least partly monomer-flooded conditions but later progressed into starved conditions during monomer addition. Similar to the batch operation, the increase in the rate of reaction in the presence of silica nanoparticles can partly be attributed to the larger number of particles initially formed, as shown in Figure 5.1.4c.

Significant coagulation occurred in the later stage of the polymerisation in the presence of silica nanoparticles, as shown in Figure 5.1.4b and c. In semicontinuous process, monomers are continuously fed to the aqueous phase. The monomer then diffuses toward the surface of polymerising particles where it is polymerised. As a result, silica nanoparticles which have already adhered onto the surface of polymer particles are gradually buried in the particles and

cannot provide sufficient electrostatic stability to the particles anymore leading to severe coagulation.

Another important point to notice is the possible effect of ionic strength on the colloidal stability of the system. For polymerisation with neat MMA via both batch and semicontinuous processes, the conductivity is around 0.45-0.58 ms·cm^{-1} throughout the reactions. When polymerisations were carried out in the presence of silica nanoparticles under acidic conditions, the conductivity increased to 2.4-2.6 ms·cm^{-1} for both processes. Such an increase in ionic strength may affect the stability of polymer particles by suppressing their double layers since no surfactant was present. This causes primary polymer particles to become even less stable and undergo homocoagulation.

The evolution of PSD during semicontinuous process of MMA in the presence of silica nanoparticles was measured by DLS and shown in Figure 5.1.5.

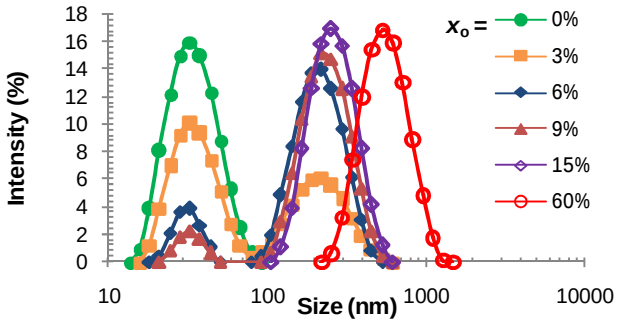

Figure 5.1.5. Overall conversion evolution of PSD during semicontinuous polymerisation of MMA in the presence of silica nanoparticles, the same reaction as shown in Figure 5.1.4.

Comparing to the batch process (Figure 5.1.3), a clear bimodal PSD was observed in the early stage of reaction ($x_o \leq 9\%$) in which the peak for free silica nanoparticles gradually shrank with time while the peak for the polymer particles incorporated with silica particles (hybrid or composite particles) evolved. The average size of the distribution (peak) at the higher end represents the diameter of nanocomposite particles, as shown in Figure 5.1.4b. This diameter was in fact used to calculate N_p for the current system using Equation 5.1.2. The weight of the incorporated silica particles ($m_{i,s}$), to be used in aforementioned equation, was estimated by intensity fraction of the free silica nanoparticles as represented by the corresponding peak. The details have been discussed in Appendix F.

This method is believed to give a better estimation of number of nanocomposite particles with time, in comparison to the one used for the batch process, which are shown in Figure 5.1.4c. As polymerisation progressed, the PSD transformed to a unimodal one in 20 min. For the batch process, a skewed monomodal distribution was obtained right from the beginning of reaction suggesting that all silica nanoparticles were involved in homo or hetero-coagulation. This is mainly because the growing polymer particles expand their interface very quickly in the batch

process. Figure 5.1.5 suggests that, unlike batch process, silica nanoparticles in the semicontinuous process are gradually attached to the growing particles due to their relatively low rate of surface expansion.

Morphology of PMMA/SiO_2 hybrid nanoparticles

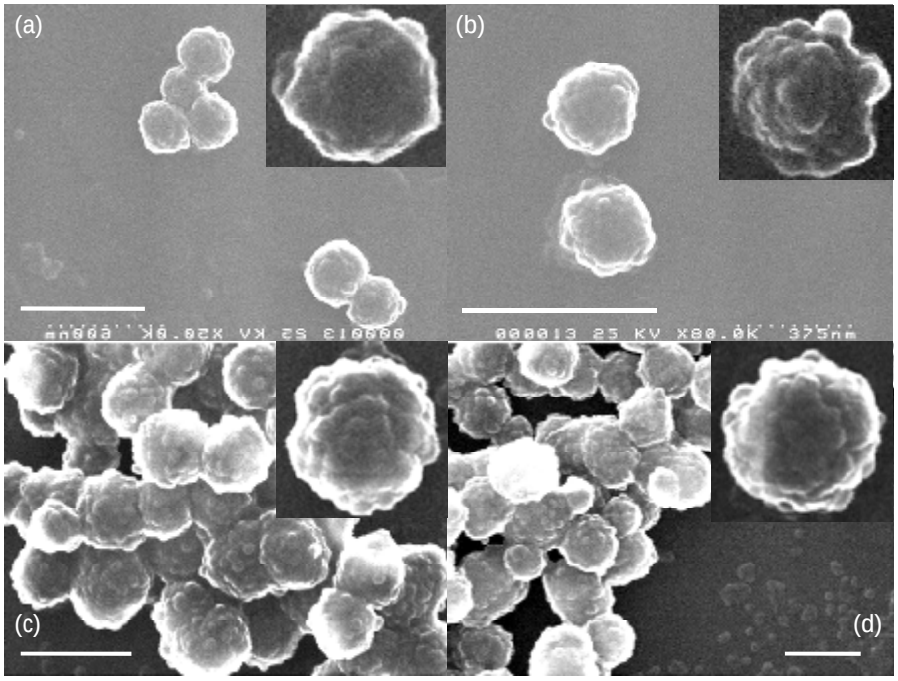

Figure 5.1.6. SEM images of nanocomposite particles produced via (a-b) batch process; (e-f) semicontinuous process; bar: 600 nm. Recipes can be found from Figure 5.1.2 and 5.1.4.

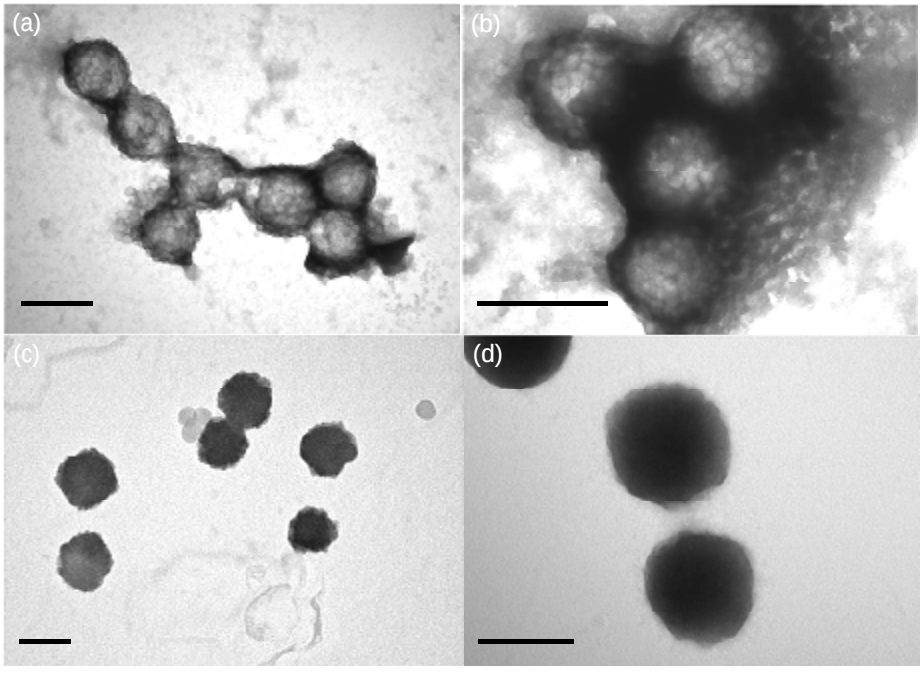

Figure 5.1.7. TEM images of nanocomposite particles produced via (a-b) batch process, (c-d) semicontinuous process (100 min reaction), bar: 300 nm. Samples are stained with a negative stain agent, 1wt% phosphotungstic acid solution. Recipes can be found from Figures 5.1.2 and 5.1.4.

In order to investigate the morphology of the hybrid particles, images (Figure 5.1.6) from SEM were studied. In the SEM images, the outline of the silica nanoparticles can be found on the surface of hybrid particles from both batch and semicontinuous processes, which indicates a significant adhesive attachment between PMMA and silica particles. Raspberry-like morphologies were obtained via both processes.

To further study the surface composition of nanocompoite particles, they were stained with 1wt% phosphotungstic acid solution and observed by TEM. When negative staining agent is applied, polymer becomes dark. By contrast, silica nanoparticles are brighter. In the TEM images produced, different colours can be observed for nanocomposite particles produced via batch and semicontinuous processes. Figure 5.1.7a-b show a bright surface for particles from batch process with tiny particles packed on suggesting a silica armored structure of nanocomposite particles. For semicontinuous process, as shown in Figure 5.1.7c-d, the surface of particles is dark. This suggests that the top surface layer is more polymer chains. Furthermore, a nonspherical shape of the nanocomposite particles implies the presence of buried silica nanoparticles inside the hybrid particles.

Cross-section Morphology of PMMA/SiO_2 hybrid nanoparticles

The cross-section morphology of the hybrid particles was studied using TEM. Before proceeding, some explanation about the methodology used to interpret the resulting images is essential. Electrons can go through the resin and polymer and get stopped by any material which has a high enough atomic number to deflect the electrons, i.e., silica. An image is ultimately rendered with different levels of black, grey and white colours. Black/grey indicates areas of the samples which are not transparent to the beam (electron dense, i.e., silica nanoparticles) and white parts are where the sample is transparent to the beam (i.e., polymer, resin).

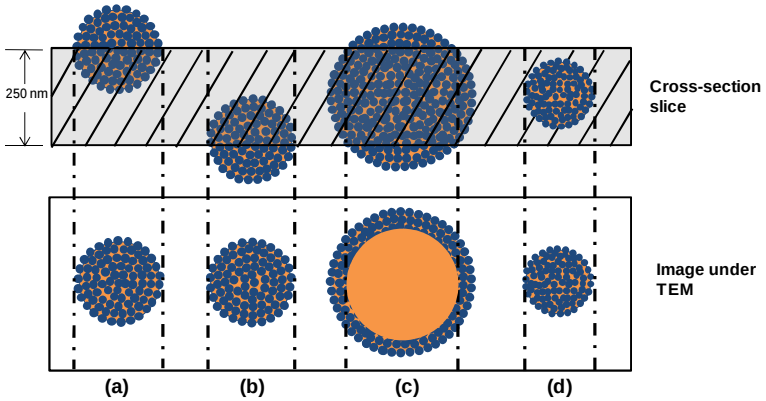

Figure 5.1.8. (a) Cross-section of particles at different positions inside the film. (b) The normal view of the particles morphologies under TEM.

Four different positions can be envisaged for a particle in relation to the microtomed section thickness, as shown in Figure 5.1.8. Morphologies (a) and (b) can be obtained for a core-shell particle if the slice of cross-section has gone through either the top or bottom of the particle. The

2D projection of such samples from TEM image gives both surface and internal information, which cannot be distinguished. Only cross-sections of particles which are cut from both top and bottom, can reveal the internal structure of the core-shell nanocomposite particles (morphology (c)). Furthermore, the possibility to obtain information on the internal structure of particles depends on their size. If the entire particle is located within the thickness of the resin section, a similar projection will be found as morphologies (a) or (b), though it may be denser (darker) since the silica nanoparticles at both top and bottom of composite particles are superimposed in the image (morphology (d)). By contrast, the larger particles would be more likely to be cut twice from top and bottom, comparing with small ones, as shown in Figure 5.1.8c-d.

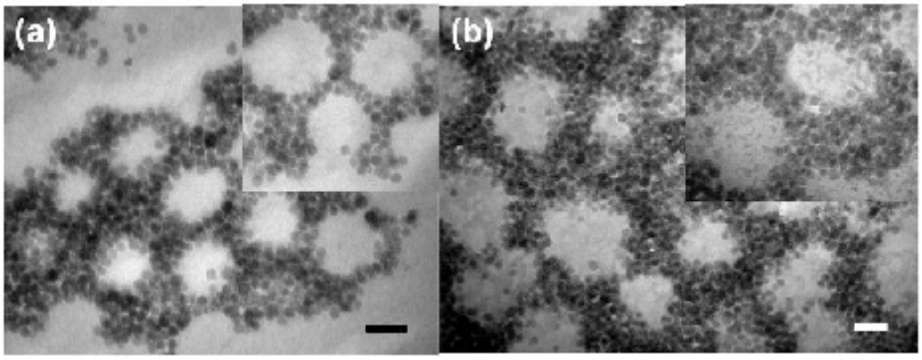

Figure 5.1.9. TEM images of the cross-section of final hybrid samples obtained from (a) batch process (c) semicontinuous process (at reaction time of 100 min). bar: 100nm. Samples are unstained. Recipes can be found from Figure 5.1.2 and 5.1.4.

The cross-section morphology of PMMA/SiO_2 hybrid nanoparticles, which were synthesized by either batch process or semicontinuous process, was found to be of core-shell structures via observation by TEM, as shown in Figure 5.1.9. For batch process, silica-free PMMA cores can be found from the Figure 5.1.9a, which indicates a core-shell structure with silica nanoparticles adhered onto the surface of polymer particles. On the images, there are also a few particles fully covered with silica nanoparticles. It is likely that these morphologies correspond to the cases (a), (b) or (d) shown in Figure 5.1.8. In comparison, more silica-free cores can be found in the figure for semicontinuous process due to larger particles obtained at the end of polymerisation, which made cross-sectioning more successful (Figure 5.1.4b). One important difference appears to be that there are much thicker silica shells for particles produced by semicontinuous process, comparing with that produced by batch process, as shown in the insets of Figure 5.1.9.

5.1.3.2.2 Synthesis of PVA/SiO_2 hybrid nanoparticles

Experiments were carried out using VA in the presence of silica nanoparticles via batch and semicontinuous processes at 65°C. The temperature was taken lower than that used in the previous experiments in order avoid VA evaporation in the vicinity of its boiling point (bp = 72.7°C). Similar to MMA system, the pH of the dispersion was adjusted to 5.0±0.5 before polymerisations started. Polymerisations of VA in the absence of silica nanopartcles were carried out for comparison.

Batch Process

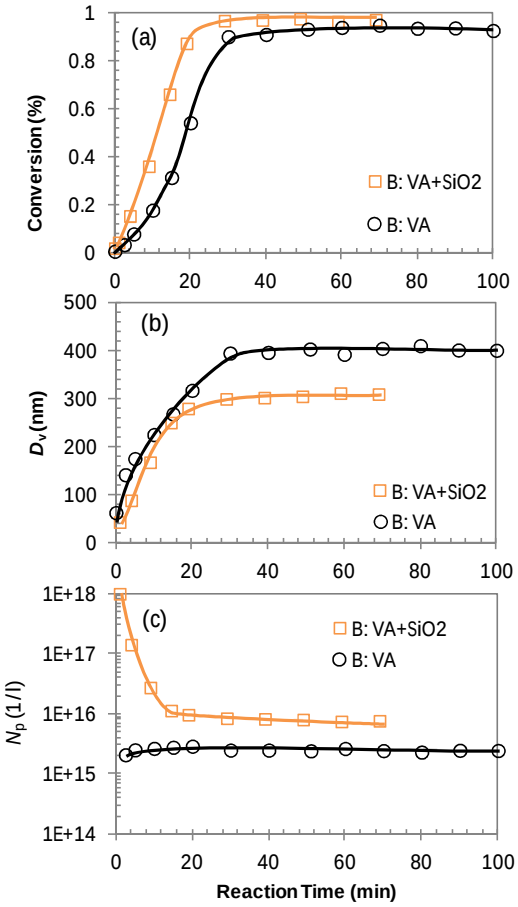

Figure 5.1.10. (a) Conversion, (b) volume average size of particles and (c) number of particles produced versus reaction time for batch reactions. [KPS] = 2 mmol·l_{aq}^{-1}; water: 450 ml; VA: 50 ml; SiO2/VA(g/g): 1:1. pH = 5.0±0.5

Figure 5.1.10 shows conversion, volume-average size and number of particles formed in the course of batch polymerisation. The rate of polymerisation as well as the final conversion increased in the presence of silica particles and more particles with smaller size were obtained at the same time (Figure 5.1.10b-c). It appears that silica nanoparticles could enhance the colloidal stability of PVA particles, which is similar to MMA/SiO_2 system.

Similar to batch polymerisation of MMA with silica nanoparticles (Figure 5.1.3), broad PSDs are observed in the early stage of reaction ($x \leq 15\%$), which eventually transformed to narrow PSDs, as shown in Figure 5.1.11.

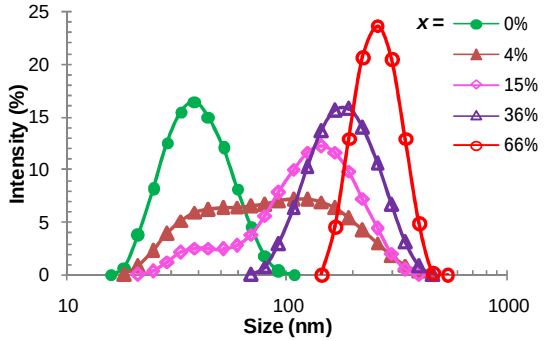

Figure 5.1.11. Conversion evolution of PSD during batch polymerisation of VA in the presence of silica nanoparticles, the same reaction as shown in Figure 5.1.10.

Semicontinuous process

For the semicontinuous process, as shown in Figure 5.1.12, the presence of silica had little effect on the rate of polymerisation, which was tightly controlled by the rate of monomer addition. A higher number of particles was initially formed in the presence of silica nanoparticles. However, coagulation of particles occurred during the whole process. Finally, only a slight increase in the number of particles as well as a slight decrease in particle size was obtained, as shown in Figure 5.1.12b-c.

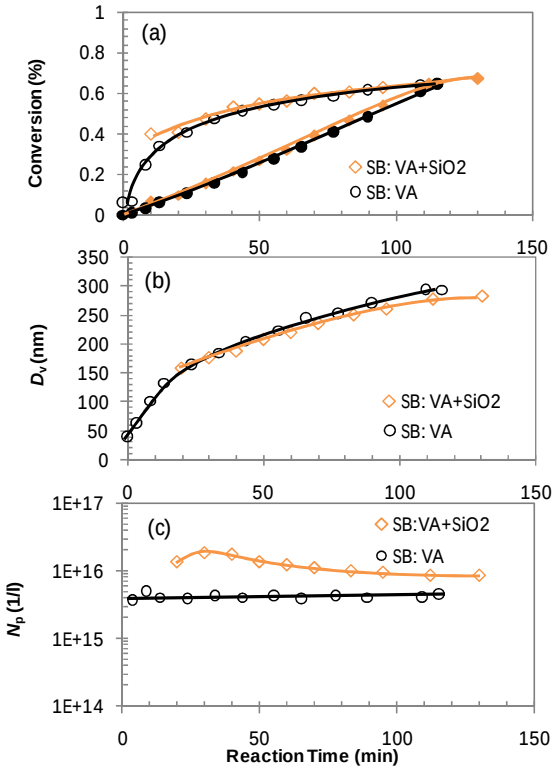

Figure 5.1.12. (a) Conversions, (b) volume average size of particles, and (c) number of particles produced versus reaction time for semicontinuous reactions, same recipe as batch process, 2h feeding time. pH = 5.0±0.5.

Similar to semicontinuous reaction of MMA, a gradual attachment of silica nanoparticles to the polymer particles can be observed from Figure 5.1.13, in which a bimodal PSD exists in the

early stage of reaction ($x_o \leq 10\%$). A correction similar to that explained for MMA, has been made for N_p data shown in Figure 5.1.12c.

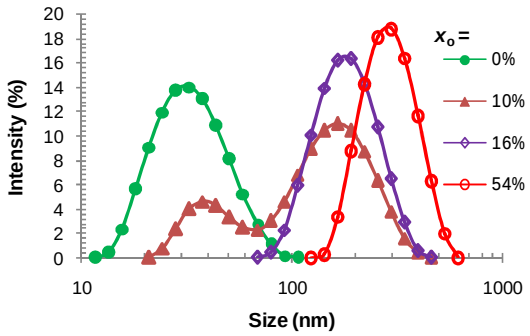

Figure 5.1.13. Overall conversion evolution of PSD during semicontinuous polymerisation of VA in the presence of silica nanoparticles, the same reaction as shown in Figure 5.1.12.

Morphology of PVA/SiO_2 hybrid nanoparticles

As discussed before, the electrostatic repulsion between silica nanoparticles and polymer particles is depressed at pH around 5.0. The driving force for the adhesion between polymer and silica particles is wetting of silica nanoparticles by the polymer chains, which is strongly dependent on the hydrophilicity of the polymer. Therefore, it is expected that PVA can be armed with more silica nanoparticles, than MMA for example. Figure 5.1.14 shows the surface morphology of the PVA/silica nanocomposite particles. Comparing with PMMA/silica, as shown in Figure 5.1.6, aggregation of silica nanoparticles can be observed on the surface of PVA/silica nanocomposite particles produced via both processes.

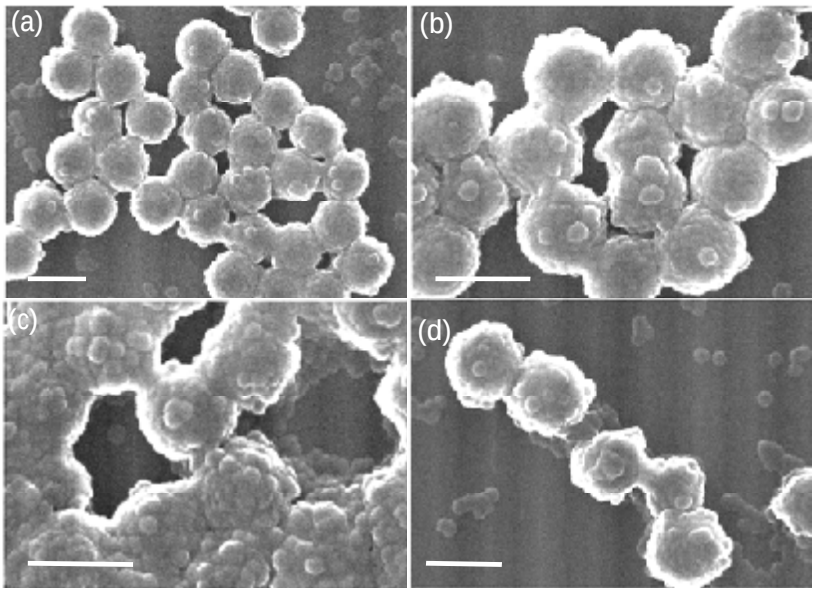

Figure 5.1.14. SEM images of PVA/SiO_2 nanocomposite particles produced via (a-b) batch process and (c-d) semicontinuous process in the presence of silica nanoparticles, bar: 300 nm; pH = 5.0±0.5.

In order to further verify the adhesion of silica nanoparticles, selected PMMA and PVA hybrids latexes produced by either batch or semicontinuous process were centrifuged. Large polymer particles as well as hybrid particles are believed to be settled down to the bottom of the centrifuge tube. The solids content in the top layer of the hybrid samples is composed of tiny polymer chains and particles, salt and free silica particles. The solids contents in the top layer of the samples were then measured by gravimetric method. By comparing these with the solids content of the top layer of the samples produced in the polymerisation with neat monomers, the concentration of free silica nanoparticles in the top layer can be estimated. The values are shown in Table 5.1.2. Their difference from 10wt%, which is the weight ratio of silica nanoparticles used in the recipe, is a rough estimation of the percentage of silica nanoparticles adsorbed or incorporated into polymer particles.

Table 5.1.2. Solids content (wt%) of the top layer of the samples in the centrifuged tube for different experiments.

Material	Batch process (wt%)	Semi process (wt%)
MMA	0.06	0.06
MMA/SiO2	5.46	4.28
VA	0.09	0.15
VA/SiO2	1.46	1.20

For the batch process, the results show that 54.6wt% of silica were present as free particles in the PMMA/SiO_2 latex, while only 13.7wt% of silica were present as free particles in the PVA/SiO_2 latex. The results suggest that PVA can absorb more silica particles than PMMA. Wu's group [19] suggested a driving force for PVA/SiO_2 absorption through the hydrogen-bonding interaction between the silanol groups of the silica particles and the hydroxyl groups of PVA, which can be another explanation for the results. The same conclusion can be found for samples produced by semicontinuous processes. Furthermore, the results indicate that more silica nanoparticles were attached to the hybrid particles produced by semicontinuous processes, comparing with batch process. Aggregations of silica nanoparticles can be observed on the surface of nanocomposite particles from TEM images for both processes, as shown in Figure 5.1.15.

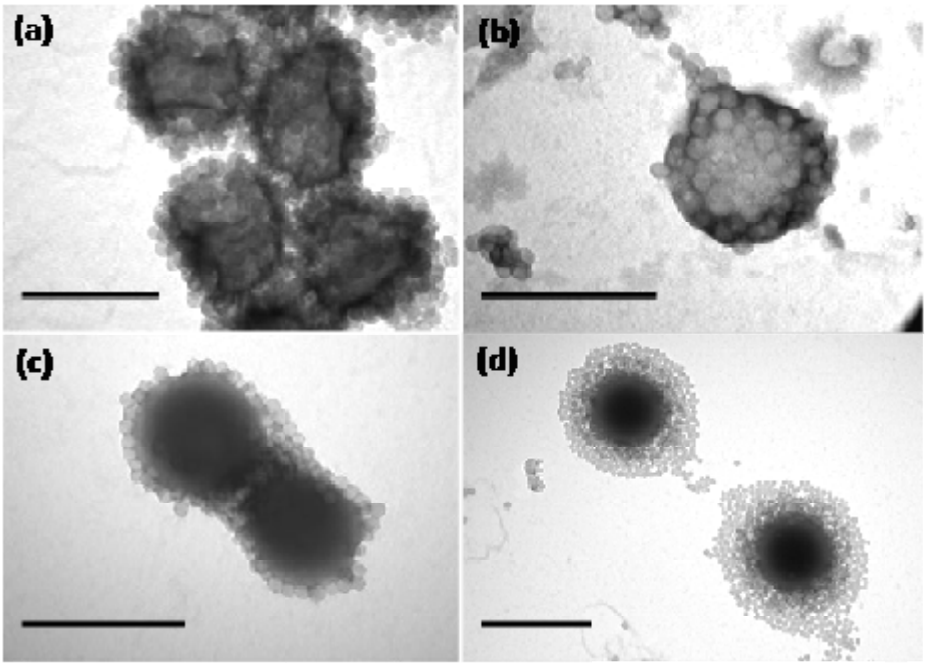

Figure 5.1.15. TEM images of PVA/SiO_2 nanocomposite particles produced via (a-b) batch process, bar: 20 nm; Samples are stained with a negative stain agent, 1wt% phosphotungstic acid solution; (c-d) semicontinuous process. Bar: 100 nm. pH = 5.0±0.5.

Cross-section Morphology of PVA/SiO_2 hybrid nanoparticles

Cross-section of the hybrid particles produced via semicontinous process is shown in Figure 5.1.16. As previously discussed, the circular void areas (bright area in Figure 5.1.16a and dark area in Figure 5.1.16b) can be taken as the polymeric cores of the particles. The average size of silica-free cores is found to be around 150 nm. The final diameter of hybrid particles was 300 nm (see Figure 5.1.12b). Therefore, silica shells with thickness of around 150 nm are formed. The results suggest formation of core-shell PVA/silica nanocomposite particles with a thick silica shell.

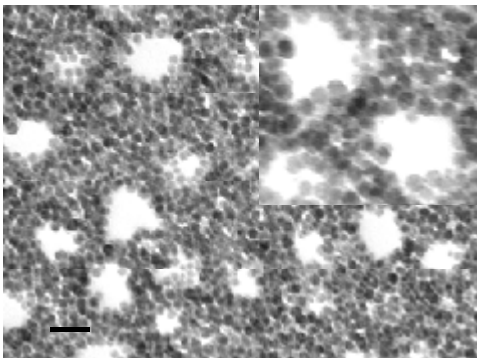

Figure 5.1.16. TEM images of the cross-section of nanocomposite particles obtained via semicontinuous process. Sample was unstained; Bar: 100nm. Recipes can be found from Figure 5.1.12.

5.1.3.3 Effect of pH

Bon's group [22] studied the effect of pH in an emulsifier-free emulsion polymerisation in which colloidal stability was provided by Ludox silica nanoparticles with 25 nm in diameter. No adhesion between silica and polymer was observed at pH = 10.0, while insufficient electrostatic stability through charge repulsion was observed at pH = 3.0. In order to study the effect of pH of the dispersion, the original silica latex with pH = 9.8±0.2 was used for polymerisations of both MMA and VA monomers. One thing should be noticed that the effect of pH on the water solubility of MMA and VA can be ignored (see Appendix G).

The semicontinuous polymerisation of MMA was carried out in the presence of silica nanoparticles at pH = 9.8±0.2. Severe coagulation of PMMA particles occurred in the early time so that the reaction did not proceed any further, as shown in Figure 5.1.17. Under base conditions, silica nanoparticles cannot attach to the polymer particles due to strong electrostatic repulsion force. In such a case, polymer particles will undergo homocoagulation because of their insufficient colloidal stability in the absence of surfactant. Furthermore, the effect of ion strength on the colloidal stability of the system could be also responsible for the coagulation. The conductivity was around 1.0-1.5 $ms \cdot cm^{-1}$ in the presence of silica nanoparticles (pH = 9.8±0.2), which is slightly higher than that for neat MMA polymerisations (0.45-0.58 $ms \cdot cm^{-1}$). The non-spherical morphology of polymer particles from SEM image supports this point (Figure 5.1.18)

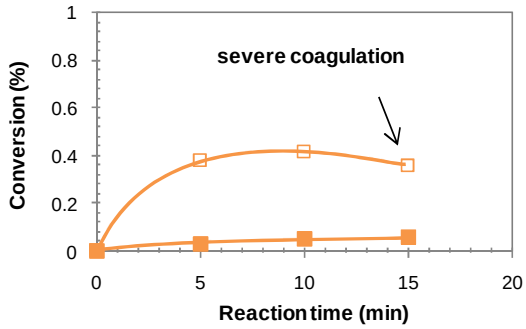

Figure 5.1.17. Conversions versus reaction time for semicontinuous process. [KPS] = 2 $mmol \cdot l_{aq}^{-1}$; water: 450 ml; MMA: 50 ml; SiO2/MMA(g/g): 1:1. pH = 9.8±0.2.

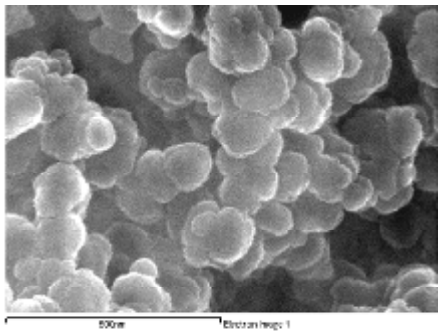

Figure 5.1.18. SEM images of particles produced via semicontinuous polymerisation of MMA in the presence of basic silica particles. Bar: 600 nm. pH = 9.8±0.2.

Batch polymerisation of VA with silica nanoparticles under basic conditions (pH = 9.8±0.2) was carried out and the results are compared with that at pH = 5.0±0.5 in Figure 5.1.19. The rate of polymerisation as well as final conversion decreased under basic conditions, comparing with the reaction under acidic conditions in the presence of silica nanoparticles.

One may conclude from this graph that the decrease in the rate of polymerisation was due to depressed rate of particle formation in the early stage under basic conditions (Figure 5.1.19c). For VA as case I monomer, the rate of polymerisation reaction should be almost independent of the number of particles formed. This suggests that there is another factor contributing to the reduction in the rate of reaction, which could be the slower rate of thermal decomposition of potassium persulfate under basic conditions [23].

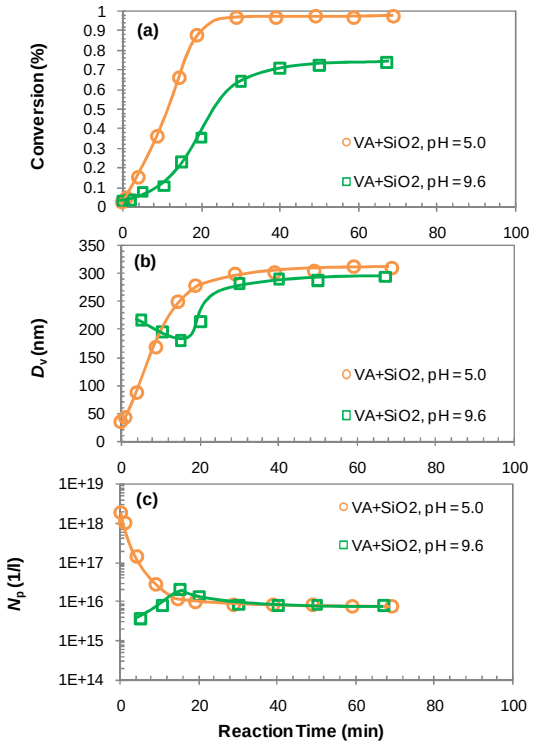

Figure 5.1.19. (a) Conversions, (b) volume-average diameter of particles and (c) number of particles produced versus reaction time for batch process under basic conditions. pH = 9.8±0.2. [KPS] = 2 mmol·l_{aq}^{-1}; water: 450 ml; VA: 50 ml; SiO2/VA(g/g): 1:1. Batch polymerisation of VA/SiO_2 under acidic conditions is shown for comparison.

In contrast to the batch polymerisation of VA with SiO_2 nanoparticles under acidic conditions (Figure 5.1.11), clearly bimodal PSDs were found in the early stage of the reaction ($x \leq 11\%$) under basic conditions, as shown in Figure 5.1.20. As mentioned before, corrections have been made for N_p in order to eliminate the effect of free silica nanoparticles in the system on the size. Note that fewer hybrid particles with larger size were initially formed under basic conditions (Figure 5.1.19b-c). It indicates that the adhesion of silica nanoparticles to the surface of polymer particles was suppressed due to significant electrostatic repulsion between two types of particles under basic conditions.

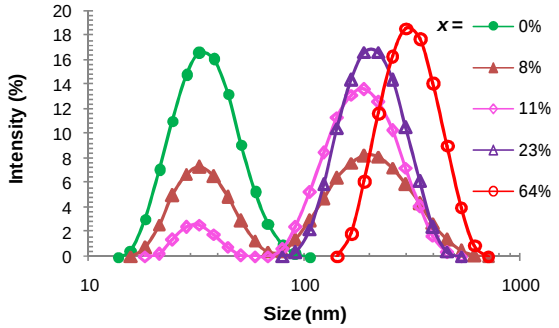

Figure 5.1.20. Evolution of PSD during batch polymerisation of VA in the presence of silica nanoparticles under basic conditions.

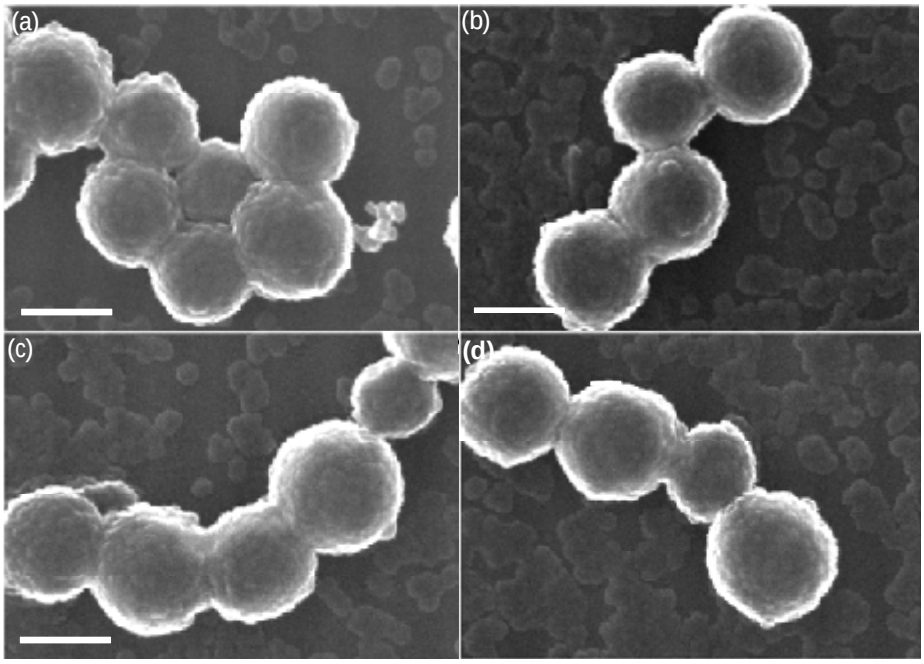

Figure 5.1.21. SEM images of PVA/SiO_2 nanocomposite particles produced batchwise in the presence of original silica nanoparticles. pH = 9.8±0.2, bar: 500nm.

Figure 5.1.21 indicates that the surfaces of the composite particles produced at pH = 9.8±0.2 are smoother than those produced under acidic conditions and a larger number of free silica particles can be found in the background. This implies that the polymer-silica particles collisions become less frequent due to the significant electrostatic repulsion between the negatively charged silica and polymer particles. For the same reason, aggregation of silica nanoparticles with each other, and less importantly their collapse on the surface of nanocomposite particles, became insignificant resulting in a rather smooth particle surface. However, stable PVA/silica nanocomposite particles were still obtained due to the affinity between PVA and silica nanoparticles.

5.1.3.4 Semibatchwise addition of silica nanoparticles

In the previous section for semicontinuous process, all silica nanopartiles were initially charged in the reactor while monomer was continuously added. As a result, most of silica nanoparticles were first captured and then buried in growing polymer particles during reaction. Therefore,

composite particles eventually suffered from lack of stability and underwent massive coagulation in the later stage of reaction. In order to enhance the stability of polymer particles, part of silica nanoparticles was added semibatchwise. The total amount of silica nanoparticles was kept constant, but only half of it was initially charged in the reactor. The rest of silica latex was fed into the reactor in the course of polymerisation at the rate of 17.9 $ml \cdot h^{-1}$. The additions of both monomer and silica latex were completed simultaneously. During the course of the addition, the pH of the latex increased as silica dispersion was continuously fed into the reactor. In order to minimise the effect of pH, an HCl solution (0.1 $mmol \cdot l_{aq}^{-1}$) was used to adjust the pH of the latex around 5.0±1.0 during polymerisation. The conductivity continuously increased with silica addition and finally reached 2.6 $ms \cdot cm^{-1}$.

The reaction data for the semicontinuous polymerisation of MMA is shown in Figure 5.1.22. The data for the reaction with silica nanoparticles initially charged is shown for the sake of comparison.

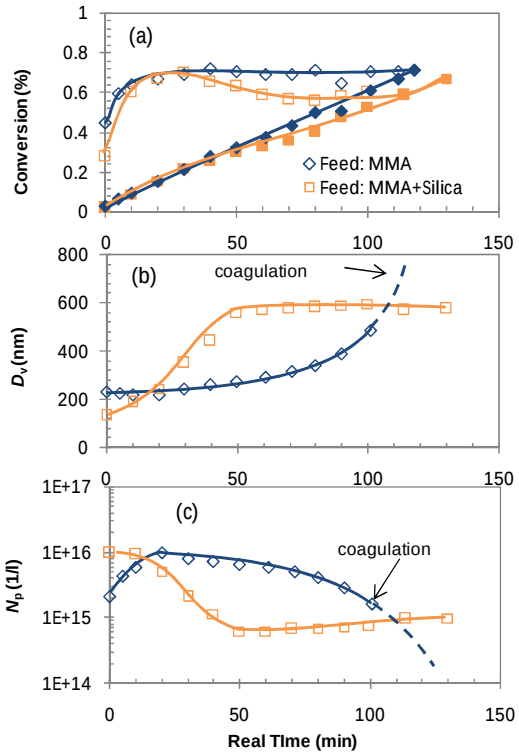

Figure 5.1.22. (a) Conversions, (b) volume average size of particles and (c) number of particles produced versus reaction time for semicontinuous polymerisation of MMA in the presence of silica with different feeds. pH = 5.0±1.0

As shown in Figure 5.1.22a, the initial rate of polymerization was not sensitive to the initial concentration of silica nanoparticles present in the system. Significant coagulation was observed after 10 min of the reaction with silica feed which caused a decrease in the rate of polymerisation, as shown in Figure 5.1.22a and 5.1.22c. Despite coagulation initially aggravated when silica particle concentration in the initial charge was halved, but later became almost negligible so that stable composite particles could be obtained (Figure 5.1.22c). This clearly

confirms that the hypothesis suggested, ***buried silica particles and loss of stability***, is credible. Moreover, an indication of secondary nucleation of particles can be observed in the later stage of reaction (Figure 5.1.22c).

One should note that the effect of variations in ionic strength, due to continuous addition of silica dispersion, on particle coagulation can be ruled out on the ground that the initial conductivity of the reaction mixture with silica dispersion feed (1.8 $mS \cdot cm^{-1}$) was lower than that for the polymerisation with silica nanoparticles initially charged (2.6 $mS \cdot cm^{-1}$).

In order to investigate incorporation of silica nanoparticles into hybrid particles, their morphology was observed via SEM as shown in Figure 5.1.23.

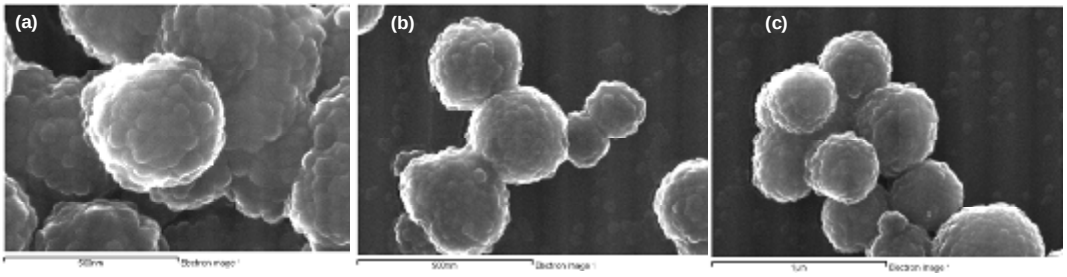

Figure 5.1.23. SEM images of PMMA/SiO2 nanocomposite particles produced via semicontinuous process with silica dispersion feed. Bar: (a) 500nm; (b) 900nm; (c) 1000nm. pH = 5.0±1.0.

Comparing with composite particles produced via initially charged silica nanoparticles, as seen in Figure 5.1.6c-d, particles appear to be more spherical which implies an improved contribution of silica nanoparticles to the colloidal stability of nanocomposite particles.

Following the same process as PMMA/SiO_2 nanocomposite particles, the effect of semibatchwise addition of silica nanoparticles was studied for PVA/SiO_2 system. The pH was controlled around 5.25±0.75 using 0.1 $mmol \cdot l_{aq}^{-1}$ HCl solution. The results are shown below.

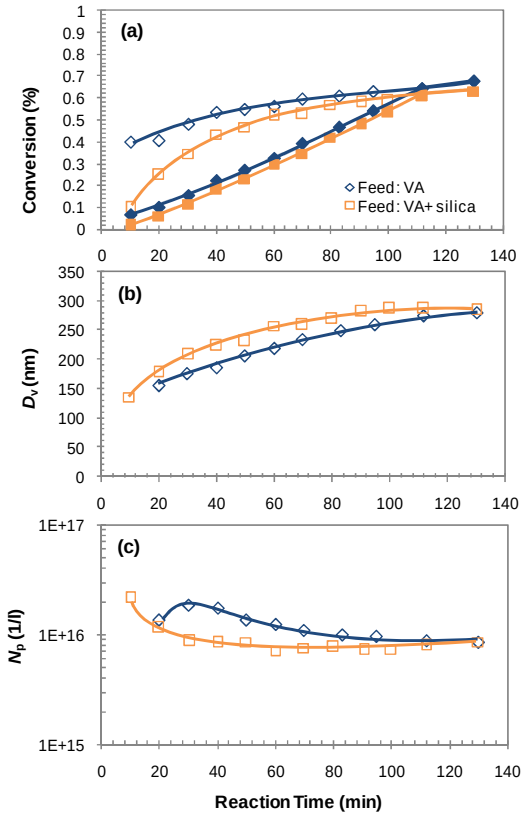

Figure 5.1.24. (a) **Conversions, (b) volume average size of particles and (c) number of particles produced versus reaction time for semicontinuous process. [KPS] = 2 mmol·l_{aq}^{-1}; water: 450 ml; VA: 50 ml; SiO2/VA(g/g): 1:1. pH = 5.25±0.75.**

The rate of polymerisation is not affected by different methods of feeding, as shown in Figure 5.1.24a. Similar to MMA/SiO_2 system (Figure 5.1.22), a stronger rate of coagulation is observed in the early stage of polymerisation with silica feed (Figure 5.1.24c). Finally, stable latexes of similar sizes were obtained for both runs.

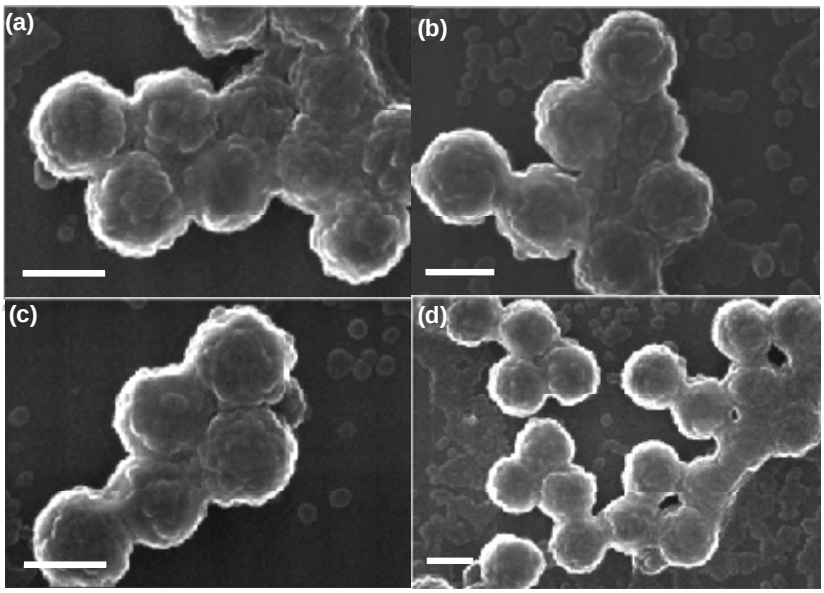

Figure 5.1.25. SEM image of the PVA/SiO_2 nanocomposite particles produced via semicontinuous process with addition of silica nanoparticle, bar: 200nm. pH = 5.25±0.75.

SEM images, as shown in Figure 5.1.25, show a more spherical morphology for nanocomposite particles produced via silica feed, compared with those produced with silica nanoparticles initially charged (Figure 5.1.14). The silica feeding policy provides an improved usage of silica nanoparticles as stabiliser in the formation of nanocomposite particles.

5.1.3.5 Glass transition temperature (T_g)

Nanocomposite particles can exhibit significant improvement in mechanical and thermal properties in comparison with their parent polymer systems (nano-effect). Glass transition temperature (T_g) is the temperature where the polymer goes from a hard glass like state to a rubber like state. The nano-effect of nanoparticles on the T_g of polymer nanocomposite particles has been studied widely in the literature. The attractive or repulsive interactions between the nanoparticle surface and local polymer chain segments alter the mobility of the polymer segments. Recent work revealed that T_g increased for nanoparticles with attractive interaction with polymer matrix in the interfacial region [24-25,30], and decreased with repulsive polymer-nanoparticle interaction [26] which induces free volume at the interface and thus assists the large-scale segmental motion of the polymer. The extent of change in T_g, which is attributed to the confinement effect of nanoparticles, also depends on the degree of intermixing of polymer and inorganic particles. It has been reported that the deviations from T_g of neat polymer can be as large as tens of degrees in the nanocomposite systems [26-31]. For core-shell particles with little intermixing such as core-shell particles, the effect in T_g should not be very significant.

In order to better clarify the morphology of nanocomposite particles produced, glass transition temperatures of the final products were studied by DSC. The results are shown in Table 5.1.3. The main result is that the T_g of nanocomposite particles were not much different from those of neat polymers confirming that the morphology of particles is core-shell one.

The T_g of neat PMMA produced via semicontinuous process was around 3ºC lower than that produced via batch process. In the literature [32], the expression relating the glass transition temperature to the molecular weight of amorphous polymer is generally accepted as follows:

$$T_g = T_{g,\infty} - K/\bar{M}_n \qquad (5.1.7)$$

where $T_{g,\infty}$ is the glass transition temperature when polymer molecular weight approaches infinity. K is a constant and $\bar{M}_n$ is the number-average molecular weight of the polymer. The increase in the polymer chain length tends to decrease the chain mobility and therefore increase the glass transition temperature of the polymer.

In order to verify the effect of molecular weight on T_g, selected final samples were dissolved in toluene and the weight-average molecular weight ($\bar{M}_w$) of polymers was measured. The results show a lower T_g for polymer with a lower molecular weight (10.4 kDa; for polymer produced

via semicontinuous process) than that for higher molecular weight (79.4 kDa; via batch process), which is consistent with the theory (Equation 5.1.7). By contrast, T_g of the neat PVA did not vary much (< 1ºC) for different processes, which is simply because of the similar $\bar{M}_w$ produced via both processes (8.0 kDa for batch process and 10.9 kDa for semicontinuous process).

Table 5.1.3. Summary of T_g (°C) of nanocomposite particles.

Material	Batch process		Semi process	
		Basic silica		Feeding Silica
PMMA	126.3	-	123.5	-
PMMA/SiO_2	128.5	-	128.1	127.1
PVA	41.5	-	40.6	-
PVA/SiO_2	40.3	40.7	36.0	37.6

The nanocomposite particles exhibited single T_g, which suggests a homogeneous morphology. A slight increase in T_g (2-3°C) of the PMMA/SiO_2 nanocomposite particles produced via both batch and semicontinuous processes, in comparison with those of neat polymers, can be observed. It suggests an attractive interaction between silica nanoparticles and PMMA in the shell. One important point to notice is that T_g of nanocomposite particles produced via semicontinuous process with continuous silica addition is 1°C lower than that produced via semicontinuous process with all silica particles initially charged. This suggests that fewer silica nanoparticles were incorporated into polymer particles (less polymer-silica intermixing) for the run with silica feeding, which is consistent with the previous discussion.

For PVA, the presence of silica nanoparticles decreased the T_g of the nanocomposite particles by 1-4ºC. Furthermore, the decrease in T_g is more significant for the composites produced via semicontinuous process than those produced via batch process. The possibility of decrease in T_g upon incorporation of silica into polymer composites has been reported in the literature [33-34]. When hydrophilic silica nanoparticles are used, it is likely that they absorb water molecules on the surface that are not compatible with the polymer matrix [33], leading to the formation of free volume at the silica-polymer interface. This possibility appears to be more likely for more hydrophilic polymers such as PVA. As a result, the crystallinity of PVA chains can decrease in PVA/silica nanocomposite particles leading to relatively easier movement of polymer chains, and thus the depression of glass transition temperature [34]. In this case, a more significant decrease in T_g for semicontinuous process could be due to an increasing interface area of polymer and silica particles and associated plasticising water.

5.1.3.6 Mechanism of formation of hybrid core-shell particles

From the experimental results presented, one can draw the morphology of PMMA/silica and PVA/silica nanocomposite particles formed via batch and semicontinuous processes as given in Figure 5.1.26. Nanocomposite particles produced via semicontinuous process have a thicker shell of silica nanoparticles compared to that produced by batch process.

In the batch process, particles stop to grow by polymerisation when the critical conversions, 0.33 and 0,21 (x_{cr}) for PMMA and PVA, respectively, are reached (interval ш). After this conversion, all unreacted monomer is contained inside the particles so that particles do not grow by propagation anymore. As a result, coagulation might become progressively less important as particles may become glassy at high conversions. Therefore, the interaction period between polymer and silica nanoparticles is relatively short and limited to particle formation stage. For semicontinous process, particles kept growing during the whole addition period by polymerisation as well as by coagulation, resulting usually larger particles, comparing with batch process. However, on the other hand, the particle interaction period was as long as the monomer addition time. As a result of these, nanocomposite particles produced by semicontinuous process incorporate more silica nanoparticles than those made by batch process. Nanocomposite particles with thinner silica shell and more spherical morphology were produced via batch process.

Furthermore, the surface of nanocomposite particles produced by the batch process is believed to be smoother than those produced by the semicontinuous process. This is thought to be due to the fact that adsorption of silica particles or lumps during batch polymerisation occurs at low to intermediate conversions where polymer is soft and can accommodate silica particles to produce smooth surface. Whereas particle adsorption in the semibcontinuous operation occurs at high conversions where the polymer is semi-solid (close to glass transition temperature) and hardly can deform.

On the other hand, the presence of almost silica-free polymer core for both processes indicates that the primary nucleation occurs by limited flocculation of primary polymer nuclei probably due to their high instability. When the primary particles acquire sufficient stability, they start coagulating with silica nanoparticles and form core-shell structures. Phase separation may also assist in formation of core-shell morphologies.

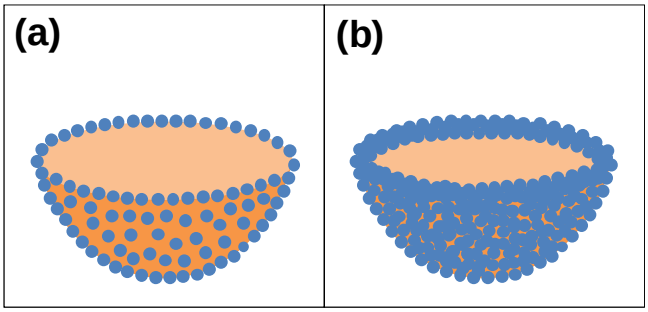

Figure 5.1.26. Morphology of polymer/silica nanocomposite particles produced via (a) batch and (b) semicontinuous process.

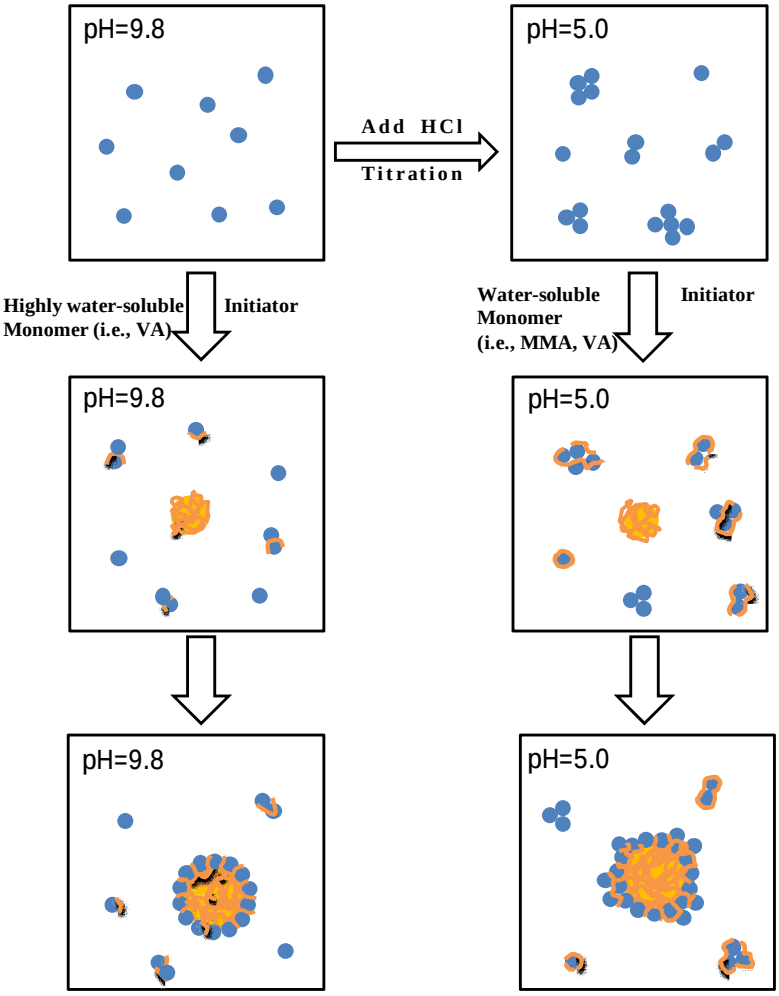

Figure 5.1.27. Scheme of particle formation of nanocomposite particles under different pH.

The TEM images of stained samples from the early stage of the batch polymerisation (pH = 5.0) clearly show that there is a thin layer of polymer around and within flocs, as shown in Figure 5.1.28. A thin layer of polymer can also be observed around free silica particles.

Based on these new evidences, the schematic of underlying mechanisms for formation of nanocomposite particles is deliberated and shown in Figure 5.1.27. Under basic conditions (pH

= 9.8), silica nanoparticles dispersed in the water phase are highly charged (Figure 5.1.1). When a highly water-soluble monomer (i.e., VA) is polymerising, silica nanoparticles can absorb water-soluble oligomeric chains which are formed by termination of propagating radicals in water. Furthermore, the soft precipitated polymer chains on the surface of silica particles may facilitate the adsorption of oligomeric radicals from the water phase by silica particles in the course of polymerisation so that polymerisation could occur on the surface of silica particles. Such surface polymerization is believed to be more important in the batch polymerization, than the semicontinuous process, because the monomer concentration in water phase is higher. These events can lead to the formation of silica nanoparticles partly covered by polymer chains, which can promote their adhesion to polymer particles in the later stage of polymerisation. However, silica particles are still able to keep their identity and avoid flocculation at basic pH thanks to their strong electrostatic stability. It is the adsorption of partly polymer-covered silica nanoparticles by the polymer particles that makes it possible to give smooth core-shell structure to the nanocomposite particles at basic pH, as shown in Figure 5.1.21. Note that the hydrophilicity of monomer is a key factor for the adhesion between polymer and silica particles. MMA did not produce composite particles under basic conditions (Figure 5.1.18) probably due to its insufficient water solubility.

By contrast, at acidic conditions (pH = 5.0), the surface charge on the silica nanoparticles is suppressed, which causes silica-silica flocculation in the water phase (Figure 5.1.1) and an increase in the average particle size. At acidic pH, the electrostatic repulsion among particles is already weak so that particles flocculate to some degree. Each floc contains several silica nanoparticles. The same pattern, as described above, follows; the polymer chains as well as polymeric radicals are adsorbed by silica flocs and assist their further flocculation. Polymer-silica coagulation occurs later during reaction and finally composite particles with rough surfaces and raspberry structures are formed, as shown in Figure 5.1.6 and 5.1.14.

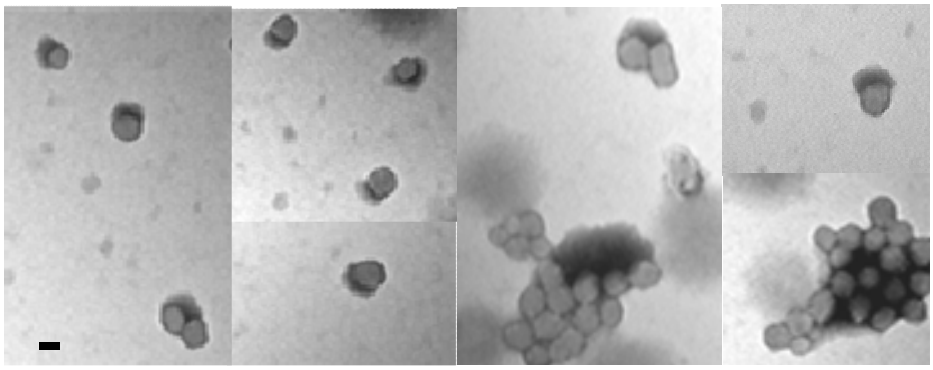

Figure 5.1.28. TEM images of stained samples from the early stage (x ≈ 30%) of batch polymerisation of VA in the presence of silica nanparticles under acidic conditions. Black layers represent stained polymer and spheres are silica nanparticles. Bar: 20 nm. pH = 5.0±0.5.

5.1.4 Conclusions

In this work, core-shell nanocomposite particles have been produced by surfactant-free emulsion polymerisation via both batch and semicontinuous processes in the presence of silica nanoparticles (Ludox TM-50, ca. 25 nm in diameter).

The rate of polymerization as well as the number of particles increased significantly in the presence of silica particles for the batch process. For the semicontinuous process, the overall rate of polymerization is controlled by the rate of monomer addition and is independent of the presence of silica nanoparticles. Larger particles were produced via semicontinuous process, in comparison to batch process, due to the lack of stability caused by continuous burial of silica particles into the polymer shell. Comparing with conventional batch process, nanocomposite particles produced by semicontinuous process can incorporate more silica nanoparticles on the shell, due to continuous growth of particles in the course of monomer addition. The usage of silica nanoparticles as stabilizer was improved by gradually feeding silica nanoparticles in the course of semicontinuous polymerisation. However, the pattern of particle growth was opposite to that of conventional semicontinuous process. For initially charged silica particles, the rate of coagulation was minimal in the beginning of the reaction but gradually increased in the course of reaction until a mass coagulation occurred. For the run with silica feed, polymerisation started with limited coagulation until intermediate conversions, but later on particle sizes became stable. In line with what has been reported in literature, it has been found that the hydrophilicity of monomer is the key factor for the adhesion between polymer and silica particles. However, the new discovery is that such affinity is facilitated by polymerisation of monomers on the surface of silica particles in the course of reaction.

The effects of pH on morphology of composite particles are reported for very first time. MMA did not produce composite particles under basic conditions (pH=9.8), at which silica nanoparticles are highly negatively charged. This extreme stability can be easily overcome by changing the initial pH of the emulsion to acidic conditions (pH=5.0), under which silica nanoparticles are less stable and coagulate with PMMA particles to form raspberry core-shell particles. By contrast, highly water-soluble monomers like vinyl acetate (VA) can easily yield nanocomposite particles over a wide range of pH. Under basic conditions, raspberry structures with smoother surface of nanocomposite particles were obtained, comparing with those produced under acidic conditions. The mechanistic insights into morphology evolution of composite particles were presented.

5.1.5 Reference

[1] Sanchez, C., Julian, B., Belleville, P., Popall, M. Applications of Hybrid Organic-inorganic Nanocomposites. *Journal of Materials Chemistry*, 2005, v15, pp3559.
[2] Saunders, B.R., Turner, M.L. Nanoparticle-Polymer Photovoltaic Cells. *Advances in Colliod and Interface Science*, 2008, v138, pp1.
[3] Leszczynska, A., Njuguna, J., Pielichowski, K., Banerjee, J.R. Polymer/Montmorillonite Nanocomposites with Improved Thermal Properties. Part II. Thermal Stability of Montmorillonite Nanocomposites Based on Different Polymeric Matrixes. *Thermochimica Acta*, 2007, v454, pp1-22.
[4] Nguyen, D., Ravaine, S., Bourgreat-Lami, E., Duguet, E. About the Suitability of the Seeded-Dispersion Polymerization Technique for Preparing Micron-Sized Silica-Polystyrene Clusters. *Journal of Materials Chemistry*, 2010, v20, pp9392-9400.
[5] Reculusa, S., Poncet-Legrand, C., Ravaine, S., Mingotaud, C., Duguet, E., Bourgeat-Lami, E. Syntheses of Raspberrylike Silica/Polystyrene Materials. *Chemistry of Materials*, 2002, v14, pp2354-2359.
[6] Hatto, N., Cosgrove, T., Snowden, M.J. Novel Microgel-Particle Colloids: the Detailed Characterisation of the Layer Structure and Chain Topology of Silica : Poly(NIPAM) Core-Shell Particles. *Polymer*, 2000, v41, pp7133-7137.
[7] Balmer, J.A.; Schmid, A., Armes, S.P. Colloidal Nanocomposite Particles: Quo vadis?. *Journal of Materials Chemistry*, 2008, 1v8, pp5722-5730.
[8] Schmid, A., Fujii, S., Armes, S.P. Synthesis of Micrometer-sized Silica-Stabilized Polystyrene Latex Particles. *Langmuir*, 2005, v21, pp8103-8105.
[9] Tiarks, F., Landfester, K., Antonietti, M. Silica Nanoparticles as Surfactants and Fillers for Latexes made by Miniemulsion Polymerization. *Langmuir*, 2001, v17, pp5775-5780.
[10] Bon, S.A.F., Colver, P.J. Pickering Miniemulsion Polymerization using Laponite Clay as a Stabilizer. *Langmuir*, 2007, v23, pp8316-8322.
[11] Barthet, C., Hickey, A.J., Cairns, D.B., Armes, S.P. Synthesis of Novel Polymer-Silica Colloidal Nanocomposites via Free-Radical Polymerization of Vinyl Monomers. *Advanced Materials*, 1999, v11, pp408.
[12] Percy, M.J., Barthet, C., Lobb, J.C., Khan, M.A., Lascelles, S.F., Vamvakaki, M., Armes, S.P. Synthesis and Characterization of Vinyl Polymer-Silica Colloidal Nanocomposites. *Langmuir*, 2000, v16, pp6913.
[13] Chen, M., Wu, L.M., Zhou, S.X., You, B. Synthesis of Raspberry-like PMMA/SiO2 Nanocomposite Particles via a Surfactant-free Method. *Macromolecules*, 2004, v37, pp9613.
[14] Chen, M., Zhou, S.X., You, B., Wu, L.M. A Novel Preparation Method of Raspberry-like PMMA/SiO2 Hybrid Microspheres. *Macromolecules*, 2005, v38, pp6411.
[15] Luna-Xavier, J., Guyot, A., Bourgeat-Lami, E. Preparation of Nano-sized Silica/Poly(Methyl Methacrylate) Composite Latexes by Heterocoagulation: Comparison of Three Synthetic Routes. *Polymer International*, 2004, v53, pp609-617.
[16] Luna-Xavier, J., Guyot, A., Bourgeat-Lami, E. Synthesis and Characterization of Silica/poly (Methyl Methacrylate) Nanocomposite Latex Particles through Emulsion Polymerization using a Cationic Azo Initiator. *Journal of Colloid and Interface Science*, 2002, v250, pp82-92.
[17] Lapeyre, V., Renaudie, N., Dechezelles, J.F., Saadaour, H., Ravaine, S., Ravaine, V. Multiresponsive Hybrid Microgels and Hollow Capsules with a Layered Structure. *Langmuir*, 2009, v25, pp4659-4667.

[18] Colard, C.A.L., Teixeira, R.F.A., Bon, S.A.F. Unraveling Mechanistic Events in Solids-Stabilized Emulsion Polymerization by Monitoring the Concentration of Nanoparticles in the Water Phase. *Langmuir*, 2010, v26, pp7915-7921.

[19] Wen, N.G., Tang, Q.Q., Chen, M., Wu, L.M. Synthesis of PVAc/SiO2 Latices Stabilized by Silica Nanoparticles. *Journal of Colloid and Interface Science*, 2008, v320, pp152-158.

[20] Xu, P., Wang, H., Tong, R., Du, Q., Zhong, W. Preparation and Morphology of SiO2/PMMA Nanohybrids by Microemulsion Polymerisation. *Colloid and Polymer Science*, 2006, v284, pp755-762.

[21] Chen, Y., Sajjadi, S. Particle Formation and Growth in ab initio Emulsifier-free Emulsion Polymerisation Under Monomer-Starved Conditions. *Polymer*, 2009, v50, pp357-365.

[22] Colver, P.J., Colard, C.A.L., Bon, S.A.F. Multilayered Nanocomposite Polymer Colloids Using Emulsion Polymerization Stabilized by Solid Particles. *Journal of the American Chemistry Society*, 2008, v130, pp16850-16851.

[23] Kolthoff, I.M., Miller, I.K.J. Study of the Thermal Decomposition of Potassium Persulfate by Potentiometry and Capillary Electrophoresis. *Journal of the American Chemistry Society*, 1951, v73, pp3055.

[24] Starr, F.W., Schroder, T.B., Glotzer, S.C. Molecular Dynamics Simulation of a Polymer Melt with a Nanoscopic Particle. *Macromolecules*, 2002, v35, pp4481-4492.

[25] Rittigstein, P., Torkelson, J.M. J. Polymer-Nanoparticle Interfacial Interactions in Polymer Nanocomposites: Confinement Effects on Glass Transition Temperature and Suppression of Physical Aging. *Journal of Polymer Science Part B-Polymer Physics*, 2006, v44, pp2935-3943.

[26] Van Zanten, J.H., Wallace, W.E., Wu, W.L. Effect of Strongly Favorable Substrate Interactions on the Thermal Properties of Ultrathin Polymer Films. *Physical Review E*, 1996, v53, ppR2053-R2056.

[27] Rittigstein, P., Priestley, R.D., Broadbelt, L.J., Torkelson, J.M. Model Polymer Nanocomposites Provide an Understanding of Confinement Effects in Real Nanocomposites. *Nature Materials*, 2007, v6, pp278-282.

[28] Ramanathan, T., Liu, H., Brinson, L.C. Functionalized SWNT/polymer Nanocomposites for Dramatic Property Improvement. *Journal of Polymer Science Part B-Polymer Physics*, 2005, v43, pp2269-2279.

[29] Avella, M., Errico, M.E., Gentile, G. Nylon 6/calcium Carbonate Nanocomposites: Characterization and Properties. *Macromolecular Symposia*, 2006, v234, pp170-175.

[30] Ash, B.J., Schadler, L.S., Siegel, R.W. Glass Transition Behavior of Alumina/polymethylmethacrylate Nanocomposites. *Materials Letters*, 2002, v55, pp83-87.

[31] Tate, R.S., Fryer, D.S., Passqualini, S., Montague, M.F., Pablo, J.J.D., Nealey, P.F. Extraordinary Elevation of the Glass Transition Temperature of Thin Polymer Films Grafted to Silicon Oxide Substrates. *Journal of Chemical Physics*, 2001, v115, pp9982-9990.

[32] Fox, T.G., Loshaek, S. J. Influence of Molecular Weight and Degree of Crosslinking on the Specific Volume and Glass Temperature of Polymers. *Journal of Polymer Science*, 1955, v15, pp371.

[33] Sun, Y., Zhang, Z., Moon, K., Wong, C.P. Glass transition and relaxation behavior of epoxy nanocomposites. *Journal of Polymer Science, Part B-Polymer Physics*, 2004, v42, pp3849-3858.

[34] Sarkar, M.D., Deb, P. Synthesis and Characterization of Hybrid Nanocomposites Comprising Poly(vinyl Alcohol) and Colloidal Silica. *Advances in Polymer Technology*, 2008, v27, pp152-162.

5.2 Synthesis and Characterisation of Thermal-Sensitive SiO_2/polymer Nanocomposite Particles via Semicontinuous Polymerisation

Abstract: Uniform Poly(*n*-isopropylacrylamide)(polyNIPAM)/silica nanocomposite particles have been synthesised via emulsifier-free emulsion polymerisation using semicontinuous approach. The batch process could only produce nanocoposite particles with core-shell morphologies due to rapid rate of growth of polyNIPAM particles, which then acted as core material to attract silica nanoparticles. In both processes, stable nanocomposite particles were only obtained if stable silica nanoparticles were used (basic conditions). Application of silica nonoparticles with intermediate stability (acidic conditions) led to mass coagulation. This was attributed to super high affinity between silica nanoparticles and polyNIPAM, assisted by surface polymerisation of the monomer on silica particles. Furthermore, it was found that the presence of silica nanoparticles can improve the dissolution behaviour of crosslinker-free polyNIPAM particles.

5.2.1 Introduction

Poly(*n*-isopropylacrylamide) (PolyNIPAM) is a thermal-sensitive polymer exhibiting a reversible phase transition behaviour at around 32°C, which makes it a popular material for many applications [1-3].

The main motivation for the design of hybrid materials is the fact that properties of different components can be combined in one material. As a result, the performance of materials, such as mechanical, optic, magnetic or catalytic properties can be modified depending on the nature of the inorganic component used [4-12].

In the previous section (Chapter 5.1), synthesis of raspberry-like nanocomposite particles in the presence of silica nanoparticles was reported. It was found that the morphology of hybrid particles can be varied either by changing the hydrophilicity of monomer or the type of process used. In this work, we examine the interaction of a highly water-soluble monomer, NIPAM, with silica nanoparticles via both batch and semicontinuous processes.

Table 5.2.1. Typical recipes for the polyNIPAM latexes prepared by surfactant-free emulsion polymerisation in the presence of Ludox TM-50 silica nanoparticles. [KPS] = 4 mmol·l_{aq}^{-1}. Water: 450 ml.

Reaction	R_a ($gmin^{-1}l_{aq}^{-1}$)	[M] (wt%)	NIPAM/silica (g/g)	T (°C)	[KPS] ($mmol \cdot l_{aq}^{-1}$)
Batch		3	1:1	60	4
Batch		3	1:3	60	4
Batch		2	1:1	60	4
Batch		2	1:3	60	4
Semi	0.18	3	1:1	60	4
Semi	0.18	3	1:3	60	4

5.2.2 Experimental Work

The procedure and measurements have been given in the previous subchapter (see Chapter 5.1, page 154). Conversion, z-average diameters (D_z), and the morphology of the nanocomposite particles have been measured and characterized. The volume-average diameter and number of particles have been calculated.

5.2.3 Crosslinker-free polyNIPAM/SiO_2 hybrid particles

5.2.3.1 Primary Experiments

Surfactant-free emulsion polymerisation of NIPAM in the presence of silica nanoparticles, with recipes specified in Table 5.2.1, was studied. Several preliminary experiments were conducted before a workable polymerisation condition was found.

Initially, the same recipe used for producing PMMA/SiO_2 and PVA/SiO_2 nanocomposite particles, which involved 10wt% monomer concentration and 2 $mmol \cdot l_{aq}^{-1}$ KPS in the presence of silica nanoparticles (NIPAM/silica(g/g) = 1:1) under acidic conditions (pH = 5.0±0.5), was utilised. However, the batch polymerisation was interrupted by a severe coagulation of particles early in the reaction. Based on the conclusion drawn from the work reported in Chapter 4.1, monomer concentration was decreased to 3wt%, in order to reduce the rate of particle growth. Unexpectedly, the problem was not resolved as significant gel-like precipitation was still observed as soon as polymerisation started. Interestingly, the resulting gel was insoluble in water below LCST even in the absence of crosslinker.

In order to further study the interaction between polymer and silica nanoparticles under acidic conditions, the reaction was carried out using a lower monomer concentration via semicontinuous process. The reactor was initially charged with 1wt% silica nanoparticles at pH = 5.0±0.5. The feeding rate of NIPAM monomer was set at a relatively low value (0.06 $g \cdot min^{-1} \cdot l_{aq}^{-1}$) in order to be able to control the rate of polymerisation. The results are shown in Figure 5.2.1. The results show a gradual coagulation in the course of polymerisation. Silica nanoparticles are less stable and tend toward increased coagulation under acidic conditions (see Chapter 5.1). Moreover, since NIPAM is highly water-soluble, surface polymerisation on the silica nanoparticles could be significant. This can promote hetero-coagulation between polymer and silica particles. Similar to batch process, the resulting gels from senicontinuous process were insoluble in water below LCST. The instantaneous conversion data were all above 100% (Figure 5.2.1a), which indicate the presence of water trapped in the samples, which could not be removed during drying. This again proves the formation of crosslinked gels in the course of polymerisation [13].

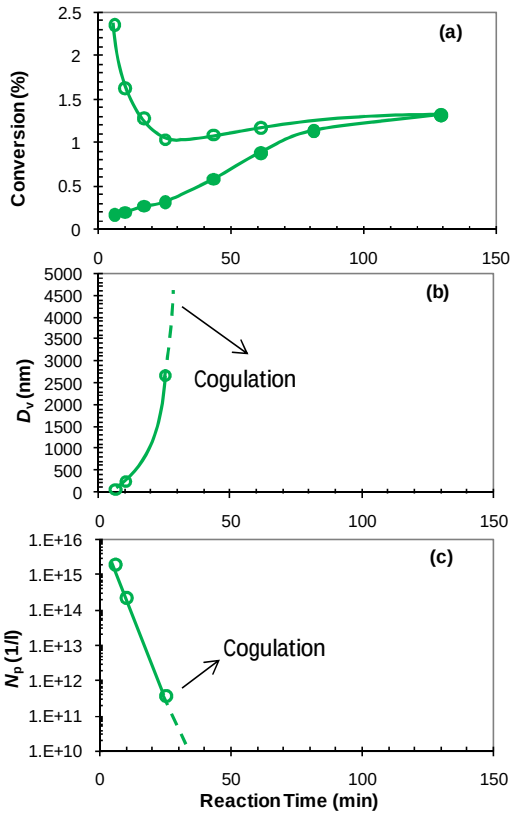

Figure 5.2.1. (a) Conversions, (b) volume average diameter of particles and (c) number of particles produced versus reaction time for semicontinuous process. Water: 450 ml; [NIPAM] = 0.5wt%; T = 60°C, [KPS] = 2 mmol·l_{aq}^{-1}. pH = 5.0±0.5; R_a = 0.06 g·min^{-1}·l_{aq}^{-1}.

To further improve the colloidal stability of the system, the reaction was conducted under basic conditions (pH = 9.8±0.2), under which the zeta potential of silica nanoparticles is as high as -52 mv. This implies good electrostatic stability of silica nanoparticles against homo and hetero-coagulation. This appeared to be a workable recipe to produce stable composite particles. The concentration of KPS was also increased from 2 mmol·l_{aq}^{-1} to 4 mmol·l_{aq}^{-1} in order to provide more anionic sulfate groups and therefore enhance the stability of polymer particles. This formulation turned out to be successful, as reported in the succeeding sections.

Before proceeding to the result section, it is worth mentioning the effect of pH on water solubility of NIPAM, which was studied and reported in Appendix G. The results indicate a decrease in water solubility of NIPAM with increasing pH. However, one thing should be noticed is that the maximum concentration of NIPAM used in this work is 3wt%, which is much lower than its water solubility (~20wt%) at pH = 7.0. Therefore, the effect of pH on the monomer concentration in the water phase in the course of polymerisation can be ignored.

Effect of silica nanoparticle concentration on rate of reaction, particle size and size distributions

Batch Polymerisation

The batch polymerisation of NIPAM in the presence of silica nanoparticles was conducted using different concentrations of monomer and silica nanoparticles. Batch polymerisations using 3wt% NIPAM were firstly carried out. Different concentrations of silica latex were used in terms of weight ratio of NIPAM/SiO_2, as 1:0, 1:1, and 1:3.

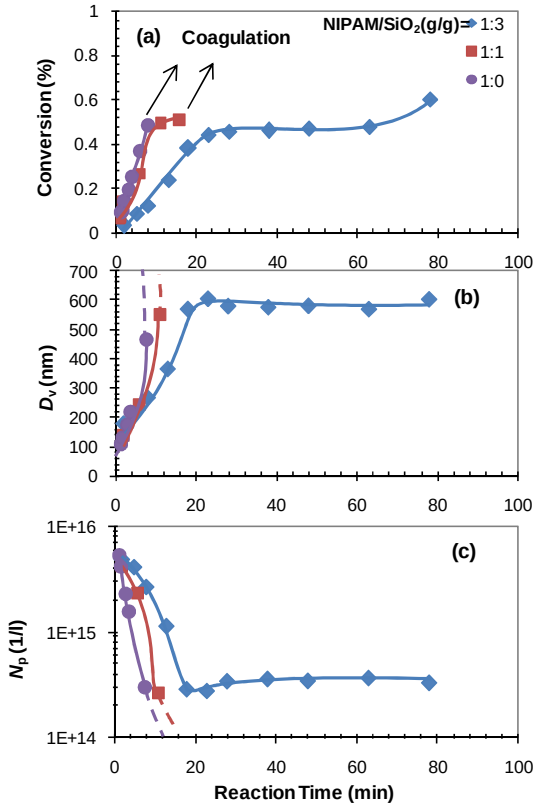

Figure 5.2.2. (a) Conversions, (b) volume-average size of particles and (c) number of particles produced versus reaction time for batch reactions with different concentrations of silica latex. Water: 450 ml; [NIPAM] = 3wt%; T = 60°C, [KPS] = 4 mmol·l_{aq}^{-1}.

Severe coagulation occurred during the early stage of polymerisation (x < 50%) for most of polymerisations except for the one with the highest concentration of silica nanoparticles (1:3). The rate of polymerisation decreases in the presence of silica nanoparticles and the decrease in the rate becomes more significant with increasing amount of silica latex. This feature is due to the effect of pH, which increased from 5.4±0.5 for silica-free (NIPAM/SiO_2=1/0) system to 9.8±0.2 when silica nanoparticles were added. The same observation was found and explained in the previous section (see Chapter 5.1; 5.1.3.3) for VA/SiO_2 system, which is due to the suppressed rate of thermal decomposition of potassium persulfate under basic conditions.

The results indicate that the presence of silica nanoparticles improved the colloidal stability of the system and stable latexes were obtained, as shown in Figure 5.2.2b and c.

In order to be able to study and compare the properties of final products under different conditions, highly stable latexes are desired. Therefore, the concentration of NIPAM monomer was decreased to 2wt% and results are shown in Figure 5.2.3.

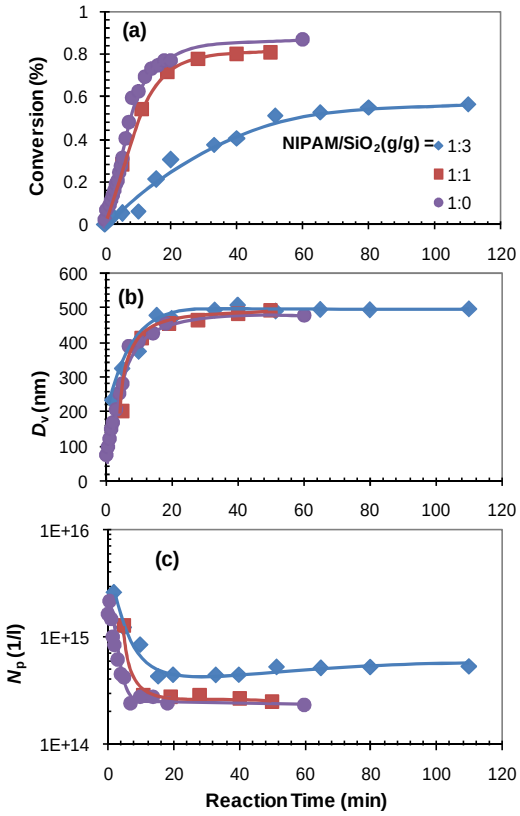

Figure 5.2.3. (a) Conversions, (b) volume-average size of particles and (c) number of particles produced versus reaction time for batch process with different NIPAM/SiO_2 ratios. [KPS] = 4 mmol·l_{aq}^{-1}; water: 450 ml; [NIPAM] = 2wt%; T = 60°C.

Similar to the observation from Figure 5.2.2, the rate of polymerisation as well as the final conversions decreased in the presence of silica nanoparticles at basic conditions (pH = 9.8±0.2), as shown in Figure 5.2.3a. The size of composite particles produced was not sensitive to the presence of silica nanoparticles (Figure 5.2.3c). One may notice that although less polymer was formed in the presence of silica nanoparticles (1:3), however, particles richer in silica were produced (Figure 5.2.3b) suggesting a significant interaction between polymer and silica particles at NIPAM/SiO_2 = 1/3.

The PSDs evolution with conversion for the silica-polymer composite particles with different NIPAM/SiO_2 ratios and NIPAM monomer concentrations are shown in Figure 5.2.4. The PSD at x=0% represents the distribution of silica nanoparticles.

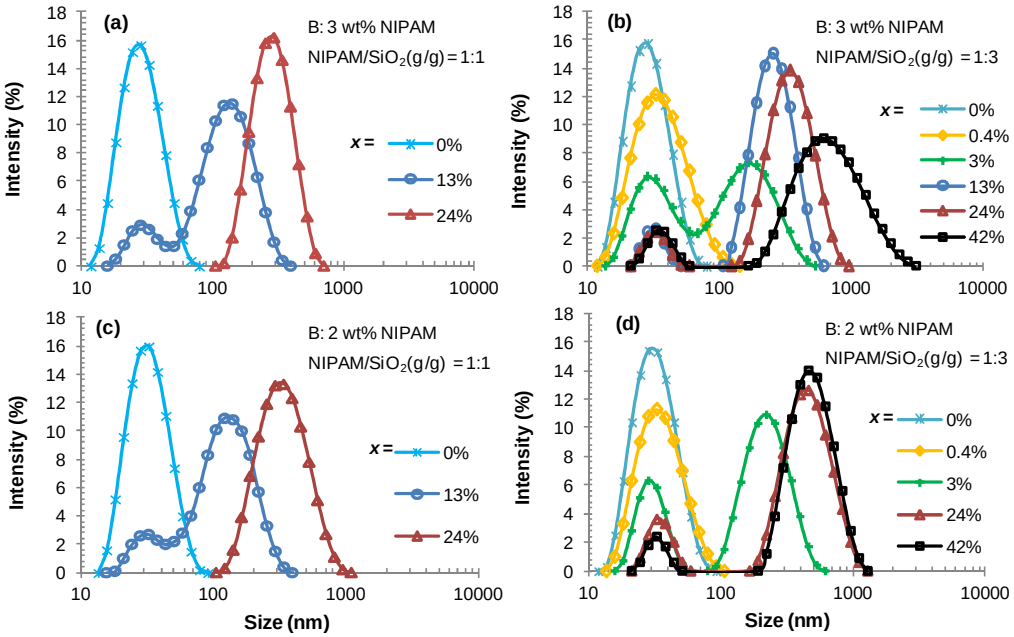

Figure 5.2.4. Evolution of PSD during batch polymerisations with different concentration of NIPAM monomer and silica nanoparticles (a) 3wt% NIPAM, NIPAM/SiO_2 = 1:1; (b) 3wt% NIPAM, NIPAM/SiO_2 = 1:3; (c) 2wt% NIPAM, NIPAM/SiO_2 = 1:1; (d) 2wt% NIPAM, NIPAM/SiO_2 = 1:3.

It can be seen that the peak representing silica nanoparticles shrinks during polymerisation for all reactions. The PSD transformed from bimodal to unimodal rather in the early stage of reaction (x = 24%) in the presence of a low concentration of silica nanoparticles (Figure 5.2.4a and c). By contrast, bimodal PSDs are observed from the beginning to the end of reactions when a higher concentration of silica nanoparticles was applied (Figure 5.2.4b and d), which indicates that an excessive amount of silica nanoparticles was present in the system. Note that the median size of the peak at the higher size range was used as the size of nanocomposite particles. Similar to previous work (see Chapter 5.1, Equations 5.1.4 and 5.1.5), the weight of the incorporated silica particles was estimated by the intensity fraction of free silica nanoparticles. Corrections have been made for N_p in order to eliminate the effect of free silica nanoparticles in the system on the size.

The important finding is that silica nanoparticles are quickly attached to the growing polymer particles while they are highly charged under reaction conditions (pH = 9.8±0.2). This suggests that a second mechanism such as surface polymerisation of NIPAM, which covers the surface of silica nanparticles with polyNIAPM and promotes the adhesion of silica nanoparticles to polymer particles, should be in place. This idea can be further confirmed by the slight broadening of PSDs in the very early stage of reaction (x = 0.4%), as shown in Figure 5.2.4b and d. This broadening suggests that silica nanoparticles undergo coagulation as soon as polymer is formed.

Semicontinuous Polymerisation

For the semicontinuous process, 3wt% of NIPAM and different silica concentrations were used. The rate of monomer addition was controlled at 0.18±0.03 $g \cdot min^{-1} \cdot l_{aq}^{-1}$ for NIPAM/SiO_2 ratios of 1:0, 1:1 and 1:3.

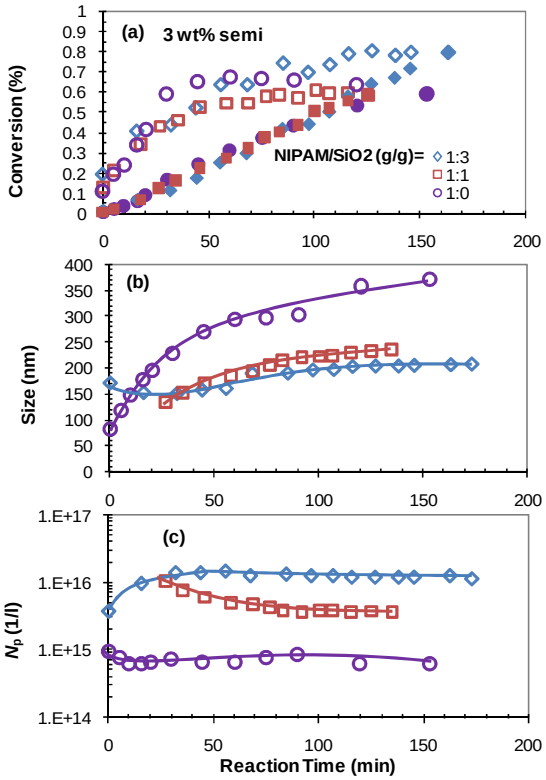

Figure 5.2.5. (a) Conversions, (b) volume-average size of particles, and (c) number of particles produced versus reaction time for semicontinuous reactions in the presence of different concentrations of silica nanoparticles. [KPS] = 4 $mmol \cdot l_{aq}^{-1}$; water: 450 ml; NIPAM: 3wt%; T = 60°C. R_a = 0.18±0.03 $g \cdot min^{-1} \cdot l_{aq}^{-1}$.

Figure 5.2.5 shows that the overall rate of polymerisation is not much sensitive to the presence of silica nanoparticles. This indicates the rate of polymerisation is controlled by the rate of monomer addition. Interestingly, and different from the batch process, the presence of silica nanoparticles decreased the size of nanocomposite particles significantly, as shown in Figure 5.2.5b. As a result, more particles were produced with increasing silica concentration (Figure 5.2.5c). The PSDs evolution with overall conversion in the presence of different concentrations of silica nanoparticles are shown in Figure 5.2.6.

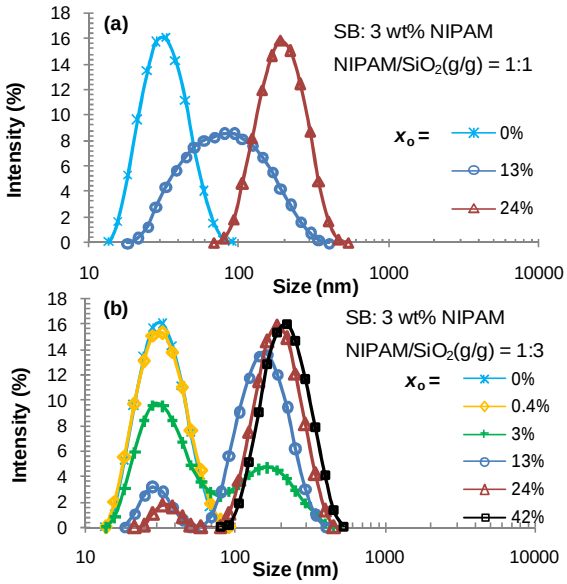

Figure 5.2.6. Evolution of PSD with overall conversion during semicontinuous polymerisation of 3wt% NIPAM in the presence of different concentrations of silica nanoparticles (a) NIPAM/SiO_2 = 1:1; (b) NIPAM/SiO_2 = 1:3, the same reaction as shown in Figure 5.2.5.

Comparing with batch processes (Figure 5.2.4a-b), the peak representing silica nanoparticles shrinks more slowly in the course of polymerisation for both concentrations of silica nanoparticles. It indicates that in the semicontinuous process silica nanoparticles were gradually attached to the growing particles due to the limited rate of surface expansion of latter particles, comparing with that in the batch process. Moreover, it is found that even at high concentration of silica nanoparticles, the PSDs eventually transformed to unimodal distribution after conversion of 42%, unlike batch process in which they always remained binary, as shown in Figure 5.2.4b. This suggests an improved usage of silica nanoparticles in the semicontinuous process.

5.2.3.2 Thermal behaviour

The phase transition behaviour of selected samples has been studied by DLS and UV spectrometer. The samples for size measurements were diluted with de-ionized water and kept at 60ºC in the water bath. The measurements were started from 60ºC as the temperature was gradually decreased to 20ºC at a constant rate of 1ºC·min^{-1}. The samples for UV measurements were directly taken from the latexes in the reactor. The turbidity of the samples was measured as a function of temperature at a wavelength of 600 nm as they were gradually cooled down from 50°C by heat transfer to surroundings (2°C·min^{-1} until 31°C and 1°C·min^{-1} until 20°C).

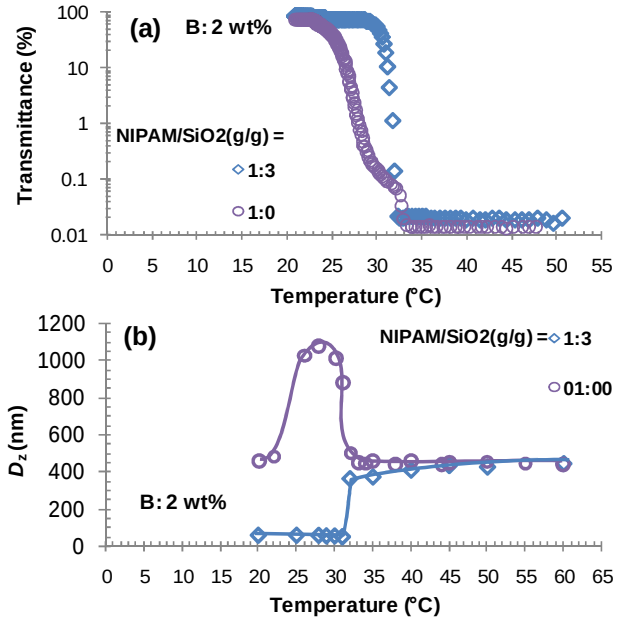

Figure 5.2.7. The evolution of (a) transmittance and (b) z-average size of particles with temperature of final products from batch process using 2wt% NIPAM with different concentration of silica latex.

It has been found that polyNIPAM chains produced by batch process are partly insoluble below LCST even in the absence of crosslinker (see Chapter 4.1). Neat polyNIPAM particles underwent significant swelling during the phase transition of polymer chains (Figure 5.2.7b). Interestingly, for composite particles produced by batch process, the rate of phase transition as well as the final turbidity increased (from 69% to 83%), and swelling did not occur during phase transition stage, as shown in Figure 5.2.7. LCST did not vary in the presence of silica nanopartilces, as shown in Figure 5.2.8. One may argue that the drop in average size during phase transition stage may be due to the release of silica nanoparticles from composite particles, which can cause particle size to be significantly underestimated. This could also be one of the reasons for not being able to detect swelling, as seen in Figure 5.2.7b. However, the turbidity measurement (Figure 5.2.7a) strongly supports the point that the dissolution behaviour of cross-linker free polyNIPAM was improved with the help of silica nanoparticles.

This interesting phenomenon has not been reported in the literature before. We think that this may be due the interaction between silica particles and polymer chains, which could hinder the chain entanglements within the particle. Such an interaction has been observed for water soluble monomer, VA (see Chapter 5.1).

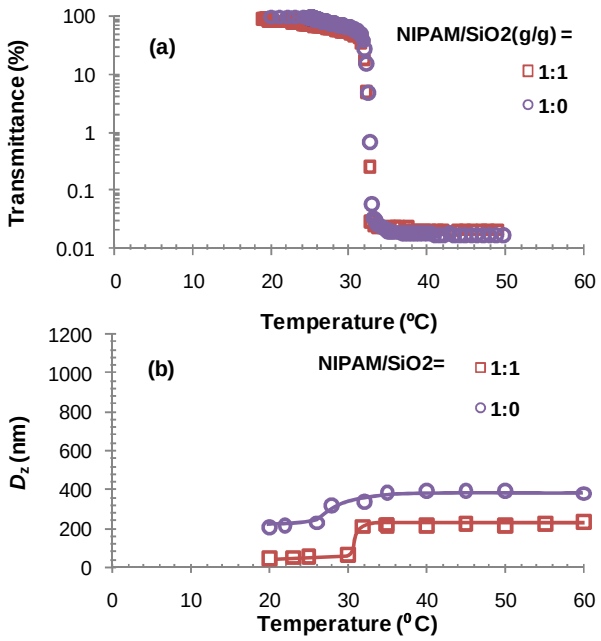

Figure 5.2.8. Particle size and transmittance versus temperature for final products via semicontinuous process with 3wt% NIPAM. [KPS] = 4 mmol·l_{aq}^{-1}; water: 450 ml; NIPAM/SiO2 = 1:1; T = 60°C.

Figure 5.2.8 shows the thermal-responsive behaviour of the product with 3wt% NIPAM via semicontinuous process. Comparing with neat polyNIPAM nanoparticles, the phase transition behaviour did not vary significantly when silica nanoparticles were used. The particles did shrink right after LCST without going through temporary swelling. Note that semicontinuous polymerisation of NIPAM could also produce such thermal behaviours (see Chapter 4.2 and 4.3). The slight drop in final transmittance (from 98% to 86%) is probably due to the presence of silica nanoparticles in the final polymer solution. The results also show that the LCST is not sensitive to the presence of silica particles.

Similar to Figure 5.2.7, the slight decrease in particle size may be due to the effect of released silica nanoparticles below LCST on the average size.

5.2.3.3 Adsorption test

Very good affinity between polyNIPAM and silica has been found in the experiments. Based on the point proposed in the previous chapter (see Chapter 5.1), such affinity is facilitated by polymerisation on the surface of hydrophilic silica nanoparticles. One may argue that the adhesion between silica and polymer particles is strong enough to guarantee formation of composite particles. In order to verify this, proper experiments were designed. Crosslinker-free polyNIPAM particles were produced via batch process using 1wt% NIPAM. The resulting latex was incubated at 80°C for 24h to decompose the remaining KPS ($t_{1/2} \approx$ 2h, 80°C) in the reactor. Adsorption tests were carried out by adding 1wt% silica nanoparticles to the polymer latex at both basic conditions (pH = 9.8) and acidic conditions (pH = 5.0) at reaction temperature (60°C) under continuously stirring. The evolution of PSD was monitored by DLS and shown below.

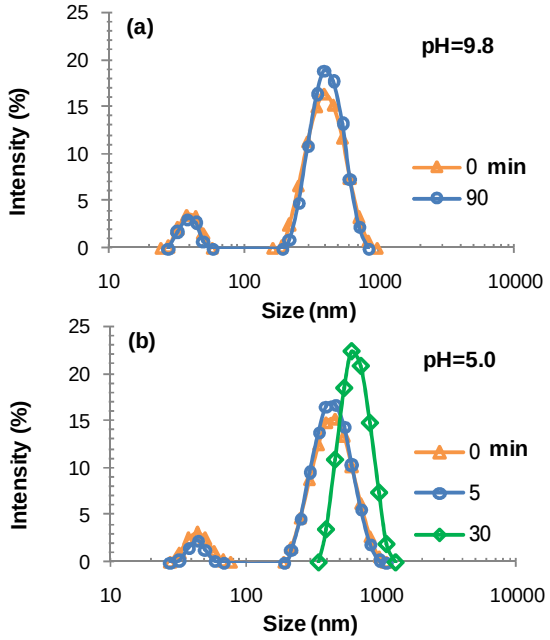

Figure 5.2.9. Incubation time evolution of PSD of 1wt% polyNIPAM particles in the presence of 1wt% silica nanoparticles under (a) basic conditions, pH = 9.8; (b) acidic conditions, pH = 5.0.

The peaks within the small size range (10-100 nm) and large size range (100-1000 nm) represent free silica nanoparticles and polymer (composite) particles, respectively. It is seen that the intensity of peak for free silica nanoparticles decreases with stirring time.

Under basic conditions, as shown in Figure 5.2.9a, only a small amount of silica nanoparticles had been adsorbed by polyNIPAM particles after 90 min of stirring. By contrast, the PSD transformed from bimodal to unimodal and shifted to larger size range after 30 min of stirring under acidic conditions (Figure 5.2.9b), which indicates strong adsorption of silica nanoparticles. The TEM images, as shown in Figure 5.2.10, also support these points.

Therefore strong adsorption of silica nanoparticles onto polyNIPAM particles at basic pH and under polymerisation conditions can only be attributed to surface polymerisation. The results clearly suggest that surface polymerisation can reconcile highly charged and stable nanoparticles with polymer particles. The electrostatic repulsion between charged silica particles and growing polymer particles would not allow these particles to attach to polymer colloids and merge. Therefore, polymerisation on the surface of charged silica nanoparticles is a prerequisite for the interaction between silica and polymer particles in order to produce hybrid particles, as shown in Figures 5.2.4 and 5.2.6.

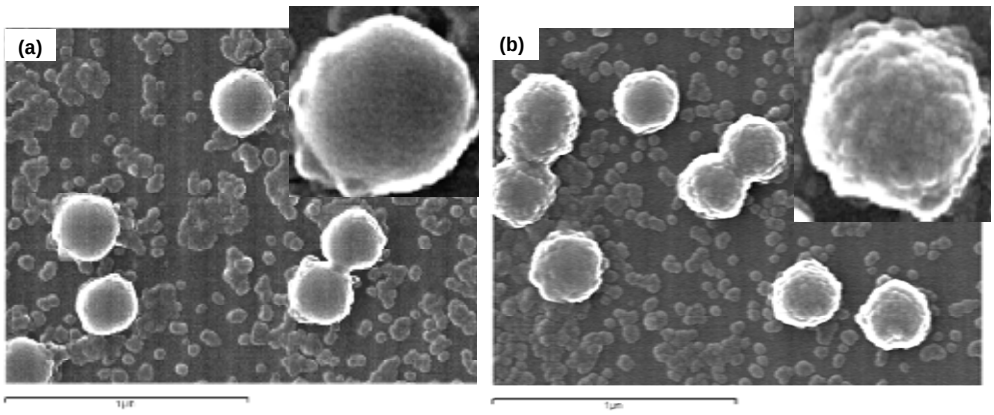

Figure 5.2.10. SEM images of samples obtained after 30min of stirring under (a-b) basic conditions, pH = 9.8; and (c-d) acidic conditions, pH = 5.0. Bar: 1000nm.

5.2.3.4 Morphology of composite particles

Figure 5.2.11 shows SEM images of crosslinker-free nanocomposite particles produced via both batch and semicontinous processes with different monomer concentrations. Hardly any particle can be identified from these images.

Phase study suggests that these particles are water-soluble below LCST (Figures 5.2.7 and 5.2.8). Even if sampling is carried out at a temperature above LCST, polyNIPAM chains are so soft (have a very low T_g) that they would likely undergo coalescence and form film during sample preparation.

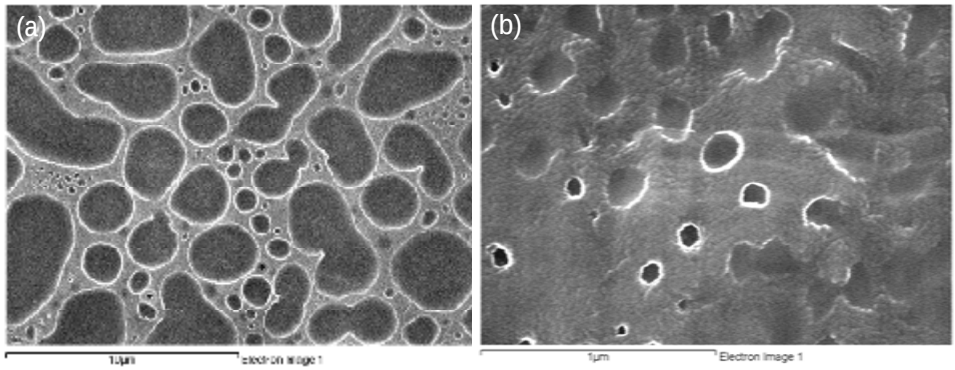

Figure 5.2.11. SEM images of samples produced with (a) 2wt% NIPAM via batch process, bar: 10 µm and (b) 3wt% NIPAM via semicontinuous process, bar: 1 µm. [KPS] = 4 mmol·l_{aq}^{-1}; water: 450 ml; T = 60°C.

5.2.4 PolyNIPAM/SiO_2 hybrid microgels

5.2.4.1 Synthesis of hybrid microgels

In order to produce insoluble polyNIPAM/silica hybrid microgels, MBA was used as crosslinker to obtain more rigid particles. The use of cross-linker is not expected to affect the surface affinity of particles significantly, but makes it possible to observe and analyse silica-polymer interactions.

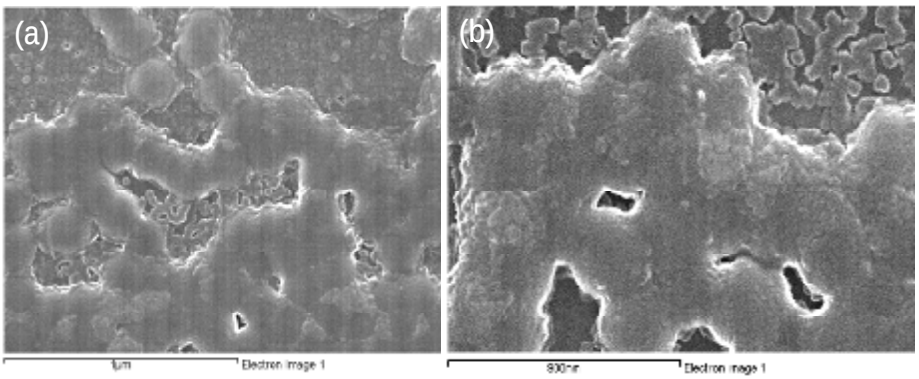

Figure 5.2.12. SEM images of samples produced with (a) 2wt% NIPAM via batch process, bar: 1000 nm and (b) 3wt% NIPAM via semicontinuous process, bar: 900 nm. [KPS] = 4 mmol·l_{aq}^{-1}; water: 450 ml; T = 60°C, NIPAM/silica(g/g) = 1:1; MBA/NIPAM(g/g) = 1:50; pH = 9.8±0.2.

Initially, 2wt% of MBA based on the weight of NIPAM was used. The SEM image shown in Figure 5.2.12 indicates that particles were still not fully crosslinked. For this reason, the concentration of MBA was then raised to 10wt%. Reactions with 3wt% and 1wt% NIPAM monomer concentrations were carried out via both batch and semicontinuous processes, as shown in Figure 5.2.13 and 5.2.14.

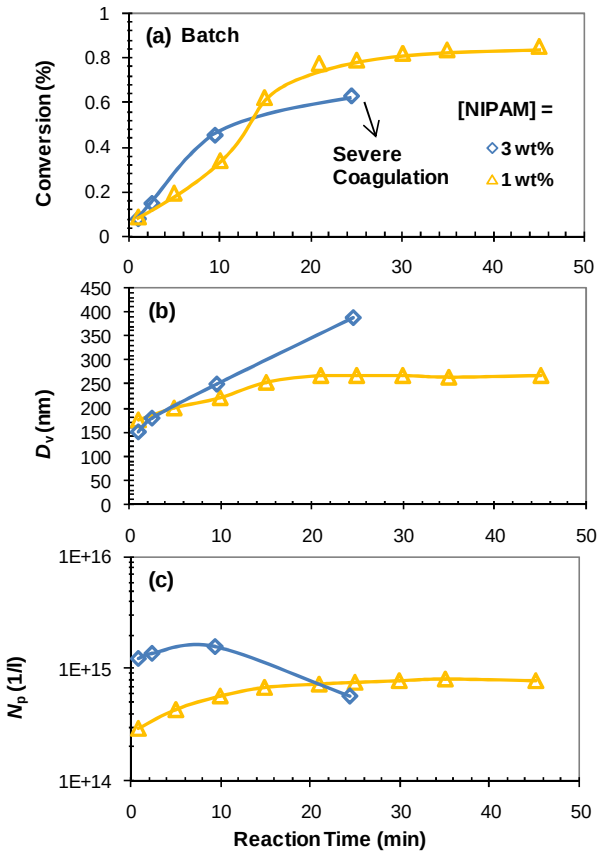

Figure 5.2.13. (a) Conversion, (b) volume average size of particles and (c) number of particles produced versus reaction time for batch reactions with different concentrations of NIPAM monomer. [KPS] = 4 mmol·l_{aq}^{-1}; water: 450 ml; NIPAM/silica(g/g) = 1:1; MBA/NIPAM(g/g) = 1:10; T = 60°C. pH = 9.8±0.2.

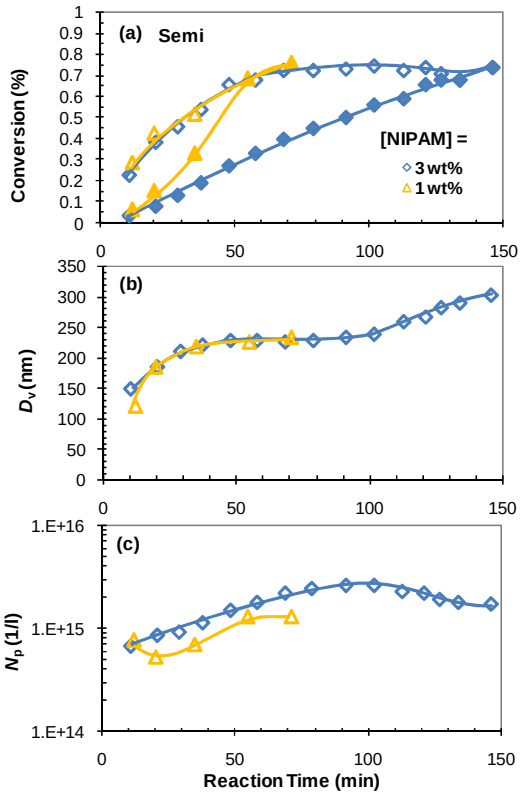

Figure 5.2.14. (a) Conversions, (b) volume-average size of particles and (c) number of particles produced versus reaction time for semicontinuous reactions with different concentrations of NIPAM monomer. [KPS] = 4 mmol·l_{aq}^{-1}; water: 450 ml; NIPAM/silica(g/g) = 1:1; MBA/NIPAM(g/g) = 1:10; T = 60°C; pH = 9.8±0.2; R_a = 0.18±0.03 g·min^{-1}·l_{aq}^{-1}.

5.2.4.2 Morphology of hybrid microgels

As shown in Figure 5.2.13, the batch reaction with 3 wt% NIPAM monomer concentration was interrupted in the early stage by severe coagulation. The samples produced with 1 wt% NIPAM via batch process, 1 wt% and 3 wt% NIPAM via semcontinuous process, were used for the further investigations.

Figure 5.2.15 shows the morphology of hybrid microgels produced with 10wt% MBA under SEM. The outline of silica particles can be found from the surface of the particles, which indicates a good adherence of silica nanoparticles onto polyNIPAM ones.

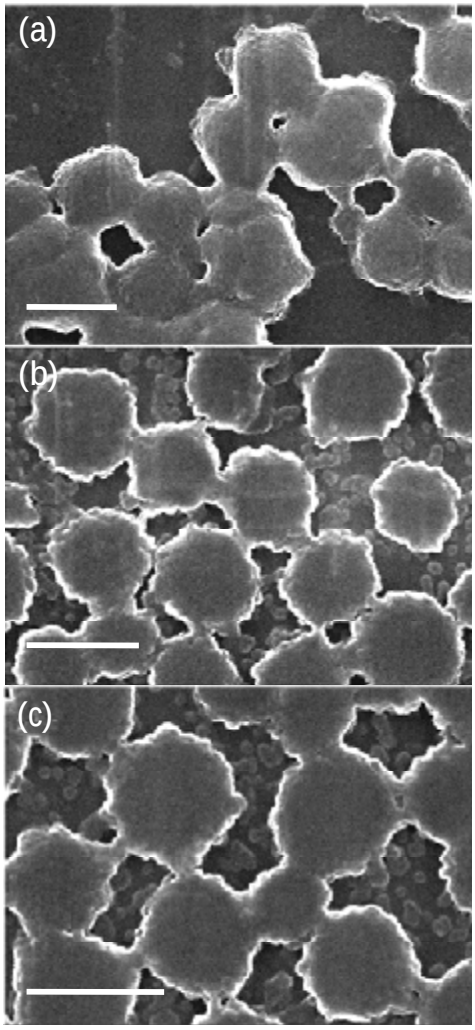

Figure 5.2.15. SEM images of microgels produced with (a) 1wt% NIPAM via batch process, bar: 250 nm; (b) 1wt% NIPAM semicontinuous process, bar: 250 nm; and (c) 3wt% NIPAM semicontinuous process, bar: 250 nm. [KPS] = 4 mmol·l_{aq}^{-1}; water: 450 ml; T = 60°C, NIPAM/silica(g/g) = 1:1; MBA/NIPAM(g/g) = 1:10; pH = 9.8±0.2.

Samples were also investigated under TEM. As shown in Figure 5.2.16, good adherence between silica nanoparticles and crosslinked polyNIPAM can be found out from all of the images. For batch process, silica nanoparticles were more packed on the surface of microgels, leading to core-shell structures. For semicontinuous process, the microgels were filled with silica nanoparticles. The results indicate that different morphologies and structures of nanocomposite particles can be obtained by different processes of polymerisation.

The interesting finding from the images, consistent with the conclusion from SEM images, is that silica naoparticles incorporated into polymer particles are very finely distributed on the surface and within the polymer particles without any obvious flocculation, especially for the semicontinuous process This is because of stability of particles at pH = 9.8 which makes them stable against flocculation. On the other hand, due to the high water solubility of NIPAM monomer, the surface polymerisation on the silica nanoparticles may occur so fast that they are quickly covered by polyNIPAM chains and form tiny core-shell silica-polymer nanocomposites,

which are very unstable due to lack of electrostatic stability and large surface energy. Therefore, they coagulate with each other and form larger nanocomposite particles, as shown in Figure 5.2.18. For batch process, the monomer concentration in the water phase is high, which can enhance homogeneous nucleation of neat polyNIPAM primary particles, followed by their heterocoagulation with silica nanoparticles. In this case, it is more likely to have core-shell structures of nanocomposites due to the rapid growth of particles. Comparing with batch process, the rate of polymerisation as well as particle growth are controlled by semicontinuous process. Composite particles continuously grow in the course of polymerisation via both homo and hetero-coagulation between silica and polymer particles, resulting finely distributed structures.

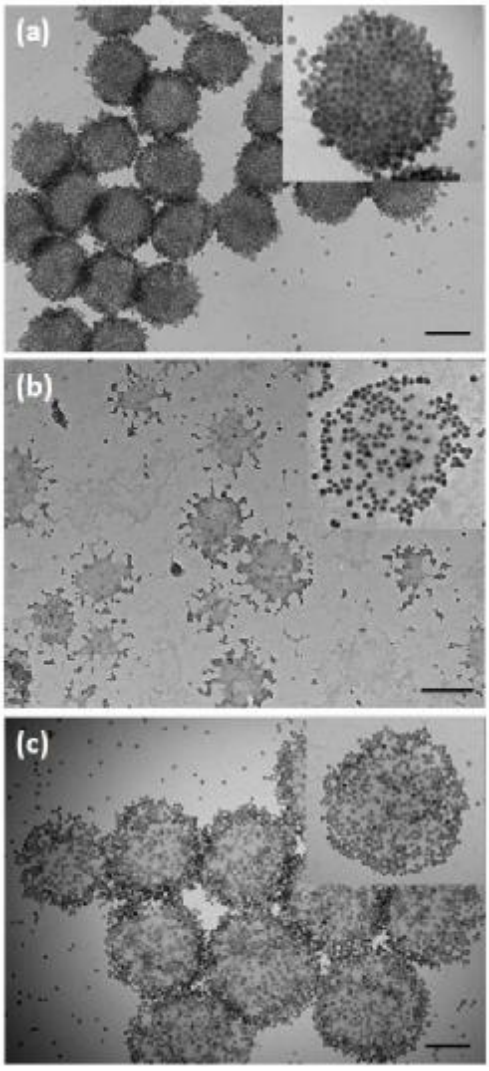

Figure 5.2.16. TEM images of polyNIPAM/SiO_2 nanocomposite particles produced via (a) 1wt% batch process and (b) 1wt% semicontinuous process. (c) 3wt% semicontinuous process, Bar: 100 nm. [KPS] = 4 mmol·l_{aq}^{-1}; water: 450 ml; T = 60°C, NIPAM/silica(g/g) = 1:1; MBA/NIPAM(g/g) = 1:10.

5.2.5 Conclusions

In this work, uniform polyNIPAM/SiO_2 hybrid particles were produced via surfactant-free emulsion polymerisation using both batch and semicontinuous approaches. Very good affinity between silica and polyNIPAM was found, which is attributed to the high water-solubility of NIPAM and polymerisation on the surface of hydrophilic silica nanoparticles. This is consistent with the conclusion obtained from previous work (see Chapter 5.1).

Interestingly, at pH = 5.0, where the silica particles were slightly unstable, agglomeration of polymer particles with silica particles was significant resulting insoluble gels in the absence of crosslinker.

At pH = 9.8, where silica particles were quite stable, uniform silica armored polyNIPAM particles were obtained via both processes. Since silica nanoparticles are quite stable under basic conditions, they could not be involved in reaction before their surface was sufficiently masked by polymer layers.

The presence of silica particles depressed the rate of polymerisation for the batch process, but had no significant effect on that for the semicontinuous process. Interestingly, the dissolution behaviour of resulting crosslinker-free hybrid particles was improved, comparing with neat polymer particles.

PolyNIPAM/silica hybrid microgels have also been produced. SEM and TEM show different morphologies for hybrid microgels were produced via different processes. Core-shell structures were obtained via batch process, while more homogenous structures were obtained via semicontinuous process.

5.2.6 Reference

[1] Chapter 4.1: Synthesis of Thermo-responsive Water-Soluble Poly(n-isopropylacrylamide) Colloids
[2] Chapter 4.2: Fast Dissolving PolyNIPAM Nanoparticles via Semicontinuous Emulsion Polymerisation
[3] Chapter 4.3: A Novel Method for Preparation of Thermosensitive Nanocapsules by Semicontinuous Emulsion Polymerisation
[4]Zhu, Y., Ni, C.H., Shao, D., Jiang, X. The preparation of Composites of Poly(N-isopropylacrylamide) with Silica and Its Application in HPLC for Separating Naphthalene Derivatives. *Polymer Composites*, 2008, v29, pp 415-420.
[5]Alvarez-Puebla, R.A., Contreras-Caceres, R., Contreras-Caceres, R., Pastoriza-Santos, I., Perez-Juste, J., Liz-Marzan, L.M. Au-PNIPAM Colloids as Molecular Traps for Surface-enhanced, Spectroscopic, Ultra-sensitive Analysis. *Angewandte Chemie International Edition*, 2009, v48, pp138-143.
[6] Pich, A., Karak, A., Lu, Y., Ghosh, A.K., Adler, H-J.P. Preparation of Hybrid Microgels Functionalized by Silver Nanoparticles. *Macromolecular Rapid Communications*, 2006, v27, pp344-350.
[7] Zhu, Y., Ni, C.H., Shao, D., Jiang, X. The preparation of Composites of Poly(N-isopropylacrylamide) with Silica and Its Application in HPLC for Separating Naphthalene Derivatives. *Polymer Composites*, 2008, v29, pp415-420.
[8] Duan, L. Chen, M., Zhou, S., Wu, L. Synthesis and Characterization of Poly(N-isopropylacrylamide)/silica Composite Microspheres via Inverse Pickering Suspension Polymerisation. *Langmuir*, 2009, v25, pp3467-3472.
[9] Chai, S., Zhang, J., Yang, T., Yuan, J., Cheng, S. Thermoreponsive Microgel Decorated with Silica Nanoparticles in Shell: Biomimetic Synthesis and Drug Release Applciation. *Colloids and Surfaces A: Physicochemical and Engineering Aspects*, 2010, v356, pp32-39.
[10] Yang, J., Hu, D., Fang, Y., Bai, C., Wang, H. New Method for Preparation of Structural Microspheres Poly(n-isopropylacrylamide-co-acrylic acid)/SiO2. *Chemistry of Materials*, 2006, v18, pp4902-4907.
[11] Hatto, N., Cosgrove, T., Snowden, M.J. Novel Microgel-Particle Colloids: The Detailed Characterization of the Layer Structure and Chain Topology of Silica: Poly(NIPAM) core-shell particles. *Polymer*, 2000, v41, pp 7133-7137,
[12] Cao, Z., Du, B., Chen, T., Nie, J., Xu, J., Fan, Z. Preparation and Properties of Thermo-sensitive Organic/Inorganic Hybrid Microgels. *Langmuir*, 2008, v24, pp12771-12778.
[13] Rasmusson, M., Vincent, B. Flocculation of Microgel Particles. *Frontiers of Polymer Colloids*, 2004, v58, pp203-211.

Chapter 6 Conclusions and Recommendations for Future Work

This chapter is subdivided into three sub-sections. The objectives and research tasks carried out are summarised in the first section. In the second section, the main findings of the research are highlighted. Finally, in the third section, recommendations are made for future research.

6.1 The Present Study

The major aim of the research presented in this thesis is to investigate the kinetics and particle formation in semicontinuous emulsion polymerisation for a better understanding as well as explore potentials of this process in order to produce advanced materials.

Semicontinuous microemulsion polymerisation of styrene during particle nucleation stage has been investigated and reported in Chapter 3. The effects of process parameters, such as rate of monomer addition (R_a) and surfactant concentration ([S]) have been studied. Later, reactions under extreme conditions, such as high [S], low R_a and high reaction temperature, have been carried out to explore the minimum size of particles achievable. A water-soluble chain transfer agent (CTA), 2-Butanethiol, has been used as an alternative way to reduce the particle size by hindering the particle growth.

Thermo-responsive and water-soluble poly(*n*-isopropylacrylamide) (polyNIPAM) colloids have been synthesised and reported in Chapter 4. The effects of monomer concentration on the kinetics of polymerisation and properties of the polymer particles produced have been studied. The dissolution behaviour of crosslinker-free polyNIPAM has been further investigated via semicontinuous approaches. The results clearly unravel a novel way of making fast-dissolving temperature-sensitive colloids, which has then been used to fabricate thermally-responsive nanocapsules.

Polymer/silica hybrid particles have been studied and reported in Chapter 5. Rasperberry-like nanocomposite particles have been produced by surfactant-free emulsion polymerisation via both batch and semicontinuous processes in the presence of silica nanoparticles. Consistent with the literature, it has been found that the hydrophilicity of monomer is the key factor for the adhesion between polymer and silica. However, new results and concepts are presented in order

to explain variations in particle morphology with polymerisation conditions and properties of silica nanoparticle.

6.2 Main Findings

6.2.1 Microemulsion Polymerisation of Styrene

- In all research works on semicontinuous microemulsion polymerisation reported in the literature, experimental data are from the runs which either ended with incomplete initiation of free emulsifier micelles or underwent particle growth during post nucleation so that the true features of polymerisation cannot be exploited. In this work, the mechanistic information on particle formation was obtained by decoupling particle nucleation stage from particle growth via close monitoring of the end of nucleation. It was found particle nucleation period can be prolonged by either decreasing rate of monomer addition (R_a) or increasing surfactant concentration [S]. As a result, more particles can be produced.

- Except for one or two contributions, the whole bulk of literature on semicontinuous microemulsion polymerisation is experimental with surprisingly no or little attempt to justify the results against theoretical predictions. In this contribution, a major step was taken forward to reconcile experiments with theory. The exponent dependence of the number of particles produced in terms of R_a and [S] was found to approach those theoretically predicted, -2/3 and 1.0, respectively. The results indicate that the average size of particles as well as the particle size distribution (PSD) at the end of nucleation is almost independent of [S] for low R_a. Furthermore, PSDs at the end of nucleation narrowed with decreasing R_a. This is in contrast with the early literature which indicates particle nucleation under monomer-starved conditions will lead to the formation of polymer latexes with broad size distributions, but is consistent with recent theoretical developments.

- The weight-average molecular weights of polymer produced decreased with decreasing R_a. Secondary radical entry was found to be the dominant mechanism of chain termination in semicontinuous microemulsion polymerisation. Single-chain polymer particles could only be formed at early stage of nucleation.

- As general rules of thumb, high [S] and low R_a are pre-requisite to produce small nanoparticles by semicontinuous microemulsion polymerisation. Interestingly, the results show a limit to which the size of particles can be reduced, as the average particle size approached constant values with increasing [S] and decreasing R_a. It was found that excess surfactant micelles at the end of polymerisation, in order to avoid secondary radical entry, are required in order to achieve smallest particles.

- An attempt was made to reduce the particle size by using a water-soluble chain transfer agent (CTA) in order to stop the particle growth. The adopted policy could reduce the average particle size by almost 25% under given conditions.

- Comparing with conventional batch process, semicontinuous process can produce much smaller particles at a constant rate of polymerisation and provide a better controllability over particle size and molecular weight of polymer. The process lends itself easily to production of nanolatexes with high solids content. Particles as small as 10 nm could be easily produced by the end of feeding.

- Using semicontinuous process at an extremely low rate of monomer addition, the size evolution of particles could be captured. Particles as small as 6 nm, which is close to the size of micelles, were detected in the early stage of feeding.

6.2.2 Smart Particles

- There is little information in the literature on crosslinker-free polyNIPAM colloids despite their growing potential applications. A set of kinetic data is reported for neat NIPAM polymerisation using a wide range of monomer and surfactant concentration for the first time. The evolution of conversion, particle size, and number of particles in the course of polymerisation, which are mostly ignored in previous works, were monitored and reported. Unlike other contributions, all particle sizes were measured at the reaction temperature. The rate of polymerisation, average size of particles and molecular weight of final products increased with NIPAM concentration.

- Controversial issues exist in the literature regarding colloidal stability of crosslinker-free polyNIPAM particles below the lower critical solution temperature (LCST). Whether the batch NIPAM polymerisation in the absence of crosslinker can

yield water-soluble colloids below LCST has not been clarified in the previous works. Our results show that crosslinker-free polyNIPAM particles produced via batch process were partly insoluble below LCST, which is due to the occurrence of both self-crosslinking and chain entanglement during the polymerisation.

- The dissolution/swelling behaviour of resulting polyNIPAM colloids was monitored. With decreasing temperature of polymer particles, their PSD evolved as binary distributions representing two competing effects; particle swelling because of absorption of water and particle shrinking due to chain disintegration and dissolution of polymer chains in water. Only small particles formed with low monomer concentration depicted a single shrinking PSD.

- Polymerisation of NIPAM in the presence of sodium dodecyl sulphate (SDS) revealed two new features. First unlike conventional emulsion polymerisation of vinylic monomers, the rate of NIPAM polymerisation was independent of the concentration of SDS over a wide range. Second, the number of particles showed a maximum with increasing SDS concentration. The latter was explained by the interaction of SDS with polyNIPAM; by SDS being incorporated into polymer particles and causing them to swell with water at reaction temperature.

- Consistent with the literature, polymerisation of NIPAM in the presence of *N*,*N*,*N*',*N*'-tetramethylenediamine (TEMED) can produce completely water-soluble particles. However, it was found that the colloidal stability of the latexes was weakened due to too many uncharged radicals generated by TEMED, an effect which has not been reported before.

- Moreover, it can also be suggested that the semicontinuous technique can be applied to produce stable water-soluble polyNIPAM latexes with high solids content.

- A model for orientation of polymer chains within particles produced via both batch and semicontinnuous processes has been suggested. A novel method for fabrication of fast dissolving colloids was designed based on the understanding that chains formed via surface polymerisation through semicontinuous process, disintegrate and dissolve in water phase before they can swell to a measureable extent, making the dissolution time

very short. By contrast, particles formed via the conventional batch process had to undergo swelling first before the chains could disintegrate and dissolve in the water.

- The application of above model was extended to fabrication of polyNIPAM nanocapsules. Conventionally, crosslinker-free polyNIPAM particles produced via batch process are used as core templates to produce nanocapsules. However, the batchwise made core materials could not be fully removed from particles due to their chain entanglements. By contrast, the core produced by semicontinuous process undergoes fast dissolution and can be easily removed via self-removing process at room temperature.

6.2.3 Composite Particles

- The surfactant-free emulsion polymerisation of several monomers in the presence of silica nanoparticles and in the absence of any auxiliary materials mostly resulted in formation of polymer/silica core-shell particles. Comparing with conventional batch process, hybrid particles produced by semicontinuous process can incorporate more silica nanoparticles into the shell.

- It was found that the rate of polymerisation as well as the number of particles increased significantly in the presence of silica nanoparticles for conventional batch process. By contrast, the rate of polymerisation in the semicontinuous process remained constant as it was tightly controlled by the rate of monomer addition.

- Large particles were produced via semicontinuous process, in comparison to batch process, due to lack of stability caused by continuous burial of silica nanoparticles in the polymer shell. The usage of silica nanoparticles can be improved by gradually feeding silica nanoparticles in the course of monomer addition, resulting more stable hybrid particles.

- A mechanistic scheme for particle formation of hybrid particles under different pH was developed. Monomers with intermediate water solubility like methyl methacrylate (MMA) do not produce composite particles under basic condition (pH=9.8), at which silica nanoparticles are highly negatively charged and stable. This lack of adhesion can be overcome by changing the initial pH of the dispersion to acidic condition (pH=5.0).

By contrast, vinyl acetate (VA) can easily yield composite particles at both basic and acidic conditions. Polymerisation on the surface of silica nanoparticles is believed to occur in the course of polymerisation for water-soluble monomers, which can overcome the electrostatic repulsion between negatively charged silica and polymer particles and thus promote the adhesion of silica and polymer. Raspberry structures with smoother surface were obtained under basic conditions, comparing with those produced under acidic conditions.

- Very good affinity between silica and polyNIPAM was found, which is attributed to the high water solubility of NIPAM and its polymerisation on the surface of silica nanoparticles. Interestingly, under acidic conditions (pH=5.0) where silica particles were not quite stable, agglomeration of growing polymer particles with silica particles was extensive, resulting insoluble gels (even in the absence of crosslinker). Under basic conditions (pH=9.8), however, uniform silica armoured polyNIPAM particles were formed. The rate of batch polymerisation was reduced in the presence of silica nanoparticles under basic conditions. By contrast, the rate of polymerisation was well controlled via semicontinuous process.

- Crosslinker-free hybrid particles produced via batch process were dissolved more easily in water than those produced in the absence of silica. This new finding, apparently due to interaction of polymer with silica, has not been observed and reported before.

- PolyNIPAM/silica hybrid microgels with core-shell structures were obtained via batch process, while more homogeneous structures were obtained via semicontinuous process.

6.3 Recommendations for Future Work

- The work presented in this study provides new insights into semicontinuous emulsion polymerisation. The results show the size of particles approached a constant value or even experienced a rise under extreme conditions, which is mainly due to the depletion of initiator radicals in the course of polymerisation. This shortcoming can be overcome by continuous addition of an initiator into the reactor, which makes it possible to achieve smallest particles.
- The research can be extended to semicontinuous microemulsion copolymerisation of monomers with a wide difference in water solubility, in particular for theoretical considerations. The particle size as well as the number of particles can be controlled by varying the composition of feeding monomer in the course of polymerisation, which has not been extensively explored.
- It has been observed from the results that semicontinuous technique can be used to synthesis fast dissolving water-soluble polyNIPAM colloids via controlling the orientation of polymer chains within the particles. It is interesting to apply the same strategy to microgels and investigate the effect of chain orientation on swelling and deswelling behaviour, in order to produce fast swelling thermal-sensitive microgels.
- The nature of the silica nanoparticles, such as particle size and surface charge can affect the morphology of resulting polymer/silica hybrid particles. Therefore, it is possible to design new morphologies of hybrid particles using different types of silica nanoparticles via semicontinuous process.
- Considering the effect of pH on the surface charge of silica nanoparticles, the synthesis of polymer/silica hybrid particles can be carried out under the conditions of isoelectric point, under which silica nanoparticles are neutral and extremely unstable. Such policy is expected to produce homogeneous silica-polymer nanocomposites.
- The work can be extended to inverse dispersions via inverse polymerisations, which are attractive processes for many applications, especially for encapsulation of waterborne substances, such as proteins, DNAs and functionalised inorganic nanoparticles.

Appendix A

Instruments

A.1 Zetasizer Nano (Malvern)

The Zetasizer Nano instrument provides the ability to measure three characteristics of particles or macromolecules in a liquid medium, which are size, zeta potential and molecular weight. The main advantage of the instrument is that all information can be obtained in the order of minutes. Furthermore, it is almost completely automated so that routine measurements are easily reproduced.

Figure A.1. Nanosizer (Malvern)

A.1.1 Dynamic Light Scattering (DLS)

The size measurements are preformed using a process called dynamic light scattering (DLS), which measures Brownian motion of the particles or macromolecules and relates this to the size of the particles. It does this by illuminating the particles with a laser and analysing the intensity fluctuations in the scattered light. The resulting hydrodynamic size is the diameter of sphere that diffuses at the same speed as the particle being measured. When particles are illuminated by the laser of Zetasizer (fitted at 633 nm), they will scatter the light in all directions but at different frequencies. If a screen is held close to the particles (Figure A.2), the screen will be illuminated by the scattered light and show a speckle pattern as Figure A.3 shown.

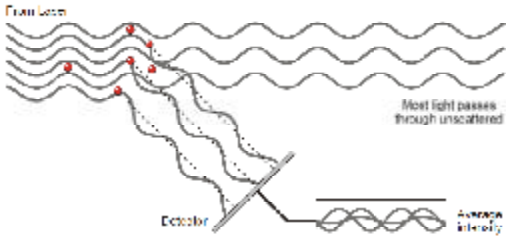

Figure A.2. Propagated waves from the light scattering by particles.

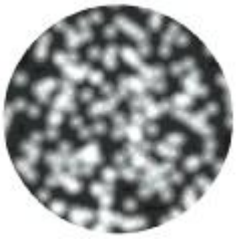

Figure A.3. The speckle pattern consisting of bright light and dark areas from constructive and destructive interference, respectively.

The bright areas of light are where the light scattered by the particles arrive at the screen with the same phase and interferes constructively to form a bright patch. The dark areas are where the phase additions are mutually destructive and cancel each other out.

In practice, particles suspended in a liquid are randomly moving due to Brownian motion which is attributed to the bombardment by the molecules that surround them and the speed of movement is size dependent. Small particles move quickly and large particles move more

illuminated particles will also appear to move. When large particles are being measured, the intensity of the speckle pattern will fluctuate slowly since they are moving slowly. On the other hand, a much faster fluctuation of intensity of the speckle pattern will be measured for small particles. The Zetasizer measures the rate of variation of the fluctuation intensity and uses it to calculate the average size of the particles from the translational diffusion coefficient by using the Stokes-Einstein equation:

$$d(H) = \frac{kT}{3\pi\eta D} \qquad (A.1)$$

where d(H) is the hydrodynamic diameter, *k* is Boltzmann's constant, T is absolute temperature and η is the viscosity of the medium. *D* is the translational diffusion coefficient, which depends not only on the size of particle 'core', but also on any surface structure, as well as the concentration and type of ions in the medium.

Within the instrument, a digital correlator is used to measure the degree of similarity between the signal and itself at varying time intervals. If period of interval δt, is small enough, there will be a strong relationship or correlation between the intensities of two signals. If the original signal was then compared to a signal a little further ahead in time, there would still be a relatively good comparison between the two signals, but it would not be as good as the first. The correlation is therefore reducing with time. The δt is usually very small, maybe nanoseconds or microseconds and is called the sample time of the correlator. And $t = \infty$ may be of the order of a millisecond or tens of milliseconds. Figure A.4 shows the typical correlation function for large and small particles. Perfect correlation is represented as 1.0 and no correlation is reported as 0.0. As can be seen, the rate of decay for the correlation function is related to particle size since the rate of decay is much faster for small particles than that for larger particles.

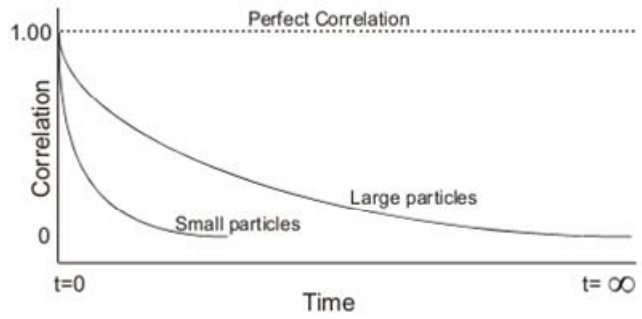

Figure A.4. Typical correlation functions from samples containing large particles and small particles in which the correlation of signals decays with time.

By viewing the correlation function from a measurement, the mean size as well as the size distribution of the sample can be obtained from the time when the correlation starts to significantly decay and the decay rates for a number of size classes, respectively. The size distribution can be obtained directly from DLS measurement is the intensity size distribution, which is weighted according to the scattering intensity of each particle family and proportional

to the square of the weight of particles. Thus the intensity distribution can be misleading, in that a small amount of aggregates or larger particles can dominate the distribution. For example, considering a sample contains only two sizes of particles (D), 5 nm and 50 nm, but with equal numbers of each size particle. The first graph shown in Figure A.5 is a number distribution. As expected the two peaks are of the same size (1:1) as there are equal numbers of particles. The second graph is the volume distribution, which shows the volume composition of mixture ($\propto D^3$). Therefore, the area of the peak for 50 nm particles is 1000 times larger than that for 5 nm. The third one is an intensity distribution. Based on the Rayleigh's approximation, the intensity of scattering light of a particle is proportional to the sixth power of its diameter ($\propto D^6$), as seen in Figure A.5.

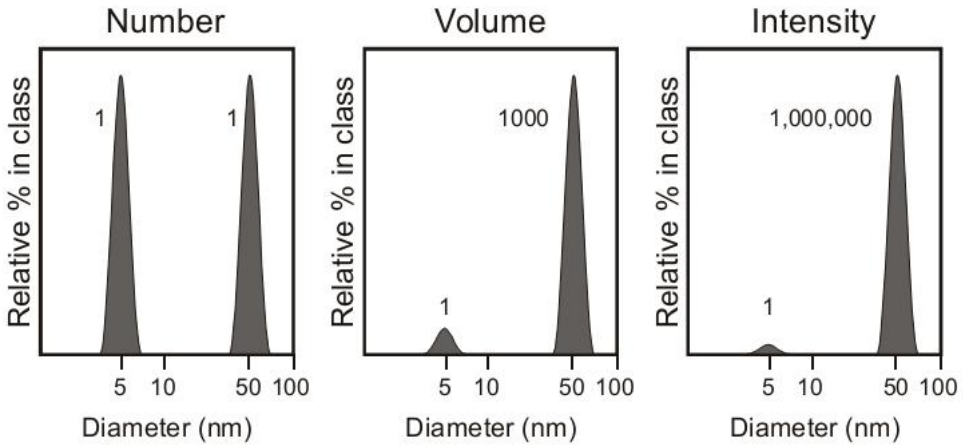

Figure A.5. (left) number distribution, (middle) volume distribution and (right) intensity distribution of a mixture of 5 and 50 nm particles, with equal numbers of particles [1]

Since the mean size derived from DLS is the intensity weighted average hydrodynamic size of the collection of particles (z-average size), any polydispersity or breadth of the particle size distribution will bias the z-average toward the larger particle sizes. On the other hand, the mean size obtained from transmission electron microscopy (TEM) or scanning electron microscopy (SEM) is a number weighted average size of a dehydrated hard sphere. Therefore, z-average diameter is always larger than the TEM measured diameter.

A.1.2 Static Light Scattering (SLS)

The molecular weight measurements were performed using a process called static light scattering (SLS). Similar to DLS, the macromolecules in a sample are illuminated by the laser, with the scattering light in all directions. But, instead of measuring the time-dependent fluctuations in the scattering intensity, SLS makes use of the time-averaged intensity of scattered light. The intensity of light scattered over a period of time, 10 to 30 s, is accumulated for a number of concentrations of the sample. This time averaging removes the inherent fluctuations in the signal. The Rayleigh equation is applied:

[1] Zetasizer Nano user manual, Chapter 13. Size Theory , pp13-5.

$$\frac{KC}{R_\theta} = \left(\frac{1}{\bar{M}_W} + 2A_2C\right)P(\theta) \quad (A.2)$$

where R_θ the Rayleigh ratio, which is the ratio of scattered light to incident light of the sample. $\bar{M}_w$ and C are weight-average molecular weight and concentration of samples, respectively. P_θ the angular dependence of the sample scattering intensity, $A_{2,}$ the 2nd virial coefficient, is a property describing the interaction strength between the macromolecules and the solvent. When $A_2 > 0$, the macromolecules 'like' the solvent more than itself, and tend to stay as a stable solution. When $A_2 < 0$, the macromolecules 'like' itself more than the solvent and therefore may aggregate. When $A_2 = 0$, the particle-solvent interaction strength is equivalent to the molecule-molecule interaction strength, the solvent can then be described as a theta solvent. K is the optical constant and can be defined below:

$$K = \frac{4\pi^2}{\lambda_o^4 N_A}\left(n_o \frac{dn}{dc}\right)^2 \quad (A.3)$$

where N_A the Avogadro's constant, λ_o the laser wavelength and n_o the solvent refractive index. *dn/dc* is the differential refractive index increment. This is the change in refractive index as a function of the change in concentration.

When macromoleclues in solution are much smaller than the wavelength of the incident, P_θ will reduce to 1.0 and the angular dependence of the scattering intensity is ignored. As a result, the Rayleigh equation can be simplified as:

$$\frac{KC}{R_\theta} = \left(\frac{1}{\bar{M}_W} + 2A_2C\right) \quad (A.4)$$

For molecular weight analysis, a key parameter in the determination of the scattering signal is the use of a reference standard. A common standard used in SLS is toluene, the Rayleigh ratios of which are suitably high for precise measurements and known over a range of wavelengths and temperatures. A Debye plot of the concentration dependence of the sample scattering intensity (KC/R_θ) at fixed angel is measured by Nanosizer and compared with that of the standard. $\bar{M}_w$ is determined from the intercept at zero concentration and expressed in Daltons (or $g \cdot mol^{-1}$). The 2nd Virial Coefficient (A_2) is determined from the gradient of the Debye plot.

A.1.3 Laser Doppler Velocimetry (LDV)

The zeta potential measurements are calculated by performing an electrophoresis experiment on the sample and measuring the velocity of the particles when an electrical field is applied using laser Doppler velocimetry technique (LDV).

When an electric charged particle is suspended in liquid, ions of an opposite charge will be attracted to the surface of the suspended particle. The inner region, where ions are close to the surface of the particle and strongly bound, is called Stern layer; the outer region, where ions are further away and less firmly attached, is called Diffuse layer. Therefore, an electrical double layer exists around each particle, as shown in Figure A.6.

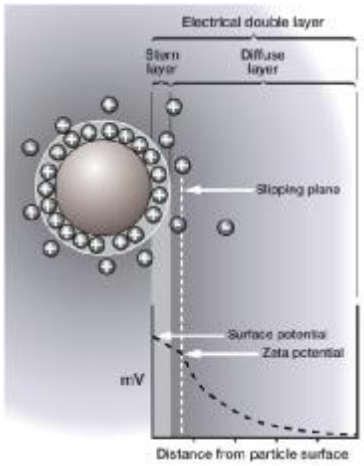

Figure A.6. Scheme of the distribution of ions in the surrounding interfacial region of a charged particle.

Within the diffuse layer there is a notional boundary inside which the ions and particles form a stable entity. When particle moves, ions within the boundary move with it, but any ions beyond the boundary do not travel with the particle. This boundary is called the surface of hydrodynamic shear or slipping plane. The potential that exists at this boundary is known as the zeta potential.

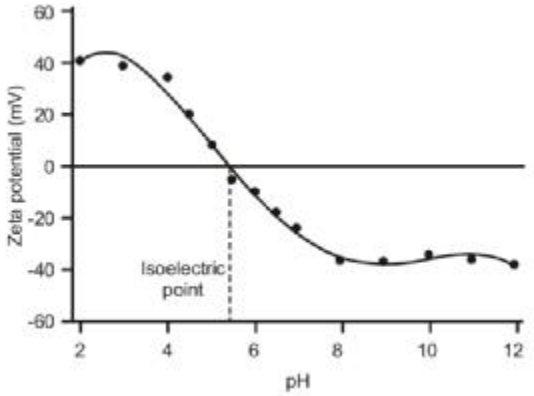

Figure A.7. Typical plot of zeta potential versus pH of the dispersion.

The magnitude of the zeta potential gives an indication of the potential stability of the colloidal system. If particles have a large negative or positive zeta potential then they will repel each other and there is no tendency to flocculate. However, if the particles have low zeta potential values then there is no force to prevent the particles from flocculating.

The general critical value between stable and unstable suspensions is ±30 mV. Particles with zeta potential more than ±30 mV are normally considered stable. The most important factor that affects zeta potential is pH. A zeta potential value on its own without a quoted pH is a meaningless number. The point where the plot passes through zero zeta potential is called the Isoelectric point. It is normally the point where the colloidal system is least stable. A typical plot of zeta potential versus pH is shown in Figure A.7.

The electrophoretic mobility can be measured directly, which is used for obtaining zeta potential of the particle by application of the Henry equation:

$$U_E = \frac{2\varepsilon z f(Ka)}{3\eta} \quad \text{(A.5)}$$

where z is the zeta potential, U_E is electrophoretic mobility, ε is the dielectric constant and η is the viscosity of medium. In the device used, $f(Ka)$ is the Henry's function and referred to as the Smoluchowski approximation, using a value of 1.5 for larger particles (>200 nm) in aqueous media. For small particles in low dielectric constant media (non-aqueous media), $f(Ka)$ becomes 1.0, which is referred to as the Huckel approximation.

During the measurement, a laser is used as the light source and split to provide an incident and reference beam. The incident laser beam passes through the centre of the sample cell, and the scattered light is detected at a forward angle (17°). In combination with the reference beam, a fluctuating intensity signal can be produced, where the rate of fluctuation is proportional to the speed of the particles. A digital signal processor is used to extract the characteristic frequencies in the scattered light.

A.2 Soxhlet Extractor

In year 1879, Franz von Soxhlet invented the Soxhlet extractor, which was originally designed for the extraction of a lipid form a solid material. Typically, a Soxhlet extractor is only required where desired compound has a limited solubility in a solvent, and the impurity is insoluble in that solvent. Normally a solid material containing some of the desired compound is placed inside a sample holder made from thick filter paper, which is loaded into the main chamber of the Soxhlet extractor. The Soxhlet extractor is placed onto a flask containing the extraction solvent and equipped with a condenser, as shown in Figure A.8.

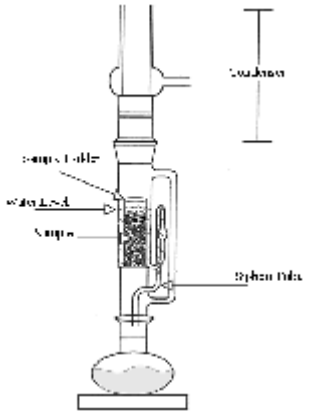

Figure A.8. A schematic representation of a Soxhlet extractor.

The solvent is heated to reflux. The solvent vapour travels up a distillation arm and floods into the chamber containing the sample holder. The condenser ensures that any solvent vapour cools and drips back down into the chamber. When the chamber is almost full, the solvent is automatic drained by a siphon side arm. This cycle is allowed to repeat over days to dissolve desired compound in the warm solvent. In this research, we used Soxhlet extractor to determine the amount of insoluble polymer chains.

A.3 Differential Scanning Calorimeter (DSC, Mettler Toledo)

A differential scanning calorimeter (DSC) measures the heat flow that occurs in a sample when it is heated, cooled or held isothermally at constant temperature.

It can detect endothermic and exothermic effects, transition and reaction enthalpies and specific heat capacity, and thus measures the physical and chemical properties, such as melting point, crystallization behaviour, glass transition of amorphous materials, chemical reactions and et al. In this research, we used DSC in order to measure the glass transition temperature of polymer products.

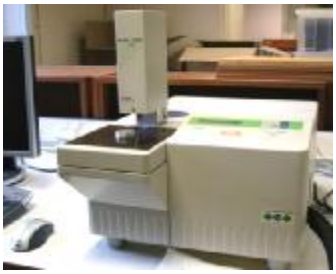

Figure A.9. DSC (Mettler Toledo)

The heat flow, Φ, flows through thermal resistance R_{th} of the sensor. The temperature difference across this thermal resistance is measured by thermocouples. From Ohms's law, the heat flow on the sample side is given by:

$$\Phi_1 = \frac{T_s - T_c}{R_{th}} \tag{A.6}$$

and similar on the reference side:

$$\Phi_2 = \frac{T_r - T_c}{R_{th}} \tag{A.7}$$

The DSC signal, Φ, the heat flow to the sample, corresponds to the difference between the two heat flows:

$$\Phi = \Phi_1 - \Phi_2 = \frac{T_s - T_r}{R_{th}} \tag{A.8}$$

where T_s, T_c, T_r are the temperature of sample, furnace and reference, respectively.

A.4 Ultraviolet-visible Spectroscopy (UV-Vis, PerkinElmer)

UV-Vis refers absorption spectroscopy uses light in the visible and adjacent (near-UV) ranges. It measures the intensity of light passing through a sample (I), and compares it to the intensity of light before it passes through the sample (I_o).

Figure A.10. UV-vis (PerkinElmer)

The ratio I/I_o is called the transmittance and is usually expressed as a percentage (%T). The absorbance, A, is based on the transmittance:

$$A = -\log(\%T/100\%) \tag{A.9}$$

A.5 Luminescence Spectrometer (LS50B, PerkinElmer)

Luminescence or fluorescence spectrometer can analyze fluorescence from a sample. It measures the different wavelength of fluorescent light emitted by QDs, holding the excitation light at a constant wavelength, which is called emission spectrum.

Figure A.11. LS-50B (PerkinElmer)

An excitation spectrum is the opposite, whereby the emission light is held at a constant wavelength, and the excitation light is scanned through many different wavelengths. It is usually measured at a 90° angle relative to the excitation light in order to avoid interference of the transmitted excitation light.

A.6 Electron Microscopy

Scanning electron microscopy (SEM; Hitachi, S4000) and transmission electron microscopy (TEM; Nippon, 200 kv) have been used to measure the size and observe the morphologies of resulting particles. Details for specific uses and sample preparations have been explained where appropriate.

Appendix B

Concentration dependence of turbidimetric measurements

To study the temperature dependence of the phase transition of the polyNIPAM, turbidity of the latexes was measured using UV-vis spectroscopy at a wavelength of 600 nm. The samples were heated up to 50°C and gradually cooled by heat transfer to the surroundings. The initial rate of cooling was around 3°C·min^{-1} until 33°C and then decreased to around 1°C·min^{-1}.

In order to verify the effect of the concentration of latexes on the measurements, samples with different concentrations were prepared by diluting parent 1.0wt% polyNIPAM latex (original latex) to 0.5wt%, 0.25wt% and 0.1wt%. The transmittance curves are shown in Figure B.1. It can be seen that the initial transmittance of the samples before phase transition (40-50ºC) decreased with decreasing the concentration of latex. Furthermore, it was found out that the LCST of the samples become unclear at lower concentrations. Therefore, for all turbidimetric measurements, original samples were directly used without dilution, in order to avoid artificial results.

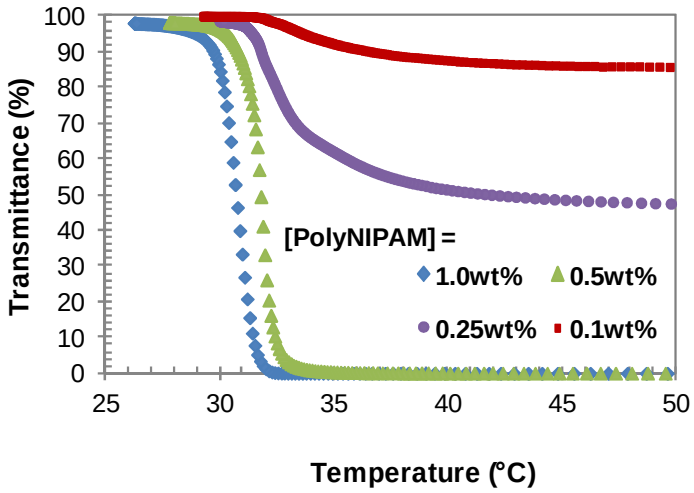

Figure B.1. The evolutions of transmittance of latexes with temperature for different concentrations of polyNIPAM samples.

Appendix C

Reproducibility

Some examples of reproducibility checks are given below in Figures C.1 to C3 for different polymerisation conditions.

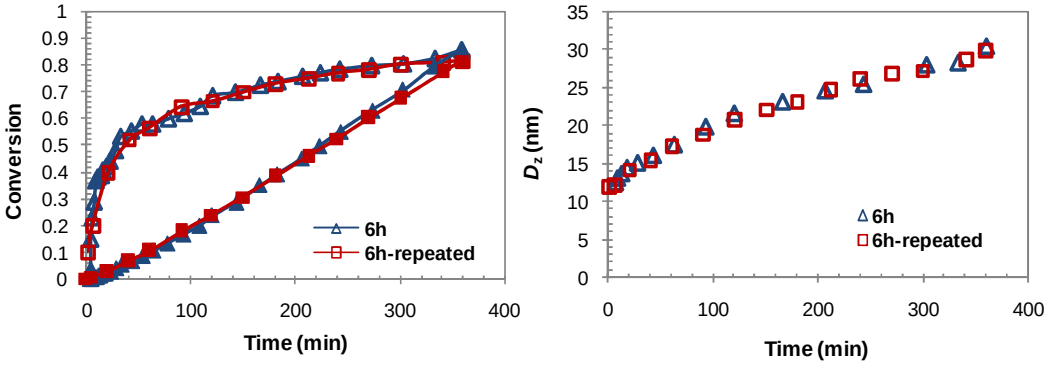

Figure C.1. Two runs for conversions and z-average sizes of particles in the course of semicontinuous microemulsion polymerisation of styrene, [*S*] = 10 g·l$_{aq}^{-1}$; t_{add} = 6h; T = 70°C.

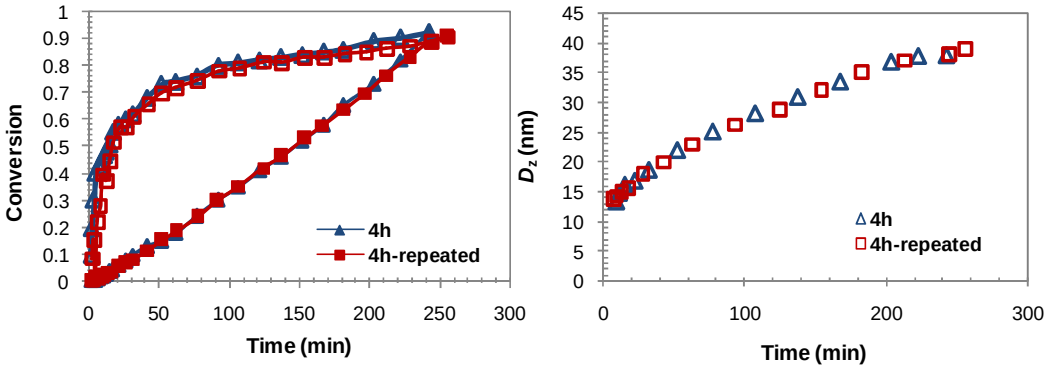

Figure C.2. Two runs for conversions and z-average sizes of particles in the course of semicontinuous microemulsion polymerization of styrene with 4wt% CTA, [*S*] = 10 g·l$_{aq}^{-1}$; t_{add} = 4h; T = 70°C.

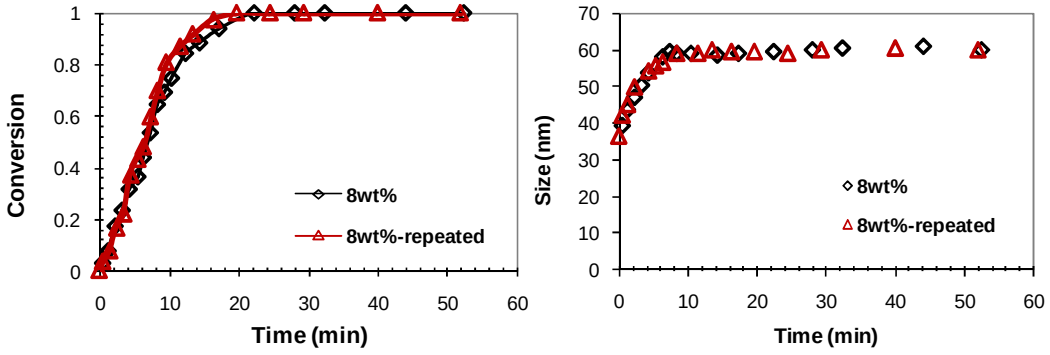

Figure C.3. Two runs for conversions and z-average sizes of particles in the course of batch polymerisation of 8wt% NIPAM, [*S*] = 4 g·l$_{aq}^{-1}$; T = 60°C.

Appendix D

Synthesis and Characterisation of Quantum Dots (QDs)

D.1 Introduction

Inorganic quantum dots (QDs) exhibit strongly size-dependent optical and electrical properties [1-3], and have gained a great interest for application in many fields such as optics, electronics, catalysis and magnetic storage [4-7]. Recently, considerable attention has been paid to using QDs as fluorescent labels for biological applications [8-10]. Aqueously prepared QDs have been suggested to be an attractive alternative to traditional organometallic approaches [11], as the synthetic pathways are cheaper and of lower toxicity [12]. Especially, the products are both water and biological compatible.

In this work, thiol-stabilized cadmium tellurium (CdTe) nanocrystals were synthesized in the aqueous phase. cysteine ($HSCH_2CH(NH_2)COOH$) was used as capping agent because its thiol group has the ability to bond strongly to the metal ions by chemisorptions. The hydrophilic end group (carboxyl) extends into the water to achieve water-compatibility and also serves as a binding site of chemical attachment for biomolecules. Also cysteine, which is a kind of amino acid, is nontoxic or less toxic compared with other modifiers [13]. Traditionally, the precursor molar ratio of Cd : Te : cysteine (RSH) used in the synthesis is 1:0.5:2.4, which makes it possible to obtain perfect crystal structure of $Cd_{17}Te_4(SR)_{26}$ and $Cd_{32}Te_{14}(SR)_{36}$ [12,14]. The capping agent used to form the Cd-SR complex compounds to control the amount of free cadmium ions via the complex-equilibrium process [15].

$$Cd^{2+} + RSH \rightarrow Cd(RS)^{+} + H^{+} \quad (D.1)$$

$$Cd(RS)^{+} + RSH \rightarrow Cd(RS)_2 + H^{+} \quad (D.2)$$

These complexes are insoluble at low pH (< 7.0). With increasing pH to 11.2, they become soluble. The strong coordination bond between Cd^{2+} ion and capping agent can only lead to formation of a low concentration of free Cd^{2+} ion, which keeps the growth of QDs under control. The decomposition of the Cd-SR complexes, which is the rate-limiting process, continuously provides Cd^{2+} ions. The excess of cadmium relative to tellurium is essential, allowing the cadmium-rich particle surface to react with the sulfur precursors (H_2S) generated by thermal decomposition of L-cysteine [16] and resulting a CdS shell on the surface of CdTe QDs.

It has been demonstrated that using inorganic semiconducting materials with broader band-gap (such as CdS) to form a shell structure on the surface of QDs with narrower band-gap (such as CdTe) is an effective approach to reduce the surface traps of the core and thus raise the fluorescence quantum yield (QY) [10].

D.2 Main Experimental Work

To produce and characterise water-soluble core-shell CdTe-CdS particles, the following stages are adopted [13].

D.2.1 Synthesis of Te Precursor, $(NH_4)_2Te$

$(NH_4)_2Te$ is chosen as the tellurium precursor, which is sensitive to oxygen and has to be stored as an aqueous solution under nitrogen atmosphere. However, this precursor is much safer and easier to handle comparing with other type of precursors [13]. The reaction proceeds as follows [17]:

$$3Te + 6NH_4OH + 2Al \rightarrow 3(NH_4)_2Te + 2Al(OH)_3 \qquad (D.3)$$

Al powder (0.77 g, 28 mmol) and Te powder (1.30 g, 10 mmol) were added into a 100 ml one-neck flask. Then 60 ml of deionised water was added to the flask and stirred under nitrogen purging for 1h. 5 $mol \cdot l_{aq}^{-1}$ Ammonium hydroxide solution (14 ml, 70 mmol) was added, forming a violet colour in 2 min. The mixture was stirred for one day, during which the colour lightened. After standing for an additional 2 days, the supernatant of the solution was used for further reactions (Figure D.1).

Figure D.1. (left) Set up and (right) resulting Te precursor solution.

D.2.2 Synthesis of CdTe Precursors

Cadmuim acetate dihydrate (0.42 g, 1.58 mmol) and 3.8 mmol of L-cysteine were dissolved in 60 ml of ultrapure water forming a cloudy dispersion. The pH was then altered to ca. 11.2 using sodium hydroxide (2 $mol \cdot l_{aq}^{-1}$). Above pH of 9.0, the solution cleared. The reagents were then degassed by bubbling dry nitrogen through the aqueous solution for 3h, followed by flushing with nitrogen.

To the reaction flask, 5 ml of a 0.16 $mol \cdot l_{aq}^{-1}$ aqueous solution of $(NH_4)_2Te$ was added, causing an immediate clear dark brown coloration. The reaction was allowed to stir under nitrogen for 3h. The CdTe precursors are formed at this stage, which is accompanied by a change in the solution colour. The precursors show an absorption spectrum being unstructured in the visible spectral region with a tail extending to 650-700 nm and no luminescence. The solution should not be exposed to air at this stage due to the risk of oxidation of Te^{2-} ion.

Figure D.2. Set up and resulting latxes of CdTe precursors

The chemical reactions are shown below [15]:

$$Cd(RS)_2 \rightarrow Cd(RS)^+ + RS^- \quad (D.4)$$

$$Cd(RS)^+ \rightarrow Cd^{2+} + RS^- \quad (D.5)$$

$$nCd^{2+} + mTe^{2-} + 2nRS^- \rightarrow [Cd_nTe_m(RS)_{2n}]^{2m-} \ (n>m) \quad (D.6)$$

D.2.3 Particle Growth, Ostwald Ripening, S^{2-}release, CdS Shell Formation

High temperatures can accelerate the decomposition of Cd-SR complexes, leading to the fast growth of QDs. The aqueous solution of cysteine-capped QDs was heated to reflux temperature under nitrogen gas with a condenser attached (Figure D.3). The refluxing lasts up to 60 min. Excessive prolonged heating resulted in the growth of bulk cadmium telluride. Under refluxing and in the presence of an excess amount of thiols, the partial hydrolysis of thiols can cause an incorporation of the sulfur from the thiol molecules into the growing nanoparticles [10].

Figure D.3. Set up of refluxing

$$2HSR \text{ (cysteine)} \rightarrow RSSR \text{ (cystine)} + H_2S + NH_3 \text{ (needs heat)} \quad (D.7)$$

$$Cd^{2+} + S^{2-} \rightarrow CdS \quad (D.8)$$

D.2.4 Post Preparation to Enhance the Fluorescence of QDs via Ripening Process

The latex was cooled down and left at room temperature for up to 2 weeks to in order to stop the growth process. This stage is based on the Ostwald ripening phenomenon. Further particle growth occurs via dissolution of small clusters in favour of the growth of larger particles. As a result, precipitations of CdTe were formed. However, there always exists a fraction of particles in the supernatant with equal rates of growth and dissolution, which is preferable for high photoluminescence quantum efficiencies and photostability [13].

D.3 Improvement of Standard Synthesis of QDs

When Cd : Te : cysteine= 1:0.5:2.4 was used, stable complex (1:2 Cd-SR) is dominant in the system which limited the amount of free Cd^{2+} ion concentration. The formation of CdTe nuclei is depressed and a large amount of Te^{2-} ions was left for the further growth before refluxing. As a result, big size QDs was obtained in the end due to fast growth. In this case, the surface structure of QDs may not be optimized by the location of the monomers on the most favourable sites, which required an equilibrium growth to further perfect the nanocrystal surface [13]. The resulting latex exhibits dark red color (Figure D.4), which indicates the formation of large QDs. The formula was modified by decreasing the concentration of Te^{2+} ion to Cd : Te = 1:0.3. The resulting latex shows a strong orange colour, as shown in Figure D.5.

Figure D.4. The resulting latex with a formula of Cd : Te : cysteine = 1:0.5:2.4.

Figure D.5. The resulting latex with a formula of Cd : Te : cysteine = 1:0.3:2.4.

It also has been reported [10,18] that by decreasing the capping agent/Cd ratio from 2.4 to 1.1, a drastic increase in the photoluminescence quantum efficiency was observed. Optimised values of 1.3-1.5 were found for the efficiency [10]. However, it should be noticed that such improvement is gained at the cost of the stability of QDs. The zeta potential of QDs were measured and shown in Table D.1.

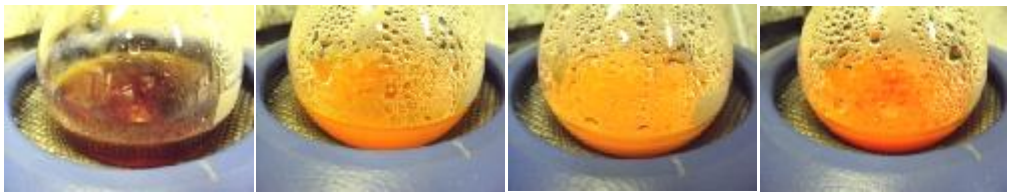

Figure D.6. Evolution of the colour of the latex with refluxing period from left to right; 0 min, 15 min, 30 min and 60 min. Cd : Te : cysteine = 1:0.3:1.5.

Table D.1. Zeta potential of resulting QDs

Cd:Te:cysteine	Zeta potential (mv)
1:0.5:2.4	-25
1:0.3:2.4	-22
1:0.3:1.5	-13

D.4 Stability of CdTe QDs

Significant oxidation was found when QDs solutions were exposed to air overnight. The black colour, as shown below, is attributed to the oxidation of Te^{2-} ions on the surface of CdTe QDs.

Figure D.7. QD solutions just produced (left) and after overnight exposure to ambient room conditions (right). Up: Cd:Te:cysteine=1:0.5:2.4; middle: Cd:Te:cysteine=1:0.3:2.4; bottom: Cd:Te:cysteine=1:0.3:1.5

D.5 Characterization of QDs

UV-vis spectrometer was used to measure the absorption spectrum of resulting QDs. The samples were diluted with water to obtain a clear solution with absorbance around 0.15-0.25, in order to avoid self-quenching. The resulting spectrum is presented as a graph of absorbance (A) versus wavelength of the excitation light, as shown in Figure D.8.

The first excitonic absorption peak can be considered as the range of the band edge of the QD, and its wavelength, λ=560 nm, is related to the particle size (D) according to [1]:

$$\text{CdTe: } D = (9.8127\text{e-}7)\lambda^3 - (1.7147\text{e-}3)\lambda^2 + (1.0064)\lambda - 194.84 \qquad \text{(D.9)}$$

which suggests that particles have an average diameter of 3.34 nm.

The emission spectrum of the sample can be obtained from fluorescence spectrometer, in which the different wavelengths of fluorescent light emitted by the sample are measured at a constant wavelength of excitation light (Figure D.8). In order to obtain the strongest signal of emission, an optimised wavelength of excitation light need to be found out from the excitation spectrum.

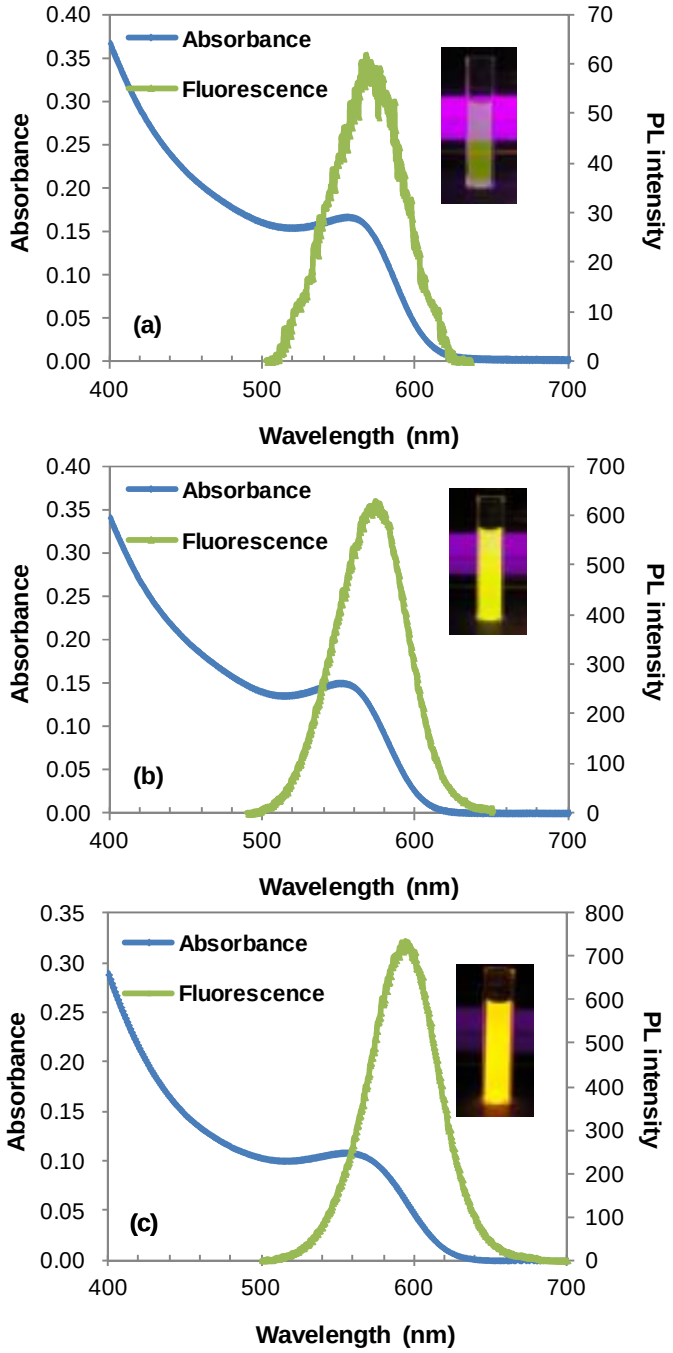

Figure D.8. Absorption and emission spectra (PL stands for photoluminescence) for crysteine-capped CdTe QDs produced by (a) Cd:Te:crysteine=1:0.5:2.4; (b) Cd:Te:crysteine=1:0.3:2.4; (c)Cd:Te:crysteine=1:0.3:1.5. The optimised wavelength of excitation light is λ_{exc}= 390 nm.

D.6 Reference

[1] Yu, W.W., Qu, L.H., Guo, W.Z., Peng, X.G. Experimental Determination of the Extinction Coefficient of CdTe, CdSe, and CdS Nanocrystals, *Chemistry of Material*, 2003, v15, pp2854-2860.
[2] Finlayson, C.E., Ginger, D.S., Marx, E., Greenham, N.C. Electrical and Optical Properties of Semiconductor Nanocrystals, *Philosophical Transactions A*, 2003, v361, pp363-377.
[3] Nirmal, M., Brus, L. Luminescence Photophysics in Semiconductor Nanocrystals, *Accounts of Chemical Research*, 1999, v32, pp407.
[4] Lesser, C., Gao, M., Kirstein, S., Highly Luminescent thin films from alternating deposition of CdTe Nanoparticles and Polycations, *Materials Science & Engineering C- Biomimetic and Supramolecular Systems*, 1999, v8-9, pp159-162.
[5] Greenham, N.C., Peng, X.G., Alivisatos, A.P. A CdSe Nanocrystal MEH-PPV Polymer Composite Photovoltaic, *Future Generation Photovoltaic Technologies*, 1997, pp295-301.
[6] Harrsion, M.T., Kershaw, S.V., Burt, M.G., Rogach, A.L., Kornowski, A., Eychmuller, A., Weller, H. Colloidal Nanocrystals for Telecommunications. Compete Coverage of the Low-loss Fiber Windows by Mercury Telluride Quantum Dots, *Pure and Applied Chemistry*, 2000, v72, pp295-307.
[7] Colvin, V.L., Schlamp, M.C., Alivisatos, A.P. Light-Emitting-Diodes Made From Cadmium Selenide Nanocrystals and A Semiconducting Polymer, Nature, 1994, v370, pp354-357.
[8] Gao, X.H., Cui, Y.Y., Levenson, R.M., Chung, L.W.K., Nie, S.M. In Vivo Cancer Targeting and Imaging with Semiconductor Quantum Dots, Nature Biotechnology, 2004, v22, pp969-976.
[9] Zhang, H.Y., Sun, P., Liu, C., Gao, H.Y., Xu, L.R., Fang, J., Wang, M., Liu, J.L., Xu, S.K. L-cysteine Capped CdTe-CdS Core-shell Quantum Dots: Preparation, Characterization and Immuno-Labeling of Hela Cells, Luminescence, 2011, v26, pp86-92.
[10] Taniguchi, S., Green, M., Rizvi, S.B., Seifalian, A. The one pot Synthesis of Core/shell/shell CdTe/CdSe/ZnSe Quantum Dots in Aqueous Media for in vivo Deep Tissue Imaging, Journal of Materials Chemistry, 2011, v21, pp2877-2882.
[11] Hines, M.A., Guyot-Sionnest, P. Synthesis and Characterization of Strongly Luminescing ZnS-Capped CdSe Nanocrystals, Journal of Physical Chemistry, 1996, v100, pp468-471.
[12] Bao, H.B., Gong, Y.J., Li, Z., Gao, M.Y. Enhancement Effect of Illumination on the Photoluminescence of Water-Soluble CdTe Nanocrystals: Toward Highly Fluorescent CdTe/CdS Core-Shell Structure, Chemistry of Materials, 2004, v16, pp3853-3859.
[13] Green, M., Harwood, H., Barrowman, C., Rahman, P., Eggeman, A., Festry, F., Dobson, P., Ng, T. A Facile Route to CdTe Nanoparticles and Their Use in Bio-labelling, Journal of Materials Chemistry, 2007, v17, pp1989-1994,
[14] Vossmeyer, T., Reck, G., Schulz, B., Katsikas, L., Weller, H. Double-Layer Superlattice Structure Built Up of $Cd_{32}S_{14}(SCH_2CH(OH)CH_3)_{36}$ $4H_2O$ Clusters, Journal of the American Chemical Society, 1995, v117, pp12228-12882.
[15] Li, Z., Wang, Y.X., Zhang, G.X., Han, Y.J. Luminescent Properties Dependence of Water-Soluble CdTe Quantum Dots on Stabilizing Agents and Reaction Time, Journal of Central South University of Technology, 2010, v17, pp1148-1154.
[16] Routh, J.I. The Decomposition of Cysteine in Aqueous Solution, Journal of Biological Chemistry., 1939, v130, 297.
[17] Boudjouk, P., Remington, M.P., Grier D.G., Triebold W., Jarabek, B.R. 2,2,4,4,6,6-Hexabenzylcyclotristannatellurane, $(Bn_2SnTe)_3$. Synthesis and Structure Characterization of an Organometallic Single-Source Precursor to Phase-Pure, Polycrystalline SnTe. Organometalllics, 1999, v18, pp4534.

[18] Rogach, A.L., Franzl, T., Klar, T.A., Feldmann, J., Gaponik, N., Lesnyak, V., Shavel, A., Eychmuller, A., Rakovich, Y.P., Donegan, J.F. Aqueous Synthesis of Thiol-Capped CdTe Nanocrystals: State-of-the-Art. Journal of Physical and Chemistry, 2007, v111, pp14628-14637.

Appendix E

Investigation of synthesis of novel polyNIPAM/quantum dots (QDs) composite particles

E.1 Introduction

Exploring novel materials based on QDs and polyNIPAM has attracted great interest in recent years [1-4]. Since QDs are very sensitive to environmental changes via varying their photoluminescence (PL) efficiency, the incorporation of QDs with thermal-sensitive polyNIPAM microgels can provide a new generation of fluorescence markers for biological applications [2]. In our previous work (see Chapter 5.2), very good affinity has been found between polyNIPAM and hydrophilic silica nanoparticles. Therefore, thiol-stabilized CdTe QDs were first produced in the water phase (Cd:Te:cysteine = 1:0.3:1.5; see Appendix D) and then used for the synthesis of polyNIPAM/QDs composite particles.

E.2 Results and Discussions

Surfactant-free emulsion polymerisation of NIPAM in the presence of QDs was first conducted at 60ºC via semicontinuous process. Monomer emulsion, containing 20wt% NIPAM monomer, 2wt% MBA crosslinker and 0.02wt% QDs, was continuously fed into the reactor in the course of polymerisation at the rate of 4.76 $ml \cdot h^{-1}$. The results are shown in Figure E.1. Limited coagulation was observed in the later stage of reaction. According to SEM image (Figure E.2), very good affinity can be found between QDs and polyNIPAM particles. In semicontinuous process, QDs are gradually buried in the polymer particles and cannot provide sufficient electrostatic stability to the particles anymore leading to significant hetero-coagulation between polymer and QDs. Furthermore, the prepared QDs are not quite stable (zeta potential of -13 mv, see Appendix D), so they promote hetero-coagulation between QDs and polymer.

Unexpectedly, the resulting latex did not exhibit any photoluminescence. This may be due to the oxidation in the presence of KPS leading to the fluorescence quenching of QDs. In order to verify the effect of KPS on the fluorescence of QDs, 10.8 mg KPS was added to 10 ml QDs solution (10 $mg \cdot l_{aq}^{-1}$). Fluorescence quenching of QDs was observed after 20 min. Similar observation has been reported in the literature [5].

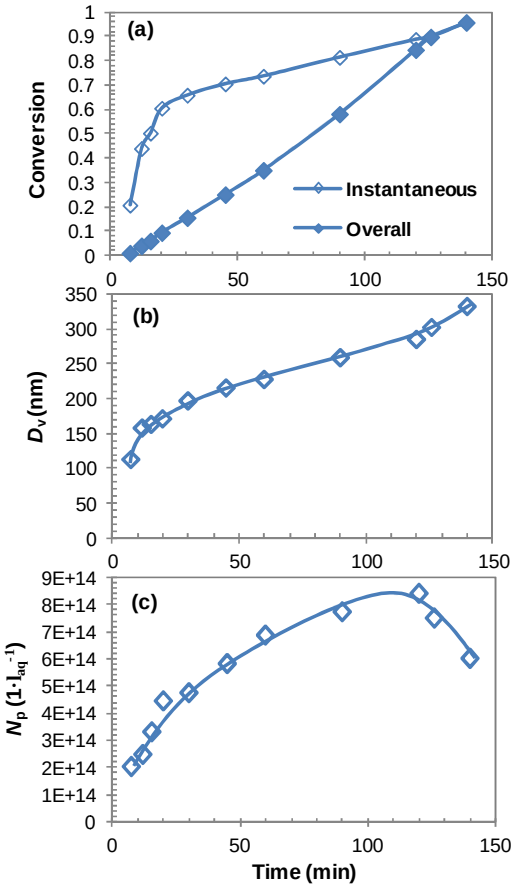

Figure E.1. (a) Conversions, (b) volume-average size of particles and (c) number of particles produced versus reaction time for semicontinuous surfactant-free emulsion polymerization of NIPAM in the presence of QDs. T = 60°C; KPS = 4 mmol·l_{aq}^{-1}; pH = 9.8; R_a = 4.76 ml·h^{-1}. Monomer emulsion: 20wt% NIPAM, 0.02wt% QDs.

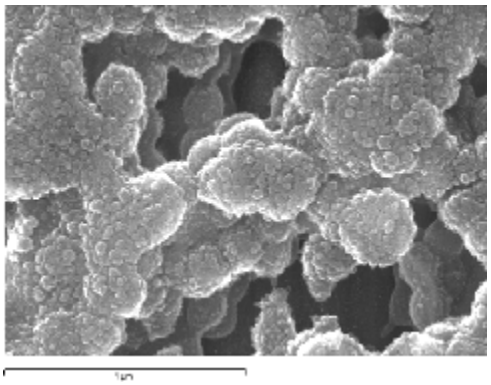

Figure E.2. SEM image of polyNIPAM/QDs hybrid particles produced by the reaction shown in Figure E.1.

Since the use of persulfate initiators can hardly be avoided in the conventional emulsion polymerisations, inverse systems were introduced and investigated as an alternative method that can use other types of initiator. In contrast to conventional systems, inverse polymerisations involve aqueous droplets (or micelles) containing water-soluble NIPAM monomer and hydrophilic QDs dispersed with the aid of oil-soluble surfactant in continuous organic phase. When polymerisation starts at room temperature (below LCST), hydrophilic polyNIPAM chains formed tend to stay in the aqueous droplets, resulting stable colloidal particles containing QDs.

As a fist trial, hexane and dioctyl sodium sulfosuccinate (AOT; HLB=10.2) were chosen as the continuous phase and surfactant, respectively. The stability of the inverse emulsion was tested. 20wt% aqueous phase containing 82wt% water, 16.4wt% NIPAM monomer, and 1.6wt% MBA was dispersed in the oil in the presence of 1wt%, 3wt% and 5wt% AOT, respectively. As shown in Figure E.3, highly viscous emulsions were formed, which could not be used for polymerisation.

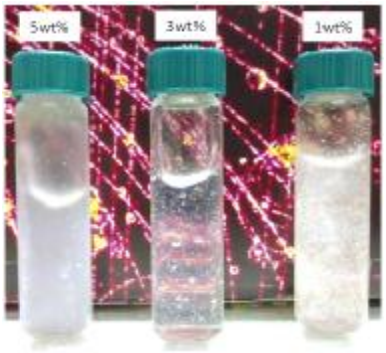

Figure E.3. Inverse emulsions with 5wt%, 3wt% and 1wt% AOT; Continuous phase: hexane; 20wt% Aqueous phase: 82wt% water, 16.4wt% NIPAM and 1.6wt% MBA.

The continuous phase was then replaced by toluene. Finally, milky emulsions with mild viscosity were obtained, which could be a workable system (Figure E.4).

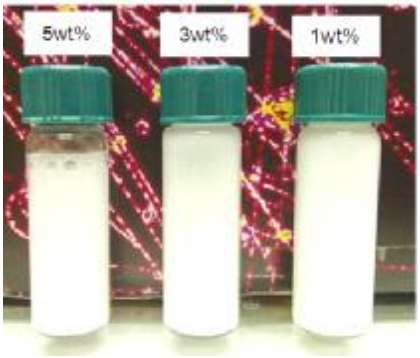

Figure E.4. Inverse emulsions with 5wt%, 3wt% and 1wt% AOT; Continuous phase: toluene; 20wt% Aqueous phase: 82wt% water, 16.4wt% NIPAM and 1.6wt% MBA.

Benzoyl peroxide (BP)/TEMED redox pair was first selected for initiation. BP was placed in the oil phase but TEMED in the water phase. In this case, oil-soluble BP and water-soluble TEMED will only meet up and generate radicals at the oil-water interface, which can promote polymerisation reaction followed by the phase separation of crosslinked polyNIPAM at the interface and form polymer shell/water core structures. Several polymerisations with different recipes and processes were conducted, as shown in Table E.1. However, the results were not ideal and low values of final conversions were obtained after 4h reaction. In order to find out the reason, the solubility of NIPAM monomer in toluene at 20ºC was tested and found to be more than 50wt%, which is much higher than that in the water phase (~20wt%). In this case, most of the NIPAM monomer would remain in the oil phase, due to low aqueous phase ratio (5- 17wt%), leading to low conversions. Similar recipe has been used in the literature [6]; however, no

conversion data was reported. The final sample was observed under SEM, film of polymer was found and individual particles can be hardly identified, as shown in Figure E.5. It is believed that the formation of polymer film is due to insufficient crosslinking density in the particle. Since MBA is a water-soluble crosslinker, most of the crosslinker monomer stays in the water droplets, in which the monomer concentration is very low, as mentioned above. In this case, crosslinker monomer is likely to be used up in the early stage of reaction and the resulting crosslinked particles will be covered by crosslinker-free polymer chains as polymerisation continuing. In order to overcome this problem, MBA is replaced by DVB, which is an oil-soluble crosslinker monomer. However, unexpectedly, no reaction was detected after 2h.

Table E.1. Summary of inverse polymerisations initiated by BP/TEMED redox pair. Continuous phase: 200 ml toluene; T = 20ºC. [AOT] = 5.0wt%. MBA/NIPAM(g/g) = 1:10.

Code	Process	Water (wt%)	NIPAM (wt%)	BP/NIPAM (g/g)	TEMED/BP (mol/mol)	Description
[1]	Batch	17	3.4	0.01	1:1	x_{final} = 54%
[2]	Batch	17	3.4	0.02	1:1	x_{final} = 25%
[3]	Batch	7	5	0.02	1:1	x_{final} = 12%
[4]	Semi	5	1	0.02	3:1	x_{final} = 10%

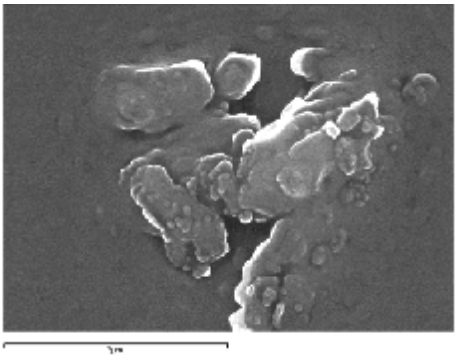

Figure E.5. SEM image of sample produced by inverse batch polymerisation, recipe [1] as shown in Table E.1. Bar: 3 μm.

The redox pair was then changed to BP/4,N,N-Trimethylaniline (Tri). Since both components are oil soluble, the rate of radical generation was expected to be improved. Several polymerisations were carried out and shown in Table E.2. However, none was successful due to significant coagulation in the early stage of polymerisation, which might have been caused by rapid homogeneous nucleation in the oil phase, since free radicals were all generated in the continuous phase. Due to high monomer concentration in the oil phase, the system could undergo homogeneous nucleation much faster in toluene than in water. As a result, bulks of polymer were formed.

Table E.2. Summary of inverse batch polymerisations initiated by BP/Tri redox pair. Continuous phase: 200 ml toluene; T = 20ºC. Tri/BP(mol/mol) = 1:1. MBA/NIPAM(g/g) = 1:10.

AOT (wt%)	Water (wt%)	NIPAM (wt%)	BP/NIPAM (g/g)	Description
5	1.25	0.25	0.446	Coagulations occurred within 18-30 min into reaction
10	1.25	0.25	0.446	
5	5	1	0.111	
5	16.5	3.3	0.03	
5	5	1	0.03	no reaction at all

To hinder homogeneous nucleation, the availability of monomer in the continuous phase should be limited. Therefore, hexane was brought up again, since the solubility of NIPAM in the hexane (< 1wt%) is much lower than that in the water phase at 20ºC. In order to produce workable inverse emulsion, AOT was replaced by Span80. Several experiments were carried out, as shown in Table E.3. Generally, the system was stable in the course of polymerisation (Figure E.6). Most of conversions were all above 1.0, which usually indicates the presence of trapped water molecules in the crosslinked polymer networks, which cannot be removed by conventional drying. However, unexpectedly, particles could hardly be identified in the SEM image (Figure E.7). A film of polymer was formed during the sample preparation, which suggests lack of cross-linked network in the particles. Use of oil-soluble crosslinker (DVB) also did not resolve this problem.

At this point, further research was directed toward silica composite materials, as described in Chapter 5.

Table E.3. Summary of inverse polymerisations initiated by BP/Tri redox pair. Continuous phase: 200 ml hexane; T = 20ºC. Tri/BP(mol/mol) = 1:1. [Span80] = 5wt%. MBA/NIPAM(g/g) = 1:10.

Process	Water (wt%)	NIPAM (wt%)	BP/NIPAM (g/g)	Description
batch	19	3.8	0.038	insufficient cross-linking density
batch	5	1.0	0.147	
semi	5	1.0	0.147	

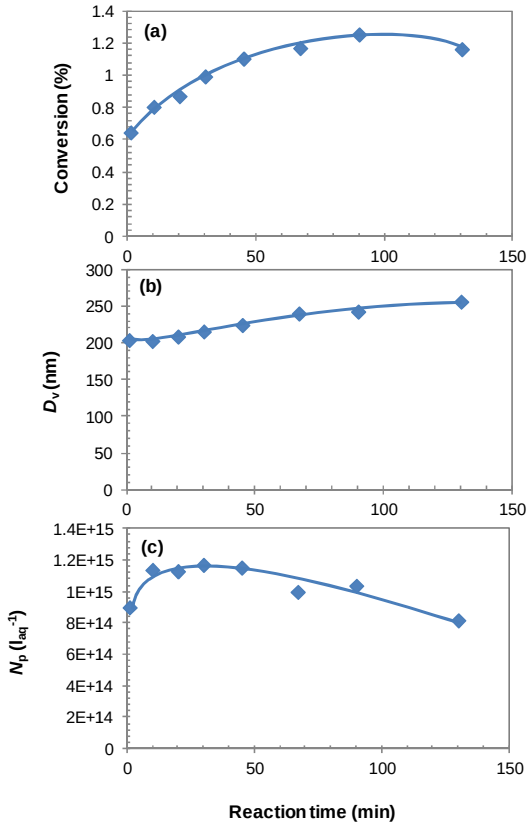

Figure E.6. (a) Conversions, (b) volume-average size of particles and (c) number of particles produced versus reaction time for inverse batch polymerization of NIPAM. T = 20ºC; Oil phase: hexane; Aqueous phase: 5wt% water, 1wt% NIPAM, 0.1wt% MBA. BP/NIPAM(g/g) = 0.147.

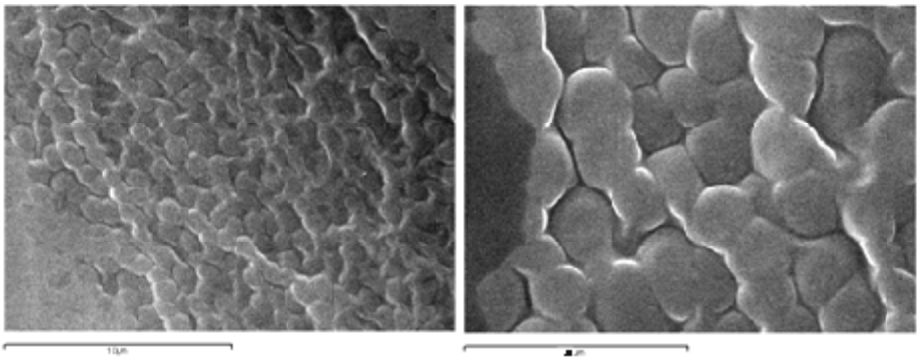

Figure E.7. SEM image of polyNIPAM particles produced by inverse batch polymerisation shown in Figure E.5. Bar: (left) 10 µm; (right) 3 µm.

E.3 Reference

[1] Kuang, M., Wang, D.Y., Bao, H.B., Gao, M.Y., Mohwald, H., Jiang, M. Fabrication of Multicolor-Encoded Microspheres by Tagging Semiconductor Nanocrystals to Hydrogel Spheres. *Advanced Material*, 2005, v17, pp267-270.

[2] Agrawal, M., Rubio-Retama, J., Zafeiropoulos, N.E., Gaponik, N., Gupta, S., Cimrova, V., Lesnyak, V., Lopez-Cabaros, E., Tzavalas, S., Rojas-Reyna, R., Eychmuller, A., Stamm, M. Swichable Photoluminescence of CdTe Nanocystals by Temperature-Responsive Microgels, *Langmuir*, 2008, v24, pp9820-9824.

[3] Li, J., Hong, X., Liu, Y., Li, D., Wang, Y.W., Li, J.H., Bai, Y.B., Li, T.J. Highly Photoluminescent CdTe/Poly(N-isopropylacrylamide) Temperature-Sensitive Gels, *Advanced Material*, 2005, v17, pp163-166.

[4] Shen, L., Pich, A., Fava, D., Wang, M.F., Kumar, S., Wu, C., Scholes, G.D., Winnik, M.A. Loading Quantum Dots into Thermo-Responsive Microgels by Reversible Transfer from Organic Solvents to Water. *Journal of Materials Chemistry*, 2008, v18, pp763-770.

[5] Yang, Y.H. Preparations and Properties of Fluorescent Microbeads Incorporated with CdTe Nanocrystals, PhD Thesis, Graduate University of Chinese Academy of Sciences, 2006.

[6] Fernandez, V.V.A., Tepale, N., Sanchez-Diaz, J.C., Mendizabal, E., Puig, J.E., Soltero, J.F.A. Thermoresponsive Nanostructured Poly(N-isopropylacrylamide) Hydrogels Made via Inverse Microemulsion Polymerisation. *Colloid and Polymer Science*, 2006, v284, pp387-395.

Appendix F

Calculation of the mass of incorporated silica nanoparticles into composite particles from intensity size distribution

Since we were not able to separate free silica nanoparticles from the hybrid particles before the size measurements, the size data obtained from DLS presents the average size of all particles present in the sample. Thanks to intensity size distribution data, we were able to estimate the weights of free silica nanoparticles and incorporated silica particles. The latter was then used to calculate the number of nanocomposite particles. One should notice that this method is only valid for clear bimodal size distributions, as shown in Figure F.1.

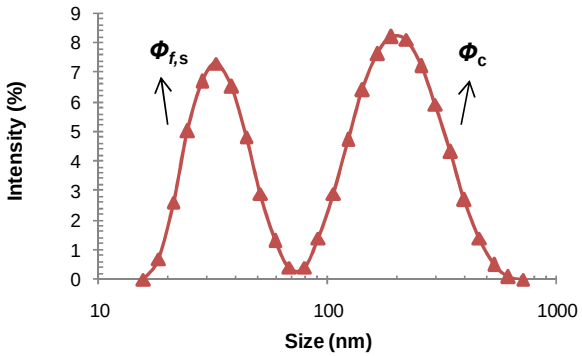

Figure F.1. A typical bimodal size distribution. The peak within the small size range (10-70 nm) represents free silica nanoparticles, while the peak within the large size range (80-700 nm) represents composite particles.

Based on the Rayleigh's approximation, the intensity of scattering light of a particle is proportional to the square of its volume ($\propto V^2$; see Appendix A.1.1). Therefore, the intensity ratio between free silica nanoparticles and composite particles ($\emptyset_{f,s}/\emptyset_c$) should be equal to the ratio of the square of their volumes ($V_{f,s}^2/V_c^2$), so that:

$$\emptyset_{f,s}/\emptyset_c = V_{f,s}^2/V_c^2 \tag{F.1}$$

The volume of composite particles can be calculated as:

$$V_c = V_P + V_{in,s} \tag{F.2}$$

where V_p is the volume polymer formed at given time (t), which can be obtained from conversion data (x), weight of monomer used (m_{mon}) and the density of polymer (ρ_p), so that $V_p = m_{mon} \cdot x \cdot t/\rho_p$. The volume of incorporated silica particles, $V_{in,s}$, can be solved using mass balance equation for silica nanoparticles as:

$$V_{t,s} = V_{f,s} + V_{in,s} \tag{F.3}$$

where $V_{t,s}$ is the total volume of silica nanoparticles used in the recipe.

Equations F.1, F.2 and F.3 can be simultaneously solved to obtain $V_{in,s}$, which can be used to obtain the weight of the incorporated silica nanoparticles ($m_{in,s}$), so that $m_{in,s}=V_{in,s}\cdot\rho_s$.

In order to check the reliability of the method, a weighted quantity of polyNIPAM particles were mixed with different amounts of silica nanoparticles under basic conditions. Since the adhesion between silica and polyNIPAM particles was negligible at pH = 9.8 (see Chapter 5.2), the weight of the added silica nanoparticles was considered as that of free silica nanoparticles. Clear bimodal intensity size distributions were obtained from DLS. The results are shown below.

Table F.1. Weight fraction of free silica nanoparticles (w_s), ratio of the square of volume of silica and polymer particles and intensity ratio between silica and polymer particles as a function of amount of silica nanoparticles added.

w_s	V_s^2/V_p^2	$\emptyset_s/\emptyset_p$
0.09	0.00	-
0.18	0.01	0.07
0.29	0.04	0.09
0.36	0.08	0.11
0.43	0.14	0.13
0.50	0.23	0.14
0.57	0.41	0.16
0.61	0.59	0.19
0.65	0.76	0.22
0.70	1.29	0.26
0.75	2.06	0.32

Based on the hypothesis (Equation F.1), V_s^2/V_p^2 should be equal to $\emptyset_s/\emptyset_p$. V_s^2/V_p^2 ratios were calculated form polymer/silica ratios used in the recipe. $\emptyset_s/\emptyset_p$ ratios were obtained from DLS distribution curves. From Table F.1 and Figure F.1, it can be found that the experimental $\emptyset_s/\emptyset_p$ data approaches those predicted by theory up to V_s^2/V_p^2 = 0.2, corresponding to w_s = 0.5, which covers the range of silica particles used in the study as explained in Chapter 5. Significant deviation can be observed when more silica particles were added.

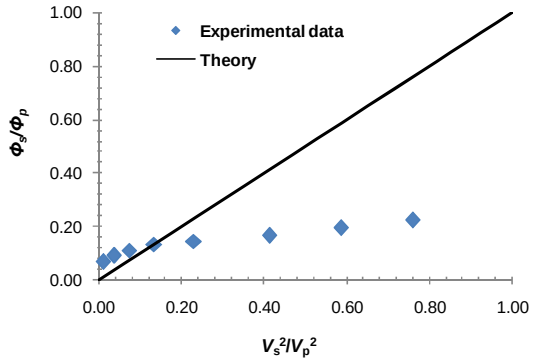

Figure F.1. A comparison of experimental $\emptyset_s/\emptyset_p$ data with theoretical ones.

Appendix G

Effect of pH on the water solubility of monomers

In order to investigate the effect of pH on the water-solubility of NIPAM monomer, oversaturated NIPAM dispersion (30wt%) was firstly obtained at room temperature (pH=7.0). After standing for 5 min, phase separation occurred, resulting a NIPAM monomer-rich layer in the upper phase and a saturated NIPAM solution in the lower layer. 4 ml of monomer-saturated solution was then placed in a glass tube. By adding 0.5 ml of sodium hydroxide solution (2 $mol \cdot l^{-1}$), the monomer solution became turbid, as shown in Figure G.1a. By contrast, no change was observed by adding 0.1 ml of HCl solution (10 $mol \cdot l^{-1}$).

To further study the water solubility of NIPAM at acidic conditions, 2 ml of oversaturated NIPAM dispersion (30wt%) was then used (pH=7.0). By adding 0.1 ml of concentrated HCl solution (10 $mol \cdot l^{-1}$), the solution became clear, as shown in Figure G.1b. Therefore, it can be concluded that the water solubility of NIPAM decreases with increasing pH.

The same method has been applied to MMA and VA monomers. However, no change was observed via altering the pH from acidic to basic conditions. Therefore, the effect of pH on the water solubility of MMA and VA monomers can be ignored.

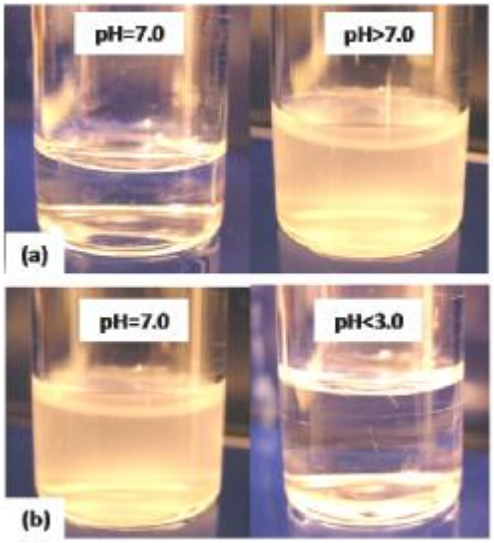

Figure G.1. NIPAM solution at different pH; a) saturated sample with NIPAM at pH = 7.0 (left) followed by an increase in pH (right), b) Sample oversaturated with NIPAM at pH = 7.0 (left) followed by a decrease in pH (right)

Publications

1. **Chen, Y.**, Sajjadi, S. Particle Formation and Growth in ab initio Emulsifier-free Emulsion Polymerisation Under Monomer-Starved Conditions. ***Polymer***, 2009, v50, pp357-365.

2. **Chen, Y.**, Sajjadi, S. Novel Method for Synthesis of Fast Dissolving PolyNIPAM Colloids. **To be Submitted**.

3. **Chen, Y.**, Sajjadi, S. A Novel Method for Synthesis of Temperature-responsive Nanogel Capsules. **To be Submitted**.

4. **Chen, Y.**, Sajjadi, S. Synthesis of Thermo-responsive Water-Soluble Poly(*N*-isopropylacrylamide) Colloids. **To be submitted**.

5. **Chen, Y.**, Jahanzad, F., Sajjadi, S. New Insights into Semicontinuous Microemulsion Polymerisation as a Mean to Produce Nanolatexes: Analysis of Nucleation Stage. **To be submitted**.

6. **Chen, Y.**, Sajjadi, S. Exploring the Minimum Particle Size Achievable via Semicontinuous Microemulsion Polymerisation. **To be submitted**.

7. **Chen, Y.**, Sajjadi, S. Synthesis of Ultrafine Nanolatexes using Chain Transfer Agent via Semicontinuous Microemulsion Polymerisation. **To be submitted**.

8. **Chen, Y.**, Sajjadi, S. Synthesis and Characterisation of Polymer/SiO_2 Core-Shell Nanocomposite Particles by Semicontinuous Polymerisation. **To be submitted**.